Cranfield University

Andrea I Marasco

Analysis and evaluation of mechanical performance of reinforced sandwich structures: X-Cor™ and K-Cor™

School of Industrial and Manufacturing Science

PhD Thesis

Cranfield University
School of Industrial and Manufacturing Science
Advanced Materials Department

PhD Thesis
Academic years: 2002 – 2005

Andrea I Marasco

Analysis and evaluation of mechanical performance of reinforced sandwich structures: X-Cor™ and K-Cor™

Supervisor: Professor Ivana K Partridge

December 2005

Abstract

X-Cor™ and K-Cor™ are foam based lightweight structural cores reinforced with Z-Fiber® rods oriented in a truss pattern. They can generate sandwich structures which possess strength- and stiffness-to-weight ratios such to compete with aerospace grade honeycomb constructions. The enhanced tailoring ability to specific design needs, the flexibility in reinforcement type and arrangement, the variety between closed cell foam-filled or hollow core configurations for ultimate weight savings or structural multifunctionality, while utilising manufacturing procedures similar to traditional honeycomb sandwich structures (low cost out-of-autoclave manufacturing techniques included) make these novel materials an attractive alternative. The process of their implementation into current engineering practice requires a parallel comparison with existing competitor cores and a critical evaluation of their performance, identifying advantages and disadvantages.

This study represents one of the first attempts to create a rigorous methodology for the analysis and evaluation of their mechanical behaviour and manufacturing sensitivities. The balance of out-of-plane properties (shear and compression), fundamental for a sandwich core material, has been investigated. The material energy absorption capacity for the aforementioned loading cases, as well as for in-plane crushing was evaluated. For this purpose, a new quasi-static test for progressive crushing of flat sandwich laminates was designed successfully. The experimental data gathered validate proposed analytical models which allowed further deductions on core parameters influence to be made. Those parameters were the pin insertion angle, pin lay-out, pin density and the role of the foam. A local-global FE modelling approach for Z-pinned sandwich cores is also provided and validated for X-Cor™ structures. Structural differences between X-Cor™ and K-Cor™ are at the base of a diverse mechanical response; their performance is sensitive to the manufacturing process, as it determines the quality of the pin-skin and pin-adhesive film interfaces. An ‘improved’ manufacturing technique designed for X-Cor™ resulted in a sandwich panel able to offer the same mechanical performance of a Nomex® honeycomb structure for a 25% of weight saving.

To Maria José

Caminante, son tus huellas
el camino, y nada más;
caminante, no hay camino,
se hace camino al andar,
Al andar se hace el camino,
y al volver la vista atrás
se ve la senda que nunca
se ha de volver a pisar.
Caminante, no hay camino,
sino estelas en el mar.

Antonio Machado,
Proverbios y Cantares, XXIX

Acknowledgements

I would like to express my gratitude to Professor Ivana K Partridge for giving me this opportunity and for her continuous support throughout the research work.

I would like to thank Professors M. Rink, R. Frassine and A. Pavan from the Politecnico of Milan which encouraged me to embark on this PhD course at Cranfield.

Thanks must go to Dr. D. Cartié, Dr. G. Allegri, Mr. J. Hurley and Mr. G. Iacopino for always answering all my questions which, at times, generate interminable discussions on thesis related subjects and beyond. Thanks also to Dr. M. Troulis for carefully reading the final version of the manuscript and to Dr. G. Marengo for his support during the last phase of this work. A special appreciation goes to Mr. H. Zervos, for having the patience to proof read the initial version of this work. Thanks also to Giuseppe, Simon, Matt, James, Ryan, Michel, Gavin, Zahir and Ben from the Composites group for all the nice moments in the office, the lab and the CSA pub.

I would like to remember Mr. T. Bonnington (president of Aztex Inc.) whose contagious enthusiasm and commitment gave us the strength to go on in hard times.

Thanks to all the companies involved in the projects for advice and supply of free material, especially Aztex Inc., BAE SYSTEMS (Dr. A. Rezai) and Jaguar Racing (Mr. S. Foster) and to Professor A. Pickett and Mr. A. Mills for their support in the CIMS project.

I should not forget the rest of the people in Cranfield who helped in their way, especially: Marcello, Sareta, Axel, Luca, Magalie, Laura, Alessandro A., Alessandro G. and Mimmo.

Last but not least I thank my parents, my sister, Maria José and friends in Italy who coped with me being away for so long and whose love and support made all of this possible.

Table of contents

List of figures

List of tables

Nomenclature

A	Specimen cross-section
b	Specimen width
d	Pin diameter
D	Flexural rigidity
D_c	Flexural rigidity of the core
D_f	Flexural rigidity of the facesheet about its neutral axis
D_0	Flexural rigidity of the facesheet about the centroidal axis of the sandwich
D_{eq}	Equivalent flexural rigidity
E	Tensile modulus
E_c	Core tensile modulus
E_f	Facesheet tensile modulus
E_{f11}	Fibre longitudinal elastic modulus
E_m	Resin (matrix) elastic modulus
f	Pin volume fraction
G	Shear modulus
G_c	Core shear modulus
G_{IC}	Critical strain energy release rate (or delamination toughness) for mode I
G_{IIC}	Critical strain energy release rate (or delamination toughness) for mode II
h	Foam thickness
I	Moment of inertia
K	rotational spring constant
l	Reveal / flattened length
L	Pin length
L_{cr}	Crush length
Mc	Critical moment applied at pin interface
M_{cr}	Crushed specimen mass

$M_{ext,o}$ External moment with respect to the pole O

M_f Flexural moment

$M_{int,o}$ Internal (interfacial) moment with respect to the pole O

n_{eff} Number of effective load bearing pins

n_{th} Theoretical number of load bearing pins

N Pin axial load

N_{ss} Buckling load for a simply supported pin

N_{cr} Pin buckling load

$N_{cr,exp}$ Experimentally determined pin buckling load

N_{rs} Buckling load for a rigidly supported pin

P_B Specimen Buckling load

P_E Specimen Euler buckling load

$\overline{P_{cr}}$ Constant crush load

S Core shear buckling load

t Shear force applied on a single pin

t_s Facesheet thickness

t_c Sandwich core thickness

t_{sp} Specimen thickness

u Relative skin movement in the longitudinal direction

V_{cr} Crushed volume

W_{cr} Total crush work

α Half vertex angle of pyramidal specimen

γ Shear strain

γ_{τ_s} Shear strain to failure

δ Displacement

θ_e Pin rotation angle in the elastic phase

θ_i Pin insertion angle

v_f Fibre volume fraction

v_m Resin volume fraction

ρ Specimen density

ρ_{eff}	Effective pin areal density
ρ_{th}	Theoretical pin areal density
σ_C	Pinned core compressive strength
$\overline{\sigma_{cr}}$	Average crush stress
$\sigma_{f,T}$	Fibre failure strength
$\sigma_{1,T}$	Pin tensile strength in the longitudinal direction
τ_m	Average shear stress
τ_s	Shear strength

Abbreviations

AE	Acoustic Emission
ASTM	American Society for Testing and Materials
CAI	Compression After Impact
CSB	Crack Sandwich Beam (Fracture Test)
CF	Carbon Fibre
CFRP	Carbon Fibre Reinforced Plastic
CTA	Cold Temperature Ambient
DCB	Double Cantilever Beam
DOF	Degree of Freedom
FEA	Finite Element Analysis
FEM	Finite Element Method
HVI	High Velocity Impact
LVI	Low Velocity Impact
LVDT	Linear Variable Displacement Transformer
NDE	Non Destructive Evaluation

RFI	Resin Film Infusion
RTA	Room Temperature Ambient
RTM	Resin Transfer Moulding
SEA	Specific Energy Absorption
TTR	Through (the) Thickness Reinforcement
UAV	Ultrasonically Assisted Vibrator
UD	Uni-directional
VARTM	Vacuum Assisted Resin Transfer Moulding

Chapter 1

Introduction

Composite materials now occupy an established position within the aerospace industry and a constantly growing importance in the automotive, naval and civil sectors. Nevertheless, the manufacturing costs for composite structures have proved to be a significant obstacle to their widespread use. This is partly due to the design approach that often still considers composites in the conventional 'metal fashion'. In order to take advantage of the weight and cost benefits of these materials, design and manufacturing should be considered in parallel from the earliest stages, generating in this way more affordable and tailored structures. Before a new composite material system or structural concept can be engineered, a process involving progressive intermediate steps is needed. This allows for ad-hoc developed methodologies, a comprehensive analysis of structural behaviour and failure mechanisms, which become crucial tools for the modern structural composite engineer or designer. With this perspective, the research work carried out aims to provide an understanding of the quasi-static mechanical behaviour of novel sandwich structures named X-Cor™ and K-Cor™ and its dependence on manufacturing processes.

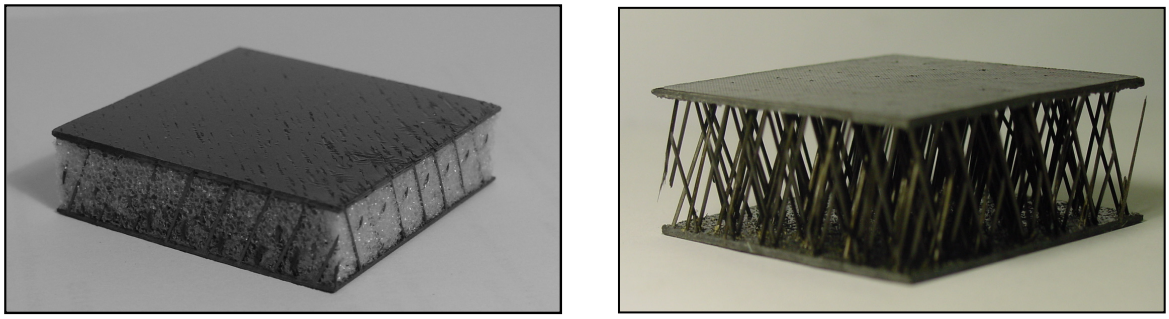

(a) *(b)*

Figure 1.1– *Reinforced foam core (a) and hollow core (b) X-Cor™ sandwich structures with carbon fibre / epoxy skins*

1.1 Background

1.1.1 Structural affordability: performance at low cost

In the emerging scenario of future composite structures for aerospace vehicles, the combination of leading-edge technologies, novel engineering tools and manufacturing techniques should lead to the improvement of structural efficiency and reduction of manufacturing costs. Structural affordability is accomplished through a design which is low in cost, but meets its target functional requirements [1]. All major aerospace companies, both in military and civil projects, are moving in this direction (figure 1.2).

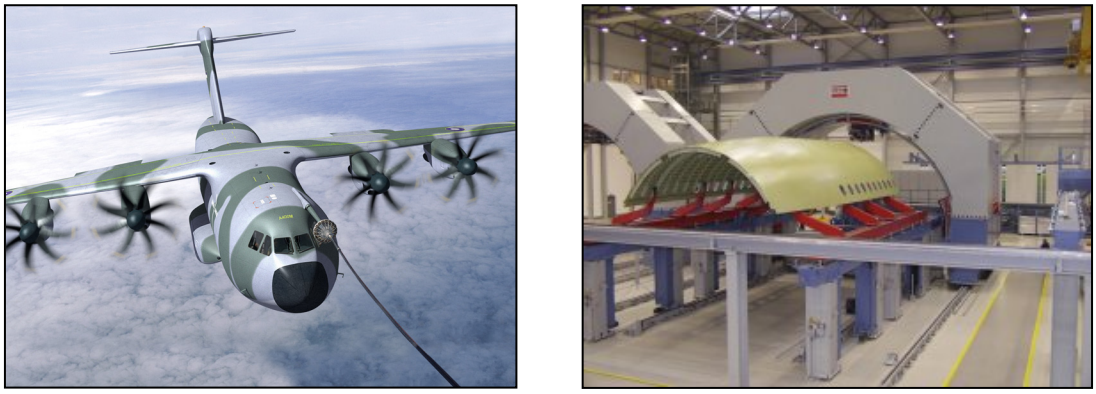

(a) *(b)*

Figure 1.2– *Application of composite technology for primary structures on the A400M large transport aeroplane wing (a) and on the A380 fuselage panels (b). Photographs courtesy of Airbus Industries*

Passenger aircraft represent a severe test for these materials, as both performance and economic aspects need to be equally justified [2]. Composites have been accepted for major primary structures on both Boeing's new 787 'Dreamliner'' and the world's largest airliner, the Airbus A380. The 787 will have half of its structural weight made of composite materials. The Airbus A380 is adopting a novel material, GLARE (glass reinforced aluminium [3]), that combines the advantages of metals and composites. A 25% weight saving over a conventional structure is achieved by using this material for over 400 m^2 of the A380's fuselage. The advantages offered by composite materials have been taken into account and put into commercial use. Weight saving, but at the same time durability, reduced need for maintenance and increased potential for

development, together with a reduced price of carbon fibre, seem to give to composites an edge over the metal counterpart.

It is in a similar scenario that Sikorsky Aircraft Corporation, in a cooperative agreement with the US Army (called Rotary Wing Structures Technology Demonstration – RWSTD), originally approached Aztex Inc., as X-Cor™ structures seemed a way forward to make military helicopters more affordable [4]. The pre-production version of the RAH-66 Comanche, the first helicopter with an all-composites primary structure [5], would have benefited from a more damage tolerant composite material for front fuselage structures (figure 1.3).

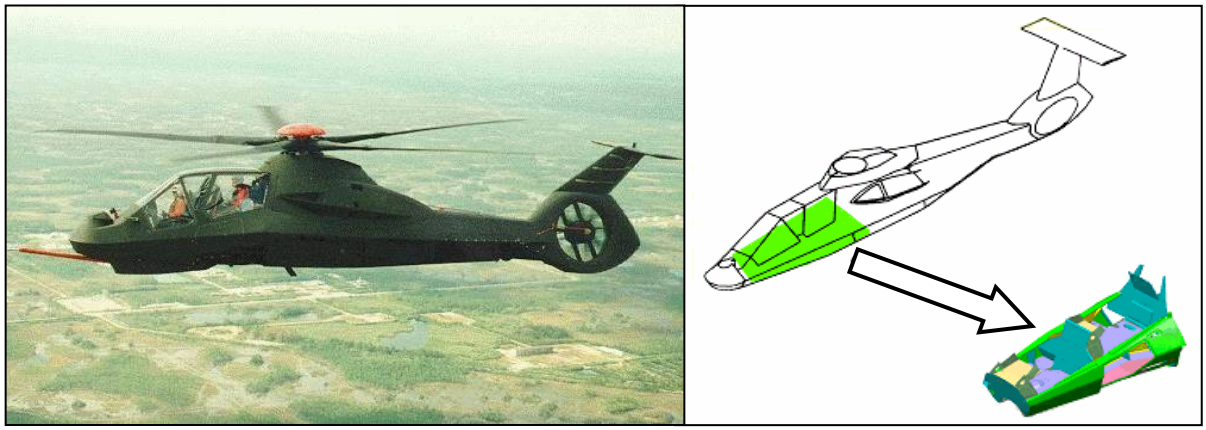

(a) *(b)*

Figure 1.3– *(a) RAH-66 Comanche (courtesy of Sikorsky Aircraft Corporation)*
(b) Front fuselage structures made of X-Cor™, adapted from [4]

The honeycomb used originally, besides not being very damage-tolerant, presented moisture absorption problems which weakened the structure. The new core had at least the equivalent mechanical properties of a honeycomb, but with greater damage tolerance. Moreover, it allowed to save roughly 10% of weight (~50lbs per helicopter), and to reduce manufacturing costs by about 25% against the honeycomb base-line [6].

1.1.2 Out-of-plane load management

The development of three-dimensional composite structures addresses effectively the issue of performance when these materials are subjected to a transverse force, albeit an impact or any other type of out-of-plane loading condition. The poor through-the

thickness properties of composites are probably the biggest compromise to carry in these materials. Since delamination initiation and propagation are thought to be matrix material dependent, a first way to improve the resin fracture toughness and damage tolerance is through the use of toughened resins and interleaves [7, 8]. A more effective enhancement is achieved by means of numerous techniques which modify the fibre architecture within the composite laminate [9]. A three-dimensional fibre network can be created either by using different textile technologies (weaving, knitting and braiding), or by placing through-the-thickness reinforcement to a conventional two-dimensional fibre configuration in the form of Z-Fiber® (rods) or yarns when stitching or tufting are used (figure 1.4). These techniques embody an attempt to achieve desirable damage tolerance properties in these structures, usually employed for their high flexural stiffness to weight ratio.

(a) *(b)* *(c)*

Figure 1.4– *Z-Fiber® reinforced composite hat stiffeners (a) for reinforcing the skin structure of the F/A-18 (b) inlet ducts replacing traditional metal fasteners (c). Saved 35lbs in weight and approximately $83000 in cost per plane [10]. (b) Photograph courtesy of Boeing Industries*

The principal failure modes of sandwich constructions are delamination between the face and the core, shear and compressive failure of the core, as well as tensile and compressive failure in the skins. Any damage of this type may reduce the stiffness and the residual strength of sandwich structures during service life. Additionally, to increase their load carrying capability, it is desirable to maximise the transverse stiffness and strength of the core [11]. Through-the-thickness reinforcement seems an effective solution for preventing skin-to-core delamination and minimising the reduction of stiffness and residual strength [12]. Sandwich structures offer the lowest weight technique for stiffening, yet are not fully exploited due to the lack of engineering

confidence deriving essentially from environmental durability (especially with honeycombs) [1]. Z-pinned sandwich structures provide a potential solution to the problem, with an enhanced skin-to-core structural interface associated to a close-cell foam or a hollow configuration.

1.1.3 Multifunctional structures

There is a growing interest in the aerospace sector in using sandwich structures which can also offer space advantages in addition to other desirable properties [13]. Multi-functionality is considered as an added value in a structure, by enhancing the use of a core beyond traditional load bearing; the idea is to 'do more with less', maximising the use of a structure [14, 15]. Among all the possible ways of space usage, wire routing, fuel storage and sensor embedding are the principal ones (figure 1.5). While foam and honeycomb cores require considerable post-fabrication machining to fulfil any additional purpose, hollow core sandwich constructions seem the ideal alternative for such functions.

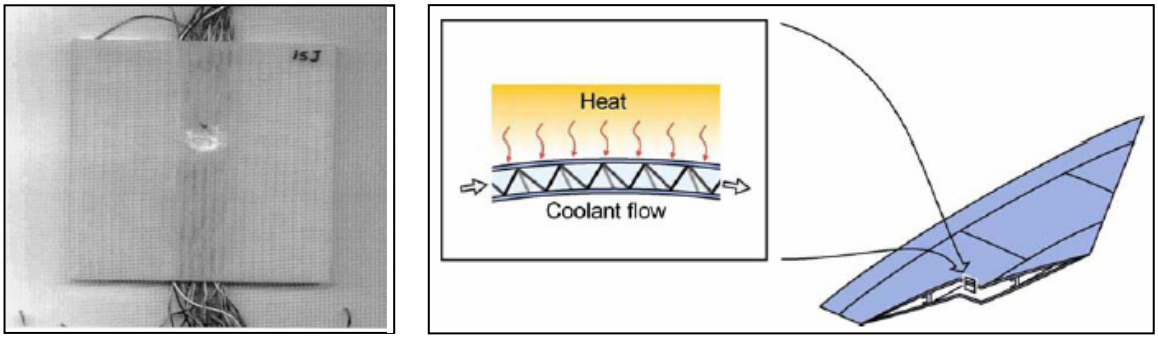

(a) *(b)*

Figure 1.5– *(a) Integrated core sandwich with wires after LVI test, from [16]*
(b) Hollow core sandwich panel wingskin for active cooling, from [15]

1.2 Thesis objectives

The principal objective of this work is to provide an in-depth understanding and a critical evaluation of the mechanical performance delivered by X-Cor™ and K-Cor™ sandwich structures through a rigorous methodology implemented for their characterization (hereafter referred to as X-Cor and K-Cor). This is used for identifying

those key parameters fundamental for the selection of an appropriate core configuration at the design stage. Methodologies to improve material performance are adopted and eventually specified throughout the work. Analytical and FE models are created, essentially as investigative tools, to predict material behaviour and to investigate possible improved configurations. The structural differences between X-Cor and K-Cor are analysed as well as their core parameter influence on mechanical response. Their behaviour is evaluated under out-of-plane shear and compressive loading conditions. The energy absorption capacity is estimated for these loading cases as well as for in-plane crushing. A new quasi-static test for progressive crushing on flat sandwich structures is proposed. Comparison with other competitor core materials (Nomex and Al honeycombs of similar density) are carried out parallel to the work done on X/K-Cor, in order to identify advantages / disadvantages and design issues related to the use of these pinned sandwich cores.

1.3 Thesis structure

A summary of the content of each chapter is presented as follows:

Chapter 1 provides the emerging scenarios in which X-Cor and K-Cor structures could potentially play a role in future applications.

Chapter 2 introduces through-the-thickness reinforcement in sandwich structures, stretching across all the different concepts and solutions. A review on the up-to-date research work done on X-Cor and K-Cor is also presented.

Chapter 3 describes the different production techniques employed for these novel materials and introduces an ‘improved’ manufacturing method for X-Cor and a specifically developed foam removal procedure. The core parameters as well as the unit cell approach followed are also detailed. A description of all the materials tested is provided.

Chapter 4 critically reviews the test methods used for out-of-plane loading and describes the data analysis technique based on the sample ‘effective area’.

Chapter 5 outlines the experimental findings for the out-of-plane shear loading test and compares the results across all the types of materials tested as function of core and manufacturing parameters. Failure modes are analysed, also involving analytical models specifically developed to evaluate pin-interface properties. A global-local FE modelling strategy for both X-Cor and K-Cor is presented along with an analytical model which provides input parameters for an X-Cor unit cell FE model. Model predictions are compared with experimental data.

Chapter 6 is dedicated to the out-of-plane compressive behaviour. Test results are presented and analysed evaluating the influence of core parameters and manufacturing techniques. Failure modes are investigated and a preliminary analytical model to evaluate the mechanical constraint acting on the pins is presented.

Chapter 7 deals with the energy absorption evaluation. An overview of in-plane crushing and different crushing tests is followed by the development of a novel in-plane crush test for flat sandwich samples. A suitable data analysis methodology is presented. Test results and specific energy absorption values are provided. A description of the main damage mechanisms and crush zone morphology in pinned core sandwich structures completes the analysis.

Chapter 8 summarises the main results and discusses selected issues further, providing a general view of the influence of the parameters analysed. Core design suggestions and potential application guidelines are also indicated.

Chapter 9 gathers the most important conclusions and suggests areas for further work.

Chapter 2

Literature review

Recent advances in core materials and through-the-thickness strengthening techniques have also generated interest in innovative reinforced sandwich structures, especially for weight-critical applications. The improved interlaminar strength results in a better damage resistance to out-of-plane loads, damage tolerance, compression-after-impact (CAI) and fracture toughness. In addition sandwich structures are less susceptible to core-skin interface delaminations. In this chapter a brief summary of the principal 'reinforcing' concepts and methods originally developed for monolithic laminates (section 2.1) and recently extended to composite sandwich constructions (section 2.2) is introduced, along with relevant references and advantages and disadvantages of each method. A detailed up-to-date review of the research activity conducted on X-Cor and K-Cor sandwich structures is also presented (section 2.3).

2.1 Enhancement of interlaminar properties in composite monolithic laminates

In the past thirty years, the sensitivity of 2D laminates to impact-induced delaminations and consequent reduction in compression strength and stiffness, low interlaminar fracture toughness and cost issues have been the driving force behind the development of new materials and fabrication processes [17-20]. The composite industry has been trying to address these issues by:

- Maintaining the traditional 2D fibre arrangement and altering the matrix material, matrix-fibre interface, fibres and laminate stacking configuration
- Developing advanced polymer composites reinforced either with 3D fibre architectures or with reinforcement placed in the z-direction

These new material concepts should provide an improved 'impact tolerance', namely a combination of impact resistance and damage tolerance. The first is defined as the ability of having a minimum amount of damage as result of a given impact event, while the latter is the ability of withstanding a given amount of damage with the minimum effect on structural integrity. The objective is to enhance the delamination resistance which is the resistance to initiate and/or propagate an existing crack in a composite system.

2.1.1 2D composite laminates

The initial approach consisted of toughening resin matrices, as the first fracture event, especially in an impact, is generally the formation of matrix cracks within the plies. Modified resins with micro-particles of rubber or thermoplastic proved to enhance the resistance to damage initiation [21, 22]. This second phase of the material absorbs energy during fracture through mechanisms such as crack blunting and void coalescence as well as promoting more extensive shear yielding in the continuous matrix resin [7, 23]. Moreover, a toughened matrix system often promotes toughening mechanisms in composites, such as fibre bridging as indicated in figure 2.1 [23, 24].

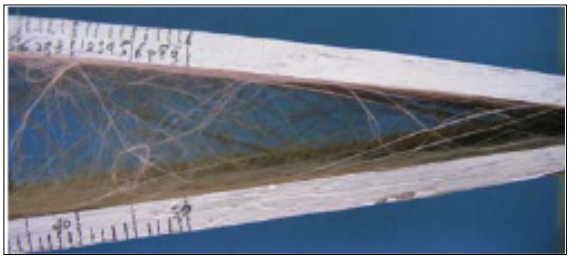

Figure 2.1– *Extensive fibre bridging in a failed glass fibre/epoxy sample under mode I loading, from [24]*

Transferring the resin system toughness into a composite material toughness is not a straightforward mechanism. Thermal history plays an important role as the presence of the fibres affects the thermal conductivity of the composite in comparison to the neat resin. Furthermore, the presence of possible residual stresses after cure as well as the diverse dispersion of toughening thermoplastic particles in the composite laminate are

additional differences from the neat resin system. Rubber toughened resin systems suffer also from compromised hot-wet performance [25].
The use of thermoplastic matrices (for example PEEK) is another option; they can absorb fracture energy through a significant amount of plastic flow [23]. However, the significant difference of the manufacturing procedure from conventional thermoset resin systems is a major disadvantage.

Interleaving represents one alternative method for improving the delamination resistance. It consists of inserting layers of a secondary material (adhesive film, self-same matrix resin or layers with toughened particles on the ply surface) at critical locations in the stacking sequence of prepreg plies [23, 26]. This method addresses the problem related to the constraining effect of the fibres on the development of large plastic deformation zones in toughened resin systems, allowing in this way the full exploitation of the matrix toughness. The benefits in delamination resistance can be up to a 10-fold increase in G_{IC} and a 7-fold increase in G_{IIC} [27]. Although these techniques have demonstrated improved damage tolerance in materials, they are characterised by an increased scatter and by a poor local distribution of the particulates which limits improvements in strength. Reduction of in-plane material properties, essentially compression and fatigue performance [23], and the increased susceptibility to processing variables are further disadvantages. More essentially the improvement in fracture toughness is not adequate for the associated weight penalty [23, 28].
The strengthening of the matrix-fibre interface involves the applications of modification methods on the surface of the fibre (coating with rubber or ductile plastic), as well as using special compatibilisers in the matrix. In some cases a controlled cooling rate may produce similar results on the interface properties, avoiding the application of chemicals [29, 30]. The consideration of the mismatch in fibre/matrix elastic property could also be taken into account in choosing, where possible, more appropriate material combinations, subsequently enhancing the delamination resistance [31]. A different approach to enhance the interlaminar properties of a composite laminate can be through an improved design which presents the advantage of not incurring the costs and timescales associated with the requalification of a new material system [23]. Panel geometry, lamina stacking sequence can be tailored to fully exploit the potential of

composites [20, 32]. Adopting a hybrid laminate combination, for example of woven and UD layers, can exploit the advantages given by the 2D fabric in terms of improved damage tolerance and the high mechanical properties assured by the unidirectional layers [23, 32, 33]. Some disadvantages associated to this method are finding a balanced stacking sequence, as well as delaminations occurring at the woven and tape lamina interfaces.

2.1.2 3D composite laminates

The techniques previously seen can improve the interlaminar properties to a certain extent, but three-dimensional composites obtained by embroidery techniques (weaving, braiding, knitting, stitching, and tufting) and Z-pinning have proved to be more effective [17, 23]. Although having reinforcement in the thickness direction improves the resistance to delamination, at the same time it may promote other failure modes [23, 34], and can affect the in-plane properties; the latter are generally lower than in a corresponding 2D configuration. With the exception of Z-pinned laminates, all the other 3D architectures are produced as fibre preforms; the resin is introduced secondarily by a suitable resin infusion process. These new composite architectures are usually coupled with low-cost, efficient manufacturing methods [34-36]. Using liquid composite moulding techniques (RTM, RFI and VARTM for example) with near-net-shape, 3-D fabric preforms radically simplifies composites manufacturing and increases its cost effectiveness [17, 37].

2.1.2.1 Textile composites

Composite structures made with 3D textile fabrics are potentially less expensive to manufacture and provide better through-the-thickness mechanical properties than composites made with the traditional 2D fabrics [17]. Despite this, the ability of 3D composites to replace 2D has been very limited in many applications.

Weaving

Weaving is the most widely used textile manufacturing technique for 2D fabrics [35] (figure 2.2); one of the advantages of 3D weaving is that preforms can be made only with minor modifications to the machinery employed for the 2D fabrics, minimising capital costs. Also the ability of 3D weaving to produce near-net-shape preforms can greatly reduce the cost of a component by reducing material wastage, the need for machining and the amount of material handled during lay-up [17, 38].

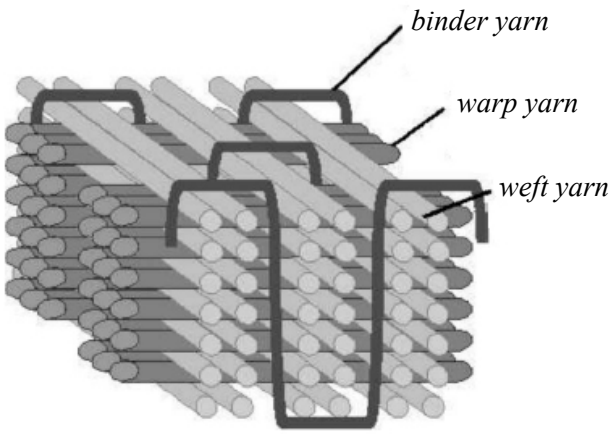

Figure 2.2– *Schematic of 3D orthogonal woven preform, adapted from [39]*

Almost any type of yarn can be used for these preforms, including carbon, glass, aramid and ceramic fibres (SiC, $A1_2O_3$) [17]. The improved damage tolerance properties compared to a similar 2D laminate are shown, for example, by the fact that the impact energy needed to initiate damage in 3D woven carbon–bismaleimide composites is up to 60% higher than in a 2D carbon–bismaleimide laminate [40]. The counter effect is that 3D composites exhibit lower in-plane mechanical properties than 2D laminates with an equivalent amount of fibres aligned in the load direction; tension and compression strengths are generally lower by 15–20% [17] and the elastic modulus at high applied stress is reduced by 20-30% [41]. One of the major drawbacks of 3D weaving is the difficulty to produce fabrics that contain in-plane yarns aligned at angles other than 0° and 90°. This results in 3D woven composites having highly anisotropic properties and poor shear and torsion properties [17]. The amount of distortion experienced by the woven fabric can be severe; the fibre architecture rarely corresponds to the idealised

structure [42]. Moreover the 3D weaving process causes abrasion damage of the yarns and breakage which affect essentially their tensile strength (reduction of 30%) [39].

Braiding

Braiding was the first textile process used to manufacture a 3D fibre preform for composite applications. It is defined as the "process of intertwining at least three parallel strands of fibre to fabricate continuous and seamless textile structure with non-orthogonal fibre orientation" [37] (figure 2.3). Their higher drapability, rotational stability and structural integrity make it possible to produce composite structures with intricate geometries to the near-net-shape [17]. One significant limitation to the use of 3D braided composites can be attributed to the manufacturing process [43]. The maximum preform size is in fact determined by the braiding machine size and most industrial machines are only able to braid preforms with a small cross-section, under 100 mm in width. Some recent developments in the manufacturing techniques provide substantial advantages over traditional 3D rotary methods and machinery; as the machine operation speed increases, these technologies become competitive [37].

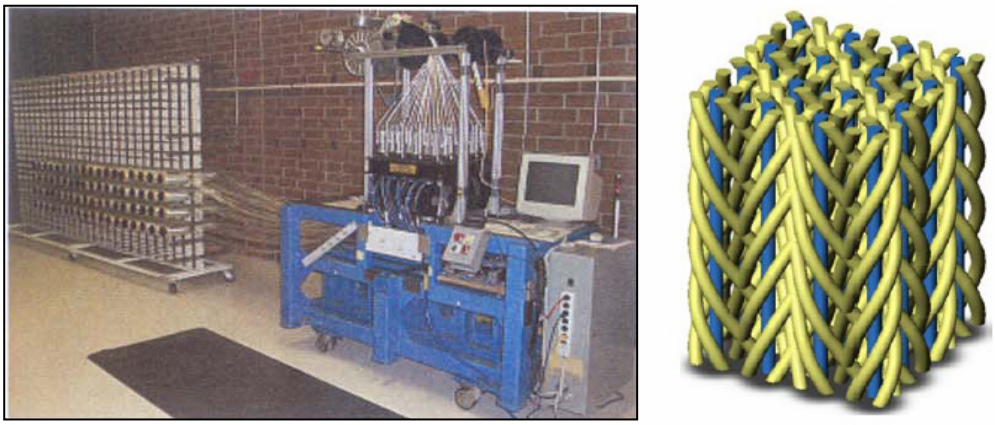

(a) *(b)*

Figure 2.3– *(a) 3TEX Inc.'s prototype: one-module 3D braider with creels for axial yarn supply [43]; (b) Design model of 3D braided preform, from [37]*

The mechanical properties of 3D braided composites are generally lower than those of 2D laminates with an equivalent weight fraction of in-plane fibres. At present the limited amount of experimental material data, along with the lack of predictive models for this type of materials, are affecting the spreading of their application.

Knitting

Knitted-fabric composites have certain advantages over woven and braided fabric composites, particularly in their ability to conform to complicated contours and to produce complex near-net-shape preforms [17, 44]. While a considerable amount of research has been performed on composites reinforced with 2D knitted fabrics [36, 45, 46], by comparison little is known about the mechanical properties and applications of 3D knitted composites [17]. Their properties are mainly dependent on the fibre volume fraction, the geometric configuration of reinforcing yarns as well as the properties of the constituent materials. The volume fraction is limited by the contact between adjacent loops with each other in either the warp or the weft direction (figure (2.4). At the same time the properties of fibres determine the minimum loop radius and consequently influence the maximum achievable fibre volume fraction. The diameter of the needle of the knitting machine plays also a fundamental role; the minimum yarn loop diameter should be greater than the diameter of the needle, in order for the needle to go through an existing loop [44].

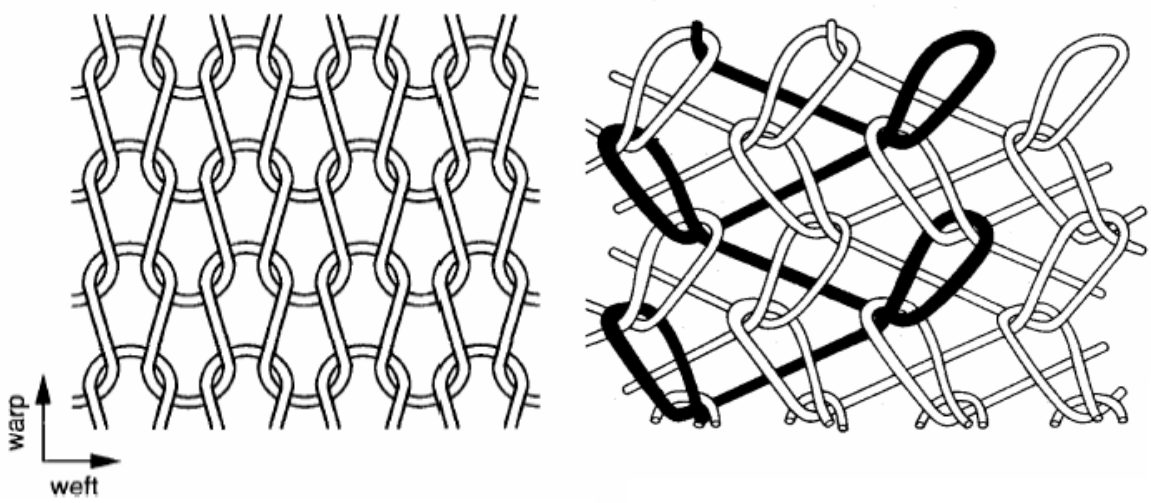

Figure 2.4– *Schematic diagrams of in-plane (a) weft- and (b) warp-knit fabrics, adapted from [47]*

Since 3D knitted sandwich composites are a recent development, there is only a small amount of published information on their mechanical properties and potential applications. The experimental results showed that the impact strength of knitted-fabric laminates was greater than that of woven-fabric laminates with the same fibre volume

fraction, while the trend is reversed for tensile strength [44] and for fatigue properties [48]. Reference [36] shows the results of an experimental characterization of different carbon fabrics knitted with Kevlar® fibres and fabricated into composite panels by resin transfer moulding. The results are compared with equivalent prepreg UD composites. Tension and compression strength reductions of knitted composites ranged from 20 to 30% compared to the UD laminates, while compression after impact strength is up to 80% higher than the strength of the baseline prepreg tape laminates.

3D textile composite materials are characterised by a fairly homogeneous structure which is generally associated with greater thicknesses; for this reasons balancing the different layers is not so important [23]. However, the improvement in impact damage tolerance is coupled with a reduction in the undamaged performance. The through-the-thickness fibres can also act as initiation sites for cracking, lowering the stress level at which damage starts to develop. The primary function of the resin system is to provide rigidity and to hold the reinforcement material in place, however the infusion process becomes more difficult in 3D composites than in conventional 2D laminates. This can lead to defect formation in large components. Additional disadvantages are the lack of flexibility of the semi-finished products and difficulty in changing the machine parameters in order to meet the dimensional requirements dictated by the stress conditions.

2.1.2.2 Through-the-thickness reinforced composites

Through-the-thickness reinforcing techniques applied on 2D laminate structures have been developed essentially in the search of methods to arrest the propagation of existing cracks in composites. Stitching, tufting and Z-pinning generally do not require a change in the manufacturing procedure, but only an additional step prior to curing. Thus, it is generally fairly simple to transfer these technologies to existing composite systems, although the 3D preform obtained is not an integral structure as for the case of 3D textiles. A further advantage, with respect to the previous technologies, is the possibility of them being used as a means of fixation.

Stitching

The stitching method has been reviewed in detail in [20, 49]. A large amount of work performed on stitched coupons and small flat panels is documented in literature, but very little research has been reported on stitched composite structures. During the process a needle is used to insert a high tensile strength yarn, usually made of aramid or glass fibres, into a prepreg laminate or a fabric preform. These materials exhibit the flexibility required for high curvatures; special partly pyrolised carbon fibres have also been developed recently for the same purpose [23]. The three most common types of stitches used are illustrated schematically in figure 2.5.

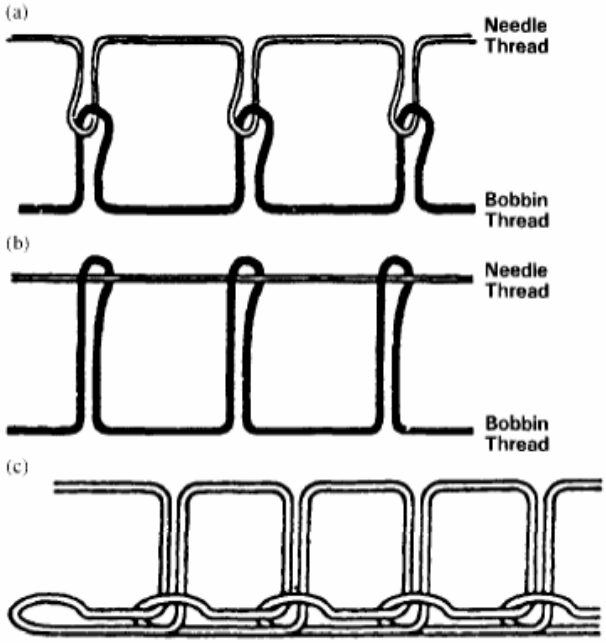

Figure 2.5– *Schematics of (a) lock stitches, (b) modified lock stitches and (c) chain stitches, after [50]*

Different types of damage occur in the composite laminate as result of the stitching process. The principal types can be summarised as:

- Localised damage due to the sewing needle and yarn penetrating the material. It consists of fibre breakage caused by the needle tip in UD laminates and by the frictional stresses generated by the needle and the yarn sliding through the fibers found in woven laminates. It can create stress concentration and subsequent crack formation (figure 2.6)

- Misalignment of fibres, as they are forced to spread around the stitches, and consequent creation of resin rich regions
- Kinking of the surface plies caused by the stitching yarn pressing on the outer surface plies between stitches for modified lock stitch or chain stitch (figure 2.7)

In general there is a dependency of the damage extent on the type of stitch used [49] as stitching generates regions of low strength and stiffness at the stitch holes and loops. Also, stitching a prepreg composite stack normally results in more induced fibre damage [20].

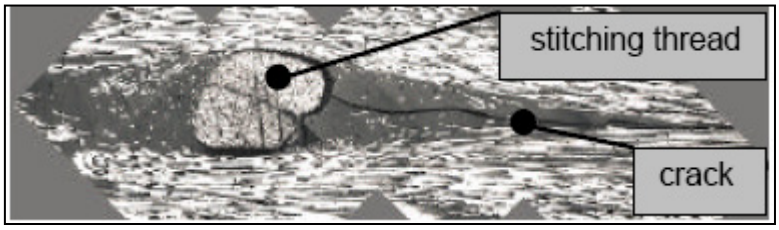

Figure 2.6– *Threads cause disturbance which can start cracks, from [51]*

The most significant improvement in mechanical performance resulting from stitching has been the increase in the interlaminar delamination resistance under Mode I [49]. Studies on this loading mode show that the strain energy G_I needed to start a delamination crack in a UD laminate is 15-80 times higher than the value for an unstitched laminate, depending on the thread type, thread diameter and stitch density [52, 53]. For steady crack growth the G_I value is raised by a factor of 3-16 [49]. The enhanced delamination resistance has been attributed to the elastic stretching of the thread, which applies crack closure forces restricting the opening displacement under tensile load [49, 52]. A considerable improvement in the mode II interlaminar fracture toughness has been also observed [54, 55]. First crack propagation becomes stable, unlike in the unstitched laminates; a 15-fold enhancement in the G_{II} values is possible [55]. Stitching generally has a negative effect on the in-plane properties [51]; Mouritz et al. [49] have noticed that only a few studies indicate that the in-plane properties were improved or not-affected by stitching. The majority of work agrees that this technique significantly reduces the in-plane performance as a result of the many defects introduced into the material, such as kinking (figure 2.7), misalignments, spreading and

breakage of the fibres, as well as formation of resin-rich volumes, porosity and resin cracks.

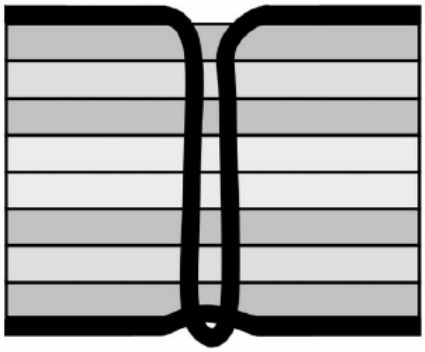

Figure 2.7– *Schematic of a stitch cross-section showing surface plies kinking [56]*

Surface plies are more greatly disturbed by the stitching yarn as its tension kinks their fibres. The compression-after-impact (CAI) strength is also improved. Reference [57] shows that a 95% improvement in CAI is achieved by introducing Kevlar® stitches in a CF / epoxy laminate, although this also results in a loss of about 30% in the undamaged compression strength. Lopresto et al. [18] have investigated the low velocity impact (LVI) behaviour on Kevlar® stitched CF/epoxy laminates, showing that apparently the presence of stitches did not affect substantially the material behaviour in terms of force–displacement curve, first failure load, and indentation. The stitched laminates exhibited a penetration energy about 30% lower than their 2D equivalent. The advantage of stitching in terms of impact damage resistance was evident only for high thickness composites; to constrain delamination in thin 2D laminates the use of stitches may be unnecessary. Hosur et al. [58] shows the high velocity impact response of stitched/unstitched woven fabric carbon/epoxy composite laminates. For fabrication of stitched laminates, a Kevlar thread was used to stitch the fabric preform in lock stitch fashion. The results indicate that the containment of the damage was superior in the case of the stitched laminates; however, the ballistic limit was found to be higher for the unstitched samples. Through the AST program [59] NASA and Boeing have joined together to perform design, analysis, fabrication, assembly and testing verification of an all composite wing structure for commercial transport aircraft. Among all the textile

composites evaluated, the results on stitching were the most encouraging, meeting the target requirements in costs and performance.

Tufting

The amount of scientific publications about tufting as a composite reinforcement procedure is very limited. Tufting as stitching is most suitable for dry fabrics; this allows liquid moulding techniques to be used and makes the process potentially cost effective. Tufting is a single-sided access method, where a single needle takes a yarn through the fabric layers and returns back along the same path, leaving a loop on the back side of the plies as illustrated in the schematic of figure 2.8. The fundamental difference to the stitching method is that the tufting loop is loose and almost tension-free and remains in position because of frictional forces acting on it. The actual reinforcement comes from the bonding between the matrix and thread and it is present only after cure [51]. This leads to a virtually tension-free structure, less waviness in the fabric and fewer problems during the resin injection [60]. Moreover the lack of thread tension allows to make oblique stitches [51]. An additional advantage with respect to traditional stitching is that the material is sewn only from one side (single thread method).

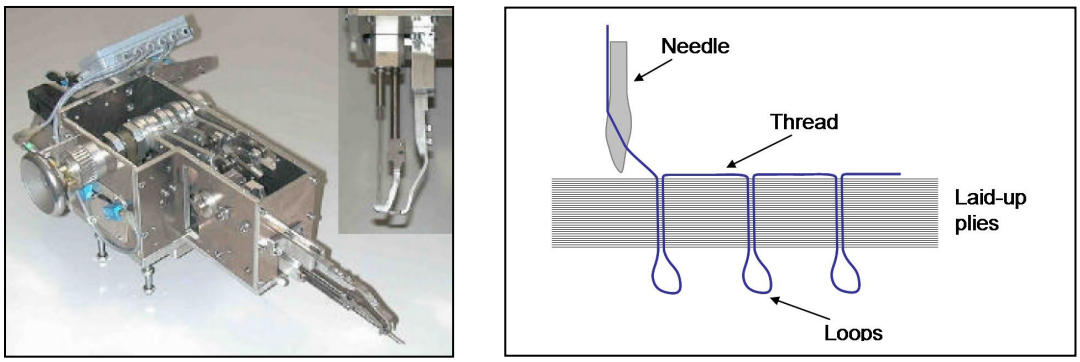

(a) *(b)*

Figure 2.8– *(a) Tufting head for conventional CNC machines, from [51]*
(b) Schematic of the yarn arrangement in a tufted preform, from [60]

A study on a tufted T-stiffener is presented in references [60, 61]. Glass fibre thread was used before the RTM injection. The pull-off resistance was determined under quasi-static conditions. As shown in figure 2.9 the peak load as well as the absorbed

energy were significantly higher than the reference case. A different failure mechanism was observed: the T-stiffener delamination was stopped and the samples failed in bending in the tufted specimen cases.

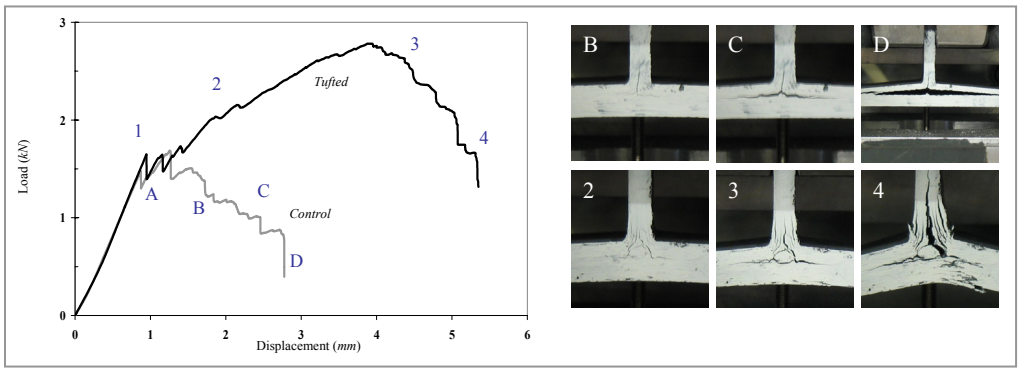

Figure 2.9– *Load/displacement curve of a tufted T-stiffener with photographs of the tested specimens [60, 61]*

Z-pinning

Z-Fiber® pins or Z-pins are rods inserted in the through-thickness direction of a laminated composite, effectively pinning the material together thanks to a combination of friction and adhesion [62-64]. The Z-Fiber® reinforcement has been proposed successfully to replace metallic fasteners, offering at the same time improved delamination strength and toughness [62, 64]. The pins can be made of a variety of materials such as for example pultruded carbon/glass fibre-epoxy/BMI resin, titanium alloy or steel (details can be found in [62, 65, 66]). After the insertion process, (figure 2.10), performed on the uncured prepreg laminate using an ultrasonic gun (ultrasonically assisted vibrator – UAV [6, 65]), the plate is cured in the autoclave using the standard cure cycle for the composite laminate. A comprehensive description and analysis of the manufacturing procedure can be found in [24, 28, 62, 64, 65]. The majority of the research work is focused on the enhanced out-of-plane properties; very little experimental work has been published on the degradation of in-plane properties [63], or on fatigue characterisation [62, 67].

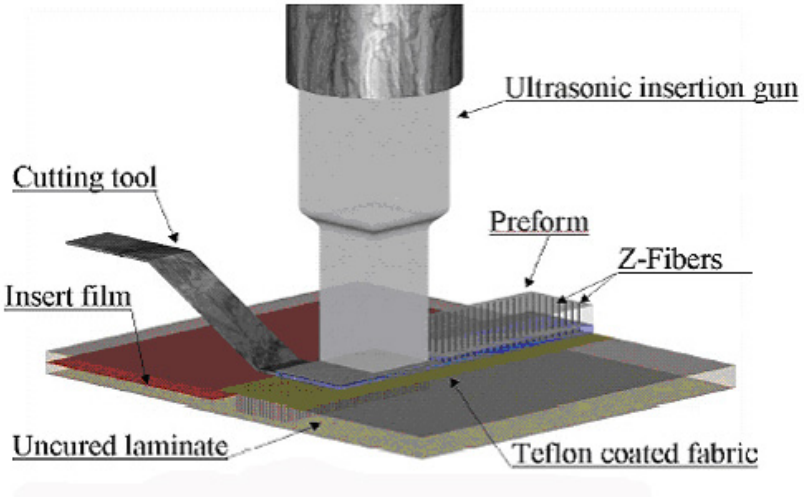

Figure 2.10– *Schematic of Z-pinning process, after [24]*

Similarly to stitching and tufting, the insertion of the reinforcement (Z-pins) into a fibre laminate leads to resin pockets, local stress concentrations and fibre waviness, which affect the in-plane tensile properties (figure 2.11).

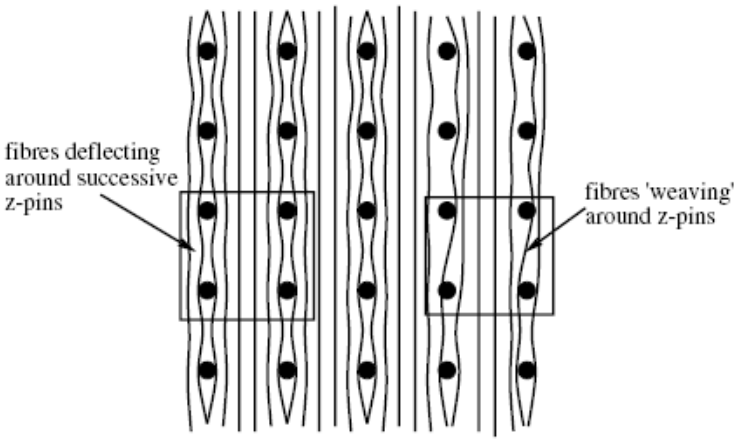

Figure 2.11– *Schematic of fibre deflecting and weaving around Z-pins from [63]*

References [62, 65, 68] have shown that, against crack propagation, interlaminar fracture toughness improves by at least an order of magnitude in mode I and significant enhancement in mode II. The test methods relating to the crack opening (Mode I) loading case are developed sufficiently to provide reliable data for analytical or FE models of localised behaviour in Z-pinned structures [69, 70]. The response of a Z-pinned laminate to shear loading (nominally Mode II) is a more complex problem, dominated by crack propagation resistance of the resin matrix itself and a multiplicity of

failure micromechanisms of the Z-pins bridging the crack [69]. Resistance to impact loading is also improved due to a reduction in crack formation (up to 30% decrease of damage area) and to an increase up to 50% in compression after impact strength [62, 65, 71]. Increasing the Z-pin density, insertion depth and laminate thickness, increases the mode I delamination resistance in Z-pinned laminates; pin diameter has the opposite effect. The effectiveness of Z-pinning reinforcement is enhanced when mode I loading conditions are favoured by design [24]. The degradation of in-plane properties measured in a recent work [63] is much higher than the values indicated in some early works on Z-pinning [28], where no decrease in compression strength and about a 10% decrease in tensile strength were indicated. Experiments and numerical simulations show that the presence of Z-pins decreases the tensile strength of the composite by 27% and the compressive strength by at least 30% [63]. The knockdown in modulus evaluated with FE techniques was estimated in 7-10% in in-plane compression and tension [70, 72]. According to [18, 23] Z-pinning is the most promising through-the-thickness reinforcement for present structures, although its associated cost is currently high. It can provide much higher areal densities of reinforcement in comparison to stitching [63]. For future structures, 3D woven materials show significant promise for impact tolerant design [23].

2.2 Through-the-thickness reinforcement methods in composite sandwich structures

The main advantage of 'thickening' a laminate by incorporating a low-density core material between two skins is the dramatic increase in flexural stiffness achieved for very little additional weight (figure 2.12). This value greatly exceeds that of a solid structure having the same total weight and made of the same material as the facings of the sandwich construction [73, 74]. For aerospace applications honeycombs are widely established as state-of-the-art choice for core materials [75, 76], although they present some drawbacks. They suffer from susceptibility to moisture intrusion resulting from their open-cell construction, which could be caused even from non-visible face-sheet damage. The moisture trapped can cause corrosion and further damage. At the point of

impact, the honeycomb core may be crushed. Such damage may result in face sheet buckling and delamination under stress. Moreover, honeycomb core panels are anisotropic in the bending plane, due to a doubling of cell wall thickness along one orientation (called the L-direction). It is costly and difficult to fabricate honeycomb structures into complex curved shapes, because of induced anticlastic curvature [75].

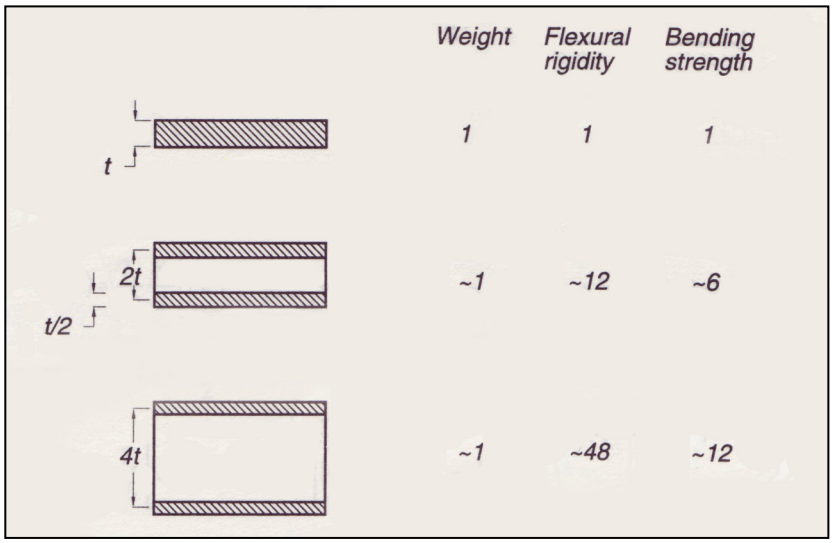

Figure 2.12– *Sandwich panel structural efficiency, from [77]*

From a manufacturing point of view there are also a few issues: the bonding area is not homogeneous; the honeycomb in fact offers a sort of bi-dimensional support to the skin. This can result in an uneven surface, noticeable as hexagonal depressions (known as the telegraphing effect) especially, in the case of thin skins associated with a co-curing process [75, 78]. As a result possible losses in strength and modulus need to be taken into account. Therefore, honeycomb core structures, although efficient because of their high strength-to-weight ratio, are not ideal for all applications. The cost of maintenance (servicing and repairing) can diminish the positive aspects of the low structural weight to the extent that heavier foam-core constructions can be more economical over the total life of the component [76]. In recent years other core solutions have started being considered as viable alternatives. Especially closed cell polymeric foams present some general advantages over honeycombs such as reduced costs of processing, mechanical isotropy and very low water absorption [75].

One first attempt has been to combine the properties of honeycomb cores with those of foams, exploiting the benefits of both and selectively eliminating their disadvantages. The cell-wall of the honeycomb is usually very thin and can experience local buckling under moderate compression (occurring even in the manufacturing process). Concentrated load can easily crush it, causing a local failure and a consequent separation of the facesheet from the core. This reduced support to the laminate skin could lead to matrix cracking and further delaminations which reduce the load carrying capabilities of the structures [79]. The foam which fills the cavities in the honeycomb provides a substantial reinforcement to the cell structure and very high mechanical properties compared to the foam itself and also to the honeycomb. In particular, compression properties are enhanced especially crushing strength in the z-direction, as well as the impact resistance capability, the induced damage in the composite skin and the extent of the crushing of the core. The principal drawback is the weight added to the sandwich panel [80]. Vaidya et al. [81] considers partially filled honeycomb cores with foam, in order to benefit from processing honeycombs with cost-effective VARTM, while at the same time enhancing damage resistance (figure 2.13). In this alternative approach the weight penalty is partially reduced, with respect to a full filled core, maintaining significant improvement over the honeycomb base material.

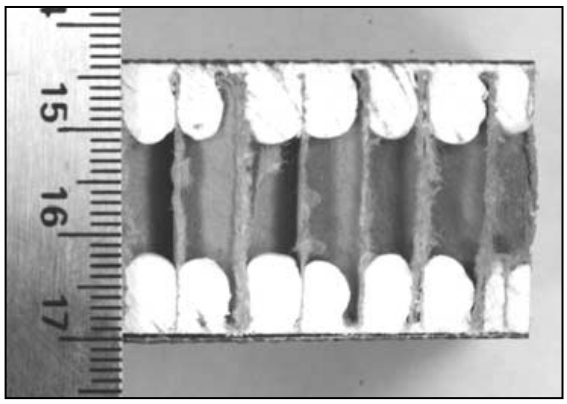

Figure 2.13– *Honeycomb partially filled with foam, after[81]*

Producing closed cell foams with higher mechanical properties, able to withstand typical autoclave temperatures and characterised by significant creep compression resistance, seems the other way forward [82]. Reference [83] shows a comparison between PU, PVC and PMI foams, all characterised by approximately 80 kg/m^3 density.

The PMI foam materials show the best strength-to-weight ratio for both tensile and shear properties. They are also reliable sandwich core materials up to a temperature of 130°C. In a comparison between PEI, PMI foams (80 kg/m^3 and 71 kg/m^3 respectively) and Nomex honeycomb (48 kg/m^3), the latter core material exhibited superior mechanical performance [75]. On the other hand, it is shown also that a foam system is more damage tolerant in out-of-plane loading conditions as the collapse of a single unit cell is not critical for the failure of the whole sandwich as in the case of honeycombs. The damage must pass through the entire specimen from the top to the bottom. Between the two foam systems PMI core sandwich samples outperformed the PEI specimens in terms of rigidity and strength in out-of-plane compression and bending tests. The PEI sandwich samples showed higher out-of-plane tensile strength and higher energy absorption capability in low velocity impact (LVI) tests where both the foam systems proved to be more damage tolerant than the honeycomb core. Similar results on post-impact residual capacity between PMI (71 kg/m^3) and Nomex honeycomb (48 kg/m^3) core sandwich with similar CF / epoxy laminated skins were also found in the work of Akay et al. [84]. As far as autoclave processability is concerned, PMI foams show a higher capacity to withstand high temperature and pressure (up to ~180°C and 0.7 MPa [83]) than all the other closed cell foam systems previously indicated. They exhibit a limited creep compression resistance during manufacturing [82].

Despite the recent improvements in performance and processability of foam cores, Al and Nomex honeycombs still exhibit a higher performance-to-weight ratio. A high-quality closed cell structural foam can only be improved in its performance by increasing its density [76]. The only way to further enhance the mechanical properties of a foam core is to combine it with a sort of an innovative through-the-thickness reinforcement. Different ways have been explored: from placing composite webs in the core [76, 85, 86] to transposing on foam sandwich structures the stitching, tufting and Z-pinning reinforcing techniques (figure 2.14). The aim of these methods is to enhance the interlaminar strength, damage tolerance and energy absorption properties and at the same time, if possible, allow for low cost processing. In particular by reinforcing the core-skin interface which is susceptible of delaminations [12], the overall strength and damage tolerance of the sandwich structure will improve. The combination of through-the-thickness reinforced carbon-epoxy structures together with sandwich structures is an

attempt to achieve the desirable properties of both types of constructions. To date very little has been published on through-the-thickness reinforcements in sandwich structures, as it is a relatively new technique.

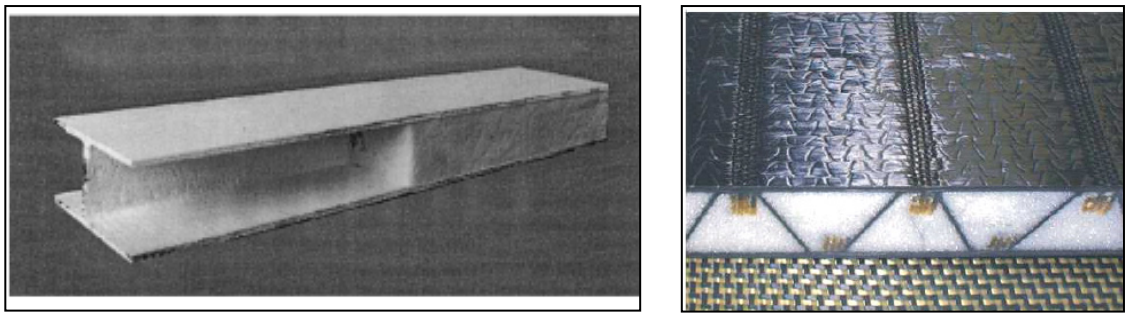

(a) *(b)*

Figure 2.14– *(a) Stiffened sandwich panel, from [87]*
(b) Stitched sandwich panel, from [76]

Stitched and tufted sandwich structures

The published work on stitched foam sandwich panels shows the feasibility and the potential benefits of this new technology. Different manufacturing methodologies are explored and an initial evaluation of the mechanical performance of this new sandwich concept can be made. Flexural strength as well as out-of-plane tensile and shear strengths are significantly improved over non-stitched reference foam sandwich samples [87-90] (figure 2.15). A significant increase in interlaminar properties and energy absorption was measured, but at the same time no appreciable effect on the load at which core failure initiated during flexure testing was noticed [88]. The work done by Lascoup et al. [89] shows that benefits brought by the addition of stitches involve both the strength and the modulus. Improvements in the out-of-plane compression and compression after impact were also found. Stitch bonded sandwich structures exhibit an interesting material behaviour in fatigue; as the number of cycles increase, the damage to the resin (a brittle epoxy) around the stitching thread increases and causes stiffness degradation as well as a consistent decrease in the bending fatigue strength (figure 2.16). The associated decrease in fatigue life is higher than those measured for the non-stitched samples for the same fatigue life [87].

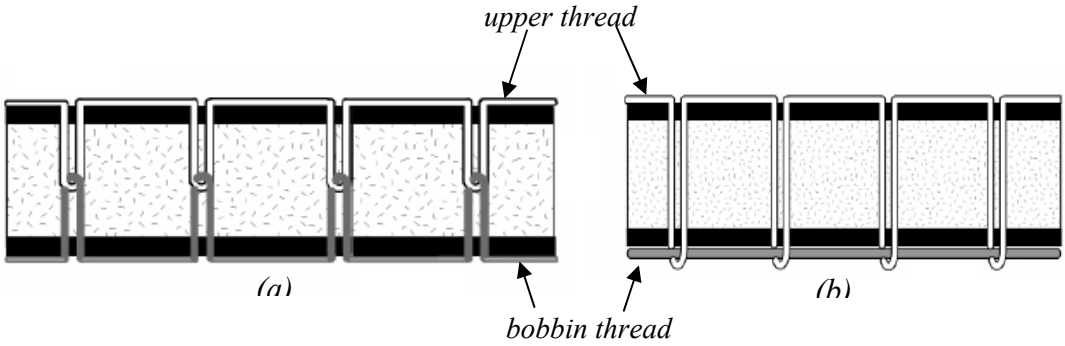

Figure 2.15– *Traditional (a) and modified (b) lock stitch and used in stitch-bonded sandwich structures, adapted from [12]*

In-plane energy absorption studies have shown an increase in energy absorption and load uniformity with diminishing stitch spacing [91]. Resistance to quasi-static indentation is generally improved by the presence of stitches and the bottom skin debonding area is reduced quite significantly [90, 92]. Singh et al. [93] carried out flexural, core shear and compression after impact tests for core stitched at 30°, 60º and 90º with respect to the facings. In flexural and shear testing the 30° configuration has a higher load capacity, while the 90° stitching exhibits the best results in compression after impact testing.

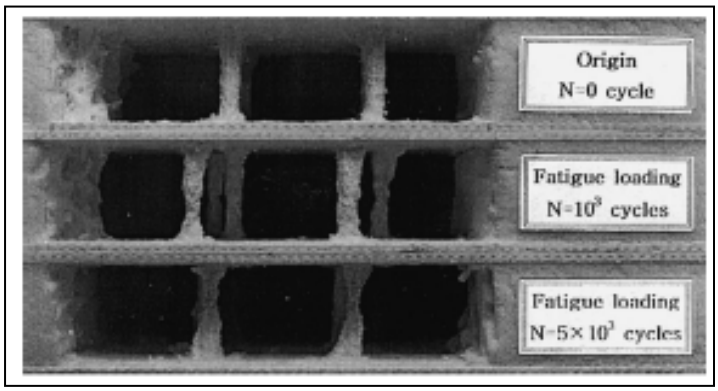

Figure 2.16– *Photos of stitched reinforced thread after fatigue loading, from [87]*

Reference [94] is at present the only speculative numerical work on the effect of stitching on the strain energy release rate for debonded sandwich beam configurations. The stitches were modelled as discrete non-linear spring elements with their compliance experimentally determined through out-of-plane tensile tests. Analysis on stitch density and rigidity coupled with a varying core modulus was carried out, defining different

optimised configurations. The small number of systematic studies on the influence of yarn distance, diameter and angle on the mechanical performance as well as predictive models still limits the exploitation of this technology. The necessity of finding an effective methodology for stitching significantly high density cellular foams appears clearly from the literature. This indicates that this technology applied to sandwich structures is still at a preliminary phase as diverse in-house stitching methods are developed [88, 90, 92]. Industrial traditional methodologies seem adequate only for low density PU foam cores [87]. The tufting technique (figure 2.17) appears to be more effective than a classic 2-sided stitching essentially for two reasons: it does not require availability of clearance underneath the part for thread manipulation and the insertion occurs along one side by only one needle minimising also the amount of damage created in the core material [95]. One sided stitching is also becoming an option, in which two needles are inserted to create an interlocked stitch on the thread [96].

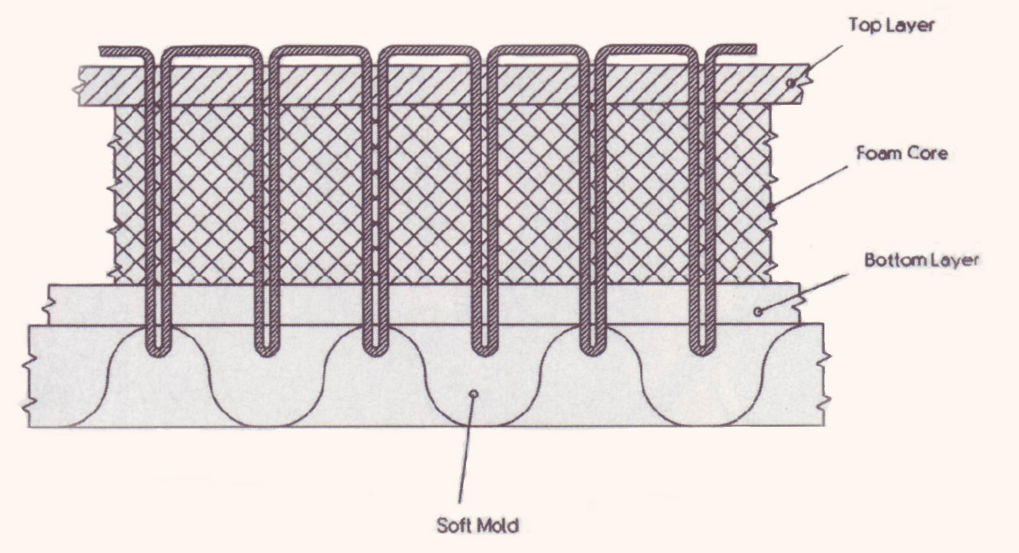

Figure 2.17– *Schematic of a tufted sandwich structure, from [95]*

Z-pinned sandwich structures: X-Cor and K-Cor

Z-Fiber® reinforced or Z-pinned sandwich structures are characterised by the presence of rods in the through-the-thickness direction. Such designation has been used to indicate two similar types of structures based on the same reinforcing technique, but applied at different stages of the manufacturing process. In the first type the reinforcement is applied directly from skin-to-skin through the core, as previously seen

for monolithic laminates [64, 97]; the panel obtained is simply indicated as a Z-pinned sandwich or as a hybrid Z-pinned laminate. They represent either early applications of this technology in the attempt of transferring such concept to sandwich structures or just ways to place an interlaminar reinforcement through the whole thickness of those constructions from skin-to-skin through the core. For example, in the work done by Wallace et al. [97, 98], a Nomex honeycomb core with composite skins was reinforced using CF / epoxy Z-pins. The Z-pin reinforcement was found to effectively improve the in-plane performance (34% increase in compressive strength), limiting the debonding of the skins from the core. Other loading conditions and the effect of pins associated with a honeycomb core were not investigated. Z-pinned sandwich panels made with this skin-to-skin technique usually have a foam core.

If the pins are inserted into foam layers at the start of the manufacturing process, they generate a new type of sandwich core material with trade name X-Cor and its alternative variation with trade name K-Cor. These through-the-thickness reinforced foam products were designed to replace honeycomb in various applications and at the same time to provide an improved durability and damage tolerance. These technologies involving the use of Z-Fiber® reinforcement have been developed and patented by Aztex Inc. [6]. The Z-Fiber® pins used for obtaining this preforms are exactly the same used for the Z-pinning of 2D laminates and, as previously mentioned, can be made of different materials. The insertion process into the foam layer is usually automated as shown in figure 2.18 and once the skins are put in place and cured a through-the-thickness reinforced sandwich structure with a truss-like core is generated (figure 2.19). The subsequent manufacturing procedure can be either autoclave cure, if prepreg skins are employed, or a low cost out-of-autoclave process such as resin transfers moulding (RTM) or vacuum assisted (VARTM) processing [99]. Usually closed-cell structural foams (PMI) are used because, among other properties, they guarantee both a high temperature resistance and a closed cell structure, allowing liquid moulding procedures to be used.

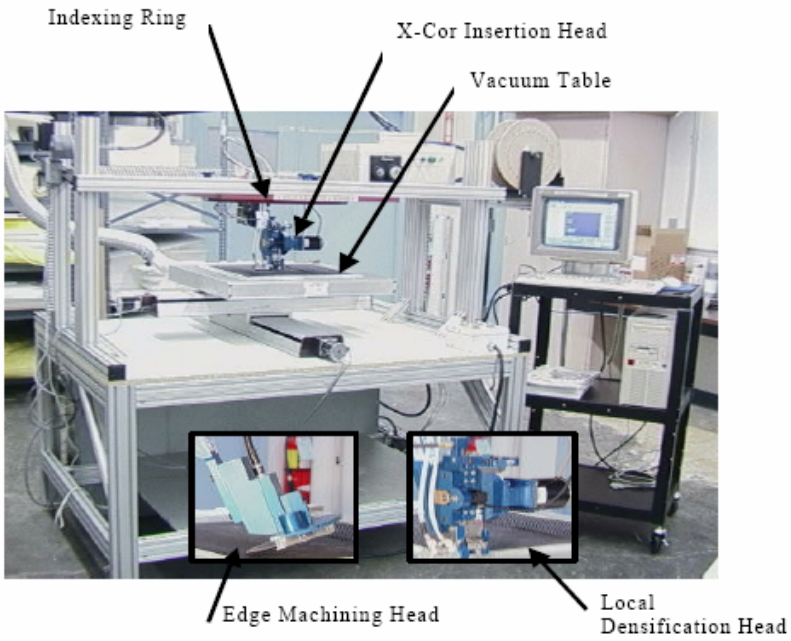

Figure 2.18– *Automated pin insertion machine for X-Cor preforms, from [99]*

In X-Cor sandwich constructions the pin tips protruding from the foam layer pierce the skins, generating a mechanical fastening (figure 2.19(a)). The pins can eventually go through the whole face-sheet thickness generating a skin-to-skin Z-pinned sandwich panel as for the previous case. It is more common to have just few plies pierced, enough for anchoring the pin and creating an efficient rotational constraint.

In K-Cor structures the protruding (undercured) pin tips are instead folded back flush the core; an adhesive bonding between core and skins guarantees in this case the integrity of the sandwich (figure 2.19(b)). A comprehensive analysis of the manufacturing procedures and of X-Cor and K-Cor structural differences can be found in Ch. 3.

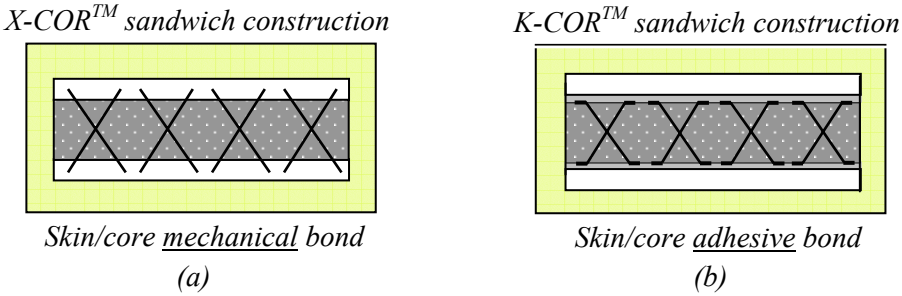

Figure 2.19– *Schematics of X-Cor (a) and K-Cor (b) sandwich structures*

What makes these sandwich structures unique is their flexibility to meet a variety of design specifications: it is possible to select a different foam system (for example with particular acoustic, thermal and electrical properties), different pin materials and diameters, different pin spacing and areal densities achieving also local densification (figure 2.20).

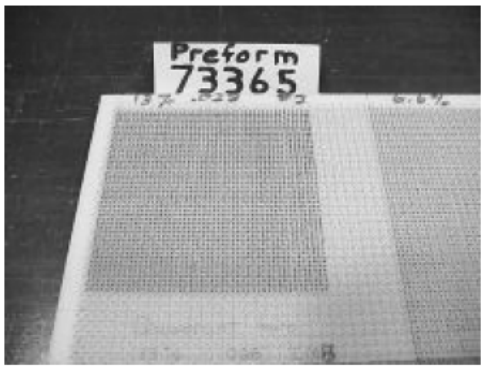

Figure 2.20– *Example of a densified preform, from [99]*

Pin insertion angle is an important variable as it changes the balance between shear and compression properties. A more vertical position of the pins enhances the compression behaviour of the sandwich structures. For shear resistance the angle of the pins should be increased. According to [62, 99], in order to match the typical honeycomb sandwich properties, the pin angle should be of 20°-30º degrees to have a good compromise in their performance.

Another advantage offered by these Z-pinned structures are the hollow sandwich configurations which are attracting a growing interest thanks to their multi-functional benefits offered by core accessibility [14]. In this sense hollow X/K-Cor structures appear more attractive than integral woven sandwich structures [100], foam-filled honeycombs or hollow stitched cores as they are conceptually closer to metal truss structures [15, 101] having the pins effectively acting as structural truss members.

2.3 Literature review on the mechanical performance of X-Cor, K-Cor sandwich structures

The first published paper on X-Cor sandwich structures, made from its homologous preform, is the work done by Carstensen et al. [99] in which the novel core concept is presented. It is shown that this new material offers major benefits over honeycomb and foam cores in terms of weight and manufacturing related cost savings. The role of the foam material (Rohacell 31 IG) needed for manufacturing the X-Cor preform is considered parasitic once the sandwich structure is consolidated. Its function is exclusively to hold the pins in place until the end of the processing phase. An eventual elimination of the foam has been considered. The X-Cor performance is compared to a baseline honeycomb core (fibreglass and aramid, not further specified) utilised by Sikorsky in airframe structures. The requirements were: 82°C wet performance, thin skins (2 plies of Hexcel 8552/IM7 plain weave fabric), directionality of the core structure (L and W directions as for honeycombs) and overall product weight. Preliminary tests have shown that the adhesive film serves no apparent purpose in these new core structures and can be eliminated. All the test results were normalised against the reference honeycomb performance.

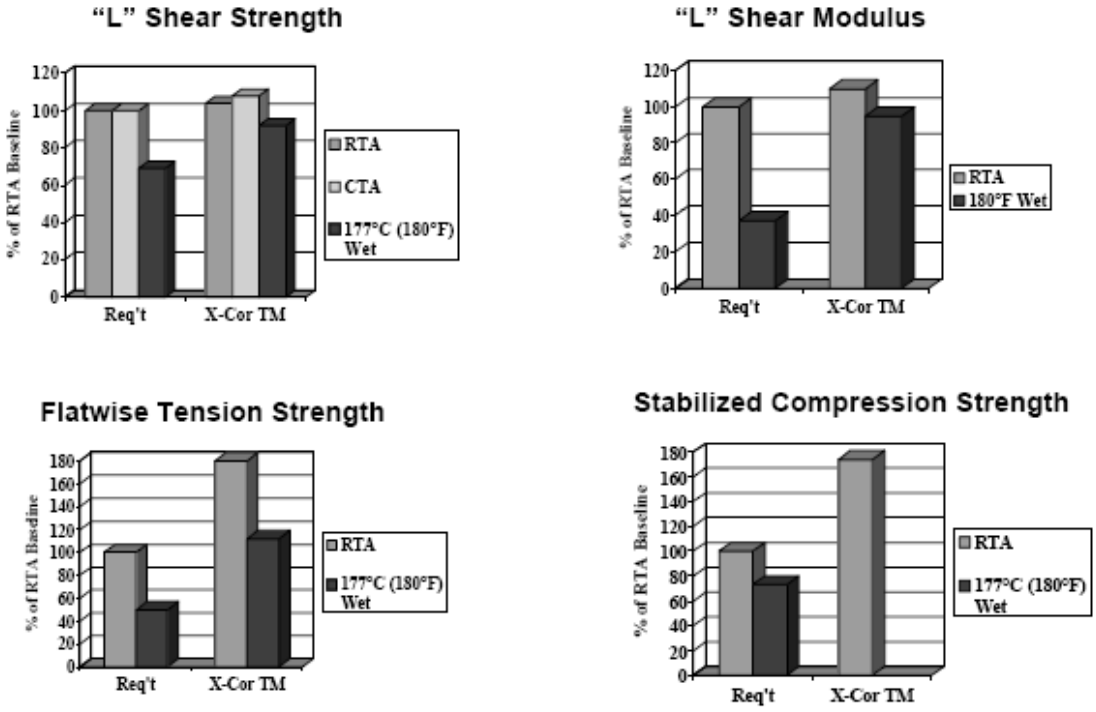

Figure 2.21– *Test results from [99]*

The first set of tests carried out was shear (ASTM C 273), out-of-plane tension (ASTM C 297) and compression (ASTM C 365); the findings are shown in figure 2.21. The three-point bend fatigue test results show that the material behaves in a similar way to the baseline honeycomb. In-plane compression on small and large panels as well as shear on large coupons were also performed in order to evaluate the damage tolerance characteristic of the materials. The results are summarised in figure 2.22.

The performance shown by the X-Cor samples is comparable to that of the baseline material for all the different load cases analysed. Pin pull-out emerges as the typical failure mechanism. The interfacial strength is addressed as one of the key parameters in the mechanical performance.

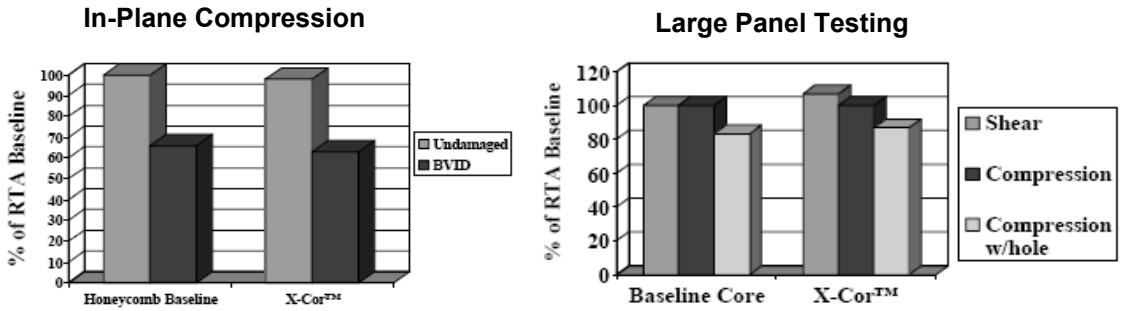

Figure 2.22– *Test results from [99]*

O'Brien and Paris [102] investigated the failure mechanisms typical of the transition regions between solid laminates and X-Cor sandwich structures. Small sub-component specimens were tested under three-point bending, uni-axial tension and a combined tension and bending loading (figure 2.23).

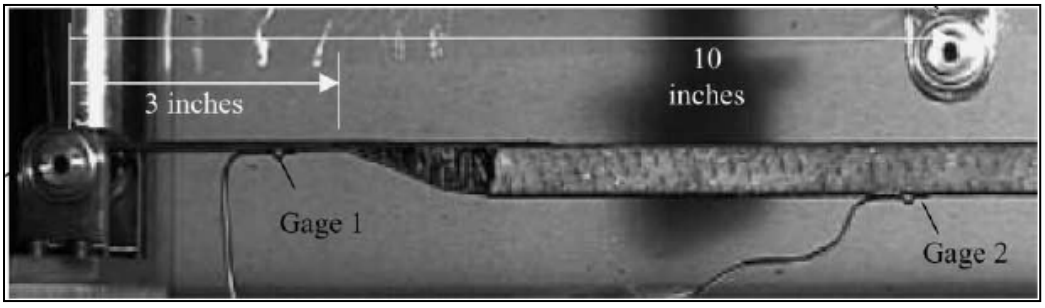

Figure 2.23– *Photograph of part of a 3-point-bend sample tested in [102]*

The most common failure modes observed were core-skin separation in the central part of the specimens and delamination between the top and the bottom skins in the transition regions. Pin buckling was also observed in the tapered parts during the application of tensile load as the distance between the two facings was reduced. It was also noticed that pin pull-out may occur without skin fracture.

The influence of pin reinforcement in X-Cor sandwich panels on out-of-plane compressive strength was investigated by Cartié and Fleck [11]. Tests were performed quasi-statically and dynamically on cores with Ti and CF pins in both hollow and foam-filled configurations. A synergistic effect due to the simultaneous presence of the pin and foam on stiffness, strength and energy absorption is observed. The foam core provides an essential lateral support which delays pin buckling. It is in fact this failure mode which determines the core strength under this loading condition. The role of the foam appears essential in enhancing core mechanical properties, differing from that observed in reference [99]. A significant elevation in peak strength during the dynamic test was also observed. A model of a simply supported beam-column on elastic foundation is suggested to represent the buckling behaviour of the pin-reinforced core. It is also argued that the pin end experiences a rotational constraint due to the fact that it is embedded in the skin.

Studies on low-velocity impact (LVI) response and damage tolerance have been published by Vaidya and co-workers [13, 103]. The results show that by reinforcing foam cores with Z-pins the low-velocity damage is more localised within the dimension of a cluster of pins, both in the core and in the skin in comparison with a reference foam core sandwich panel (figure 2.24).

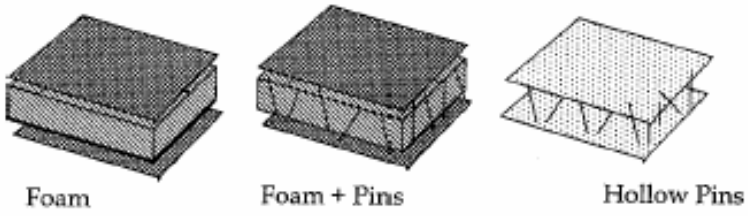

Figure 2.24– *Schematic of the different sandwich samples tested in LVI and CAI, from [103]*

The major failure mechanisms observed were localised facesheet delamination (within the distance of two pins around the impact location), skin-core debonding, pin push-out from the skins, shear cracking between plies in proximity of push-out location, fibre breakage and matrix cracking. Reference [13] indicates that the first damage to occur in an LVI event is skin-core debonding which is followed at higher loads by all the other failure modes. The presence of the pins decreases the threshold load for first damage by about 8%, depending on the impact energy, in comparison to the foam core reference sample. The initial slope of the force-time curve for the hollow core specimens is observed to be between the curves of the reference foam samples and those of the foam filled Ti pinned core specimens. In the hollow core samples pin buckling was also observed [13, 104] (figure 2.25). Apparently it was not observed in the foam-filled specimens, which shows, according to [80], the foam role in arresting this mode of failure.

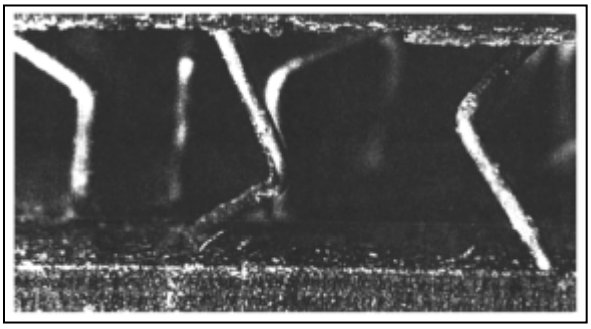

Figure 2.25– *Buckled Ti pins after an LVI test, from [103]*

Reference [103] presents an extension of the work done in [13]. The compression after impact test results show a pin spacing influence on the load bearing capacity. A closer pin spacing, associated to a better damage containment under LVI conditions, results in a lower CAI peak load. It was observed that the damage could spread across the specimen easier, in a sort of a coalescence of delaminations (also noticed in [104]). The sandwich core was found to have minimal participation under the in-plane loading condition applied to the sample tested for CAI. In the same study a finite element modelling approach is also presented for hollow core samples. The idea behind the model is to compute the axial load acting on each pin and compare its value with the critical Euler buckling load. If the load exceeds the critical value, the pin is assumed to buckle and the stiffness is reduced to 1 percent of its original value. In the dynamic

simulation the load is applied as a function of the time, obtained from the experimental results. Further details on the modelling methodology can be found in [105]. The discrepancy between the experimental results and the analysis is attributed to the facesheet failure which is not accounted for in the model and is responsible for a lower material stiffness. A technique adopted by the authors to solve this problem is to enlarge the number of pins experiencing buckling. This value is determined by matching the initial slope of the experimental results with the simulated curve; in this way the correct amount of damage introduced in the specimen is evaluated.

The work done by Palazotto et al. [104] focuses on the LVI damage threshold characterisation for Z-Fiber® reinforced sandwich panels with steel pins inserted at 10° and 20° to vertical. Same failure mechanisms were observed as in previous studies [13, 104] (figure 2.26).

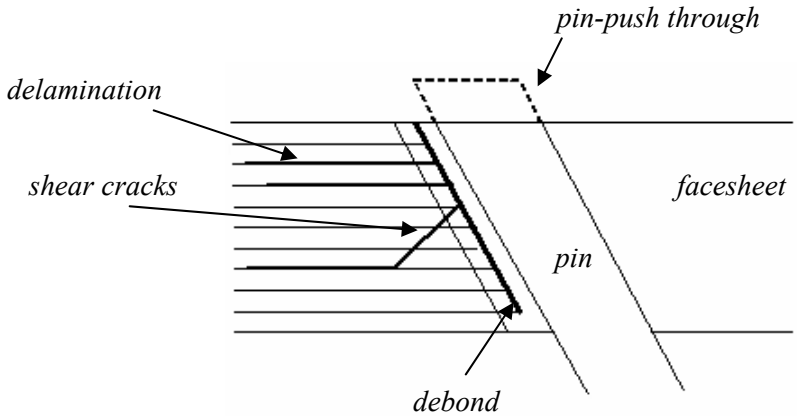

Figure 2.26– *Schematic of failure mechanisms typical of an LVI event, adapted from [104]*

The damage thresholds of pins oriented at 10° pins were associated with higher energy levels in comparison with those oriented at 20°. Quasi-static indentation tests showed approximately 90% lower peak loads in comparison with equivalent specimens tested under LVI conditions. C-scanning and acoustic emission testing were employed successfully in detecting and quantifying the damage extent.

The high velocity impact response of X-Cor structures was also investigated by Vaidya et al. [80]. Glass/epoxy, Ti and steel Z-pinned sandwich samples in both the hollow and foam filled configurations were subjected to 164-326 s^{-1} strain rate impact. All the foam filled specimens showed crushing of the foam between pins, core-skin interface

debonding and shear fractures between the foam and the pins. All the metal pins underwent buckling; the glass/epoxy pins experienced fracture and the samples exhibited almost four times higher peak stress than the Ti Z-pin reinforced core specimens. The paper concludes by stating that the pin insertion process, besides being an additional cost with respect to traditional cores, increases the core weight by ~4-12%, depending on the material chosen, but effectively suppresses extensive core crushing.

References [104, 106] show a vibration characterisation of Z-pinned sandwich plates with hollow and foam-filled cores. An FE analysis has been also conducted on hollow panels to evaluate the stiffness reduction associated with pin buckling failure [106]. Three different types of specimens were considered: reference samples made of foam IG 71, hollow and foam-filled X-Cor (skin-to-skin insertion). Ti pins were inserted at 10° to vertical. Vibration based non-destructive evaluation (NDE) was performed on the specimens before and after LVI testing. The results indicate that the impact event is very localised to the impact side skin and in the core directly beneath. The simplified FE approach considers the Z-pins and the facesheets as two distinct structures, joined together by a constraint condition. The samples are considered in a hollow configuration. The predominant failure mode of the idealised state of damage considered is pin buckling. The natural frequencies and the mode shapes were investigated with and without pin failure and simulated by reducing the pin stiffness to 1% of its original value as seen in reference [103]. The FE results show that there is no significant modification in the first three mode shapes, as found experimentally [104, 106]. The measured and predicted natural vibration frequencies do not correlate to each other, although the FEM modelling correctly predicts a reduction in frequency (related to the global change in stiffness) as a function of the number of failed pins.

The work done by Kocher et al. [107], presents an FE analysis investigation of a truss Z-pinned reinforced core in a sandwich panel. The paper shows the enhancement of the stability of the facings due to the presence of the pins (+30%) and presents a parametric analysis of the local stress distribution due to a transverse load applied on the skin for diverse pin angles. The critical location analysed was the joint between the pin and the facing; a 45° pin inclination angle showed higher stress concentration than a 30º inclination (from the vertical direction) in out-of-plane loading. The role of the foam on

the mechanical performance in this particular loading condition was found to be negligible. This result strongly disagrees with the experimental findings of reference [11]. The foam lateral support on the pin and the enhancement in its buckling strength was observed, but not considered as a probable failure mode. As result of the pin jointed-truss model (steel pin of 1mm diameter and CF / epoxy skins) used for the FE analysis, the failures modes listed in sequence are: pin penetration in the facesheets, delamination of the facings and pin buckling.

Table 2.1 summarises all the tests and material types for the analysed reference works.

ref.	*test performed*	*pinned core type*	*pin Ø [mm]*	*pin angle*	*pin material*	*skin material*	*foam type*
[11]	*o-o-p compression analytical modelling*	*H+FF X-Cor*	*0.5*	*30°*	*CF/BMI Ti*	*CF / epoxy*	*IG 31-51*
[13]	*LVI*	*H+FF X-Cor*	*0.89*	*10°*	*Ti*	*E glass / epoxy*	*IG 71*
[80]	*HVI*	*H+FF X-Cor*	*0.89*	*10°*	*glass/epoxy Ti steel*	*E glass / epoxy*	*IG 71*
[99]	*o-o-p tens/comp/shear 3-point-bend fatigue i-p compression*	*FF X-Cor*	*--*	*--*	*--*	*CF / epoxy*	*IG 31*
[102]	*3-point-bending tension tension+bending*	*FF X-Cor with transition to solid laminate*	*--*	*--*	*CF/BMI*	*CF / epoxy*	*IG 31*
[103]	*LVI CAI FE modelling*	*H+FF X-Cor*	*0.89*	*10°*	*Ti*	*CF / epoxy*	*IG 71*
[104]	*LVI indentation CAI C-scanning/AE*	*H X-Cor*	*0.508*	*10°/20°*	*steel*	*CF / epoxy*	*--*
[106]	*LVI vibration analysis*	*H+FF X-Cor*	*0.89*	*10°*	*Ti*		*IG 71*
[107]	*analytical - FE modelling*	*H+FF X-Cor*	*1.0*	*30°/45°*	*steel*	*CF / epoxy*	*PU*

Table 2.1– *List of reference works with corresponding test type and materials (significant figures from references).*
H: hollow configuration; FF: foam filled configuration

2.4 Chapter summary

1. The expansion of the use of composites from secondary to primary load-bearing applications has been accompanied by the search of improving their through-the-thickness properties as well as developing cost effective manufacturing methods.
2. The enhancement of the interlaminar properties of 2D composite with various methods has proved to be not as effective as employing 3D fibre architectures. Those are obtained either with embroidery techniques or by placing a through-the-thickness reinforcement into a 2D fibre laminate configuration. Stitching, Z-pinning and, more recently, tufting appear as more versatile technologies, simple to be transferred into existing composite systems with the advantage of being used also as means of fixation.

3. Sandwich structures represent a very efficient structural concept, with a potential yet to be exploited. Honeycombs are widely established but exhibit some drawbacks which can diminish the positive aspects of their high strength-to-weight ratio. Different solutions have been developed through the years but only recently it seems that viable alternatives have been designed. These consist of transposing the through-the-thickness reinforcing techniques developed for monolithic laminates into foam core sandwich structures.

4. The major advantages of stitched, tufted and Z-pinned sandwich structures are essentially given by the presence of a closed cell foam core and by the enhanced out-of-plane and in-plane mechanical properties in comparison with the reference foam core sandwich baseline. The overall structural performance also benefits from the improved bonding of the skin-core interface.

5. X-Cor and K-Cor sandwich structures are Z-pinned foam preforms used as cores for sandwich structures. They present the potential to substitute honeycomb constructions in certain applications. This is shown by the small number of published studies where the materials exhibit a performance comparable to that of honeycombs. The knowledge gathered so far still does not allow the industry to implement such cores into current engineering practice through exploiting their full potential.

6. At present the low-velocity impact performance represents the only loading condition extensively investigated for X-Cor structures. The small number of systematic studies, partly due to the fairly recent development of the technology, as well as due to the high number of material parameters and a variety of achievable configurations (foam-filled and hollow cores), allows only initial evaluations to be made. Very little analytical and numerical modelling work has been carried out. In particular for K-Cor sandwich constructions there are no studies available.

This work represents one of the first attempts to rigorously analyse and evaluate X-Cor and K-Cor materials. Understanding their mechanical behaviour at a meso-scale level allows us to improve the manufacturing procedures and the mechanical performance while at the same time proposing a theoretical and modelling approach.

Chapter 3

Manufacturing, materials and core structure characterisation

The manufacturing phase represents an important aspect, determining the quality of the subsequent experimental work. A preliminary stage to assess and eventually refine the production techniques used for these novel materials was carried out before adopting finalised procedures. The main objective was to obtain reproducible samples with consistent quality as a result of 'standard' and 'improved' manufacturing techniques. A variety of sandwich panels were produced and tested with the aim of evaluating the influence of core properties and parameters on the global sandwich mechanical behaviour. Different pinned cores as well as traditional honeycombs and foam cored sandwich constructions were manufactured utilising similar skins (materials and lay-up) and adhesive systems (materials and thickness). The manufacturing procedures regarding X-Cor and K-Cor are analysed in detail. For all the other materials (monolithic laminates, foam and honeycomb sandwich panels) a complete description of their manufacturing techniques can be found in [9, 108-110] along with recommendations provided by the manufacturers [6, 111-113]. A detailed analysis of K-Cor and X-Cor structures and relative core parameters, as well as a unit cell concept, is provided in order to clarify the subsequent detailed listing of manufactured panels and samples. A brief description of the basic materials used and their related mechanical properties employed in calculations and in the FE analysis is also included.

3.1 Manufacturing

3.1.1 X-Cor and K-Cor preforms

The first critical step towards the production of a pinned core sandwich panel is the placing of the through-the-thickness reinforcement into a polymeric foam layer creating

a truss pattern. The same Z-Fiber® pins can be inserted either into an uncured prepreg laminate or into polymeric foams, originating in both cases three-dimensionally reinforced composite structures [62]. In the Z-pinning of monolithic laminates, the phase before insertion consists of cutting the pins and placing them vertically into a collapsible sandwich made of two foam layers called 'preform' [62, 65]. This is only used as a carrier during the insertion into the uncured laminate through the use of an ultrasonic gantry machine and discarded afterwards (further details in [24, 62, 65]). In the case of X-Cor and K-Cor the continuous pultruded rodstock (patent held by Aztex Inc. [6]) is wound onto a spool; in this state it can either be subjected to further manufacturing steps (i.e. post-cure) or be ready for use. The pins used in this work are composite rods made of pultruded carbon fibre tows embedded either in an epoxy or a BMI resin matrix. They are inserted into layers of Rohacell foam. These are closed-cell foam cores based on PMI (polymethacrylimide), able to withstand temperatures up to 180°C, typical of an autoclave environment for aerospace materials (more details in section 3.3). The cutting takes place after the pins have been placed into a foam core. These two operations (insertion and cutting) are generally automated; if conducted manually, they are extremely time consuming and rely on the operator's skills. In this case the level of quality achieved can be appropriate only for one-off production or preliminary studies. The X-Cor and K-Cor preform panels (foam with pins inserted) constitute the cores of the homologous sandwich constructions. The foam is usually part of the sandwich structure although hollow configurations are also being used (section 3.1.2.4). All the preform panels used in this work were manufactured at Aztex Inc. and supplied in two formats $500mm \times 500mm$ and $350mm \times 350mm$, both with a nominal thickness of $12.7mm$. Figure 3.1 shows the robot arm and the recently commissioned X-Cor insertion head utilised at Cranfield University. Three different views of the same pin insertion-cutting process are shown. The production pin insertion machines are equipped with a knife-cutting tool which literally slices the pin creating a chamfered edge, inclined at ~45° with respect to its axis. This particular shape, as seen in the Z-pinning of monolithic laminates [6, 24], limits the damage in a volume of material surrounding the pin and favours its insertion process. The pin length needs to be determined on the basis of the core thickness and pin insertion angle.

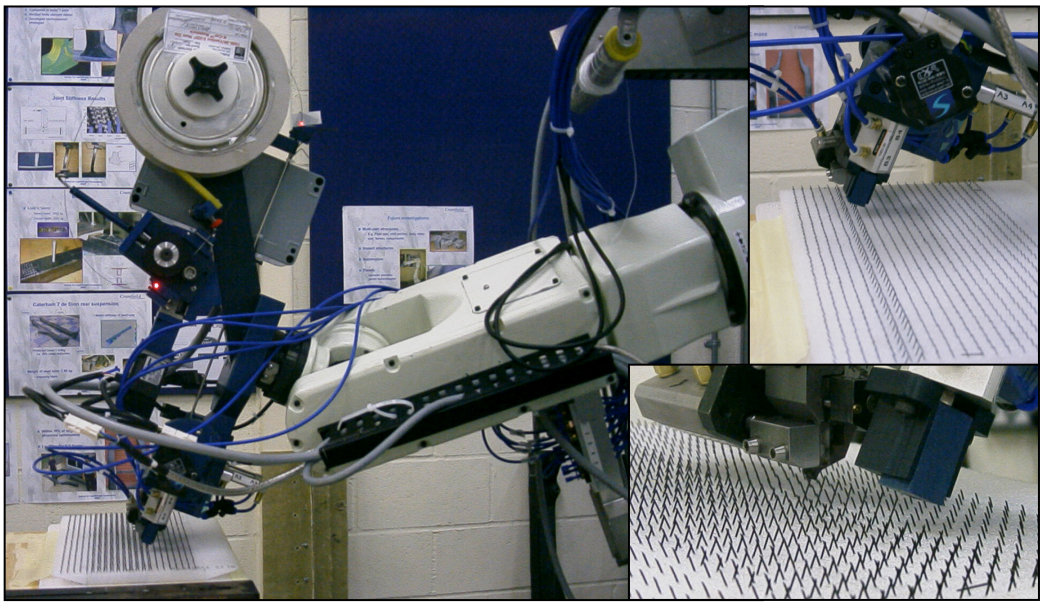

Figure 3.1– *Cranfield University X-Cor insertion head*

A characteristic parameter is the so called 'reveal length' which represents the extent of the pin beyond each surface of the foam (figure 3.2). Such length guarantees the mechanical fastening between core and skins in X-Cor structures. It needs to be able to bond at least the first three plies of the composite facesheet [62].

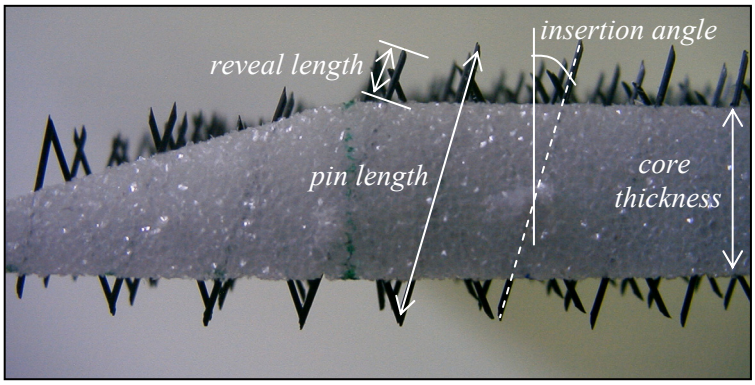

Figure 3.2– *Side view of an X-Cor preform*.

Figures 3.3(a, b) show close-up pictures of the X-Cor preform surface taken with an optical microscope with pins inserted at 11° and 33° respectively.

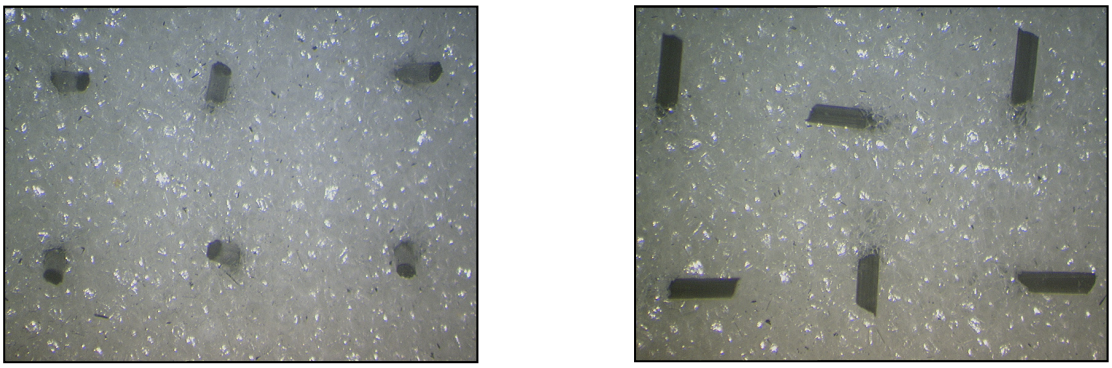

(a) *(b)*

Figure 3.3- *Top view of X-Cor preform surface: pin inserted at 11°(a) and 33°(b)*

If the pins are slightly undercured, it is then possible to fold them back with the action of moderate heat and pressure, until they flush with the foam surface. Such pinned core is called a K-Cor preform. This operation takes place in a hot press and the principal steps are the following [114, 115]:

- Heat up the hot press platens to 170ºC
- Insert the core
- Close the platens on the core over a period of 90 seconds
- Leave the core under pressure in the press for 30 minutes (or until the press has cooled to 70ºC)

The slow closing of the hot platens on the core allows the necessary time for the pin tips to heat up to plastically deform as the resin reaches its glass transition temperature. They fold over rather than crush the foam layer in which they are embedded (figures 3.4 and 3.17). After this operation the K-Cor preform is ready to be used in a sandwich construction. The pin flattened length becomes a significant core parameter, related to the reveal length of its previous X-Cor configuration.

3.1.2 Production

X-Cor and K-Cor share a few common manufacturing steps with the production of honeycomb sandwich structures. Besides similar tooling and bagging materials, they are

processed with analogous autoclave cure cycles in terms of the applied temperature and pressure. The schematic of figure 3.4 shows the principal features of their manufacturing process and their characteristic skin-to-core bond, essential for achieving structural integrity. In the case of X-Cor, the preform is initially laminated between prepreg composite skins and then co-cured. Once in the autoclave, as soon as the resin starts to flow, the skins come down over the pins; this process is also favoured by the applied pressure. The pins force their way into the facesheets and create a mechanical fastening between them and the core, achieving in this way structural integrity (figure 3.5). In contrast to traditional honeycomb sandwich processing, there is no need of an adhesive film for bonding the different parts together. Reference [99] compares the performance of two similar X-Cor structures manufactured with and without adhesive film; the tests show that there are no differences in the mechanical response. The X-Cor configuration manufactured without adhesive allows a certain weight saving for similar performance.

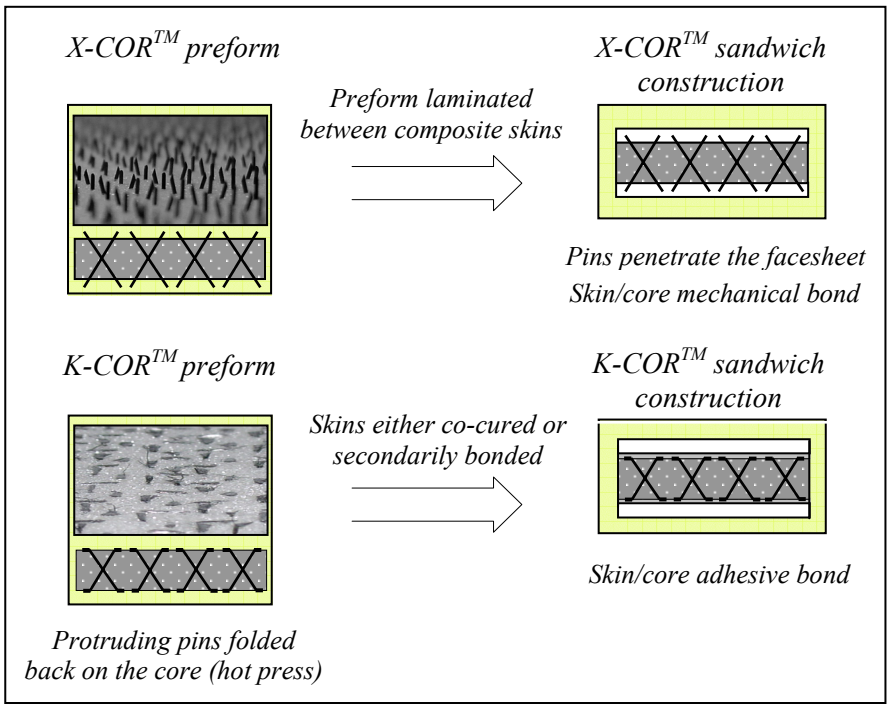

Figure 3.4– *X-Cor and K-Cor process schematic and structure differences*

Figure 3.4 shows a close-up photograph of a hollow X-Cor sample and of a pin-skin interface.

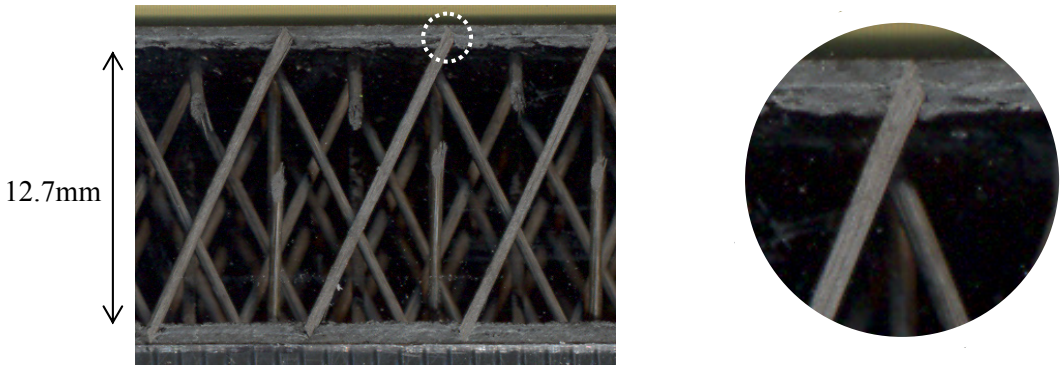

Figure 3.5– *Close-up of an embedded pin tip in a hollow X-Cor sandwich construction*

In K-Cor structures the 'sandwich effect' is achieved with the use of an adhesive film interleaving the core and the skins. As with traditional honeycomb sandwich systems, both co-curing and co-bonding processes can be used. Figure 3.6 shows a close-up photograph of a K-Cor specimen and of a flattened pin tip, typical of this core, which is embedded in the adhesive layer. In a K-Cor configuration containing foam two principal skin-to-core bond mechanisms co-exist: foam-to-skin bond and separate multiple bonds between the flattened pin surface and the skins. In the hollow K-Cor sample shown in figure 3.6, excess resin flowed along the pin external surface during the co-curing process.

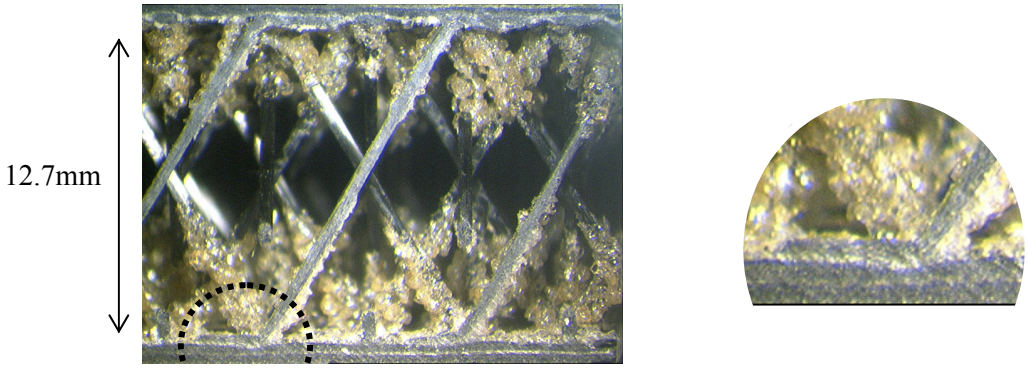

Figure 3.6– *Close-up of a flattened pin end in hollow K-Cor sandwich construction*

The pinned core panels were manufactured with two methods which are both commonly used in aerospace applications for short production series [9, 109]:

- Prepreg lay-up / co-cure 'standard' process (one-step)
- Prepreg lay-up / co-bond process (two-steps)

The first process consists of laying the laminate facings directly onto the core and then proceeding with the curing process; it can be applied to both X-Cor and K-Cor constructions. It is labelled as 'standard' because its guidelines are suggested by the manufacturer and it represents the actual industrial practice; in this way it is possible to distinguish it from a modified procedure, developed in this study for the production of X-Cor ('improved' process) and presented in section 3.1.2.2. In the second manufacturing method (co-bond process), applicable only for K-Cor, previously manufactured single-skin laminates are adhesively bonded to the core in a separate process. Both procedures require significant manual labour [110]. The only noteworthy step for the common phase of skin manufacture, is that the UD laminates were debulked every four plies under a vacuum at 60°C for 30 minutes [24]. This was adopted to previously consolidate the prepreg layers and to allow the removal of air and volatiles [108].

3.1.2.1 Prepreg lay-up / co-cure 'standard' process (one-step)

A vacuum-bag assembly specifically designed for pinned core sandwich constructions is indicated in figure 3.7. It represents one of the alternative lay-up arrangements for curing this material, suitable for the type of work conducted. The principal requirements are:

- Release film on base and upper skin of the composite stack
- Edge dam surrounding the core which extends to the top of the stack
- Caul plate extending over the edges of the dam (this improves surface finish and ensures a more evenly distributed pressure)

- Bleeder / breather cloth over the stack (this creates an even pressure around the part and at the same time allows air and volatiles to escape. It can absorb the excess resin)
- Bag film used as vacuum membrane sealed at the edge (larger than the area occupied by the composite stack to allow folds and pleats to act as stress releasers)

For X-Cor one or two layers of peel-ply on top of the release film could be also used with the function of providing an elastic surface backing the skin, in order to achieve, if needed, better pin penetration into the facesheet [114]. In the case of a co-curing process for K-Cor, adhesive film needs to be placed between the pinned core preform and the skins.

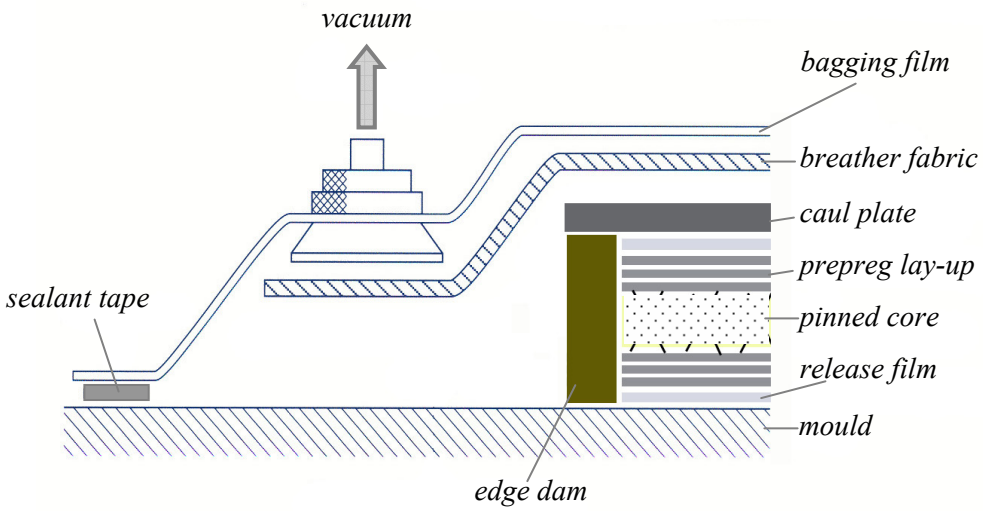

Figure 3.7– *Typical X-Cor bagging assembly schematic for a co-curing process*

The autoclave process represents the second stage of the production cycle. The material undergoes curing and compaction. For sandwich systems, as well as for thick composite laminates [116], the temperature dwell stages become important for obtaining quality panels in terms of degree of cure, low void content, low residual stresses and low distortion. Especially for sandwich constructions, due to the presence of different parts with diverse mechanical and thermal properties, a tailored curing cycle becomes necessary. The applied pressure and temperatures are chosen on the basis of the foam core, compromising the ideal curing and compaction conditions for the laminate skins

(figures 3.9(a, b) and 3.10). The high performance foam core used allows to reach temperatures in the order of 175-180°C, which represents the ideal curing temperature for most carbon/epoxy composites. The limit is on the applied pressure, which is lower than what is suggested for aerospace grade monolithic laminates (up to 7 bars). This is essential to avoid core crushing which is a typical problem encountered by foam cores in sandwich construction processing [9, 117]. It was noticed that the presence of the pins and the foam is mutually beneficial in the curing process: the foam stabilises the pins favouring their going through the skins maintaining the desired pin lay-out and insertion angle. The contribution of the pins is to prevent core crushing up to a certain extent, as they withstand most of the out-of-plane compression load acting on the composite lay-up in the curing phase. The presence of a caul plate extended over the surrounding dam prevents the inner prepreg skin from sliding inwards, especially around the edges.

The curing cycle is a two temperature-dwell process (figure 3.8); the first one allows time for the low viscosity resin to flow and for the excessive resin and trapped air to exit from the laminate under pressure and vacuum. The second dwell is necessary to allow the complete polymerization of the resin and obtain a uniform temperature throughout the panel before starting the cooling process.

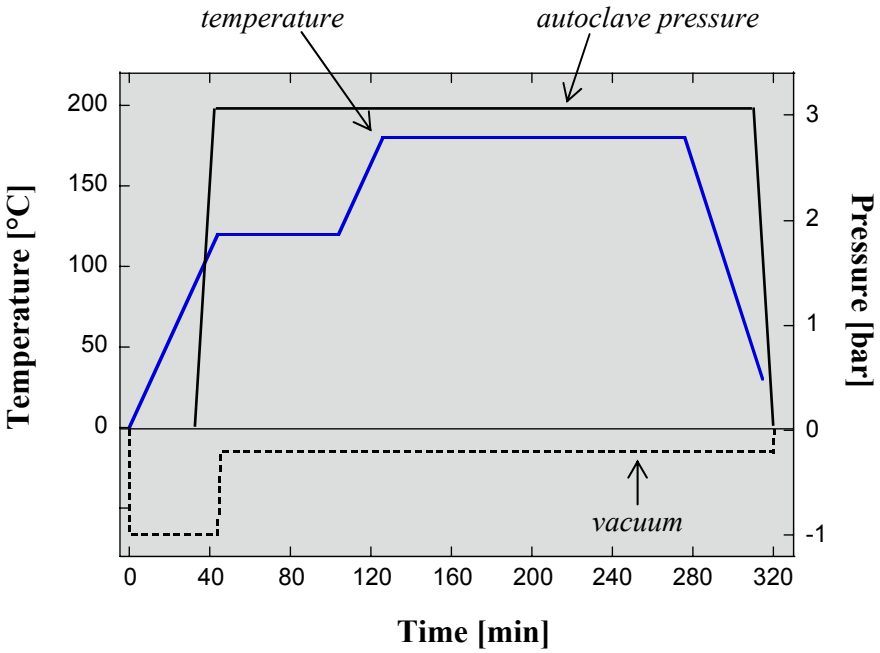

Figure 3.8– *Curing cycle adopted for Rohacell 31 IG [118] foam core and for T800/977-6 [113] and IM7/8552 [112] laminate skins*

The curing cycle consists of the following steps (temperatures and pressures optimised for the materials used):

1. Apply vacuum (1 bar)
2. Ramp (2.7°C/min) panel under vacuum to 120°C
3. When part reaches 104°C, ramp autoclave pressure to 3.1-3.4 bar
4. Reduce the vacuum to a safety value of ~0.2 bar when the autoclave pressure reaches approximately 1 bar (alternatively vent to atmosphere)
5. Hold at 120°C for 60 minutes
6. Ramp (2.7°C/min) to 177°C
7. Hold at 177°C for 150 minutes
8. Ramp down (2-5°C/min) to room temperature venting pressure when part reaches 60°C

For X-Cor with pins inserted ~10° off the vertical direction, and for K-Cor panels, a slightly lower autoclave pressure is usually recommended (3.0-3.2 bar). A concern was about the compression creep properties of the foam at such temperatures. Only for the Rohacell IG 21 foam (product still under development, section 3.3.4) a 5-10% decrease in thickness around the panel edges (areas usually characterised by the absence of pins or very low density) was found. A previous heat-treatment of the foam panel could improve its creep compression resistance [111].

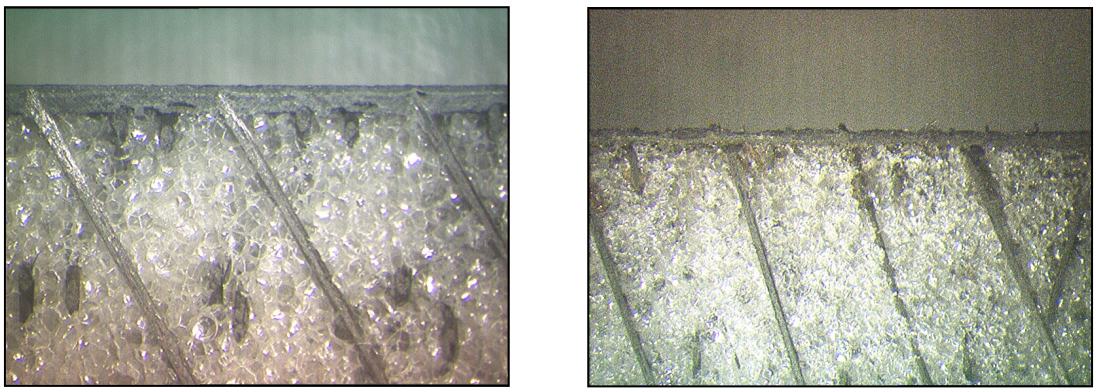

(a) *(b)*

Figure 3.9– *'Standard' X-Cor some skin porosity can be observed*

3.1.2.2 X-Cor 'improved' manufacturing process

This modification to the 'standard' manufacturing procedure originates from the fact that the pin-skin interface quality was not always found to be optimal for a particular X-Cor type. Those panels were characterised by pins of 0.51mm diameter and fabricated at Cranfield University as well as supplied by the manufacturer. As mentioned earlier, the sandwich curing cycle is not ideal for the laminate skins; this leads to a certain degree of porosity and lack of consolidation. In addition, the presence of a through-the-thickness reinforcement does not favour material compaction as also found in Z-pinned monolithic laminates [24]. Figure 3.10 shows a case of a discarded X-Cor sample compromised by excessive skin porosity.

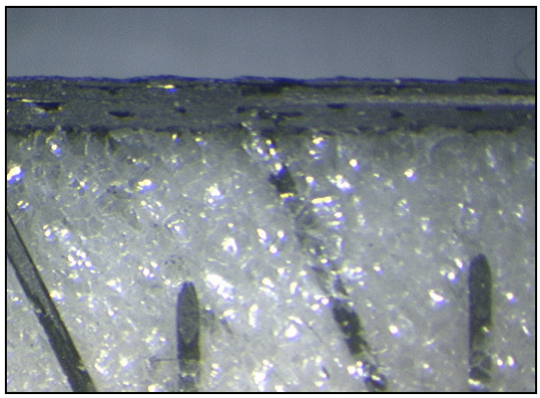

Figure 3.10– *'Standard' X-Cor specimen discarded due to unacceptable skin porosity*

Insufficient material compaction was observed especially around some of the embedded pin-tips. Moreover, a general lower pin-skin interface quality was observed in comparison to X-Cor panels with smaller pin diameter (0.25mm). As with Z-pinned monolithic laminates, the pins in X-Cor structures constitute elements of discontinuity in the laminate. This causes waviness of the fibres around the pins as well as the formation of resin rich pockets surrounding each pin [24]. In the case of Z-pinned laminates the pins are inserted in the prepreg stack before the curing cycle commences. In X-Cor this pin insertion phase takes place in the autoclave and is initiated by the decrease in viscosity of the resin and aided by the applied pressure. Higher diameter

pins face more difficulties in piercing the material and finding their way through. The discontinuities introduced in the laminate skin are certainly of a higher degree than in the case of 0.25mm pin diameter. The basic idea of the 'improved' manufacturing procedure is to reproduce conditions similar to those of a Z-pinned laminate in the X-Cor sandwich skin, before the curing process takes place. At least the initial stage of the pin insertion process takes place prior to the autoclave cycle, which has mainly the function of curing and consolidating the skin material. The obtained quality of each pin-skin interface is generally improved (figure 3.11). It seems to be also beneficial to the overall consolidation of the facesheets.

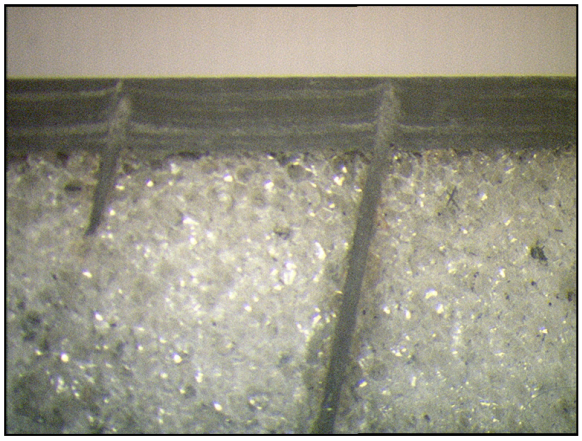

Figure 3.11– *X-Cor produced with the 'improved' manufacturing procedure. Porosity in the skin greatly reduced*

To avoid the compaction problems detailed above, an intermediate step is therefore required. It consists of placing the entire composite stack on the debulking table where a vacuum pressure of 0.6bar, at a moderate temperature between 50°- 60ºC, is applied for 30 minutes, allowing the skins to compact and the pin heads to bed into the laminate. The subsequent curing process is not changed.

3.1.2.3 Prepreg lay-up / co-bond process (two-steps)

This manufacturing process can be applied only for the production of K-Cor structures. The one-step procedures are clearly desirable from an economic point of view, but the

advantages offered by a co-bonded K-Cor can make it a valid alternative. The skins processed as monolithic laminates achieve a higher degree of material compaction and consequently of mechanical properties (figure 3.12).

An initial and fundamental step of the co-bond process is to prepare the inner face of the skin for enhancing the bond quality [108]. This means either to cure the skins with a peel-ply in order to give the laminate a rough texture or to abrade them with sandpaper. A degreasing phase is also critical before adhesive bonding. Acetone was used to remove the mould release agents and the carbon powder produced from abrasion. Adhesive layers are then positioned between the face and core material before the whole composite stack is placed in a vacuum where heat and pressure are applied. The epoxy adhesive film used (Cytec FM300-2, section 3.3) required the following curing cycle: 120°C for 90 minutes at 1.0 bar of pressure. The choice of such a pressure value was a compromise between the limitation of the vacuum table available, the low compression strength of this type of foam and the suggested adhesive bonding pressure range (1.0-6.9bar [113]). Once the panels were cured, they were left to cool down.

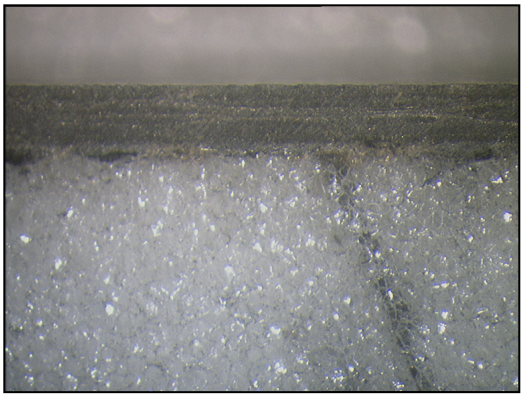

Figure 3.12- *Higher skin quality achieved with the co-bond process*

The problem of core-crushing and heat distortion associated with the high pressure and temperatures of the autoclave cycle are not encountered in this process and this makes it suitable especially for low density foams. The co-bond manufacturing process was used to produce all the K-Cor panels with a Rohacell 21 IG foam core (section 3.3).

3.1.2.4 Foam removal procedure

In order to obtain a hollow configuration of the tested material a foam removal procedure, approved by the supplier, was set up successfully [114]. This chemical process 'washes out' the polymethacrylimide (PMI) foam from the pinned cores. Prior to this method being developed there were no clear instructions on how a similar, non mechanical removal should be carried out. Attempts had been made at removing the foam mechanically with a high speed water jet stream [80] and with the use of tweezers [11]. The latter procedure was employed in the early stages of this work. Besides being time consuming, it did not give a satisfactory results in terms of quality (pin damage was observed and foam residue remained on pins). The advantages of the chemical removal process are as follows:

- Rapid and efficient method
- No material damage even for high pin densities
- Suitable for panels and structures

Some preliminary out-of-plane compression tests and optical analysis on hollow samples with the foam manually and chemically removed were performed. No differences were noticed in the mechanical performance. The chemical removal process did not show any visible degradation to the surface of either the pins or the skin.
The formation of the PMI foam occurs in two steps, a free radical polymerization followed by a heating phase (~200°C depending on the desired core properties). The mixed constituents are methacrylic acid, methacrylonitrile monomers and a blowing agent. The chemical structures of these are shown in figure 3.13.

Methacrylic acid Methacrylonitrile

Figure 3.13- *Constituents of the PMI Rohacell foam [118, 119]*

The basic polymethacrylimide monomer has the following formulation [118]:

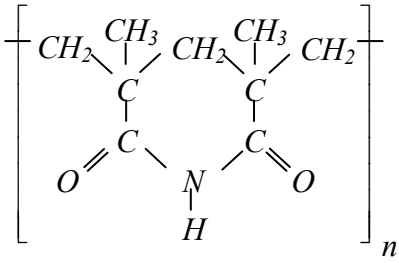

Figure 3.14– *Imidic monomer [78, 118]*

The only information made available by the supplier is that Rohacell® foam does not withstand alkaline media [118]. Under alkaline conditions a basic hydrolysis, determined by a strong base such as NaOH (solution 20-30% in water), breaks the cyclic structure of the imidic monomer attacking the Carbon-Nitrogen bond [119]. Industrial caustic soda, in the form of shiny pellets which are highly soluble in water, was used to create an alkaline solution. To speed up the reaction warm water (~40°C) and occasional stirring are necessary, for bigger parts the use of a vibrating table can be an advantage. Once the foam begins to react, it assumes a viscous consistency and can be washed away under a water flow. The author would like to make the reader aware that before attempting to repeat this process all the necessary health and safety precautions should be taken, the risks relating to handling alkaline solutions should also be properly assessed. Figure 3.15 shows a sample removed from the alkaline solution during the chemical reaction.

Figure 3.15– *X-Cor sample at the beginning of the chemical reaction (removed from the alkaline solution)*

The following figures (3.16(a)-3.16(b)) show three samples placed in warm water; gentle stirring allowed the last foam residuals trapped in between the pins to be removed.

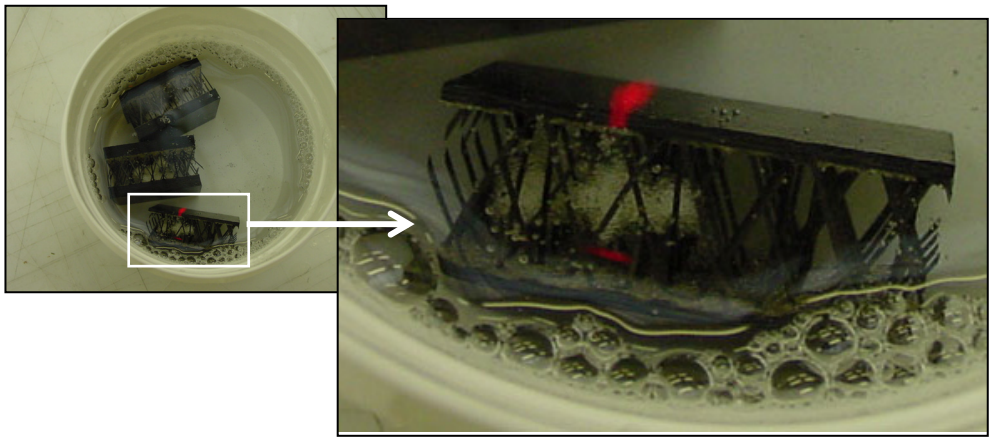

Figure 3.16– *Final stages of the foam removal process for X-Cor samples*

3.2 Core structure characterisation

The core structure properties are determined before the curing process at the stage of producing the pinned preform. Apart from the choice of pin and foam materials, the fundamental core parameters are also selected. For both X-Cor and K-Cor those are:

- Pin diameter
- Pin insertion angle (indicated in the text as θ_i)
- Pin areal density (expressed in pin/mm^2)
- Pin lay-out
- Pin reveal (X-Cor) / flattened (K-Cor) length

The curing process consolidates such core structures into an effective sandwich construction. The presence or the absence of the foam is considered as a core parameter, but it is feasible only as the last manufacturing step and not at a preform stage. All of these variables, including the manufacturing procedures, influence the mechanical performance as explained in the following chapters. The pin angle of the final product exhibits a very moderate scatter. The foam performs effectively its function of

supporting and keeping the desired pin location during either the co-cure (X-Cor and K-Cor) or the adhesive bonding (K-Cor) process. The nominal value of the insertion angle indicated by the manufacturer matched the measured angles. Similarly, for the panels manufactured at Cranfield University, the initial insertion angle corresponded to that obtained at the end of the production cycle. Pin areal density is simply determined as the number of pins in a given area. The nominal or theoretical value for this parameter is associated with ideal cores in which all the pins are undamaged and correctly fasten the two skins. Pin lay-out is the 3D truss arrangement formed by the pins in the core. The pins are usually inserted along two perpendicular directions (principal or loading directions), indicated by the manufacturer as L (principal material direction) and W (secondary material direction) respectively [99]. It is possible to vary the ratio L/W of pins obtaining isotropic and anisotropic cores. In this way it is possible, for example, to match the mechanical performance of most honeycombs which have different in-plane properties as a result of their typical production processes which create double cell walls in one direction and single walls in the other [77]. Figure 3.17 shows a magnification, obtained with an optical microscope, of the surface of a K-Cor preform. In this example the same number of pins is placed along the L and W directions (isotropic core).

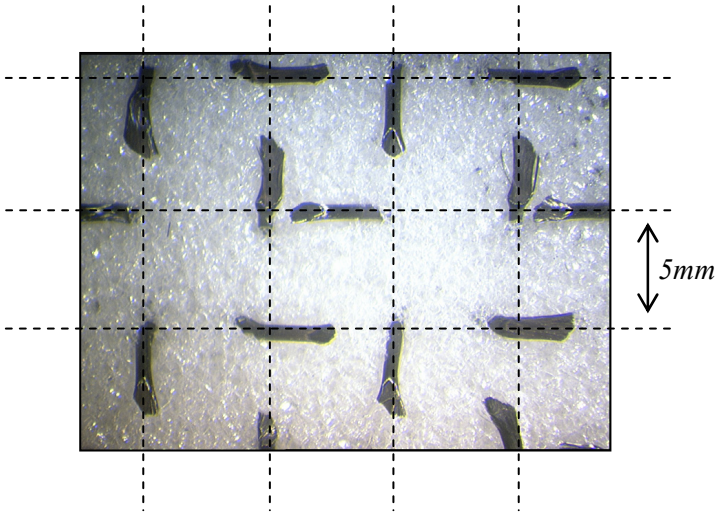

Figure 3.17– *Top view of the isotropic pin lay-out in a K-Cor preform*

Along each L and W direction, pins are usually inserted with a positive and a negative angle with respect to the vertical direction, in order to balance the mechanical properties, as indicated in figure 3.18.

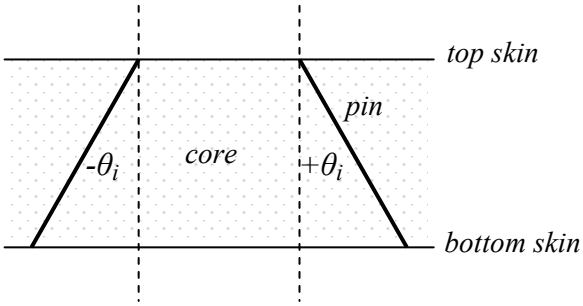

Figure 3.18– *Schematic of pin insertion in the core (lateral view)*

3.2.1 Unit cell concept

The approach followed to analyse the structure of a pinned core is based on the identification of a unit cell, defined as the smallest repeatable unit which, if translated along a longitudinal and a transversal direction, re-creates the entire core structure. The main advantage of this methodology is essentially the ease of characterising a core and its parameters as well as the possibility to associate that configuration with its mechanical performance. The same unit cell can be used also for a FE analysis in a local-global approach (section 5.3). A 3D CAD simulation of a significant portion of a hollow core based on dimensions taken from optical microscope measurements allows the determination of a unit cell representative of the core geometry. Figure 3.19 shows a hollow K-Cor specimen and the simulated core structure of a part of it.

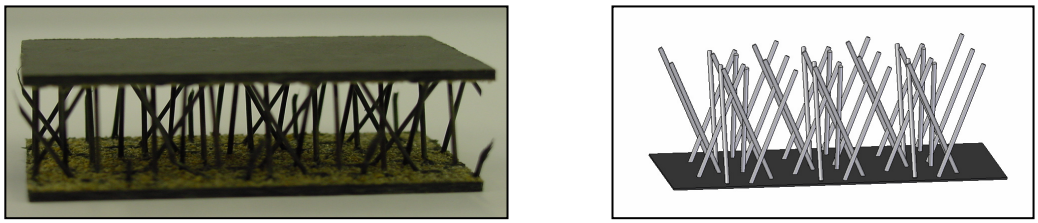

(a) *(b)*

Figure 3.19– *Hollow K-Cor sample (a) and 3D simulated pattern of the core (b)*

It is then possible to individuate a representative unit cell as shown in figure 3.20.

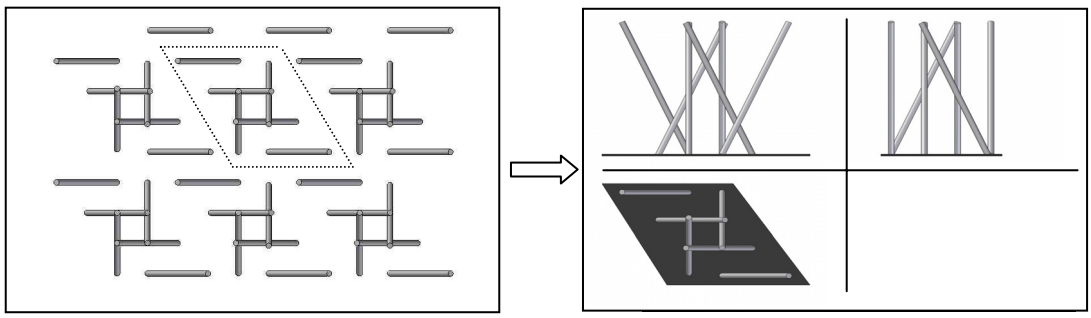

(a) *(b)*

Figure 3.20– *(a) Hollow K-Cor specimen: top view*
(b) Hollow K-Cor unit cell views

The definition of a unit cell is preferred in the determination of all the core parameters, especially for the areal or volume pin densities. Figure 3.21 shows the unit cell dimension of the K-Cor analysed in figures 3.19-20. It can be seen that this particular pin lay-out produces an anisotropic core: in one direction the number of the pins is twice (L direction) that of the perpendicular direction (W).

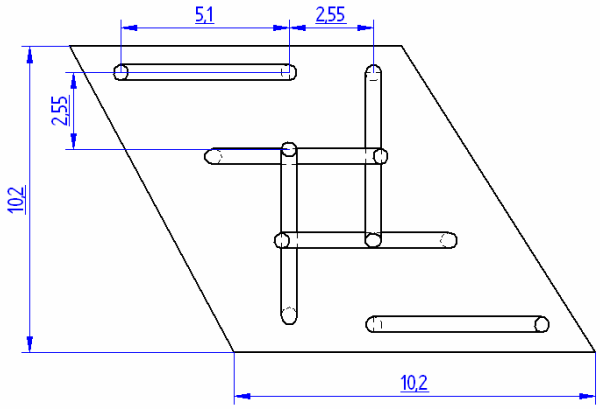

Figure 3.21– *K-Cor unit cell geometry, dimension in mm*

3.3 Materials tested

The materials used in this research work were specifically selected to evaluate the influence of pinned core parameters on the mechanical performance of X-Cor and K-Cor sandwich structures. Different configurations for each pinned core were manufactured, tested and the resulting performance was compared. To limit the influence of other variables on the mechanical behaviour, skins and adhesive systems were kept as similar as possible for all the panels. Differences in mechanical response were also evaluated with respect to competitor sandwich structures (Nomex and Al honeycombs) and reference foam cored samples. Specific tests on a single component (i.e. skin, foam etc.) of a sandwich were carried out when necessary. As a result, a variety of sandwich panels and monolithic laminates were manufactured. All the details on the manufactured panels and specimens are indicated at the end of this section.

3.3.1 Through-the-thickness reinforcement

Two different pin diameters were used: 0.25mm and 0.51mm for a total of four insertion angles. The extreme angles of this range (11° and 33°) represent also the two limits for a sensible choice in choosing a core which has a certain balance of shear and compression properties. The pin areal density was varied within a range of 0.06-0.24 pin/mm^2 and isotropic as well as anisotropic pin positioning patterns were evaluated. Tables 3.1-2 list the carbon fibre types and the resin systems used in the production of the pins together with their principal mechanical properties.

	Tensile modulus [GPa]	*Tensile strength [GPa]*
T300	*230-240*	*3.6-4.0*
T650-35	*230-240*	*4.5*

Table 3.1– *Nominal mechanical properties of carbon fibres used for producing pins, from [120]*

	Tensile modulus [GPa]	*Tensile strength [MPa]*	*Flexural strength [MPa]*
5250-4 BMI	*4.6*	*103*	*163*
8606 Epoxy	*2.5*	*64*	*103*

Table 3.2– *Neat resin properties at room temperature from [113, 121]*

The carbon fibres used were all PAN based and belong to the same 'standard' modulus band (E<256GPa, table 3.1). They are also indicated as 'high strength' fibres (HS). Table 3.3 shows the two types of pin employed. The modulus values in parenthesis are calculated applying the rule of mixtures [122]; the estimated tensile strength is determined according to the following equation from [123]:

$$\sigma_{1,T} = \sigma_{f,T}\left[v_f + \frac{v_m E_m}{E_{f11}}\right] \tag{3.1}$$

where $\sigma_{1,T}$ is the pin tensile strength in the longitudinal direction and $\sigma_{f,T}$ represents the fibre failure strength. v_f, v_m, E_{f11} and E_m are the fibre and the resin volume fractions, the fibre longitudinal elastic modulus and the resin (matrix) elastic modulus respectively.

	Nominal fibre volume fraction	*Longitudinal modulus E_{11} [GPa]*	*Transverse modulus E_{22} [GPa]*	*Tensile strength [GPa]*	*Poisson's ratio ν*
T300 / 5250-4	*0.65*	*115* (151)*	*11+ (12)*	*1.1* (2.3)*	*0.28+*
T650-35 / 8606	*0.65*	*(150)*	*(7)*	*(2.9)*	*--*

Table 3.3– *Pin properties. In parenthesis the calculated values [122, 123]. The experimentally determined values are from: * [11]; + [102]*

In the calculations a value of 115GPa for the longitudinal modulus was assumed for both pin types, although it was experimentally determined only for T300/5250-4 by [11]. Both pins have a similar theoretical modulus because they are made of carbon

fibres with similar tensile modulus; the contribution of the resin matrix, for such high fibre volume fraction, is negligible (~1%). The same scatter in properties due to materials and manufacturing conditions is assumed also for the T650-35 / 8606 pins.

3.3.2 Laminated skins

Carbon/epoxy skins were chosen for all sandwich constructions, either in a UD or fabric configuration. For the X-Cor panels manufactured the thicknesses were chosen on the basis of the 'reveal length' of the preforms (1-2mm). Tables 3.4-5 summarise the carbon fibre and resin system properties.

	Tensile modulus [GPa]	*Tensile strength [GPa]*
T800	*294*	*5.94*
IM7	*303*	*5.1-5.3*

Table 3.4– *Nominal mechanical properties of carbon fibres used for producing laminated skins, from [120]*

	Tensile modulus [GPa]	*Tensile strength [MPa]*	*Flexural modulus [GPa]*	*Flexural strength [MPa]*	*Compressive strength [MPa]*
977-6 Epoxy	--	--	*3.9*	*154.5*	*179.3*
8552 Epoxy	*4.7*	*121*	--	--	--

Table 3.5– *Nominal mechanical properties of epoxy resins used for producing laminated skins, from [112, 113]*

Table 3.6 shows the ply properties (under typical cure conditions) of the IM7 / 8552 UD and the IM7 / 8552 plain weave prepregs used [112]. The tensile and compression properties of the prepreg laminated skin ($[\pm 45, 90, 0]_{2s}$) made with T800 / 977-6 UD were required for the analysis regarding the in-plane energy absorption characterisation. They

were determined following the procedures of standards ASTM D 3039 and D 3410 [124, 125]. The skin lay-up and its mechanical properties are denoted in table 3.7.

	IM7 / 8552 UD	*IM7 / 8552 plain weave*
Resin volume [%]	*35*	*37*
0° tensile modulus [GPa]	*164*	*85*
90° tensile modulus [GPa]	*12*	*80*
0° compression modulus [GPa]	*150*	*73*$^{+}$
0° tensile strength [MPa]	*2724*	*1090*
90° tensile strength [MPa]	*111*	*945*
0° compression strength[MPa]	*1690*	--
Skin lay-up	$[\pm 45, 90, 0]_s$	$[\pm 45, 90/0, \pm 45]$

Table 3.6– *Ply properties (standard cure condition), from [112] and* $^{+}$ *from [102]*

As far as the skin manufacturing is concerned, the co-curing the process details are presented in section 3.1.2.1. For the co-bonding procedure (K-Cor) the autoclave cycle suggested by the manufacturers was followed for the production of the skins [112,113].

	T800 / 977-6 UD $[\pm 45, 90, 0]_{2s}$
resin volume [%]	*36*
0° tensile modulus [GPa]	*55*
0° compression modulus [GPa]	*46*
0° tensile strength [MPa]	*630*
0° compression strength[MPa]	*508*

Table 3.7– *Skin material properties*

3.3.3 Adhesive film

The adhesive film used in this study is the Cytec FM300-2 (table 3.8 for properties). It is an epoxy based adhesive specifically designed for co-curing and for composite and Nomex bonding applications [113]. For the curing cycle adopted refer to section 3.1.2.3.

	FM300-2 film adhesive
nominal thickness [mm]	*0.13*
nominal weight [gsm]	*145*
12.7mm (½ inch) lap shear strength at 24°C [MPa]	*27.6*
flatwise tensile strength at 24°C [MPa]	*4.1*
honeycomb sandwich peel [Nm/m of width]	*25*

Table 3.8– *FM300-2 epoxy film adhesive properties, from [113]*

3.3.4 Cores

Four different reference cores were used. Two of these, as previously mentioned, were Rohacell® foams, also used as the base layer for manufacturing the K-Cor and X-Cor preforms. The other two cores were chosen among competitor materials; these are an Aluminium honeycomb manufactured by Hexcel Inc. [112] and an unspecified Nomex® honeycomb supplied by BAE SYSTEMS ATC. The Rohacell 31 IG (IG stands for industrial grade) foam has been selected by the pinned core manufacturer, Aztex Inc., as the ideal base core for the X-Cor and K-Cor sandwich constructions because of its low weight and the excellent heat resistance which makes it suitable for autoclave processing. The other Rohacell foam product is the 21 IG and is still a development product under evaluation. Its main advantage is a similar heat resistance for a lower density. Their structure is 100% closed cell and isotropic with excellent moisture resistance, strength-to-weight ratio and creep compression properties [118]. Other advantages are the possibility to be machined using standard high-speed tools designed for wood or plastic without the use of lubricants. In terms of bonding all reaction adhesive systems are suitable for bonding this foam to itself or other materials. Tables 3.9-10 summarise materials and their mechanical properties for all the reference cores. The values marked with (*) were determined experimentally (for shear and compression properties refer to chapters 5 and 6); the other values are those provided by the suppliers [111, 112].

	Nomex® *(Aramid fibre/Phenolic resin)*	*Aluminium Alloy 5250*
nominal density ρ [kg/m³]	64	72
effective density ρ [kg/m³]	*70.7±0.1**	*72.0±0.1**
thickness [mm]	*12.7*	*10.0*
cell face side [mm]	*3.175*	*3.175*
stabiliser	*Redux 322*	--
out-of-plane compression strength [MPa]	*6.9±0.9**	*2.5±0.1**
out-of-plane compression modulus [MPa]	*257±48**	*198±10**
out-of-plane shear strength [MPa]	*2.3±0.2**	--
out-of-plane shear modulus [MPa]	*75±5**	--

Table 3.9– *Principal mechanical properties for honeycomb reference cores. (Nomex® is a registered trademark of Du Pont [126]; (* experimentally determined values)*

	31 IG	*21 IG*
nominal density [kg/m³]	*32*	--
effective density [kg/m³]	*32.0±0.1**	*22.6±0.1**
compression strength [MPa]	*0.4±0.1**	*0.2±0.1**
compression modulus [MPa]	*21±1**	*9±1**
shear strength [MPa]	*0.4*	*0.3±0.1**
shear modulus [MPa]	*13*	*11±1**
tensile strength [MPa]	*1.0*	--
tensile modulus [MPa]	*32*	--
flexural strength [MPa]	*0.8*	--
elongation at break [%]	*3.5*	--

Table 3.10– *Foam systems: properties. (* experimentally determined values)*

3.3.5 Name convention for pinned core sandwich panels and samples

A name convention to identify the different configurations among the pinned core sandwich panels and samples is used (figure 3.22). The parameters chosen to identify each configuration are:

(1) Core type
(2) Foam ('F') or hollow ('H') core
(3) Manufacturing process (standard 'S' or improved 'I')
(4) Pin diameter (expressed in mm)
(5) Nominal pin insertion angle
(6) Nominal pin areal density (expressed in pin/mm^2)

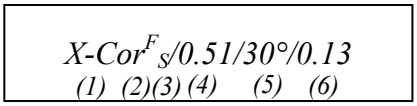

Figure 3.22- *Example of the panel name convention adopted*

Figure 3.22 shows as an example the name assigned to X-Cor panel manufactured with the standard process characterised by the presence of the foam in the core, 0.51mm pin diameter inserted at 30° and with an areal density of 0.13pin/mm^2. In the case of K-Cor the letter indicating the manufacturing procedure is omitted, being manufactured only by 'standard' procedures. The specimens are indicated with the same name convention but starting with the suffix (S) for out-of-plane shear, (C) for out-of-plane compression and (E) for samples tested for evaluating the in-plane energy absorption properties. Table 3.11 summarises all the manufactured panels, complete with relevant core parameters, used in this work. The manufacturers are also indicated (A: Aztex Inc., CU: Cranfield University; BAE: BAE SYSTEMS ATC).

sandwich panel identification	*core density [kg/m^3]*		*--------pin parameters--------*				*foam type*	*skins type*	*manufacturer / procedure*	*test type*
			areal density [pin/mm^2]	*insertion angle θ_i*		*lay-out*				
	nom	*eff*	*nom*	*nom*	*eff*					
X-Cor^F_S/0.51/22°/0.13	*~64*	*72.6±0.1*	*0.130*	*22°*	*22°*	*anisotropic*	*31 IG*	*UD*	*A / standard*	*S, C*
X-Cor^H_S/0.51/22°/0.13	*~32*	*41.4±0.1*	*0.130*	*22°*	*22°*	*anisotropic*	*--*	*UD*	*A, CU / standard*	*S, C*
X-Cor^F_S/0.51/30°/0.13	*~64*	*68.9±0.1*	*0.130*	*30°*	*32°*	*anisotropic*	*31 IG*	*UD*	*A / standard*	*S, C*
K-Cor^F/0.51/30°/0.10	*~64*	*66.8±0.1*	*0.100*	*30°*	*32°*	*anisotropic*	*31 IG*	*UD*	*A, CU co-bond/co-cure*	*S, C*
K-Cor^H/0.51/30°/0.10		*34.3±0.1*	*0.100*	*30°*	*32°*	*anisotropic*	*--*	*UD*	*A, CU co-bond/co-cure*	*C*
X-Cor^F_I/0.51/33°/0.06	*--*	*52.5±0.1*	*0.062*	*33°*	*33°*	*isotropic*	*21 IG*	*UD*	*CU / improved*	*S, C*
X-Cor^H_I/0.51/33°/0.06	*--*	*29.9±0.1*	*0.062*	*33°*	*33°*	*isotropic*	*--*	*UD*	*CU / improved*	*C*
K-Cor^F/0.51/33°/0.06	*--*	*52.5±0.1*	*0.062*	*33°*	*33°*	*isotropic*	*21 IG*	*UD*	*CU co-bond*	*S, C*
K-Cor^H/0.51/33°/0.06	*--*	*29.9±0.1*	*0.062*	*33°*	*33°*	*isotropic*	*--*	*UD*	*CU co-bond*	*C*
X-Cor^F_I/0.51/11°/0.06	*--*	*48.2±0.1*	*0.062*	*11°*	*11°*	*isotropic*	*21 IG*	*UD*	*CU / improved*	*C, E*
X-Cor^H_I/0.51/11°/0.06	*--*	*25.6±0.1*	*0.062*	*11°*	*11°*	*isotropic*	*--*	*UD*	*CU / improved*	*C, E*
K-Cor^F/0.51/11°/0.06	*--*	*48.2±0.1*	*0.062*	*11°*	*11°*	*isotropic*	*21 IG*	*UD*	*CU co-bond*	*C, E*
K-Cor^H/0.51/11°/0.06	*--*	*25.6±0.1*	*0.062*	*11°*	*11°*	*isotropic*	*--*	*UD*	*CU co-bond*	*C, E*
X-Cor^F_S/0.25/21°/0.24	*--*	*55.3±0.1*	*0.240*	*21°*	*21°*	*anisotropic*	*31 IG*	*fabric*	*A / standard*	*C*
X-Cor^H_S/0.25/21°/0.24	*--*	*23.7±0.1*	*0.240*	*21°*	*21°*	*anisotropic*	*--*	*fabric*	*A, CU / standard*	*C*
Foam 31 IG	*--*	*32.0±0.1*					*31 IG*	*UD*	*CU*	*C*
Foam 21 IG	*--*	*22.6±0.1*					*21 IG*	*UD*	*CU*	*S, C, E*
Nomex honeycomb	*64*	*70.7±0.1*						*UD*	*BAE, CU*	*S, C*
Al honeycomb	*72*	*72.0±0.1*						*UD*	*CU*	*C, E*

Table 3.11– *Sandwich panels utilised in this work*

3.4 Chapter summary

1. The manufacturing techniques employed in the production of Z-pinned sandwich panels (X-Cor and K-Cor) are explained. Although being a different type of sandwich structures, they share some manufacturing steps with more traditional honeycomb sandwich constructions in terms of similar tooling and bagging materials and autoclave cure cycles (applied temperature and pressure).

2. At a preform stage the pins (pultruded carbon/epoxy and BMI rods in this work) are placed into a foam layer (Rohacell® closed cell foams), usually through an automated process. The pins protrude from the foam core by a quantity named 'reveal length'; such a preform is called X-Cor. If the pins inserted into the foam are slightly undercured, they can be folded back easily onto the core surface with the use of heat and pressure. The preform obtained in this case is called K-Cor.

3. The making of an X-Cor sandwich panel consists initially of laminating the preform between two un-cured prepreg skins and then co-curing the whole composite stack in the autoclave. The protruding pins penetrate the skins creating a mechanical fastening and providing structural integrity to the sandwich construction. No adhesive film is needed. A K-Cor sandwich panel is obtained either by co-curing or co-bonding. The use of an adhesive film interleaving the core and the skins is necessary in this case.

4. The 'standard' co-curing procedure can present some resin compaction issues especially for pins of 0.51mm diameter. An alternative 'improved' manufacturing technique involving a preliminary debulking phase before the autoclave cycle has proved to be successful.

5. In order to obtain a hollow configuration of the tested material a foam removal procedure, approved by the supplier, was set up. This chemical process 'washes out' the polymethacrylimide (PMI) foam from the pinned cores. It consists of submerging the sample / panel in a 20-30% alkaline solution in water until the foam begins to react and assumes a viscous consistency that can be washed away.

6. The fundamental core parameters, besides the choice of the pin and foam materials, for both X-Cor and K-Cor are: pin diameter, pin insertion angle, pin areal / volume density, pin lay-out, pin reveal (X-Cor) / flattened (K-Cor) length and presence of the foam in the core. The approach followed to analyse the structure of a pinned core is based on the identification of a unit cell representative of the entire core structure.

7. The tested materials were specifically selected to evaluate the influence of pinned core parameters on the mechanical performance of X-Cor and K-Cor sandwich structures. Skins and adhesive systems were kept similar between all the panels. The mechanical response was also evaluated and compared to competitor sandwich structures (Nomex and Al honeycombs) and reference foam cored samples (table 3.11).

Chapter 4

Out-of-plane testing: methods, procedures and data analysis

This chapter describes the out-of-plane quasi-static tests performed on X-Cor and K-Cor sandwich structures. A presentation of the ASTM standards relevant to this study is followed by a detailed description of the methodology adopted in the experimental phase. A data analysis technique based on the effective sample cross-sectional area is implemented for a more appropriate evaluation of test results.

4.1 Aim and purpose of test methods

The tests carried out were out-of-plane shear and compression according to ASTM C 273 [127] and C 365 [128] respectively. These tests are typically used for the characterisation of these two fundamental sandwich core properties [129]. The structural performance of sandwich constructions is maximised only if the core is able to prevent any relative movement of the skins, especially under flexural loads [76]. The lightweight core, which is typically the weakest component of the structure, serves to place the stiffer skins further from the neutral axis, amplifying the whole structure rigidity. The facings essentially carry the bending moments as tensile and compressive stresses, while the core bears the transverse forces as shear stresses [73, 74]. At the same time the out-of-plane compression properties play a fundamental role, as a small variation in core thickness would create a large decrease in flexural rigidity and favour local and global buckling instabilities [74].

The aim of these tests is to characterise the mechanical behaviour of the different cores and explore and evaluate the balance of properties as a function of core parameters. Data on the out-of-plane properties of each sandwich construction and each core type are crucial for design purposes.

4.1.1 Out-of-plane shear test

Shear testing of composite materials has proven to be one of the most difficult areas of mechanical property testing. One of the principal difficulties is to define a rigorously correct test, especially in the out-of-plane direction, where a pure state of shear is induced in the specimen [130, 131]. For this reason there is a limited number of test methods suitable for standardisation. Especially in recent years, the aim of test protocol development is to maximise the shear stress and minimise extraneous stresses in the sample [132]. The test chosen for characterizing the shear response of X-Cor and K-Cor structures is the ASTM C 273. Alternatively a simpler bending test (ASTM C 393 [133]) could be used, however it was not considered ideal, especially for a first characterization of these novel materials, for the following reasons:

- Deflection simultaneously affected by both flexural and shear responses [133, 134]
- Scatter in the results [135]
- Eventual indentation problems (due to concentrated loads [74])

The state of shear achieved following the C 273 test is purer and consequently the results are expected to be more representative of the actual core properties [136]. The standard allows the determination of shear properties of sandwich constructions or cores, associated with shear distortion of planes parallel to the facings. The configuration does not produce a pure shear stress state in the specimen, but the sample geometry is prescribed so as to minimise secondary stresses [132]. The test is similar to a simple lap shear test, but in this case the load is applied at a slight angle with respect to the plane of the facesheets. The line of action of the direct tensile force passes through the diagonally opposite corners of the sandwich sample (figures 4.1(b), 4.6). The load applied at the ends of the rigid plates is expected to be uniformly distributed across the width of the specimen. The test can be conducted on a core bonded directly to the loading plates or on the sandwich with its skins bonded to the plates (figure 4.1(a)). For the pinned cores the presence of the skins is necessary to guarantee representative constraint at pin ends.

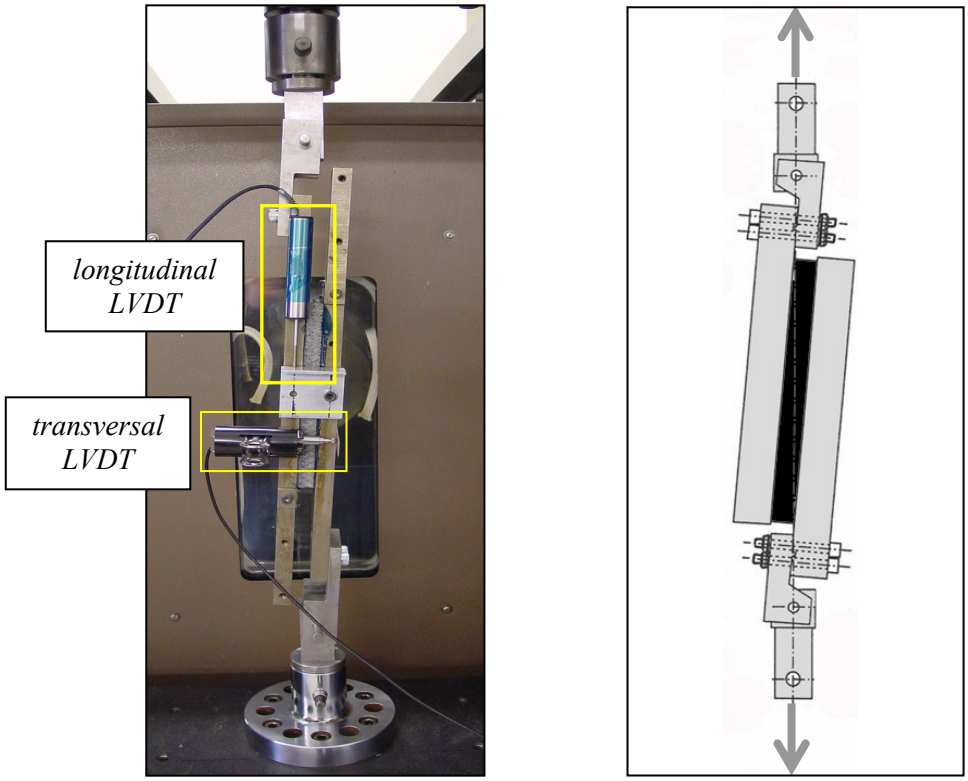

Figure 4.1– *C 273 shear test shear: (a) photograph of complete test set-up; (b) fixture schematic, adapted from [74]*

The principal parasitic effects related to the C 273 shear test, as indicated by Grédiac et al. [136], are:

- Bending of fixture steel plates (figure 4.2)
- Shear stress gradient near sample free edges

The first issue is addressed by the standard itself. It recommends a steel plate thickness, expressed as a function of the bending stiffness per unit width, greater than $2.67\times10^{6}\,Ncm^{2}/cm\ \ width$ per centimetre of core thickness. Thus, for this study the minimum allowable steel plate stiffness is $3.47\times10^{6}\,Ncm^{2}/cm\ \ width$ (core thickness is ~1.3*cm,* Ch. 3). The thickness of the steel plate used is $2cm$ which corresponds to a bending stiffness equal to $14\times10^{6}\,Ncm^{2}/cm\ \ width$. This ensured that the properties measured reflected the load response of the core only and not the fixture.

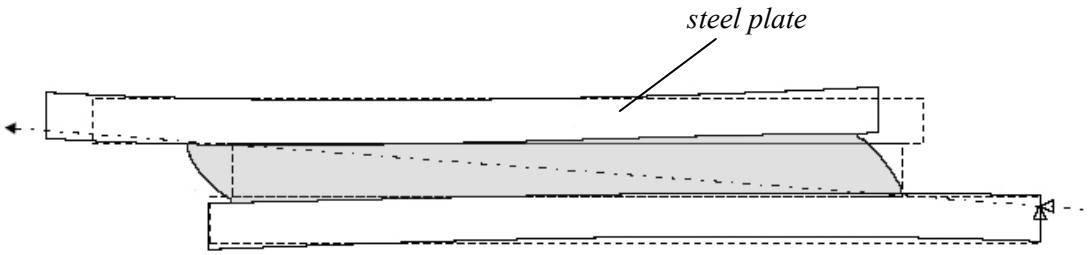

Figure 4.2– *Schematic of the steel plates bending, adapted from [136]. Loading plate displacement magnified to show the bending problem*

The shear stress was found to be approximately uniform in the central part of the specimen and up to a distance of about one half of the core thickness from the free edges, where it decreases to zero [136, 137]. This gradient affects the relative displacement between the two steel plates. The error generated was found to be dependent on the ratio *R* between the length and the thickness of the sample. The adopted sample aspect ratio (*R*=14) should lead to an error in the displacement which is less than 3%, according to the analysis performed in [137], and therefore considered negligible. To keep both the bending and shear stress gradient effects to a minimum, as recommended by [132], the relative displacement between the steel plates should be measured as close as possible to the centre lines of the sample. The longitudinal and transversal relative displacements of the plates were monitored by the use of two LVDTs, as shown in figure 4.1(a). Another common source of error for this particular test is represented by the non-parallelism of the fixture steel plates [138]. For this reason, extra care needs to be taken in the mounting of the whole fixture, in the sample adhesive bonding, as well as in the control of its thickness.

4.1.2 Out-of-plane compression test

This test method, performed according to the ASTM C365 standard, is used to determine the out-of-plane compressive strength and modulus and to investigate the failure mechanisms under this loading condition for a sandwich core. This test is straightforward and there are no complications deriving from the test apparatus, (figure 4.3), or any particular recommendations found in the literature. The only necessary

precaution is to guarantee that the load is applied perpendicularly with respect to the sample skins and that it is uniformly distributed over the sample surface.

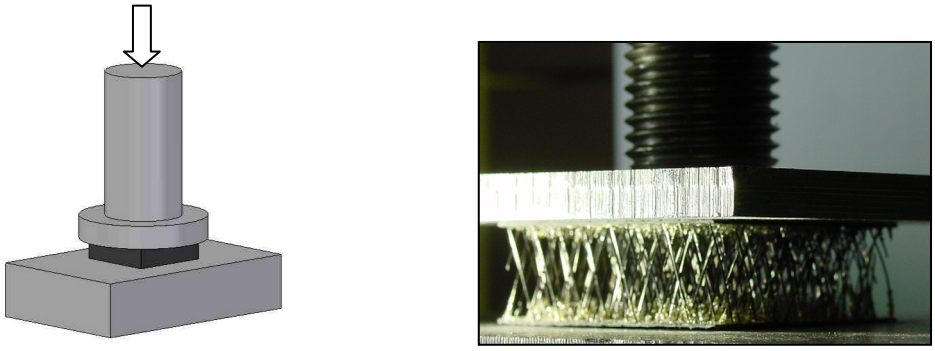

(a) *(b)*

Figure 4.3– C *365 shear test shear: (a) fixture schematic; (b) photograph of complete test set-up (*$(C)X\text{-}Cor^{H}_{S}/0.25/21°/0.24$ *sample)*

4.2 Test procedures

4.2.1 Experimental apparatus

A screw driven 6025 Instron universal testing machine with a load cell of 100kN was used for all the different tests performed [139]. A laser extensometer (EIR, LE-05 model [140]) for non-contact measurements was used for the out-of-plane compression testing (resolution 0.010*mm*; accuracy ±0.001*mm*). Two Instron LVDTs (2601 series, range ±50mm, accuracy approximately ±0.0025*mm*) were used for the out-of-plane shear test. Strain measurements were performed using a National Instruments (type SC-2345 [141]) strain gauge bridge and modules. The measurements were logged using a purpose-built LabView code.

The errors associated with the measurement of material density, sample dimension and weight, have been determined by evaluating the accuracy of the measuring instruments used (caliper accuracy ±0.01*mm*, scale accuracy ±0.1*g*). Those quantities are reported along with the final uncertainty in the results. In the stress-strain curves presented, error bars are placed at peak stress and at a convenient post-elastic stress value (usually at a plateau) to indicate the typical scatter of each sample type. The number of tests performed is denoted in tables at the beginning of each chapter. The tests were all

displacement controlled. In order to aid visualisation the number of markers shown in the graphs is a percentage (5%) of the total number of data points recorded during a test, however the graph was generated using all recorded data points. This plot style option is available in the software used (KaleidaGraph 3.5).

4.2.2 Out-of-plane shear

According to the test protocol the specimen should have a thickness equal to the thickness of the sandwich and a width of not less than 50*mm*. The requirement on the length (in order to minimize secondary stresses) is to be at least 12 times the thickness and needs to be chosen so that the line of action of the force passes through the diagonally opposite corners of the sample (as shown in figures 4.1 and 4.6). The nominal dimensions chosen for the specimen are: 50*mm* for the width and 188*mm* for the length (coinciding with the L direction of the anisotropic Z-pinned core and the honeycomb). The constant rate of movement of the cross head was set at 0.5*mm/min.* The bond surfaces were abraded with sandpaper and cleaned with acetone. The sandwich specimen facings were adhesively bonded to the fixture steel plates. The adhesive used was Araldite 420A and satisfactory performance was obtained for 150 minute cure at 70°C under slight pressure [121].

4.2.3 Out-of-plane compression

The quasi-static compression tests were conducted at a constant cross-head speed of 0.5*mm/min* on sandwich specimens of nominal dimensions 40*mm*x40*mm*. The parallelism of the skins of the sandwich construction is essential for the correctness of the test. This was insured by accepting a variability of the specimen thickness within 0.10*mm*. In order to guarantee a uniform applied load, the fixture plates were cleaned after each test of residuals from previous samples.

4.3 Data analysis

4.3.1 Load-bearing pin approach (effective area method)

The determination of the effective cross-section area of the specimen A_{eff}, which is used in the calculations of the out-of-plane stresses and moduli, is based on the actual number of load-bearing pins in each sample. This approach discounts any pin which is either damaged or not correctly fastened to both skins from the data analysis. It was originally proposed for the evaluation of the out-of-plane compression response for X-Cor structures [11], and also adopted for woven-core sandwich plates under similar loading conditions [142]. Figure 4.4 shows a close-up picture of the edges of a *(S)X-Cor$^{H}_{S}$/0.51/22°/0.13* specimen. It is evident that some of the border pins do not bridge the two facings. Depending on the pin insertion angle, pin lay-out, cutting pattern and dimensions of the sample, the number of load-carrying pins may vary.

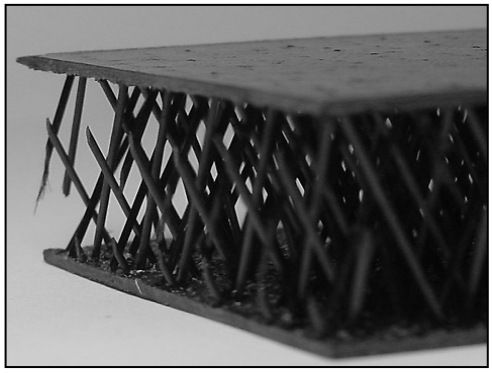

Figure 4.4– *Close-up photograph of damaged border pins. Specimen (S)X-Cor$^{H}_{S}$/0.51/22°/0.13*

The theoretical areal pin density ρ_{th} represents the theoretical number of load-bearing pins in a unit area (expressed as pin/mm^2) and is determined as follows:

$$\rho_{th} = \frac{n_{th}}{A_{nom}} \tag{4.1}$$

Here n_{th} is the number of Z-pins expected to be present in a given area A_{nom} of perfect core, based on the manufacturer's specification. The effective pin areal density ρ_{eff} is

determined experimentally by identifying the effective load bearing pins N_{eff} contained within the same nominal area A_{nom}:

$$\rho_{eff} = \frac{N_{eff}}{A_{nom}} \tag{4.2}$$

The effective area is then calculated as follows:

$$A_{eff} = \frac{A_{nom}\rho_{eff}}{\rho_{th}} \tag{4.3}$$

The effective load bearing pin number, N_{eff}, is determined by visual inspection of the specimen, discounting those border pins not spanning across the two faces. It is then double-checked by comparing it with a predicted value of a geometry based empirical method specifically developed for determining the load bearing pins as function of the specimen dimensions. This method is based on the identification of the cutting pattern for a specific sample on a simulated pin lay-out. Figure 4.5 shows an example of pin counting method for a hypothetical out-of-plane compression *(C)X-Cor$^{F}_{I}$/0.51/33°/0.06* specimen of dimensions 40*mm*x40*mm*. The tip of the arrows represents the pin part embedded in the upper skin. The grey pins are those damaged in the cutting process and discounted from calculations.

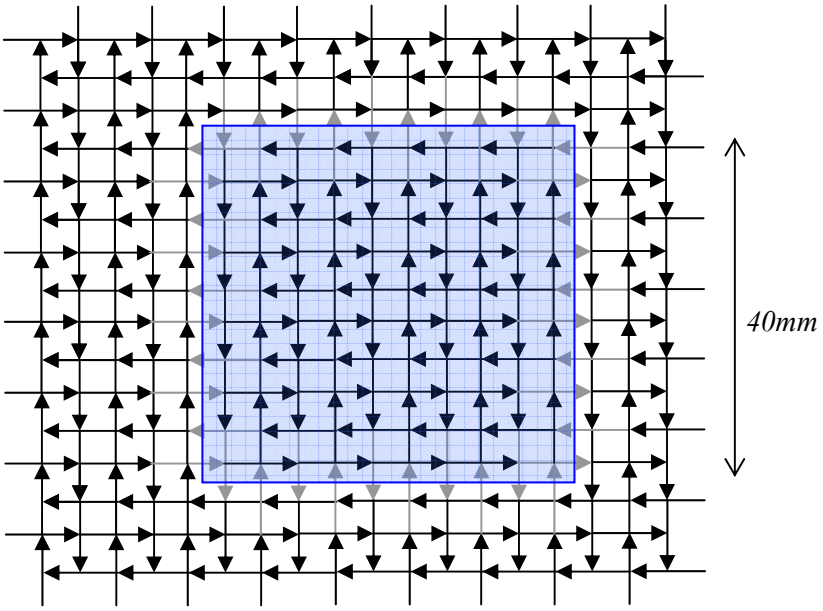

Figure 4.5– *Example of the pin counting method for a (C)X-Cor$^{F}_{I}$/0.51/33°/0.06 sample on a simulated core structure*

Good agreement has been found between the experimental and the predicted pin number (error within 6%). The effective densities denoted for convenience both in the text and in the tables, are determined by experimental measurements. Table 4.1 summarises the theoretical and effective pin densities for the specimens used and shows the extent of this effect in all the different cases.

	out-of-plane shear			***out-of-plane compression***		
	sample dimensions [mm]			*sample dimensions [mm]*		
	50 x 188			*40 x 40*		
	pin areal density [pin/mm²]			*pin areal density [pin/mm²]*		
core type	ρ_{th}	ρ_{eff}	ρ_{eff} / ρ_{th}	ρ_{th}	ρ_{eff}	ρ_{eff} / ρ_{th}
X-Cor$^{F}_{S}$/0.51/22°/0.13	*0.130*	*0.119*	*0.915*	*0.130*	*0.106*	*0.815*
X-Cor$^{H}_{S}$/0.51/22°/0.13	*0.130*	*0.119*	*0.915*	*0.130*	*0.106*	*0.815*
X-Cor$^{F}_{S}$/0.51/30°/0.13	*0.130*	*0.119*	*0.915*	*0.130*	*0.101*	*0.777*
K-Cor^{F}/0.51/30°/0.10	*0.100*	*0.086*	*0.860*	*0.100*	*0.079*	*0.790*
K-Cor^{H}/0.51/30°/0.10				*0.100*	*0.079*	*0.790*
X-Cor$^{F}_{1}$/0.51/33°/0.06	*0.062*	*0.053*	*0.855*	*0.062*	*0.050*	*0.806*
X-Cor$^{H}_{1}$/0.51/33°/0.06				*0.062*	*0.050*	*0.806*
K-Cor^{F}/0.51/33°/0.06	*0.062*	*0.053*	*0.855*	*0.062*	*0.050*	*0.806*
K-Cor^{H}/0.51/33°/0.06				*0.062*	*0.050*	*0.806*
X-Cor$^{F}_{1}$/0.51/11°/0.06				*0.062*	*0.055*	*0.887*
X-Cor$^{H}_{1}$/0.51/11°/0.06				*0.062*	*0.055*	*0.887*
K-Cor^{F}/0.51/11°/0.06				*0.062*	*0.055*	*0.887*
K-Cor^{H}/0.51/11°/0.06				*0.062*	*0.055*	*0.887*
X-Cor$^{F}_{S}$/0.25/21°/0.24				*0.240*	*0.192*	*0.800*
X-Cor$^{H}_{S}$/0.25/21°/0.24				*0.240*	*0.192*	*0.800*

Table 4.1– *Specimen attributes*

In this work the modulus and stress values calculated for the pinned specimens are all referred to the effective sample area. To determine modulus and stress values related to the nominal sample area, the ratio between the effective and nominal areas, equal to ρ_{eff} / ρ_{th}, is presented in table 4.1 for each specimen configuration used in out-of-plane shear and compression tests. For X/K-Cor samples the effective area method, as

proposed, produces consistent results, independent of sample size allowing good measurements to be made. The ASTM standards were originally created for foam/honeycomb cores, in which this particular edge effect is generally considered minimal and is neglected.

4.3.2 Out-of-plane shear and compression data analysis guidelines

The shear and compression stresses are calculated by dividing the applied load P by the effective sample area A_{eff}. For the honeycomb and foam cored samples the effective area is calculated simply as the product of the length and width of the specimen. According to the specifications found in ASTM C 273 [127], the shear strain γ is calculated through:

$$\gamma = \frac{\delta}{t_{sp}} \tag{4.4}$$

where δ is the displacement or movement of one loading plate of the specimen with respect to the other and t_{sp} is the thickness of the specimen (figure 4.6). The out-of-plane moduli are evaluated using the slope of the initial linear elastic portion of the stress-strain curves.

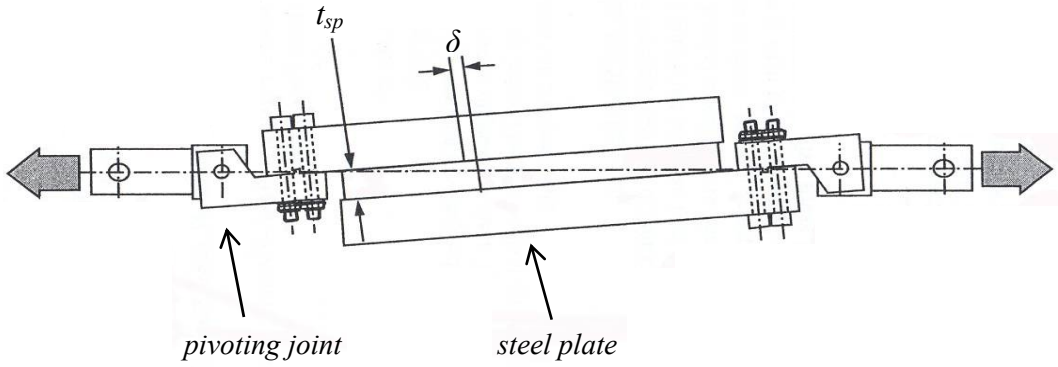

Figure 4.6– *C 273 test fixture schematic and quantities used in the analysis. Figure taken and adapted from [74]*

All the tests were carried out well beyond the end of the elastic phase, in order to evaluate the energy absorption capacity of the materials and study their failure mechanisms. In a few cases for the out-of-plane compression test, at very high strain values, the limit for reliable measurements provided by the laser extensometer was reached (the amount of deformation was such that it changed the angle of the reflecting surfaces). This imposed the application of a compliance correction method called 'direct technique' (described in reference [143]), for the evaluation of the energy absorption values from the displacement provided by the testing machine actuator. The load-displacement relationship of the testing machine is measured directly using the test setup without any sample. The actual deformation is then determined by subtracting the non-sample displacement from the total displacement recorded by the actuator. In the region where the laser extensometer gives accurate measurements, the correctness of this approach was confirmed.

4.4 Chapter summary

1. The tests carried out for the characterisation of out-of-plane shear and compression properties of X-Cor and K-Cor sandwich constructions were in accordance to the ASTM C 273 and C 365 respectively.

2. The two principal parasitic effects related to the C 273 shear test are: the bending of the fixture steel plates and an error in the displacement due to a shear stress gradient present in the sample. They were addressed by adopting fixture steel plates of prescribed thickness, [127, 136], selecting suitable specimen dimensions in order to minimise the displacement error and measuring the relative displacement at the central lines of the sample [132].

3. Out-of-plane shear specimen dimensions used were: 50*mm*x188*mm* (width and length respectively). Displacement controlled test at 0.5*mm/min* cross-head speed.
Out-of-plane compression specimen dimensions used were: 40*mm*x40*mm* (width and length respectively). Displacement controlled test at *0.5mm/min* cross-head speed.

4. The data analysis technique adopted is based on the actual number of load-bearing pins in each sample, discounting the damaged border pins [11]. This allows the determination of an effective cross-sectional area of the specimen used in the calculations. A quantity called ‘pin areal density’ is defined as the number of load-bearing pins in a unit area (expressed as pin/mm^2). The effective area method allows to measure effectively the material properties, since it produces consistent results, independent of sample size.

Chapter 5

Out-of-plane shear

In this chapter the out-of-plane shear response is investigated. A first part (section 5.1) presents all the test results for X-Cor and K-Cor (foam-filled and hollow configurations), a competitor honeycomb and a reference foam core material. This is followed by an analysis of the failure modes and of the structural differences between the pinned cores (section 5.2). Analytical models to evaluate the influence of X-Cor and K-Cor parameters on the mechanical performance are also developed. Section 5.3 introduces a general FE modelling approach for Z-pinned sandwich structures. Both an analytical and a material unit cell models are coupled and implemented into a non-linear FE analysis. Predicted results and model improvement suggestions are also provided.

5.1 Test results

The out-of-plane shear tests were performed on different material systems with the following main objectives:

- Assess the mechanical performance of the pinned cores and the influence of core parameters
- Compare their out-of-plane shear behaviour with a competitor sandwich material
- Evaluate and quantify the effects of the 'improved' manufacturing process for the X-Cor samples

The details of the ASTM C 273 test method used, including the procedures and the data analysis employed, can be found in Ch. 4. Table 5.1 shows both the nominal and the effective values of the principal core material properties for the specimens involved in

this set of tests; for more complete material and specimen specifications and analysis refer to Ch. 3.

sample type identification	*no. tests*	*core density [kg/m^3]*		*pin areal density [pin/mm^2]*		*pin insertion angle θ_i*		*foam type*	*manufact. procedure*
		nom	*eff*	*nom*	*eff*	*nom*	*eff*		
(S)X-Cor^F_S/0.51/22°/0.13	*5*	*~64*	*72.6±0.1*	*0.130*	*0.119*	*22°*	*22°*	*31 IG*	*standard*
(S)X-Cor^H_S/0.51/22°/0.13	*3*	*~32*	*41.4±0.1*	*0.130*	*0.119*	*22°*	*22°*	*--*	*standard*
(S)X-Cor^F_S/0.51/30°/0.13	*5*	*~64*	*68.9±0.1*	*0.130*	*0.119*	*30°*	*32°*	*31 IG*	*standard*
(S)K-Cor^F/0.51/30°/0.10	*5*	*~64*	*66.8±0.1*	*0.100*	*0.086*	*30°*	*32°*	*31 IG*	
(S)X-Cor^F_I/0.51/33°/0.06	*3*	*--*	*52.5±0.1*	*0.062*	*0.053*	*33°*	*33°*	*21 IG*	*improved*
(S)K-Cor^F/0.51/33°/0.06	*3*	*--*	*52.5±0.1*	*0.062*	*0.053*	*33°*	*33°*	*21 IG*	
(S)Nomex	*5*	*64*	*70.7±0.1*						
(S)Foam21IG	*3*	*--*	*22.6±0.1*					*21 IG*	

Table 5.1– *Principal characteristics of specimens used in the out-of-plane shear testing*

The performance of the pinned cores characterised by an effective density within the 66-73 kg/m^3 range (nominal value ~64kg/m^3) is initially compared to that of a Nomex® sandwich material with a measured density of 70.7±0.1 kg/m^3 and similar skins (details in section 3.3.2). It is important to observe that the pinned cores in this first comparison are all manufactured following the standard procedure as reported in section 3.1.2.1. Figure 5.1 shows the stress-strain response for the Nomex® samples and for the following specimens: *(S)X-Cor^F_S/0.51/30°/0.13* and *(S)K-Cor^F_S/0.51/30°/0.10.* Nominally all the samples should have the same weight. From the graph it is evident that although the honeycomb sandwich has a lower rigidity, it exceeds the response of pinned cores in terms of shear strength and energy absorbed (represented by the area underneath the curve) associated with the deformation process.

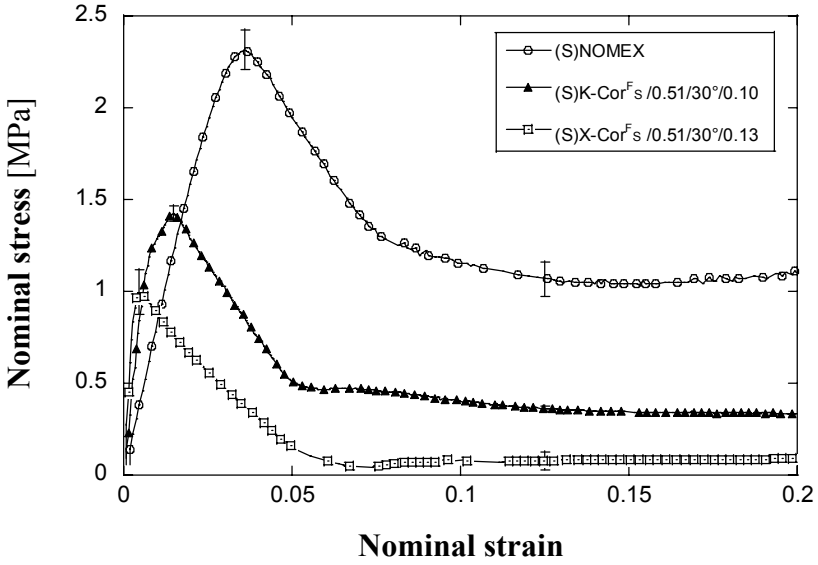

Figure 5.1– *Comparison between X/K-Cor samples ('standard' manufacturing process) and Nomex honeycomb specimens on the basis of similar core density: 66-73 kg/m^3*

Figure 5.2 compares the out-of-plane shear stress vs. strain of X-Cor samples produced with the 'standard' (*(S)X-Cor$^{F}_{S}$ /0.51/30°/0.13*) and the 'improved' (*(S)X-Cor$^{F}_{I}$ /0.51/33°/0.06*) techniques.

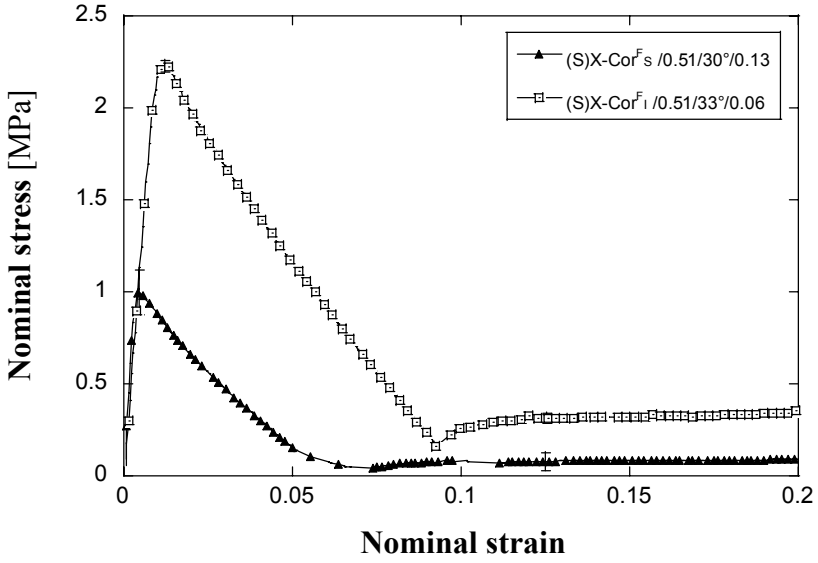

Figure 5.2– *Comparison between the 'standard' and the 'improved' manufacturing techniques for X-Cor construction*

The samples are characterised by very similar pin insertion angles (32° and 33° respectively), but by significantly different pin areal densities. The average value of the

effective number of pins present in the cores for the samples tested is 1118 for the *(S)X-Cor$^{F}_{S}$ /0.51/30°/0.13* and 498 for the *(S)X-Cor$^{F}_{1}$ /0.51/33°/0.06.* The foam core used in these latter specimens is Rohacell® 21 IG, which also has lower mechanical properties compared to 31 IG present in the other samples (section 3.3.4). The specimen with nominally the best core properties (*(S)X-Cor$^{F}_{S}$ /0.51/30°/0.13*) is outperformed by the other core (*(S)X-Cor$^{F}_{1}$ /0.51/33°/0.06*). This result shows that with the improved manufacturing procedure the mechanical properties can be improved to exceed those recorded for the X-Cor material manufactured using the 'standard' process. This sensitivity to the production method becomes therefore a crucial parameter which considerably affects the material behaviour.

Cores very similar to those which made up the previous X-Cor structures were also evaluated as K-Cor structures. In this case both *(S)K-Cor^{F} /0.51/33°/0.06* and *(S)K-Cor^{F} /0.51/30°/0.10* were produced using the co-bonded manufacturing procedure (section 3.1.2.3). As expected, the optimum performance is obtained by using the core with nominally the highest mechanical properties, figure 5.3. The other important consequence of the 'improved' X-Cor manufacturing process is that the level of performance achieved is now higher than the corresponding K-Cor structure. Under out-of-plane shear loading conditions the opposite result is obtained for the 'standard' processing method.

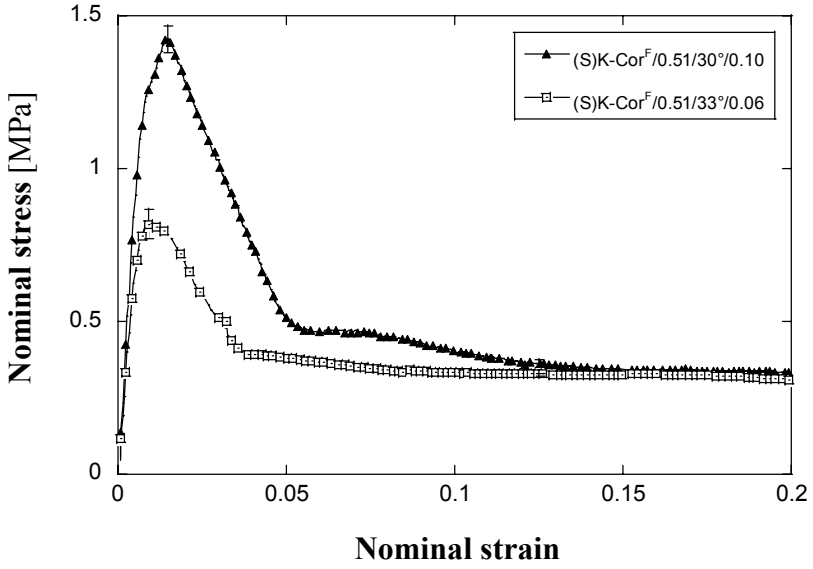

Figure 5.3– *Out-of-plane shear response of two K-Cor constructions with similar core parameters except for the pin areal density*

Figure 5.4 shows that the *(S)X-Cor$^{F}_{1}$ /0.51/33°/0.06* has the performance most comparable to that of the Nomex sandwich constructions in terms of strength.

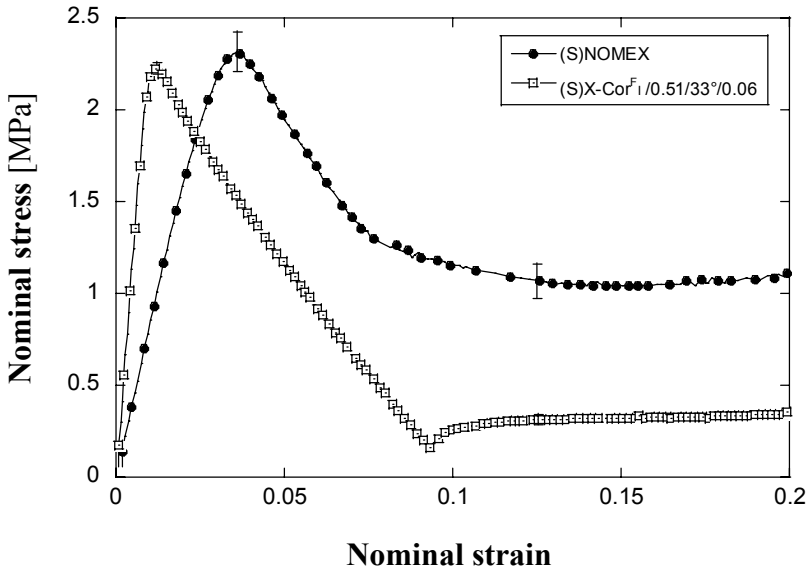

Figure 5.4– *Comparison between Nomex (70.7±0.1 kg/m^3) and X-Cor (52.5±0.1 kg/m^3) specimens. The X-Cor constructions were obtained with the improved manufacturing process*

The potential core weight saving, for the same mechanical performance, is about 25% in favour of the pinned core (value determined on the basis of the effective core densities). The main advantage of X-Cor over Nomex, as seen before, is related to its higher rigidity (241±7MPa for *(S)X-Cor$^{F}_{1}$ /0.51/33°/0.06* versus 75±5 MPa determined for the (S)Nomex samples). The mechanisms involved in the shear deformation process of the honeycomb are more efficient in terms of energy absorption, especially in the post-elastic phase.

Pin insertion angle influence

Figure 5.5 shows the mechanical response to the out-of-plane shear load of two otherwise identical X-Cor samples with different pin insertion angles (22° and 32°). The specimen types are thus: *(S)X-Cor$^{F}_{S}$ /0.51/22°/0.13* and *(S)X-Cor$^{F}_{S}$ /0.51/30°/0.13*. The

difference in performance in terms of rigidity and strength favours the core with the most inclined pins (32°).

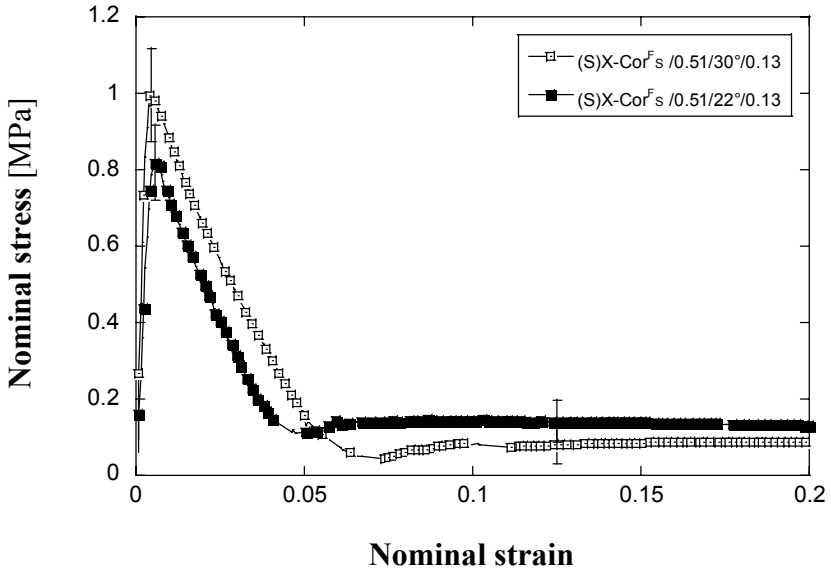

Figure 5.5– *Out-of-plane shear mechanical performance comparison between two similar X-Cor samples characterised only by different pin insertion angle*

A 10° variation in pin insertion angle significantly affects the shear stiffness of the sandwich construction which increases from 200±25 MPa to 341±25 MPa for the *(S)X-Cor$^{F}_{S}$/0.51/30°/0.13* samples.

Foam role

The foam represents another fundamental parameter for the pinned cores. Figure 5.6 shows the stress-strain curves for *(S)X-Cor$^{F}_{S}$/0.51/22°/0.13* and *(S)X-Cor$^{H}_{S}$/0.51/22°/0.13* specimens. It shows that the role of the foam is negligible in the material linear response. This allows a potential ~40% core weight saving to be achieved with the hollow configuration, whilst maintaining the same mechanical behaviour. The foam assumes a more important function in the energy absorption which is related essentially to the post elastic phase.

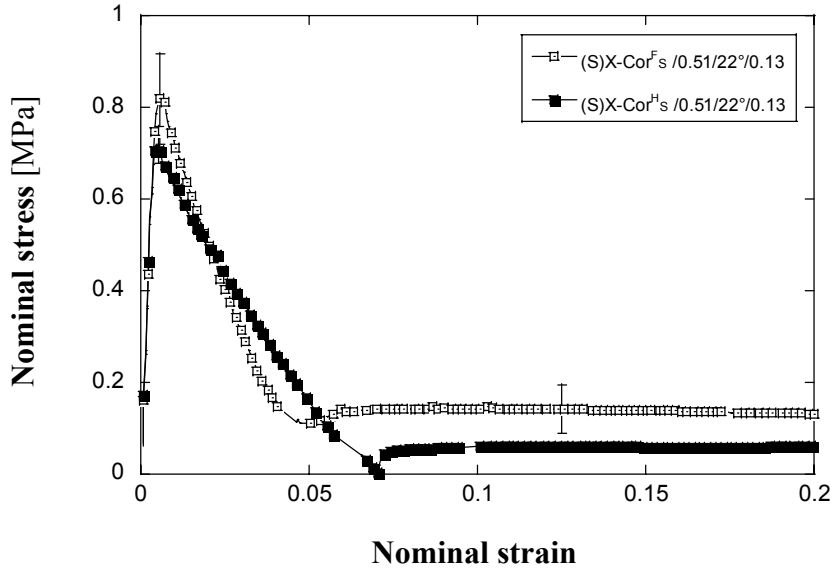

Figure 5.6– *Effect of foam on the out-of-plane shear behaviour. Foam-filled and hollow X-Cor specimens are compared*

Table 5.2 summarises the experimental results, indicating the material strengths and moduli in out-of-plane shear loading conditions. The energy absorbed in the deformation process up to a strain value of 0.2 is also indicated for each core type.

sample type identification	*core density [kg/m^3]*		*foam type*	*manufact. procedure*	*out-of-plane shear strength [MPa]*	*out-of-plane shear stiffness [MPa]*	*absorbed energy up to ε=0.2 [J]*
	nom	*eff*					
(S)X-Cor^F_S/0.51/22°/0.13	*~64*	*72.6±0.1*	*31 IG*	*standard*	*0.8±0.1*	*200±25*	*6.4±0.4*
(S)X-Cor^H_S/0.51/22°/0.13	*~32*	*41.4±0.1*	*--*	*standard*	*0.7±0.1*	*208±14*	*3.9±0.3*
(S)X-Cor^F_S/0.51/30°/0.13	*~64*	*68.9±0.1*	*31 IG*	*standard*	*1.0±0.1*	*341±25*	*6.3±0.5*
(S)K-Cor^F/0.51/30°/0.10	*~64*	*66.8±0.1*	*31 IG*		*1.4±0.1*	*176±9*	*14.1±0.6*
(S)X-Cor^F_I/0.51/33°/0.06	*--*	*52.5±0.1*	*21 IG*	*improved*	*2.2±0.1*	*241±7*	*18.8±0.4*
(S)K-Cor^F/0.51/33°/0.06	*--*	*52.5±0.1*	*21 IG*		*0.8±0.1*	*129±2*	*10.4±0.5*
(S)Nomex	*64*	*70.7±0.1*			*2.3±0.2*	*75±5*	*34.3±2.8*
(S)Foam21IG	*--*	*22.6±0.1*	*21 IG*		*0.3±0.1*	*11±1*	*1.9±0.1*

Table 5.2– *Experimental results and principal core characteristics*

5.2 Failure analysis and performance evaluation

This section deals with the common features characterising the mechanical behaviour of these sandwich structures as well as a more in-depth analysis of their specific failure micro-mechanisms. A typical out-of-plane shear deformation of a pinned sample, in this case K-Cor, is shown in figure 5.7. As expected shear cracks at about 45° of the loading axis are visible in the foam.

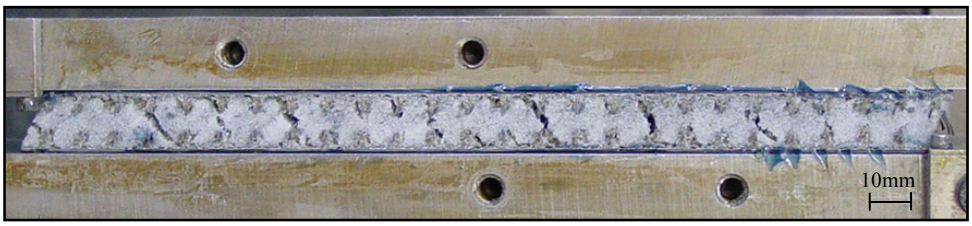

Figure 5.7– *Out-of-plane shear: post-elastic phase for a (S)K-Cor^F /0.51/30°/0.10 specimen*

Two principal failure modes in the sandwich samples tested were recognised: a core failure determined by the buckling of the honeycomb cell walls for the Nomex® specimens (figure 5.8) and generally speaking, at this stage, a skin-core interface failure for the pinned core samples, in all the different configurations, as well as for the foam core (reference) specimens.

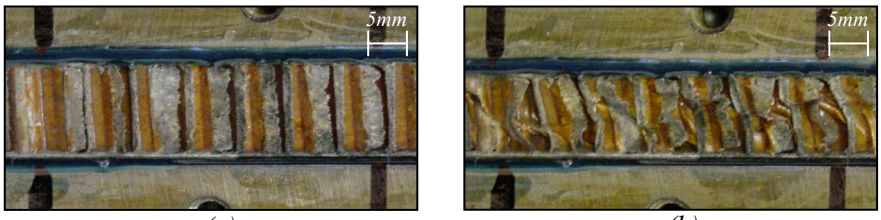

(a) *(b)*

Figure 5.8– *Nomex sample before (a) and after (b) the out-of-plane shear test. Failure mechanism is shear buckling of honeycomb cell walls*

This interface represents a typical weakness for sandwich structures and even with enhanced cores, although higher mechanical properties are achieved, it still constitutes the critical part. Figure 5.9 shows the skin-core failed interface of a K-Cor specimen;

the two steel plates have been moved slightly apart after the test to offer a better view of the failed interface.

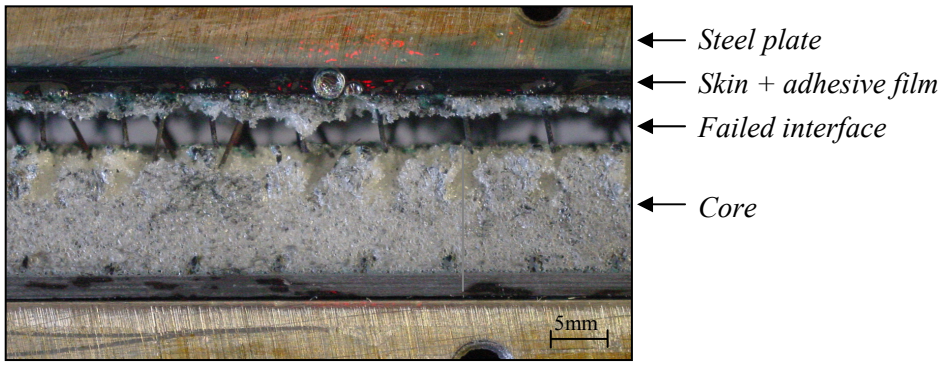

Figure 5.9– *Typical K-Cor failure mode; fixture steel plates moved apart to show the failed skin-core interface*

The most evident feature, common for both X-Cor and K-Cor during out-of-plane shear loading is an increasing skin separation due to pin rotation. This is caused by pins inserted in such a way that they counteract the applied load. Figure 5.10 shows a schematic of this opening mechanism for both cores; regardless of the type of constraint at pin-end and its failure, those pins inserted "against the nap" determine this typical behaviour. What causes pin rotation is a failure of their interface located either in the adhesive film (K-Cor) or in the skin (X-Cor). In contrast, under out-of-plane shear loading, the more traditional honeycomb sandwich systems exhibit a decreasing skin distance in the post-elastic phase (figure 5.8).

As seen in section 3.2, the pin lay-out in the core has two principal perpendicular directions along which pins are inserted. To maximise the core mechanical properties, in this case the applied shear load is parallel to one of those pin directions.

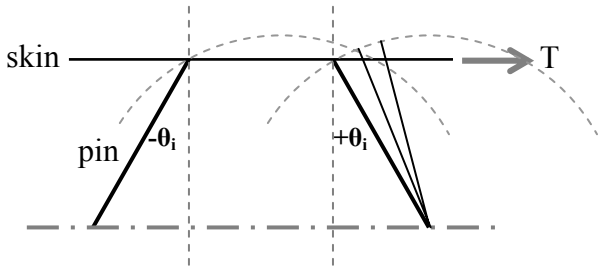

Figure 5.10– *X/K-Cor half specimen schematization. Case of pins inserted in a plane parallel to the load direction along a positive and a negative insertion angle* θ_i

As figure 5.10 shows, pins are inserted with a positive and a negative insertion angle θ_i. Using the sign convention on θ_i of the figure, the pins inserted with a positive angle in the direction parallel to the load will experience rotation; those at a negative insertion angle will be subjected to a pull-out from their original positions. The pins belonging to perpendicular planes with respect to the load direction (not shown), will also experience pull-out. The skin transversal opening mechanism applies to both types of pinned cores and it has been encountered in all the different configurations tested. The increase in the relative distance of the skins, which are integral with the fixture steel plates, was monitored by the use of a longitudinal and a transversal LVDT placed approximately at the middle of the specimen length [132, 136]. Figure 5.11 shows the applied load and displacements as functions of time respectively for a *(S)X-Cor^F_S /0.51/30°/0.13* and a *(S)K-Cor^F /0.51/30°/0.10* sample. The displacements are those measured by the two LVDTs .

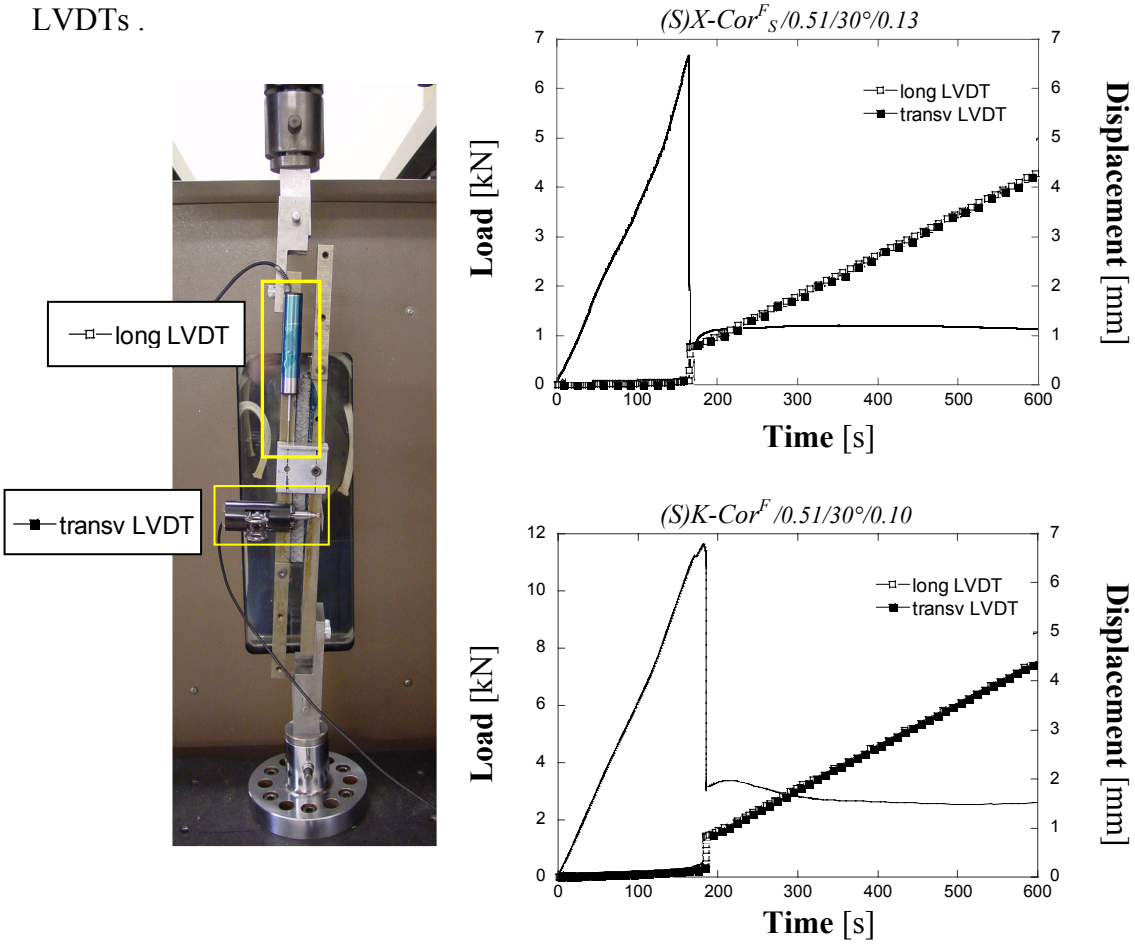

Figure 5.11– *Load and longitudinal and transversal LVDT displacements plotted versus time*

The elastic phase is characterized by a very small facesheet relative movement in both directions, as the interface around the pin tip, which represents the rotational constraint, is progressively being damaged until its failure. Once the pin is not held in place by the surrounding material, it can rotate if the applied force is high enough to overcome the friction effects and the resistance provided by the foam. As shown in figure 5.11, after the elastic phase, a linear increase of the relative longitudinal and transversal distances is registered.

For both X/K-Cor the shear strength is set by the failure of the interface at pin end. Even supposing a perfect congruence between the skins and the foam core, at the shear strain values corresponding to the sample strength, the level of deformation experienced by the foam is not critical (table 5.3).

				Experimental shear strain at peak stress	
	G [MPa]	*τ_s [MPa]*	*γ_{τ_s}*	*γ X-Cor*	*γ K-Cor*
Rohacell IG 21	*11.0*	*0.3*	*0.03*	*0.013*	*0.009*
Rohacell IG 31	*13.0*	*0.4*	*0.03*	*0.005*	*0.015*

Table 5.3– *Level of deformation experienced by the two types of foam cores at peak stress*

In table 5.3, G, τ_s and γ_{τ_s} represent respectively the foam shear modulus, shear strength and the corresponding strain to failure value determined by Hooke's law. The shear strain experienced by the core at the end of the elastic phase does not reach the foam critical values. It will eventually fail in the post-elastic phase when a higher level of core shear deformation is reached. This is caused by the difference in stiffness between the interface material at the pin end and the foam. For both X-Cor and K-Cor, it is an epoxy resin which makes up either the skin or the adhesive film. A typical range for the shear modulus for this type of resins is around 2-4GPa, while for the foam employed it is in the order of 10-20MPa, two orders of magnitude lower. As a result we can affirm that the shear load applied to the X/K-Cor specimens is essentially carried by the pins. Once the foam has failed, it will oppose the applied load by the friction effect at its contact interface. As seen in section 5.1 for the X-Cor specimens characterised by a pin insertion angle of 22°, the hollow configuration carries a minimum load in the post-

elastic phase *((S)X-Cor$^{H}_{S}$ /0.51/22°/0.13,* figure 5.6). The *(S)X-Cor$^{F}_{S}$ /0.51/22°/0.13* configuration exhibits a higher load plateau attributable to the friction arising at the foam fracture surface.

5.2.1 X-Cor out-of-plane shear failure analysis

In X-Cor constructions, the foam is not attached to the skins by means of an adhesive film. Between the core and the facesheets there is only a contact interface. The core is also internally restrained by the presence of the pins which fasten the two facesheets together allowing the foam to be sandwiched. The consequence of these boundary conditions on the foam is a non-uniform interface at failure (in contrast to what can be observed for K-Cor, figure 5.15), and a damage spread throughout the volume. Figure 5.12 shows one of the two halves of an *(S)X-Cor$^{F}_{I}$/0.51/33°/0.06* specimen.

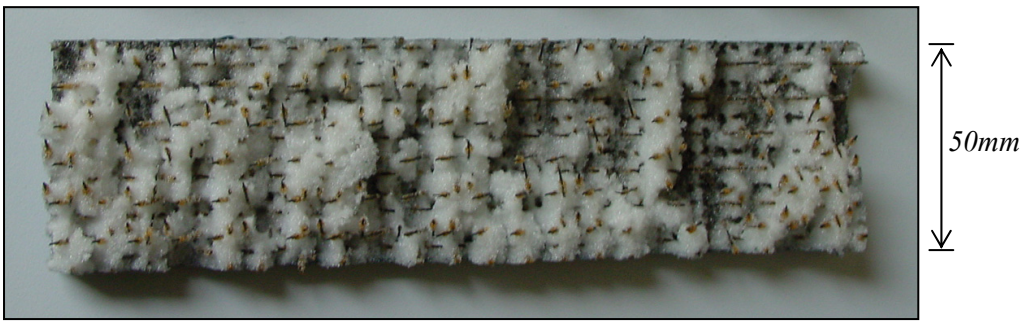

Figure 5.12– *One half of a (S)X-Cor$^{F}_{I}$/0.51/33°/0.06 sample after being tested in out-of-plane shear*

In the X-Cor, the pin-tips are embedded through a lamination process into the skins. It is plausible to consider a small surrounding volume of material around the pin tip as an interface, created during the consolidation in the curing process. It guarantees continuity between the facesheet and the pin. The stress level rises during the elastic phase until failure occurs at the pin-skin interface. This event corresponds to the end of the material elastic response. The post-elastic response is characterised essentially by pin rotation and pull-out and additionally friction effects, which also need to be overcome by the applied force. At the end of a test it is easy to separate the two halves of the sample as

the fastening mechanism provided by the embedded pin tips has failed and it is only a matter of pushing one half of the specimen away, to make the pins, still attached to the skins, go through the foam. The number of pins still fastened to each half is similar. For the hollow configurations the separation of the skins is immediate. Figure 5.13 shows one half of a hollow X-Cor specimen *((S)X-Cor$^{H}_{S}$/0.51/22°/0.13)* and a close-up of some pins.

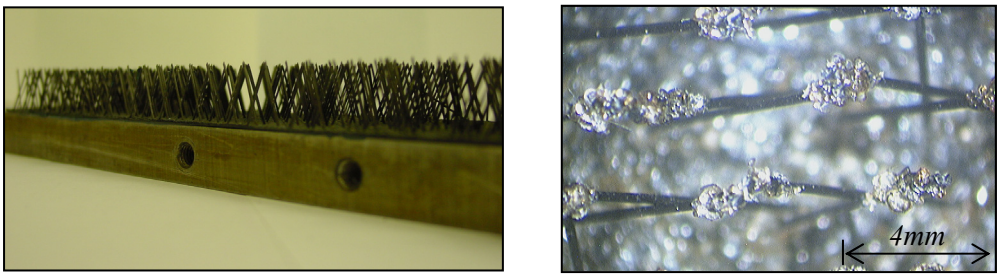

(a) *(b)*

Figure 5.13- *(a) Half (S)X-Cor$^{H}_{S}$/0.51/22°/0.13*
(b) Optical microscope close-up of pin tip

The pins, as shown in figure 5.13, do not seem particularly damaged after the testing phase. Their typical shape is still retained. A bit of resin at the pin tips is usually noticeable. Figure 5.14 shows a schematic of the failure mechanisms at the pin-skin interface. It refers to pins inserted in a plane parallel to the load direction along a positive and a negative insertion angle. Figure 5.14(b) refers to the elastic phase where the interface is progressively damaged, while figure 5.14(c) illustrates the pin behaviour in the post-elastic phase.

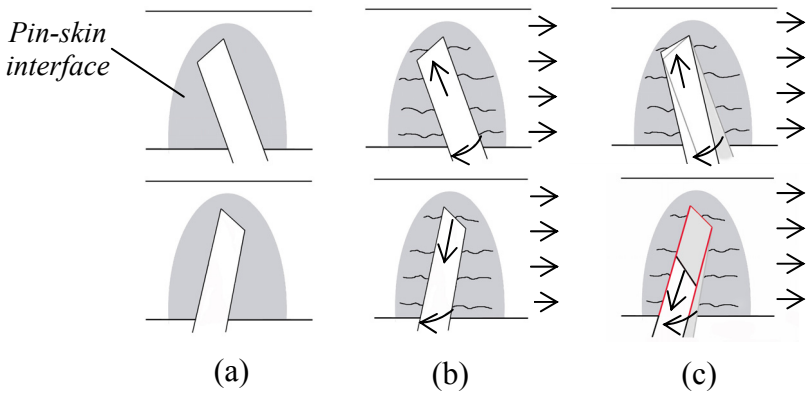

Figure 5.14– *Sketch of pin-skin interface failure mechanism. Pins inserted along a plane parallel to the load direction*

5.2.2 K-Cor out-of-plane shear failure analysis

In K-Cor structures the foam is constrained to follow the skin relative movements through the adhesive bond until the deformation experienced by the foam at those boundaries becomes critical. The failure mechanism differs from what is observed in the X-Cor specimens; the fracture front is just below the adhesive film (figure 5.15).

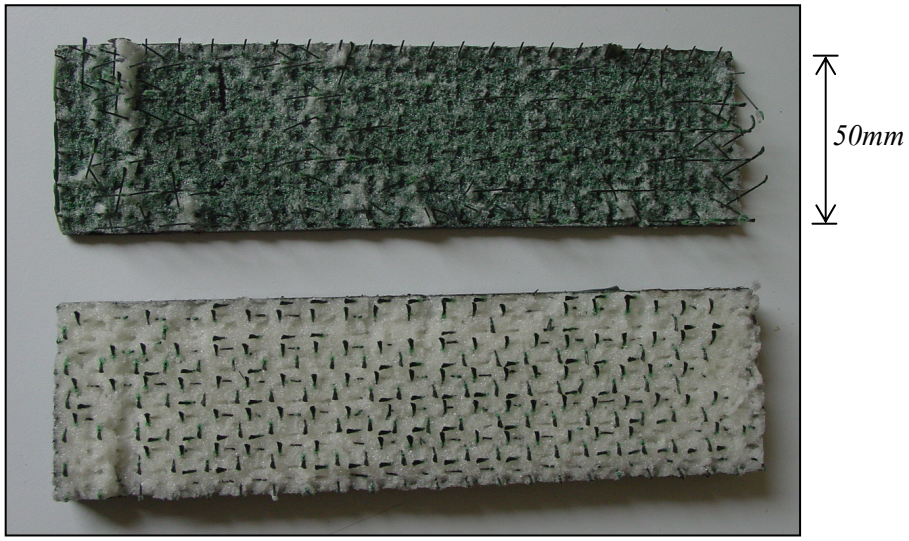

Figure 5.15– *Two halves of a (S)K-Cor^F /0.51/30°/0.10 sample*

A closer observation of the fracture surface allows few considerations to be made (figure 5.16).

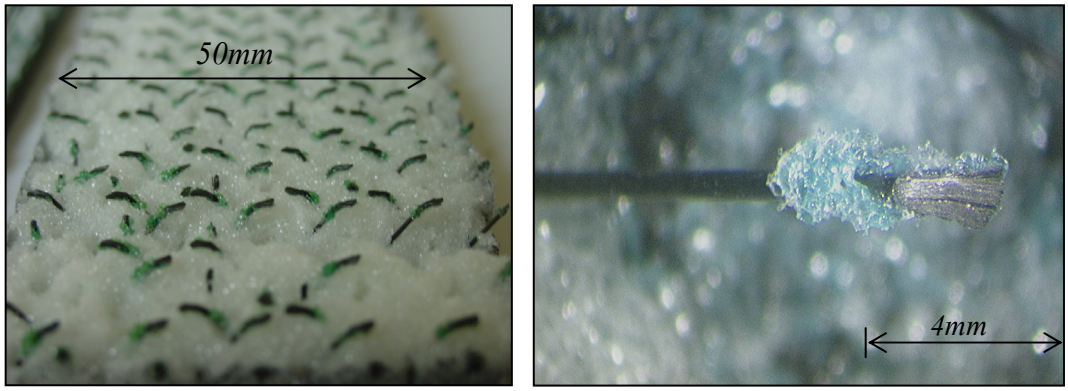

Figure 5.16– *K-Cor interface failure (a) and optical microscope magnification of a pin tip (b)*

The pin folded tips are visible on the core and this shows that the whole pin-adhesive film interface fails during the shear test. As shown in figure 5.16(b), part of the adhesive

remains connected to the pin head. The failure sequence for K-Cor is similar to that of X-Cor, although different mechanisms dominate. There is an initial failure of the pin-adhesive film interface, which corresponds to the end of the elastic phase. The foam core-adhesive interface, already damaged, fails completely in the post-elastic region when most likely critical shear deformations are reached. Figure 5.17 shows a schematic of the failure mechanisms at the pin-adhesive interface. It refers to pins inserted in a plane parallel to the load direction along a positive and negative insertion angle. It is important to notice that all the pin tip surrounding material is part of the interface; this includes mainly the adhesive, but also a small portion of the foam core below and around the flattened pin end. Figure 5.17(b) shows the progressive damage taking place in the elastic phase, where the pin-adhesive interface responds to the applied load. Figure 5.17(c) refers to post-elastic behaviour, where the pin either rotates and counteracts the load, increasing the skin separation, or rotates and experiences pull-out from the damaged interface.

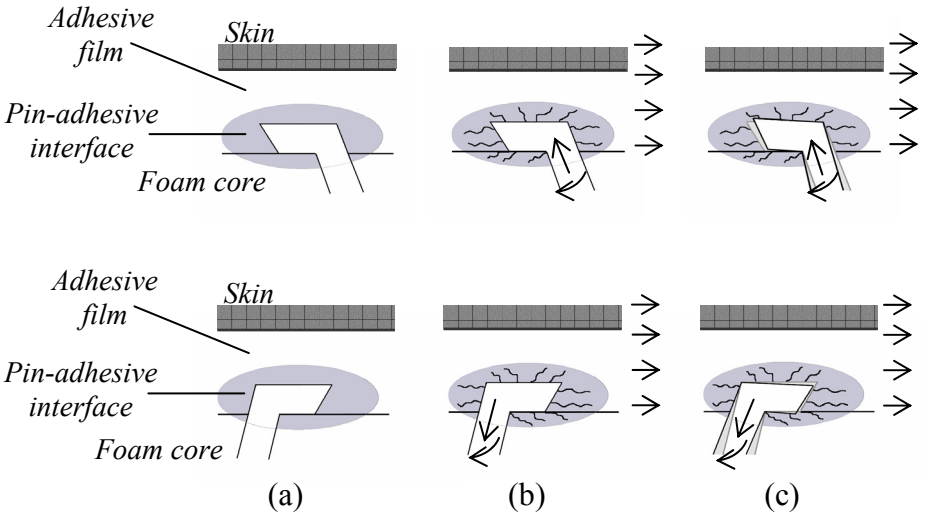

Figure 5.17– Sketch of pin-adhesive film interface failure mechanism. Pins inserted along a plane parallel to the load direction

5.2.3 Development of a pin model for X-Cor

A simple pin model is proposed (figure 5.18). It gives an indication of the critical stress condition reached at the pin-skin interface and the pin parameters influence on mechanical performance. The 2D sketch of figure 5.18 shows a simplified half pin

geometry (flat pin top, not chamfered at 45°, Ch.3). In the following analysis only a normal stress distribution of linearly varying intensity is assumed to equilibrate the flexural moment acting on the pin itself due to the applied shear load. A rotational equilibrium is considered.

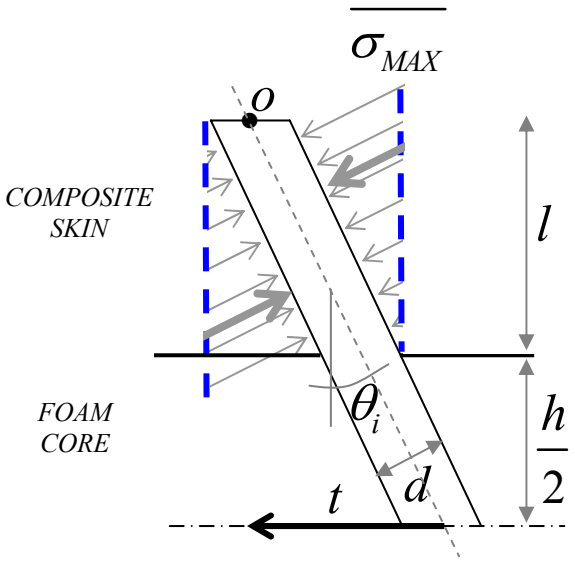

Figure 5.18- *Schematic of pin (lateral view) and quantities for the analysis*

The pin is assumed to be pinned in O. The moment equilibrium is evaluated with respect to the pole O. The external moment is given by the shear force t acting on a single pin:

$$M_{ext,o} = t\left(l + \frac{h}{2}\right) \tag{5.1}$$

where l is the pin reveal length and h is the foam core thickness. The internal (interfacial) balancing moment is the following:

$$M_{int,o} = \frac{\pi R l^2}{6\cos^2\theta_i}\overline{\sigma_{MAX}} \tag{5.2}$$

where θ_i is the pin insertion angle, R is the pin radius and $\overline{\sigma_{MAX}}$ is the average value of the normal stresses evaluated at both ends of the pin-skin interface as shown in figure 5.19.

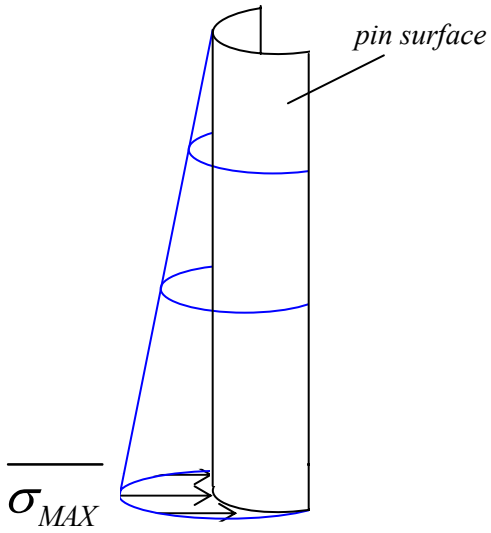

Figure 5.19- *3D schematic view of the supposed normal stress distribution around the embedded pin tip (half pin indicated)*

At equilibrium we obtain the following qualitative expression of the maximum normal stress acting at the pin-skin interface:

$$\sigma_{MAX} = \frac{6\cos^2\theta_i}{\pi R}\left(\frac{h}{2l^2}+\frac{1}{l}\right)t \tag{5.3}$$

For the cores analysed $h \sim 12l$ is generally valid, equation 5.3 yields to:

$$\overline{\sigma_{MAX}} = \frac{42\cos^2\theta_i}{\pi Rl}t \tag{5.4}$$

It is possible to identify an intensification factor in equations 5.3-4, which multiplies the applied force t on each pin. This equation is used to determine the maximum normal stress $\overline{\sigma_{MAX}}$ reached at peak load of the out-of-plane shear test for the X-Cor samples tested. The force t is obtained supposing an equally distributed shear force acting on each pin of the core. The values determined are much higher than typical resin strengths. Table 5.4 summarises those findings.

(S)X-Cor$^{F}_{S}$/0.51/22°/0.13	*(S)X-Cor$^{F}_{S}$/0.51/30°/0.13*	*(S)X-Cor$^{F}_{I}$/0.51/33°/0.06*
$\theta_i = 22^\circ$	$\theta_i = 32^\circ$	$\theta_i = 33^\circ$
$R = 0.255mm$	$R = 0.255mm$	$R = 0.255mm$
$l \sim 1mm$	$l \sim 1mm$	$l \sim 2mm$
$h = 12.7mm$	$h = 12.7mm$	$h = 12.7mm$
$N_{pins} = 1118$	$N_{pins} = 1118$	$N_{pins} = 498$
$t \sim 7N$	$t \sim 8N$	$t \sim 36N$
$\overline{\sigma_{MAX}} = 315MPa$	$\overline{\sigma_{MAX}} = 302MPa$	$\overline{\sigma_{MAX}} = 664MPa$

Table 5.4– *Average value of the maximum normal stress (calculated with eq. 5.4) experienced at each pin-skin interface. This value corresponds to the peak experimental load in the sample*

The high value of the maximum stress $\overline{\sigma_{MAX}}$ determined at the pin-skin interface shows that effectively the conditions reached in this region become progressively critical during the elastic phase until failure takes place. Those values are not realistic due to the limitations of the model adopted, but they are consistent with what was previously observed in the experimental testing phase. A stress re-distribution occurs until the damaged volume is big enough to allow pin rotation or pull-out to take place. The value for $\overline{\sigma_{MAX}}$ determined with the pin model for the *(S)X-Cor$^{F}_{I}$/0.51/33°/0.06* specimens shows that the highest performance is achieved with the 'improved' manufacturing technique together with a longer pin reveal length. Higher interfacial normal stresses are required to achieve a damage level corresponding to the end of the elastic phase.

To enhance the resistance of the pin-skin interface, given a fixed skin composition, we need to lower the value of the intensification factor and consequently of the interfacial stress distribution. The insertion angle ϑ_i (measured with respect to the vertical direction) plays an important role, confirming the experimental findings. A more vertical pin insertion determines cores characterised by lower shear properties. The reveal length l and the pin radius R have an indirect influence on the intensification factor. Thin cores, characterised by low values of thickness h, generate lower flexural moments at the pin tips, enhancing the shear properties, but at the same time reducing

the bending stiffness properties of the sandwich construction. The level of stress reached at the embedded pin tip is so high that even a simple and manageable analytical model as the one presented is suitable as an investigative tool. Higher interface stress values for the *(S)X-Cor$^{F}_{1}$ /0.51/33°/0.06* samples indicate the influence of the manufacturing procedure on the mechanical performance; an improved pin-to-skin interface due to a higher degree of material compaction is beneficial to the whole sandwich behaviour.

5.3 Finite element modelling and analysis

In this section a modelling strategy for both X-Cor and K-Cor structures is presented. The aim is to create a predictive tool for simulating the linear elastic response (stiffness and strength) in out-of-plane shear loading conditions, able to deal with the complexity of the material. The approach followed is based on a unit cell concept, which represents the smallest repeatable unit in the material. Modelling on a local scale gives the opportunity of considering all the peculiarities and essential details which characterise a material system. A local-global approach is often employed for material like sandwich structures which are made up of several components characterised by different physical properties [74, 144]. At the same time this technique could be used eventually for material improvement and optimisation by performing changes at a unit cell level and analysing the consequent change in performance. Once the mechanical behaviour is characterised at the unit cell level, it is possible to extend it to the whole panel or component with a considerable reduction of computing effort. In fact, at a global level it will not be necessary to reproduce a detailed material structure, but just to implement the mechanical properties determined at the base unit. The methodology presented is applicable to any X/K-Cor sandwich construction, although it needs to be tailored for each particular case to enable the evaluation of the effect of different material parameters. This section in particular deals with the development of a unit cell model for one type of pinned cored sandwich structure employed in the experimental work: it is an *X-Cor$^{F}_{S}$ /0.51/30°/0.13* structure, characterised by properties summarised in tables 5.1 and 5.2. More material details can be found in section 3.3. Indications on how to

employ a similar approach for K-Cor sandwich structures are also discussed throughout the section. The principal critical features which make up a pinned sandwich structure and need to be modelled at a unit cell level, in order to have an effective and realistic simulation tool, are:

- Pin
- Pin tip interface
- Foam

Although the foam does not seem to affect the material elastic response, as previously demonstrated (sections 5.1 and 5.2), it is included in the material model. In this way it would be possible to evaluate the foam strain and stress field and, eventually, validate the experimental and analytical findings.
A pin physical model is established. A pin is considered as a column of elastic-brittle material with two rotational springs at the ends which simulates the interface mechanical properties (figure 5.20).

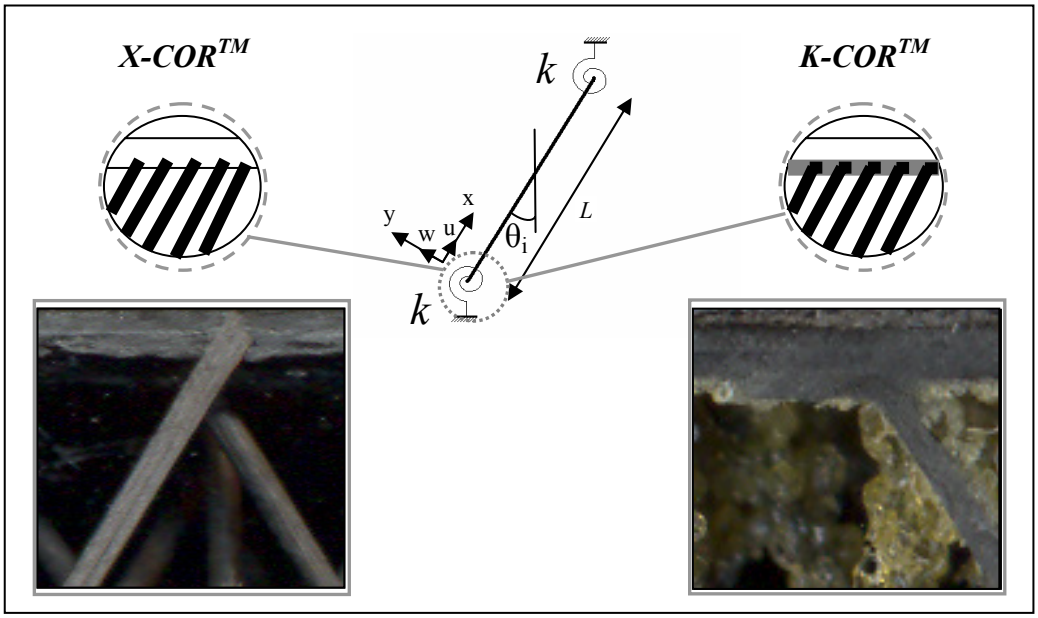

Figure 5.20– *Schematic of the pin physical model used. Rotational springs at pin-ends simulate the interface mechanical properties*

The rotational constraint provided by the springs represents a simplification of the complex pin-skin and pin-adhesive film interfaces. In the case of X-Cor there is no need to complicate the model by representing the pin embedded for a certain length (reveal length) into the skin laminate. Similarly, in the case of K-Cor, the rotational spring will take into account the flattened part of the pin bonded to the facesheet. The constant of rigidity of the rotational springs is therefore a function of a series of properties:

- Pin reveal length (X-Cor) / pin flattened end length (K-Cor)
- Pin diameter and insertion angle
- Manufacturing process and interface quality

Even at a local material level, the FE model is a simplification of a complex physical reality. To be effective it needs to take into account the main mechanisms which characterise the behaviour of pinned sandwich structures.
Another fundamental step is to input into the code the correct values of the parameters which constitute the various elements of the model. If it is not possible to experimentally determine some quantities or find them in the literature, an alternative way to estimate their values needs to be pursued. In this case the rotational constraint, which corresponds to the rigidity of the rotational spring elements, needs to be evaluated with an analytical model specifically developed for out-of-plane shear loading. The schematic of figure 5.21 summarises the local-global simulation approach.

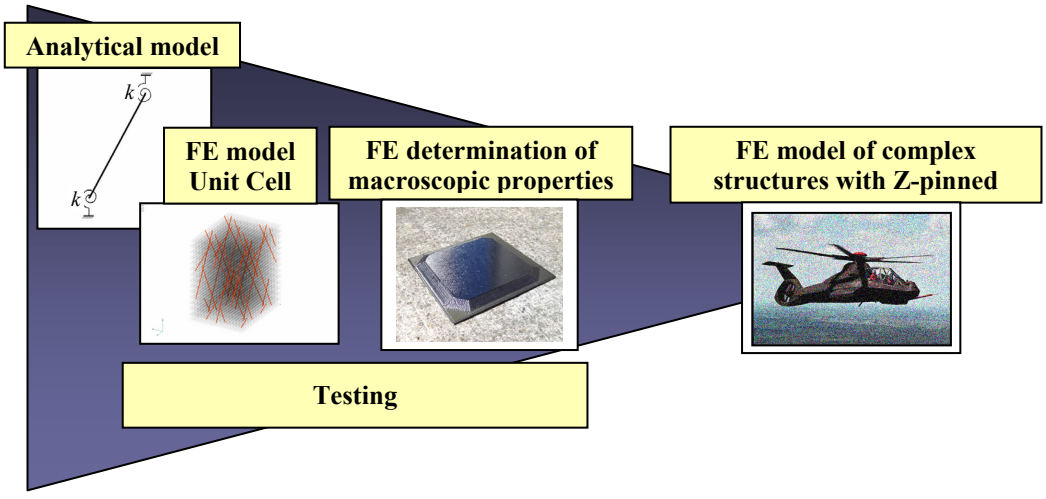

Figure 5.21– *Local-global simulation approach*

5.3.1 Analytical model

The observation of the pinned cored samples during the out-of-plane shear loading tests and the analysis of the experimental results and failure modes are the basis for the development of an analytical model in order to express experimental and core parameters as FE input values. This phase represented a fundamental step towards the recognition of the principal failure mechanisms in order to achieve a realistic model of the core behaviour. As described in section 5.2 the shear response is set by the pin tip interface properties. The increase in skin distance, due to pin rotation, is considered as a characteristic feature of this out-of-plane loading condition. The elastic phase is characterised by minimal relative movements between the specimen facesheets in the longitudinal and transverse directions. The pin rotation mechanism due to pins inserted "against the nap", (which counteract the load), is identified as typical of these cores (section 5.2). As shown in figure 5.22(a), these particular pins have a force component along the longitudinal axis which keeps them in place, causing the opening of the skins. For the other pins, figure 5.22(b, c), the same component is responsible for pull-out; their rotation also should favour a closing mechanism. For the pins belonging to planes perpendicular to the load direction, the pulling-out component of the applied force is only established when rotation starts taking place, figure 5.22(c).

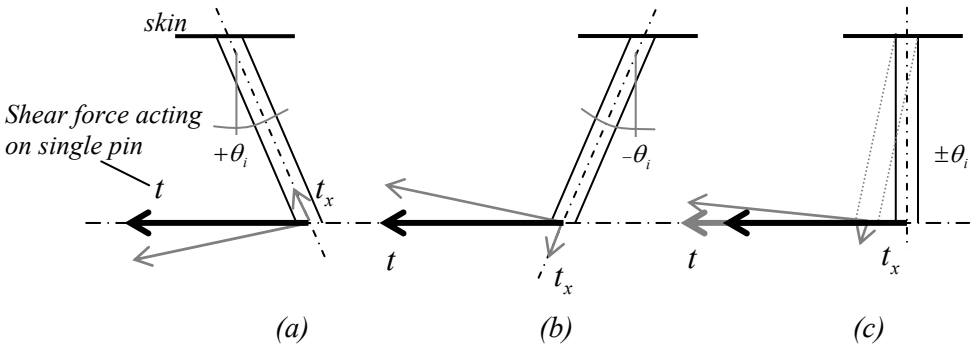

Figure 5.22– *Different pin types: (a) positive insertion angle, (b) negative insertion angle, (c) pins belonging to planes perpendicular to the load direction*

The model, for simplicity, considers only the load counteracting pins, which are those responsible for the characteristic behaviour of pinned cores in out-of-plane shear loading conditions, (figure 5.20(a)). This means that in the analytical model of the core

only those pins are present. Table 5.5 summarises the theoretical areal densities and pin numerical quantities for each one of the three pin insertion possibilities in the *(S)X-Cor$^{F}_{S}$ /0.51/30°/0.13* sample. For clarification, the specimen nominal dimensions are $180mm \times 50mm$ (section 4.2.2).

	load direction // pin insertion plane		*load direction ⊥ pin insertion plane*
pin insertion angle	$+\theta_i$	$-\theta_i$	$\pm\theta_i$
pin theoretical areal density [pin/mm^2]	*0.0433*	*0.0433*	*0.0433*
pin nominal quantity (in the sample)	*407*	*407*	*407*

Table 5.5– *Pin quantities and densities as function of insertion properties. Sign convention taken from figure 5.25*

A second assumption for the analytical model is to consider an equal distribution of the applied shear force between the counteracting pins. In this way all the pins are supposed to be in the same conditions. The analysis can be focused on one pin and then extended to the whole core. Moreover, in the model both the skins and the pins are considered as rigid bodies pinned together that experience a relative motion. For the linear response, the situation is represented in figure 5.23. The elastic deformation (and the progressive damage) is only experienced by the two connecting rotational springs. In this way all the counteracting pins, in this ideal core, experience the same angle of rotation. This assumption is also supported by the fact that the value experimentally measured by the longitudinal LVDT is an average displacement and not related to a single pin.

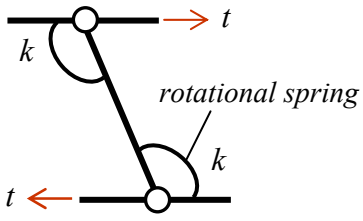

Figure 5.23– *Counteracting pins and skins considered as rigid bodies pinned together with relative movement constrained by rotational springs (approach followed in the analytical model)*

Having stated the assumptions on which the model is based, the next step is to determine a relation between an experimental measurable quantity, a core property, and the constant of rigidity to be used in the FE model.

5.3.1.1 Pin geometric and kinematics considerations

Trigonometric relations allow a correlation between the pin angle variation (pin rotation) and the global shear strain measured in the sample. This analysis is limited to the elastic response of the material. Figure 5.24 shows the global shear effect on the core (half sandwich specimen and its relative longitudinal displacement u is sketched), which is experimentally measured with of an LVDT device (section 4.1.1).

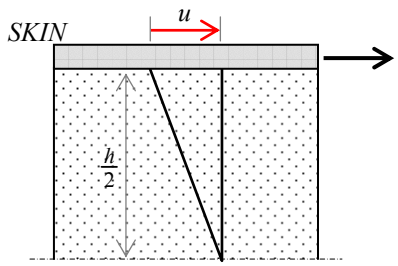

Figure 5.24- *Global shear effect on the core (half specimen represented)*

At the pin level, the local shear effect, under the assumptions made, consists of a rigid rotation. Figure 5.25 shows the effect of the loading conditions acting locally on half a pin. The two figures 5.24 and 5.25 represent the response of the same portion of material from a global and a local perspective.

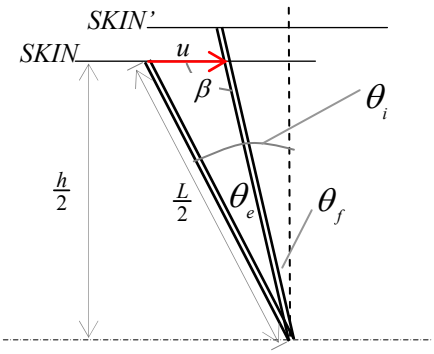

Figure 5.25– *Local shear effect on pin (quantities for the analysis shown, Appendix A for more details)*

The idea is to correlate the angle of pin rotation in the elastic phase θ_e with the global shear strain γ measured in the material:

$$\theta_e = \theta_e(\gamma) \tag{5.5}$$

The pin rotation angle of material elastic response can be obtained from the difference between the initial angle (which corresponds to the pin insertion angle θ_i) and the final pin angle θ_f at displacement u:

$$\theta_e = \theta_i - \theta_f \tag{5.6}$$

Applying the law of sines formula we obtain a relation between the pin relative displacement u and its length L with some convenient angles:

$$\frac{u}{\sin\theta_e} = \frac{L}{2\sin\beta} \tag{5.7}$$

where the angle β with simple trigonometric considerations is equal to:

$$\beta = \frac{\pi}{2} + \theta_f \tag{5.8}$$

After some computation, it is possible to obtain a correlation between the pin angle of elastic response θ_e and the global core strain γ:

$$\gamma\cos\theta_i = \frac{\sin\theta_e}{\cos\left(\theta_i - \theta_e\right)} \tag{5.9}$$

Equation 5.9 can be simplified and a more manageable relation is achieved. For very small pin angles θ_e, the following approximation is valid:

$$\theta_e \ll 1 \Rightarrow \sin\theta_e \cong \theta_e \tag{5.10}$$

and consequently the denominator of equation 5.9 can be expressed as:

$$\cos(\theta_i - \theta_e) \cong \cos\theta_i + \theta_e \sin\theta_i \tag{5.11}$$

Equation 5.9 can be re-written in the following way:

$$\theta_e = \frac{\gamma \cos^2 \theta_i}{1 - \frac{1}{2}\gamma \sin 2\theta_i} \tag{5.12}$$

which is a simpler relation between the angle of pin rotation in the elastic phase and the corresponding measurable global shear strain in the sample. It is possible to verify the agreement between the model (equation 5.12) and physical reality. In the extreme cases of pin insertion angle θ_i the relation between θ_e and γ according to eq. 5.12 is the following:

$$\theta_i = 0 \Rightarrow \theta_e = \gamma$$

$$\theta_i = \frac{\pi}{2} \Rightarrow \theta_e = 0$$

5.3.1.2 Forces and boundary conditions

The aim of the analytical model is to find an explicit expression for the spring constant of rigidity as a function of an experimentally measurable material property. For that purpose, we consider a single pin in equilibrium under the applied out-of-plane shear load and with the boundary conditions due to rotational springs at its ends. A schematic of the forces and reactions acting on a counteracting pin is presented in figure 5.26.

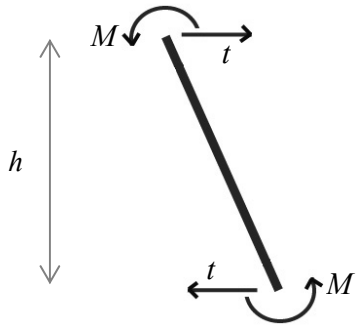

Figure 5.26– *Counteracting pin: forces and reactions due to the applied loading condition*

The moment acting on each pin end is given by the following equation:

$$M = k\theta_e \tag{5.13}$$

where k is the constant of rigidity of a spring, θ_e the angle associated to a pin rotation in the region of linear response of the pinned core and t the shear force acting on a single pin. The equilibrium of the moments with respect to a pin end gives:

$$th = 2k\theta_e \tag{5.14}$$

where h is the core thickness. To extend this result (eq. 5.14) to the whole core, we need to consider:

$$T = \sum_{i=1}^{N} t_i \tag{5.15}$$

which represents the total applied force, as N is the total number of the counteracting pins in a sample. In the modelled core the total applied shear force is shared obviously by a fewer number of pins. The constant of rigidity for the core is given by:

$$K = \sum_{i=1}^{N} k_i \tag{5.16}$$

We can extend now eq. 5.14 to the whole core

$$Th = 2K\theta_e \tag{5.17}$$

And substitute the analytical expression of θ_e as a function of core strain γ and pin insertion angle θ_i (equation 5.12):

$$Th = 2K \frac{\gamma \cos^2 \theta_i}{1 - \frac{1}{2}\gamma \sin 2\theta_i} \tag{5.18}$$

In the linear elastic domain the shear stress according to Hooke's law is given by the following relation:

$$\tau = \frac{T}{A} = G\gamma \tag{5.19}$$

where A is the sample nominal area and G is the out-of-plane shear modulus. Combining equation 5.18 and 5.19, it is possible to obtain an expression for the core shear modulus:

$$G = G(\gamma) = \frac{2K}{Ah} \frac{\cos^2 \theta_i}{1 - \frac{1}{2}\gamma \sin 2\theta_i} \tag{5.20}$$

The shear strain in the elastic region satisfies the following condition (table 5.3):

$$\gamma << 1 \tag{5.21}$$

which yields a simpler expression for the shear modulus:

$$G \cong \frac{2K}{Ah} \cos^2 \theta_i \tag{5.22}$$

This equation, together with the number of counteracting pins N in the core, allows the determination of the constant of rigidity of the rotational springs. Equation 5.22 allows the assignment of a sensible value to a parameter (k) input of the FE model, depending on the experimental evaluation of the out-of-plane shear modulus and core characteristics.

5.3.2 Unit cell FE model

A methodology for creating a complete and realistic unit cell FE model for a pinned core sandwich material is presented. General guidelines are given, although the model developed is specific for the out-of-plane shear behaviour of *X-Cor*$^{F}_{S}$*/0.51/30°/0.13*. The challenge is to build up a model which can take into account all the different material components and their relative interactions. In this way it could be suitable for more advanced simulations than the analysis presented here, represented essentially the material elastic response. The two commercial software packages used for the analysis are: MSC NASTRAN as a processor and EDS FEMAP as a pre / post-processor.

Basic assumptions in the FE unit cell model:

1. Only the counteracting pins are carrying the load. In this way continuity with the analytical model is guaranteed. This allows the values of the constant of rigidity K of the rotational springs previously determined to be used. Their stiffness value will characterise the spring elements located at the end of the pins in the FE model.

2. Perfect congruency at foam-skin and foam-pin interfaces. In reality there is contact at the foam boundaries with the other constituents of the core; this simplification puts the foam core in the worst possible case for deformation. A non critical shear strain/stress field obtained at the end of the elastic phase can be a further indicator that the linear response is set only by the pin-skin interface behaviour.

3. Rigid skins as for the analytical model. They essentially transmit the load to the pins.

Other simplifications adopted in the model are explained throughout the next sections.

5.3.2.1 Unit cell identification in the X-Cor$^{F}_{S}$*/0.51/30°/0.13*

The first step for building a unit cell model is its identification in the material core. Section 3.2.1 has fully described a unit cell recognition in a hollow K-Cor, where it was possible to unequivocally distinguish it, thanks to a low pin areal density. For the *X-Cor$^{F}_{S}$ /0.51/30°/0.13* the process of identification is more complicated. The core is characterised by a higher pin areal density (0.130 pin/mm^2) and figure 5.27 clearly suggests that from a top view similar pins overlap.

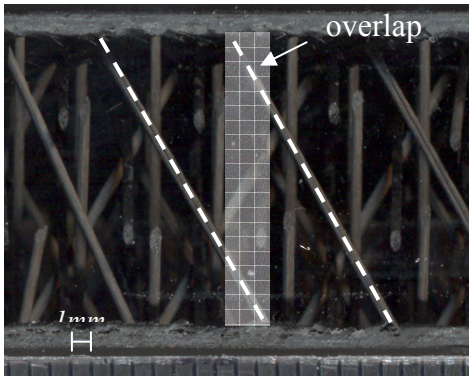

Figure 5.27- *Hollow configuration of the same core (X-Cor$^{H}_{S}$/0.51/30°/0.13)*

Consequently the smallest repetitive pattern of the core is characterised by the presence of partial pins at its borders. In order to define a unit cell, two different strategies can be adopted. The first one is based on considering only entire pins; this means combining the two corresponding parts at the boundaries to make one single pin. The advantage is dealing only with entire pins, but the unit cell in this way occupies a larger volume and to build up the core structure overlapping is necessary. The second strategy is based on a more rigorous definition of unit cell, allowing the presence of partial border pins. To evaluate the foam behaviour and benefit from symmetries, allocation of that correct portion of core to each single unit cell is required. This is adopted in the FE model, because translations of the base unit along two perpendicular directions build up the whole core structure without further complications from superimpositions. The correct portion of foam is in fact associated to each unit cell. In this analysis the interaction between each pin and the corresponding volume of foam can give a better insight on the role of the foam in the shear behaviour. The complications derived from the partial pins at the borders are addressed and presented in section 5.3.2.2. After having identified the pins belonging to a unit cell, the next step is to establish their functions and determine their exact positions. If we refer to the convention on pin positioning (pin insertion angle θ_i and plane direction) previously used and indicated in figure 5.20, it is possible to visualise clearly their functions within a unit cell. Figure 5.28 shows in red the counteracting, load carrying pins and in blue the pins inserted with a negative θ_i along planes parallel to the load direction. The yellow pins are those inserted perpendicularly to the direction of the applied load (Appendix A for a more detailed unit cell model).

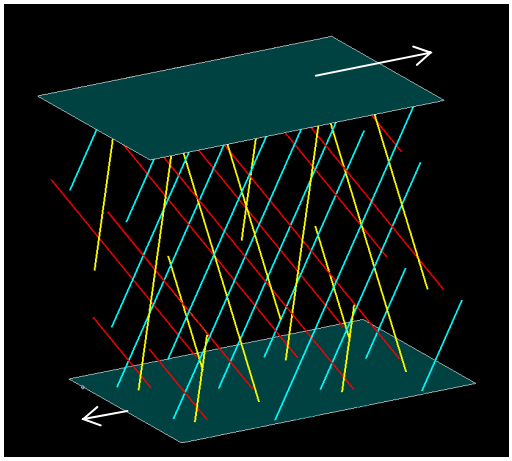

Figure 5.28- *Hollow X-Cor$^{F}_{S}$ /0.51/30°/0.13 unit cell. Pin functions are indicated with colours: red–counteracting pins; blue/yellow–non counteracting*

From figure 5.28 the partial pins at the boundaries are also evident. A top and lateral view of the unit cell schematic shows the positioning of the pins a well as their types (figures 5.29 and 5.30) together with some significant dimensions. The same colour convention as in figure 5.28 is used for pin functions.

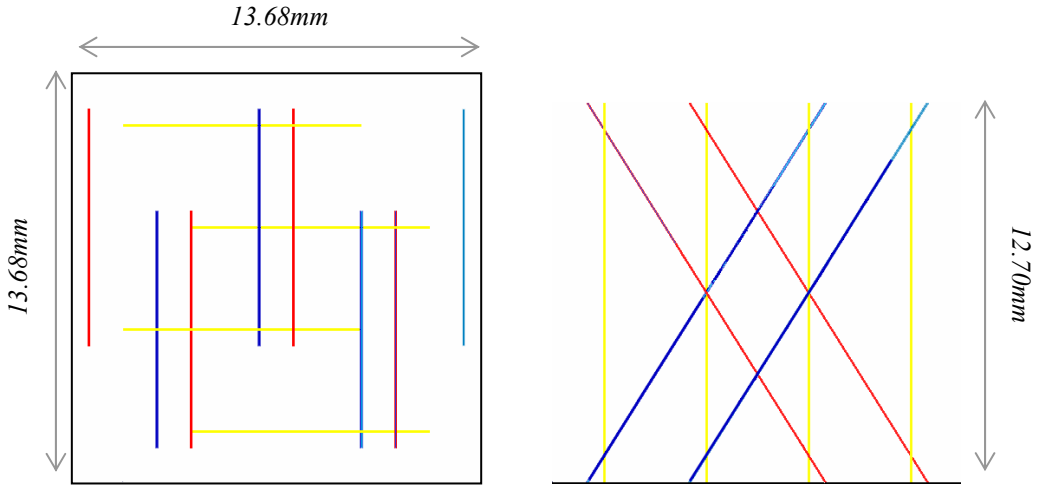

Figure 5.29- *Hollow X-Cor$^{F}_{S}$/0.51/30°/0.13 unit cell: entire pins*

Figure 5.29 shows complete pins, while figure 5.30 shows the border pins belonging to the unit cell.

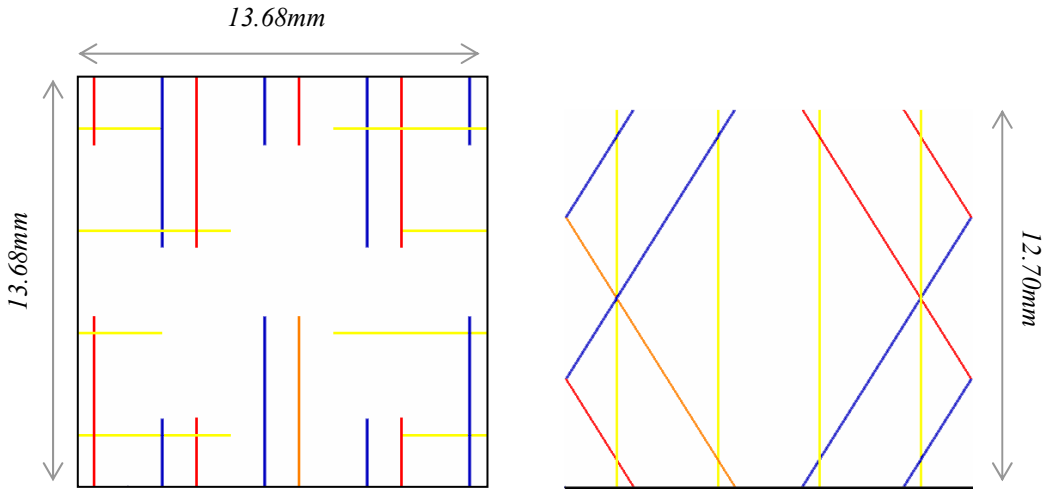

Figure 5.30– *Hollow X-Cor$^{F}_{S}$/0.51/30°/0.13 unit cell: partial (boundary) pins*

5.3.2.2 Building the unit cell FE model: elements evaluation

The materials utilised and the properties of the elements which make up the meshed unit cell are briefly summarised in table 5.6.

	material	*element*	*Nastran element type*
pin	*T300/BMI*	*beam*	*CBEAM*
foam	*Rohacell 31IG*	*solid*	*CHEXA*
skin	*rigid*	*plate*	*CQUAD4*

Table 5.6- *Materials and elements used in the FE model (for detailed element properties refer to [145]*

Foam and pin elements

A crucial aspect in building a unit cell model of a pinned sandwich structure is choosing the dimensions of the elements which constitute the core mesh. Their interactions are established by connecting nodes shared by more than one element. For this purpose the extent of each foam solid block is a compromise between the exact ratio of its

dimensions and the length of the beam elements which make up a pin. This has to be divided into an entire number of elements characterised by a length coinciding with the face diagonal of the foam brick (figure 5.31).

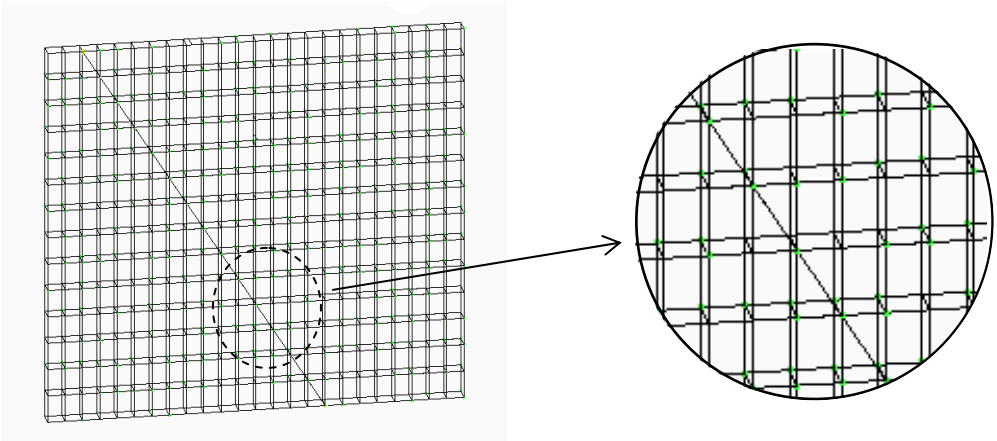

Figure 5.31– *Foam layer and pin taken from the unit cell model. Each node on the beam element is shared between eight foam solid elements*

This constitutes a limitation of this approach: if material geometrical parameters are changed, the unit cell model needs to be redeveloped.

Counteracting pins

In the case of a counteracting pin there is a spring element which regulates the rotational constraint in the direction of the applied load. This element connects the node at the pin head with the corresponding node located on the skin (coinciding but distinct nodes). This rotational spring is characterised by the stiffness value determined with the analytical model previously described (eq. 5.22). Experimentally the counteracting pins remain in the same location inside the skin, even after the interface collapses for the whole deformation process. This creates the condition for continuous pin rotation and consequently for the increasing relative distance of the skins. In the model this particular behaviour is simulated by the use of two additional extensional springs used as rigid connections. They anchor pin tip node to the skin, fixing the parallel and perpendicular translations with respect to the load direction. Table 5.7 summarises these FE elements used.

	stiffness	*element*	*Nastran element type*
Rotational spring Rx	*77000 Nmm*	*DOF spring*	*CELAS2*
Extensional spring Ty	*10^8 N/mm*	*DOF spring*	*CELAS2*
Extensional spring Tz	*10^8 N/mm*	*DOF spring*	*CELAS2*

Table 5.7- *List of the FE spring elements used [145]*

Non-counteracting pins

The node at the tips of the non counteracting pins is not connected with the corresponding skin node. In this way the load is not transmitted to them as it was assumed in the analytical model. Their presence is justified by the fact that in a realistic situation all the pins contribute in further stiffening of the foam. Their flexural stiffness is added to the shear rigidity of the foam core.

Border partial pins

According to their functions in the unit cell, the border partial pins are treated as the others when it comes to linking them to the skins. Each partial pin has on the opposite side of the cell the corresponding missing part, thanks to the core repetitive pattern as shown previously in figures 5.28 and 5.30. The model needs to guarantee that they interact within the single unit cell as if there were adjacent cells, assuring core continuity. This is achieved by connecting the extreme nodes of the two related pin parts with a rigid element which fixes the homologous translations and rotations (the six degrees of freedom). In this way the same displacements and rotations are imposed on the two correspondent parts as if it was one continuous pin. Figure 5.32 shows the partial counteracting pins in one unit cell connected with rigid elements.

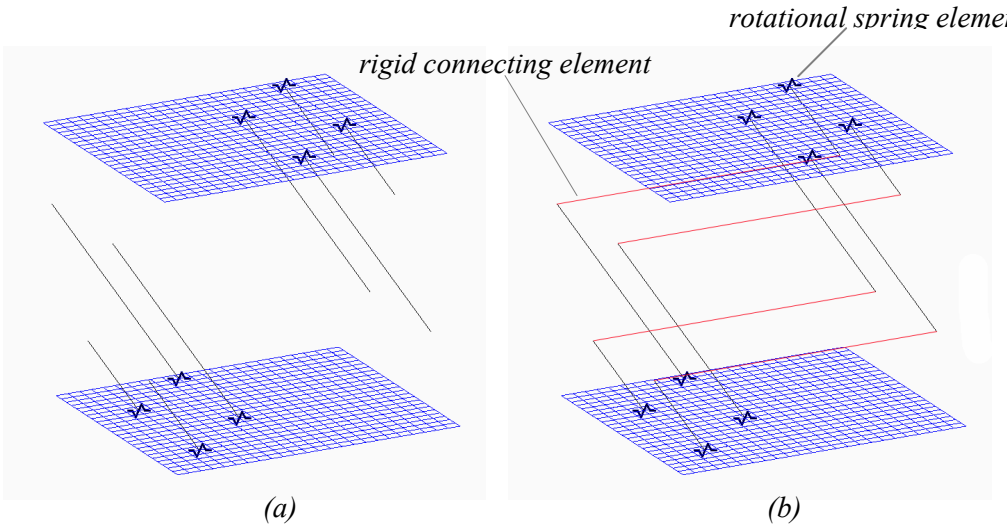

Figure 5.32– *Border counteracting pins in a unit cell (a). Rigid beam connecting elements (in red, (b)) are employed to fix the relative degrees of freedom between the two parts of each pin*

Skins

As mentioned at the beginning of this section the skins, which do not take part in the deformation process, are seen simply as means to distribute the load and to guarantee core integrity. This justifies the choice of a rigid material in the FE model. Their element dimensions coincide with the top and bottom faces of the foam solid element.

5.3.2.3 Unit cell constraints and boundaries conditions

One unit cell is representative of the whole core behaviour; this means that it needs to be restrained in such a way that at its boundaries the same interactions with the adjacent unit cells, as in the real case, are recreated. Figure 5.33 shows a unit cell surrounded by the immediate neighbouring cells from a top view of the core and the constraints acting on the nodes of the foam elements located on the lateral faces.

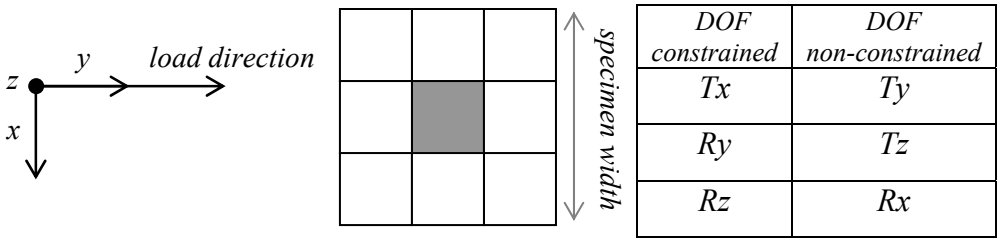

DOF constrained	DOF non-constrained
Tx	Ty
Ry	Tz
Rz	Rx

Figure 5.33– *Summary of constraints acting on the unit cell model*

The skins are glued on the metal fixtures which allow only few movements to be performed; therefore the same degrees of freedom are fixed. The allowed translations are along the y and z axes. Same constraints are obviously applied to the nodes of the top and bottom faces of the solid foam elements coinciding with the skins. The only constraint acting on the pins is that they are pinned at their middle node, defining a centre of rotation for each pin.

5.3.2.4 Unit cell loading condition

The condition of pure out-of-plane shear for the FE simulation is achieved by determining the corresponding load acting on each node of the unit cell considered. The force is considered uniformly transmitted from the steel plates to the skins and it is divided by the total number of cells (46) belonging to a sample and by the total number of nodes (576) of a single unit cell. Figure 5.34 shows the typical deformation of the unit cell achieved with the boundary and the load conditions applied (for visual convenience the deformation shown has been scaled up).

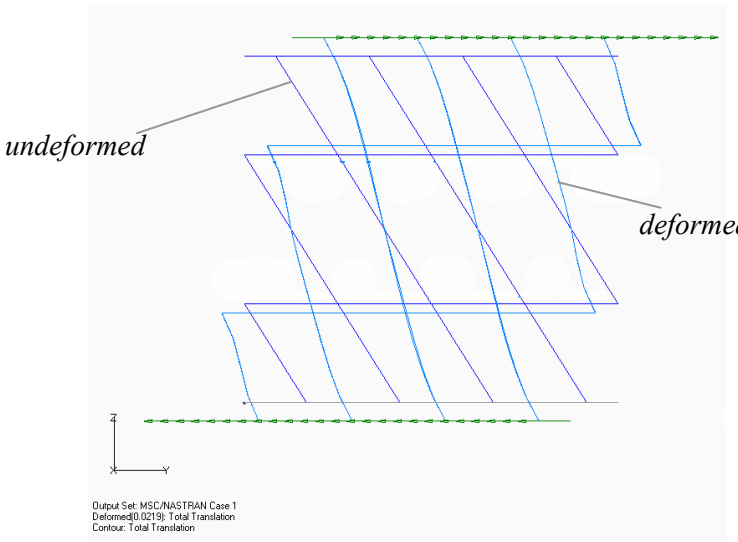

Figure 5.34– *Typical deformation of the X-Cor$^{H}_{S}$/0.51/30°/0.13 unit cell achieved with the boundary and the load conditions applied. Only the load counteracting pins are indicated*

5.3.3 FE simulation and results

Both linear and nonlinear static finite element analyses were performed on the unit cell model. The nonlinear simulation is preferred, because it accounts for material properties that are functions of the state of stress and for damage evolution [146, 147]. This allows the evaluation of both the material stiffness and strength to be performed.

5.3.3.1 Nonlinear FE analysis method

The collapse of the pin-skin interface is recognised as the dominant failure mechanism for a pinned core in a shear loading condition (section 5.2). In reality each counteracting pin is not subjected to the same applied force due to their non-symmetric geometrical distribution with respect to the unit cell barycentre. The consequence is that some interfaces will fail before others and the load will be then re-distributed among the remaining pins, which have to bear higher force values. In the core FE model this means that each pin is subjected to symmetric boundary conditions and non symmetric loads.

As a result in the simulation some rotational spring elements will reach the critical applied moment before others. Once this happens, they need to be discounted from the unit cell. In a linear static analysis the continuous damaging process in the core is not taken into account and the material strength cannot be evaluated. A nonlinear simulation is run in different incremental load steps; at the end of each one, the magnitude of the applied moment in all rotational springs is assessed. The material progressive damage is introduced in the FE model in a discrete way by removing the spring elements. As a result the total stiffness of the unit cell is lowered by a finite quantity each time a pin-skin interface fails. Figure 5.35 shows the idealisation of the method adopted. The linear analysis gives an indication of how a perfect material which maintains an undamaged state behaves; in some cases it may not be the correct approach to predict its performance appropriately. In figure 5.35 the material experimental behaviour is indicated with a continuous black line, while a dotted line shows the predicted performance result of a linear FE analysis. The broken red line represents the simulated material behaviour obtained with a nonlinear FE analysis which accounts for a discrete material damage model.

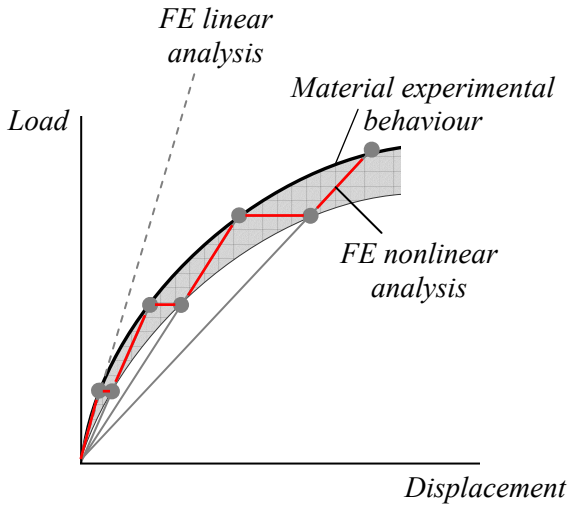

Figure 5.35– *Schematic of material response obtained experimentally as well as with a linear and nonlinear FE analysis. The progressive damage of the pinned core is introduced into the model by removing* rotational *spring elements, which cause a finite decrease in stiffness*

For the nonlinear analysis the value of the critical moment applied at the rotational spring elements is evaluated as a compromise between the material stiffness evolution and the strength value. For this pinned core the critical value is identified at $1.39 Nmm$. It represents the minimum moment applied to a counteracting pin to damage its pin-skin interface. The graph of figure 5.36 shows the agreement between the experimental curve and the curves obtained for the linear and nonlinear FE analysis.

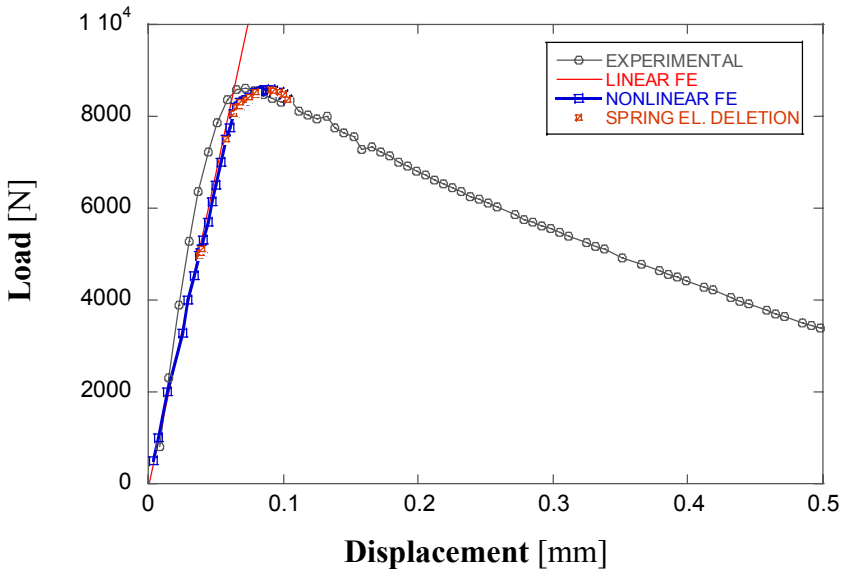

Figure 5.36– *Comparison between experimental values and linear and nonlinear analyses results. The red dots in the nonlinear curve correspond to a* rotational *spring element deletion from the model*

The material behaviour is characterised by a fairly linear response up to a peak value. The consequence is that the stiffness can be predicted also by employing a straightforward linear FE simulation using the unit cell model with all the spring elements. In the nonlinear analysis some elements need to be removed before the peak value; a red point in the graph of figure 5.36 corresponds to each rotational spring element deletion. In the interval between $8000N - 8600N$ the critical conditions are reached simultaneously for all the remaining counteracting pins. At each spring element deletion, the applied load is re-distributed among the remaining pins according to their positions in the unit cell. The loss in stiffness for this approach can be estimated to ~6% compared to the linear FE analysis. The predicted values of out-of-plane shear stiffness determined using the linear and nonlinear FE analysis are summarised in table 5.8.

	Experimental	*Linear FE*	*Nonlinear FE*
Out-of-plane shear stiffness G [MPa]	*341±25*	*283*	*263*
Error %	---	*17%*	*23%*

Table 5.8– *X-Cor^F_S/0.51/30°/0.13 : experimental and predicted values for out-of-plane shear stiffness*

The first elements deletion is at an equivalent load level of $4891N$ for the sample. This corresponds to a load of $106N$ on each unit cell and $0.185N$ applied on each node of the skins. As an example, table 5.9 shows the variation of rotational moments in the spring elements before and after removing those that have reached failure conditions at this load level. The corresponding increment in displacement for the core, under the same applied load, after the removal of the two spring elements is of $8.62E-04mm$ corresponding to a 2% increase with respect to the unit cell with all the pins.

Spring element ID.	*Moment [Nmm]* *-before el. deletion-*	*Moment [Nmm]* *-after el. deletion-*
9705	*7.154E-01*	*7.575E-01*
9706	*6.391E-01*	*6.862E-01*
9707	*5.425E-01*	*5.731E-01*
9708	*6.016E-01*	*6.292E-01*
9709	*6.235E-01*	*6.608E-01*
9710	*7.208E-01*	*7.898E-01*
9711	*6.598E-01*	*6.799E-01*
9712	*5.455E-01*	*6.813E-01*
9713	*7.480E-01*	*8.154E-01*
9714	*1.337E+00*	*1.381E+00*
9715	*7.660E-01*	*9.300E-01*
9716	*1.389E+00*	---
9717	*1.388E+00*	---
9718	*7.625E-01*	*8.363E-01*
9719	*7.230E-01*	*7.831E-01*
9720	*1.321E+00*	*1.366E+00*

Table 5.9– *Moments registered at* rotational *spring elements in X-Cor^F_S /0.51/30°/0.13 unit cell model; the applied load level is 106N in out-of-plane shear condition (it corresponds to 4981N for the tested specimens)*

Figure 5.37 shows the displacement map of a lateral section of the unit cell at peak load. In the nonlinear analysis this corresponds to $8585N$ ($\sim 187N$ applied on each unit cell) and to a total relative displacement between the two skins of $0.0909mm$. For visual convenience the deformations of the model of figure 5.37 have been scaled up to 5% of their actual values. It is worth noting the relative increasing distance between the skins during the test.

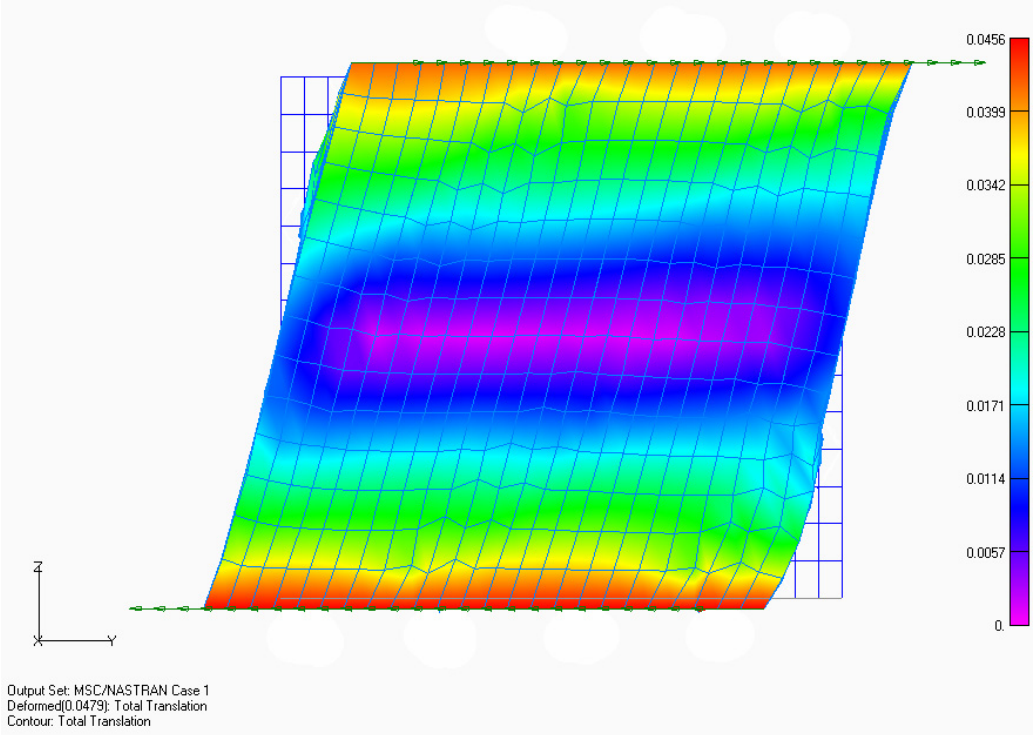

Figure 5.37– *Total translation of the unit cell at peak load (8585N). Deformations of the unit cell model drawing are scaled up 5% of their actual value*

As previously mentioned, the FE analysis allows considerations on the shear stress / strain field to be made. The displacements (figure 5.37) and the strain values achieved at peak load are not critical for the foam core. For this particular foam system (Rohacell® 31IG, section 3.3.4) the value which corresponds to the material shear failure would be of $\sim 0.38mm$, more than three times the core displacement reached by the sample at peak load. The shear stress field in the foam is evaluated along the YZ direction ($\tau_{yz} = \tau_{zy}$) since it is the most critical out-of-plane direction for this case. In fact the load application along the y axis, the constraints imposed by the testing fixture and by the presence of other unit cells prevents movements on the x direction. Figure 5.38 shows

the YZ shear stress field onto a foam layer surrounding, load counteracting pins, sliced from the central part of the unit cell. The foam shear strength is $0.6MPa$. The maximum shear stress concentration is around the pin tips and reaches values of $\sim 0.2MPa$.

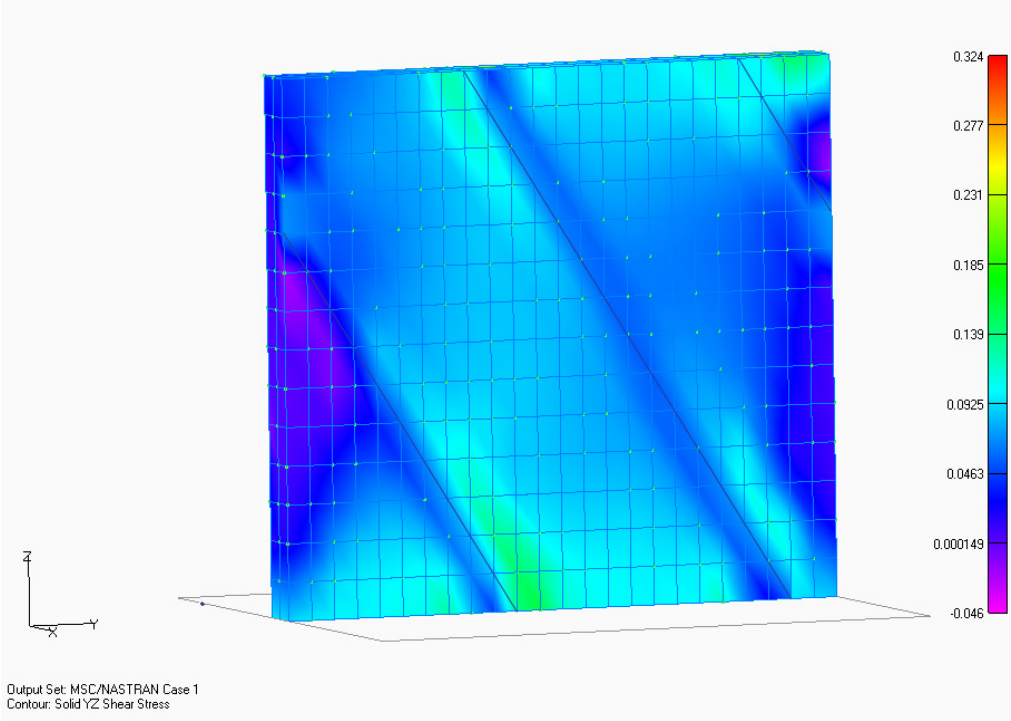

Figure 5.38– *YZ shear stress (maximum element value) in solid foam elements belonging to two central layers in the unit cell model. The corresponding counteracting pins are also indicated*

In addition, the foam core considered in the FE model has perfect congruency with the skin and pins as they share the same nodes. In reality there is a contact interface. This means that the probable strain / stress field experienced by the foam is even lower than the predicted one. In fact, the same displacement at the contact interfaces is not guaranteed (for X-Cor structures).

5.3.4 Errors in predicted stiffness values: analysis and model improvement suggestions

It is evident that both the linear and nonlinear predicted stiffnesses underestimate the experimental material value. This difference is most likely dependent on the approach

followed. The assumptions made are considered to represent an effective compromise between the complexity of the core and its mechanical response with the necessity to produce straightforward and manageable models. Three fundamental assumptions were made on:

- Load carrying pin type
- Shear force distribution
- Pin and skin rigidity

The counteracting pins are considered to characterise the out-of-plane shear behaviour (section 5.2). For this reason they are considered as the only load carrying pins in both the analytical and the FE models (sections 5.3.1 and 5.3.2). In a real core all the pin types as well as each component of the material contribute to the overall mechanical performance. All of the contributions are accounted in the out-of-plane shear stiffness G, experimentally determined, which characterises the core behaviour as a unity. The constant of rigidity of the rotational springs used in the modelled core is determined directly from this shear stiffness, allowing in this way the counteracting pins to characterise the entire core behaviour. The fundamental relation (equation 5.22) of the analytical model is obtained assuming that the shear force is equally distributed among the counteracting pins. This allows a straightforward approach, a single pin can be taken into consideration, assuming all the others to be in the same condition.

The assumption of pin rigidity, made in the analytical model, implies that the deformability is related only to the linking element (springs) at pin ends. In reality, pin deformation may have a non-negligible effect, which could be considered. A possible solution could be to adopt an analytical model based on a non-rigid pin, which takes into account for pin deformation caused by the applied shear loading. In this case the spring constant of rigidity should have higher values in order to produce a stiffer linear response. A simple evaluation of a non-rigid pin model approach is presented in Appendix A.

In the approach followed, the non-counteracting pins are assumed not to carry any load and not to contribute to the core rigidity. A more complete model could be based on

both pin types playing a role in the carrying of load for the initial shear stiffness. A consequent beneficial effect would be also to have a more realistic load distribution on each pin. An experimental characterisation of the pull-out mechanism for the pins should be also considered.

5.3.4.1 Unit cell model as a material configuration improvement tool

It is still premature to say if the unit cell approach followed for the finite element analysis could be used successfully as a material improvement tool. The two critical quantities for the spring elements (rigidity *k* and critical moment *Mc*) are still to be determined, at this stage, for each case. A set of tests is required to validate the FE results for a series of configurations developed from a basic core structure. This will contribute to the establishment of a series of trends on the variability and errors of the predictions and would allow to extend the use of the parameters (*k* and *Mc*) determined for a basic core to a comprehensive number of similar structures. At the moment the FE model can be used for material improvement only as a tool for optimising pin positioning. This is based on the evaluation of shear force distribution without involving realistic predictions on mechanical performance. In fact, the core with the most even force distribution on the pins will be able to withstand the highest applied external forces before critical conditions are reached at each pin interface and consequent load re-distribution takes place. It could be a useful tool in supporting a qualitative analysis in the selection process of improved core configurations. This analysis should be followed by experimental verification.

5.4 Chapter summary

1. The mechanical performance of different types of pinned cores and a competitor honeycomb material (Nomex®), chosen for its similar core density, has been assessed in out-of-plane shear loading. The tests were performed according to ASTM C 273 standard.

2. The pinned core sandwich structures (K-Cor and 'standard' X-Cor), compared to a traditional honeycomb (Nomex), have shown a significantly higher rigidity (2 to 4 times), but lower strength values (~50%) and energy absorption properties (~30%). A K-Cor structure outperforms a 'standard' X-Cor in terms of strength (+30%) and energy absorption (+60%) on the basis of similar core properties (foam and pin material properties, pin insertion angle and areal density).

3. The 'improved' X-Cor manufacturing procedure significantly enhances the out-of-plane shear mechanical properties of these constructions. A higher level of performance than the corresponding K-Cor structures is achieved. The core shear strength value achieved is the same as for the Nomex sandwich structure (~2.2MPa) and the difference in energy absorption between the two constructions is reduced from 80% to 45% (evaluated up to a shear strain value of 0.2). The rigidity is higher for the 'improved' X-Cor (241MPa versus 75MPa) in addition to a 25% core weight saving.

4. The role of the foam appears to be negligible in the linear response of the material where the shear load applied to the X/K-Cor specimens is essentially carried by the pins. The foam enhances the energy absorption properties particularly in the post-elastic phase. This would allow a potential ~40% core weight saving to be achieved with the hollow configuration, whilst maintaining the same mechanical performance.

5. The pin insertion angle strongly influences the mechanical performance. The cores with the highest pin insertion angle (measured from the vertical direction) achieve the best values of rigidity and strength. A 10° variation in pin insertion angle significantly affects the shear stiffness of the sandwich construction, which for the tested cores increases from 200±25 MPa ((S)X-Cor$^{F}_{S}$/0.51/22°/0.13) to 341±25 MPa for the (S)X-Cor$^{F}_{S}$/0.51/30°/0.13 samples.

6. For the Nomex® specimens core failure is determined by the buckling of the honeycomb cell walls, whilst a skin-core interface failure mechanism is typical for the pinned samples as well as for the foam core specimens. In particular for both X-Cor and K-Cor, the shear strength is determined by the properties of the interface, located at the

pin end, either in the adhesive film (K-Cor) or in the skin (X-Cor). The most evident common feature for both the pinned core types is an increasing skin separation due to pin rotation during out-of-plane shear loading. This is due to the way pins are inserted counteracting the applied load. The non-counteracting pins are instead subjected to a pull-out from their original positions.

7. In K-Cor structures the foam damage, essentially relevant in the post-elastic phase, is localised at the adhesive film interface. In X-Cor structures it is spread more throughout the whole sample volume.

8. An analytical model based on simplified pin geometry for X-Cor structures is proposed for a first evaluation of the effect of pin parameters in the mechanical performance. The pin insertion angle is shown to play an important role, confirming the experimental findings. A closer to vertical insertion angle results in cores characterized by lower shear properties. Also a longer pin reveal length is beneficial to the interface properties and consequently to the core mechanical behaviour.

9. A general FE modelling strategy for both X/K-Cor is presented for simulating the linear elastic response (stiffness and strength) in out-of-plane shear loading. A local-global approach is followed and it is based on a unit cell model, tailored for each core analysed. The FE model development for one type of the X-Cors analysed, (S)X-Cor$^{F}_{S}$ /0.51/30°/0.13, is shown in detail. The FE analysis is supported by an analytical model for the out-of-plane shear loading which provides the input parameters for the unit cell. It relates the pin rotational end constraints (interface properties) to the constant of rigidity of rotational springs placed at the end of a pin seen theoretically as a column. The predicted values obtained with both a linear and non-linear analysis underestimate the experimental shear rigidity (17% and 23% respectively). The material strength predicting using a non linear analysis corresponds to a critical value of 1.39Nmm of the rotational moment applied at each pin-skin interface.

Chapter 6

Out-of-plane compression

In this chapter the out-of-plane compression behaviour of X-Cor and K-Cor sandwich structures along with the influence of core and manufacturing parameters on their mechanical performance is investigated and compared with that of competitor honeycombs (sections 6.1 and 6.2). A failure analysis is also carried out in section 6.2. An analytical model to evaluate the pin-end rotational constraint is proposed (section 6.3) and used to further analyse the experimental results.

6.1 Test results

Out-of-plane compression tests were performed according to the ASTM C 365 standard on different materials systems with the following main objectives:

- Test X-Cor and K-Cor samples in different configurations and assess their performance as function of the following core parameters: presence of the foam, pin insertion angle and pin areal density
- Compare their performance with the out-of-plane mechanical properties of competitor sandwich materials chosen on the basis of similar core density and/or expected performance ((Nomex® and Al honeycomb samples)
- Evaluate the eventual benefits deriving from the X-Cor 'improved' manufacturing technique

The details of the test method used, including the procedures, the data analysis employed and the testing equipment can be found in Ch. 4. Table 6.1 shows both the nominal and the effective values of some of the principal sample characteristics as well as the number of tests for each core configuration. This compression test is designed

specifically for the characterisation of core material properties in the out-of-plane direction. All the cores were tested as part of a sandwich construction. Skins and adhesive films (if necessary), apart from transmitting the load from the fixture to the core, constitute the interfacial materials; in this respect they play an important role in the overall mechanical performance. The complete material specifications and the manufacturing procedures used can be found in Ch. 3.

sample type identification	*no. tests*	*core density [kg/m^3]*		*pin areal density [pin/mm^2]*		*pin insertion angle θ_i*		*foam type*	*manufact. procedure*
		nom	*Eff*	*nom*	*eff*	*nom*	*eff*		
(C)X-Cor^F_S/0.51/22°/0.13	5	~64	72.6±0.1	0.130	0.106	22°	22°	31 IG	standard
(C)X-Cor^H_S/0.51/22°/0.13	5	~32	41.4±0.1	0.130	0.106	22°	22°	--	standard
(C)X-Cor^F_S/0.51/30°/0.13	5	~64	68.9±0.1	0.130	0.101	30°	32°	31 IG	standard
(C)K-Cor^F/0.51/30°/0.10	5	~64	66.8±0.1	0.100	0.079	30°	32°	31 IG	
(C)K-Cor^H/0.51/30°/0.10	5		34.3±0.1	0.100	0.079	30°	32°	--	
(C)X-Cor^F_I/0.51/33°/0.06	5	--	52.5±0.1	0.062	0.050	33°	33°	21 IG	improved
(C)X-Cor^H_I/0.51/33°/0.06	5	--	29.9±0.1	0.062	0.050	33°	33°	--	improved
(C)K-Cor^F/0.51/33°/0.06	5	--	52.5±0.1	0.062	0.050	33°	33°	21 IG	
(C)K-Cor^H/0.51/33°/0.06	5	--	29.9±0.1	0.062	0.050	33°	33°	--	
(C) X-Cor^F_I/0.51/11°/0.06	5	--	48.2±0.1	0.062	0.055	11°	11°	21 IG	improved
(C) X-Cor^H_I/0.51/11°/0.06	5	--	25.6±0.1	0.062	0.055	11°	11°	--	improved
(C)K-Cor^F/0.51/11°/0.06	5	--	48.2±0.1	0.062	0.055	11°	11°	21 IG	
(C)K-Cor^H/0.51/11°/0.06	5	--	25.6±0.1	0.062	0.055	11°	11°	--	
(C)X-Cor^F_S/0.25/21°/0.24	5	--	55.3±0.1	0.240	0.192	21°	21°	31IG	standard
(C)X-Cor^H_S/0.25/21°/0.24	5	--	23.7±0.1	0.240	0.192	21°	21°	--	standard
(C)Foam 31 IG	2	--	32.0±0.1					31 IG	
(C)Foam 21 IG	3	--	22.6±0.1					21 IG	
(C)Nomex	5	64	70.7±0.1						
(C)Al honeycomb	3	72	72.0±0.1						

Table 6.1– *Principal characteristics of specimens used in the out-of-plane compression*

The out-of-plane compression mechanical behaviour for the pinned cores characterised by an effective density within the 66-73 kg/m^3 range (nominal value ~64kg/m^3) is initially compared to that of a Nomex® and an Al honeycomb sandwich material with a measured density of 70.7±0.1 kg/m^3 and 72.0±0.1 kg/m^3 respectively. All the X-Cor

samples of this first comparison are manufactured following the 'standard' procedure as reported in section 3.1.2.1. Figure 6.1 shows the stress-strain response for the Nomex® and Al honeycomb samples and for the following specimens: *(C)X-Cor$^{F}_{S}$ /0.51/22°/0.13* *(C)X-Cor$^{F}_{S}$ /0.51/30°/0.13* and *(C)K-Cor^{F} /0.51/30°/0.10*. The graph shows that the Nomex exhibits a lower rigidity, but exceeds the pinned cores response in terms of compression strength as well as energy absorbed (represented by the area underneath the curve) associated to the deformation process. The Al honeycomb specimens exhibit good post-elastic properties due to the plastic deformation of the metal which enhances their energy absorption capability. Among the pinned cores, the K-Cor specimens outperform the two different types of X-Cor produced with the 'standard' manufacturing technique.

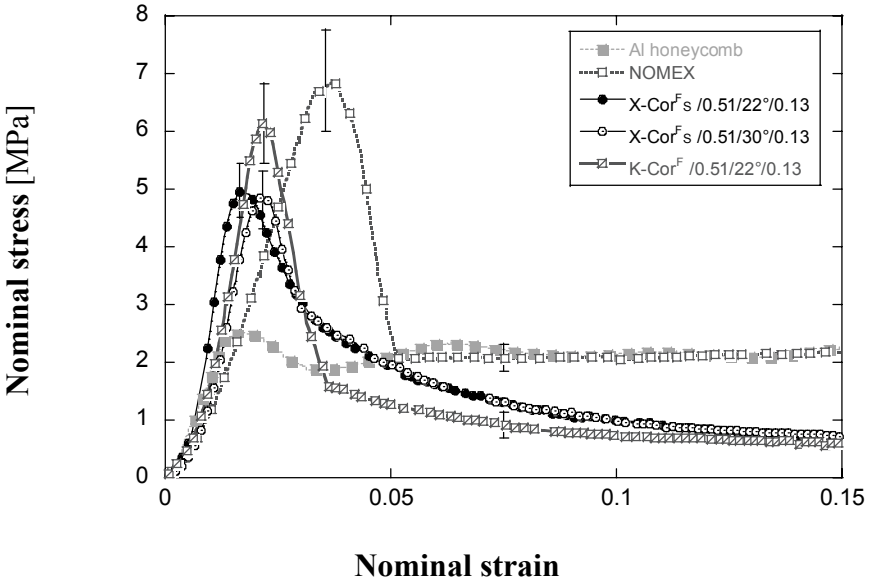

Figure 6.1– *Out-of-plane compression performance comparison between different configurations of pinned core and honeycomb sandwich structures. The X-Cor samples were manufactured using the 'standard' technique*

Figure 6.2 and 6.3 show the role of the foam in the out-of-plane compression loading condition. It significantly enhances the mechanical properties of the pinned cores. In both cases the stress-strain curve for the corresponding foam is also indicated (Rohacell 31 IG). Figure 6.2 shows the performance of a particular X-Cor characterised by a high pin areal density of 0.24 pin/mm^2 (*(C)X-Cor$^{F}_{S}$/0.25/21°/0.24* and *(C)X-Cor$^{H}_{S}$ /0.25/21°/0.24* samples). A more detailed analysis on the performance of this type of X-Cor can be found in section 6.3.5.

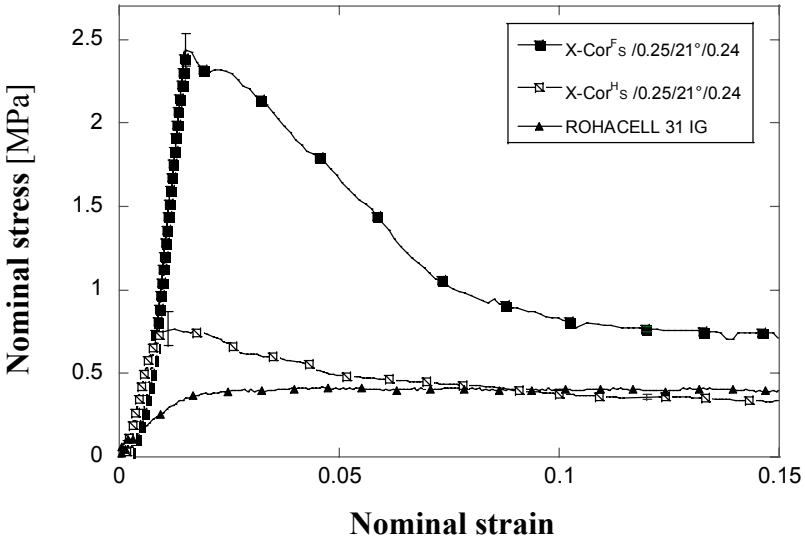

Figure 6.2– *Foam influence on the out-of-plane mechanical performance of similar X-Cor samples*

Figure 6.3 shows the foam influence on the performance of K-Cor samples (*(C)K-Cor^F/0.51/30°/0.10* and *(C)K-Cor^H/0.51/30°/0.10*).

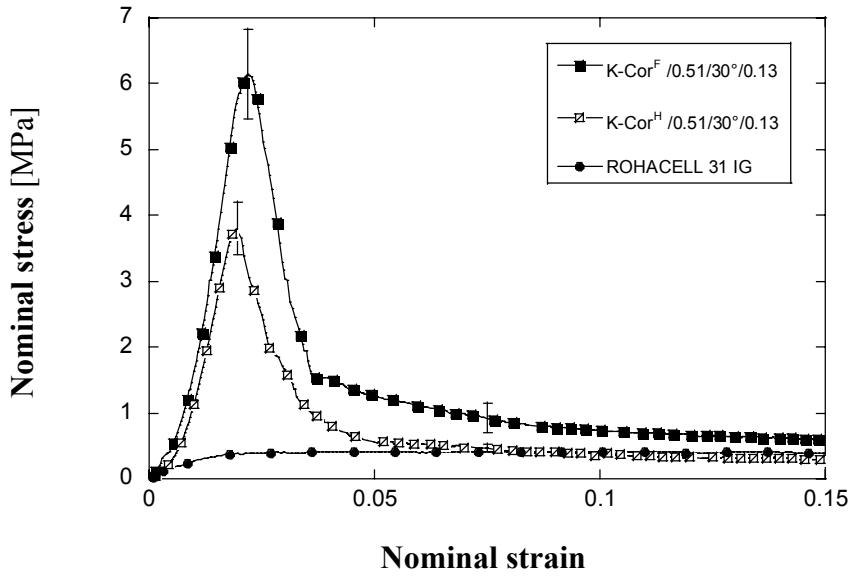

Figure 6.3– *Foam influence on the out-of-plane mechanical performance of similar K-Cor samples*

The difference in performance between K-Cor and X-Cor structures manufactured using the 'improved' procedure is shown in figures 6.4 and 6.5. The effect of the presence of the foam is also investigated. The comparison has been carried out for two core configurations characterised by different pin insertion angles ($\theta_i = 11^\circ$ and $\theta_i = 33^\circ$ respectively). All the other core parameters are kept the same. The 'improved' X-Cor samples show a superior performance with respect to K-Cor structures in all core configurations. Figure 6.4 shows pinned cores characterised by an 11° insertion angle. Those are *(C)X-Cor$^F{}_T$ /0.51/11°/0.06, (C)X-Cor$^H{}_T$ /0.51/11°/0.06, (C)K-Cor^F /0.51/11°/0.06* and *(C)K-Cor^H /0.51/11°/0.06* respectively.

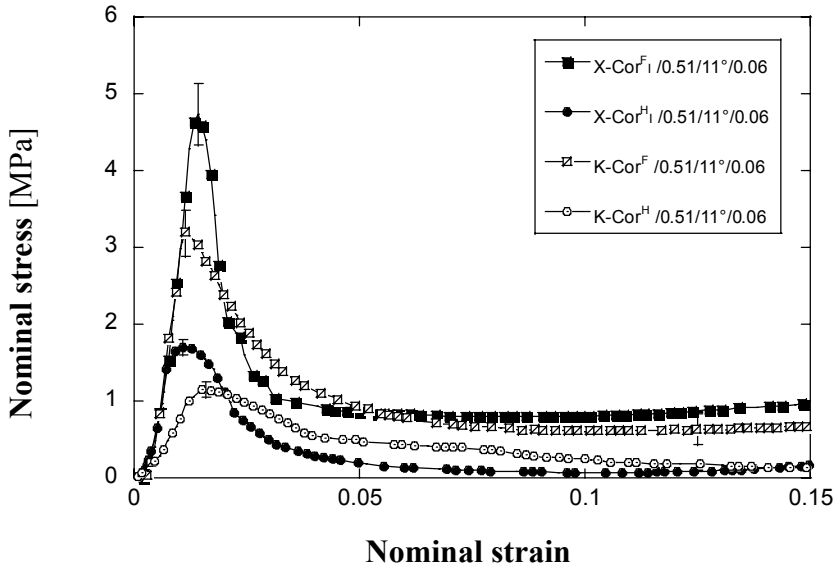

Figure 6.4– *Comparison between 'improved' manufactured X-Cor and K-Cor samples with 11° pin insertion angle and other similar core parameters in both hollow and foam-filled configurations*

It is interesting to notice that thanks to the presence of the foam both pinned core types exhibit an enhancement in strength; the K-Cor samples in particular show a significant increase in stiffness as well. A comparison between pinned cores characterised by a 33° pin insertion angle is shown in figure 6.5. Those are *(C)X-Cor$^F{}_T$ /0.51/33°/0.06, (C)X-Cor$^H{}_T$/0.51/33°/0.06, (C)K-Cor^F /0.51/3°/0.06* and *(C)K-Cor^H /0.51/3°/0.06* respectively.

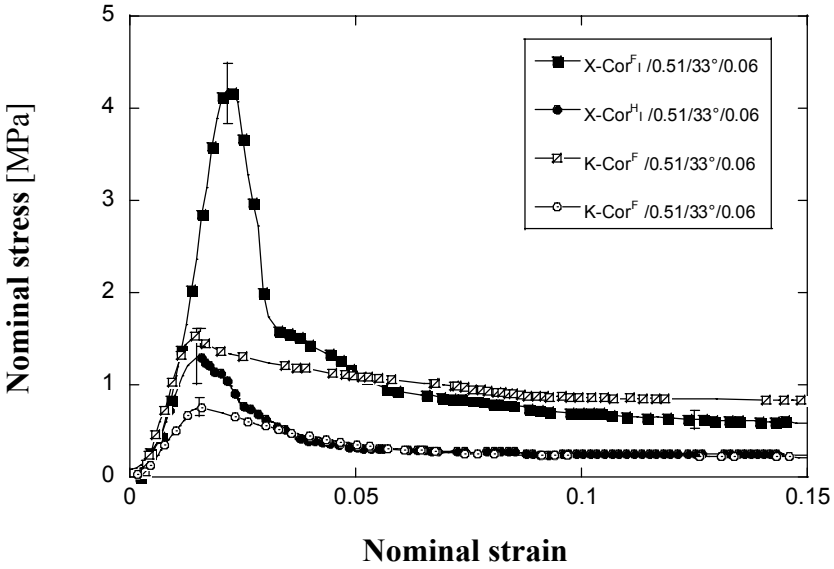

Figure 6.5– *Comparison between 'improved' manufactured X-Cor and K-Cor samples with 33º pin insertion angle and other similar core parameters in both hollow and foam-filled configurations*

The presence of the foam in this case is significantly beneficial for the strength of the X-Cor samples. Figures 6.6 and 6.7 show the influence of the pin insertion angle (11º and 33º) on the out-of-plane compressive mechanical performance for both pinned core types. Specimens in the hollow configuration are also taken into consideration.

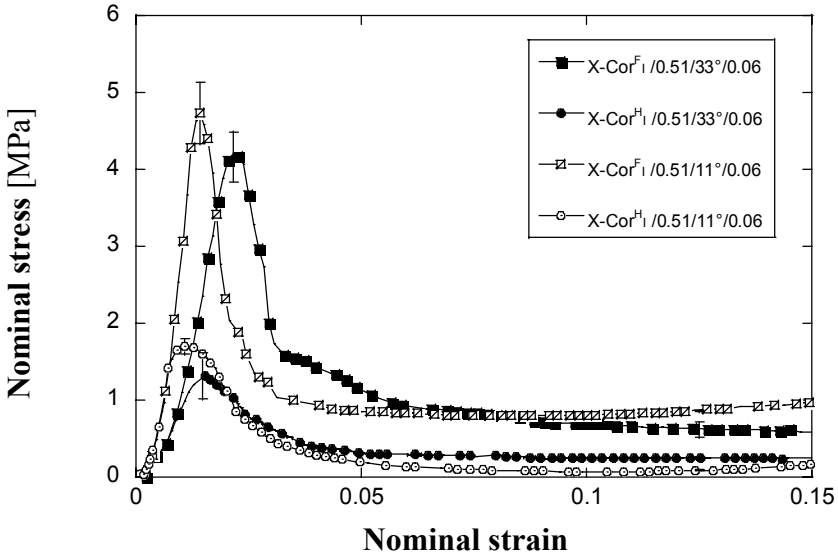

Figure 6.6– *Comparison between hollow and foam-filled X-Cor samples for two different pin insertion angles (11º and 33º)*

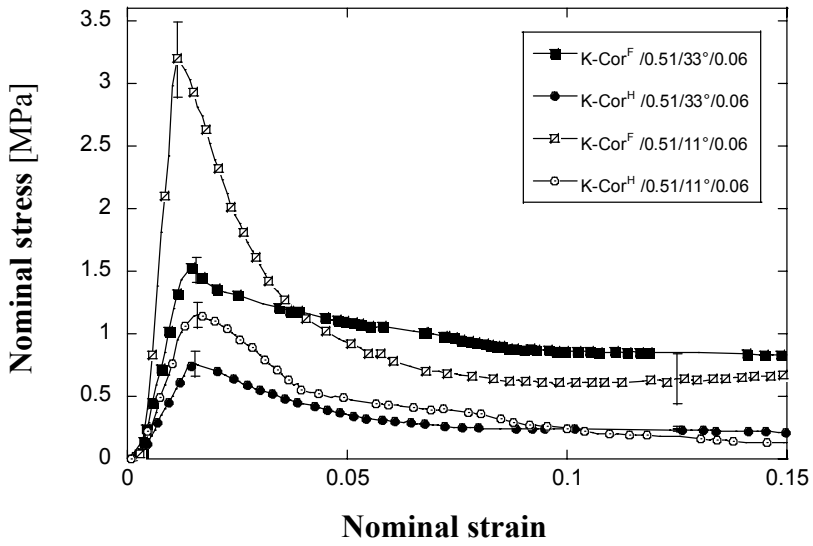

Figure 6.7– *Comparison between hollow and foam-filled K-Cor samples for two different pin insertion angles (11° and 33°)*

It is evident from the graphs, that the cores with a smaller pin insertion angle (with respect to the vertical direction) show a better out-of-plane compression performance in terms of strength and stiffness for both pinned core configurations. As a general result the mechanical performance in terms of strength and stiffness was also found to be proportional to the pin areal density. All the experimental findings are summarised in table 6.2. Considerations regarding the energy absorbing capacity for the pinned cores in out-of-plane compressive loading conditions can be found in section 7.6.1.

sample type identification	*core density [kg/m³]*	*pin areal density [pin/mm²]*		*foam type*	*manufact. procedure*	*out-of-plane compression strength [MPa]*	*out-of-plane compression stiffness [MPa]*
	eff	*nom*	*eff*				
(C)X-Cor$^{F}_{S}$/0.51/22°/0.13	*72.6±0.1*	*0.130*	*0.106*	*31 IG*	*standard*	*5.0±0.5*	*508±51*
(C)X-Cor$^{H}_{S}$/0.51/22°/0.13	*41.4±0.1*	*0.130*	*0.106*	*--*	*standard*	*4.2±0.7*	*403±83*
(C)X-Cor$^{F}_{S}$/0.51/30°/0.13	*68.9±0.1*	*0.130*	*0.101*	*31 IG*	*standard*	*4.8±0.6*	*428±40*
(C)K-Cor^{F}/0.51/30°/0.10	*66.8±0.1*	*0.100*	*0.079*	*31 IG*		*6.1±0.6*	*441±83*
(C)K-Cor^{H}/0.51/30°/0.10	*34.3±0.1*	*0.100*	*0.079*	*--*		*3.8±0.4*	*338±37*
(C)X-Cor$^{F}_{I}$/0.51/33°/0.06	*52.5±0.1*	*0.062*	*0.050*	*21 IG*	*improved*	*4.2±0.3*	*297±16*
(C)X-Cor$^{H}_{I}$/0.51/33°/0.06	*29.9±0.1*	*0.062*	*0.050*	*--*	*improved*	*1.3±0.3*	*133±19*
(C)K-Cor^{F}/0.51/33°/0.06	*52.5±0.1*	*0.062*	*0.050*	*21 IG*		*1.5±0.1*	*159±30*
(C)K-Cor^{H}/0.51/33°/0.06	*29.9±0.1*	*0.062*	*0.050*	*--*		*0.8±0.1*	*65±12*
(C)X-Cor$^{F}_{I}$/0.51/11°/0.06	*48.2±0.1*	*0.062*	*0.055*	*21 IG*	*improved*	*4.7±0.4*	*578±56*
(C)X-Cor$^{H}_{I}$/0.51/11°/0.06	*25.6±0.1*	*0.062*	*0.055*	*--*	*improved*	*1.7±0.1*	*404±51*
(C)K-Cor^{F}/0.51/11°/0.06	*48.2±0.1*	*0.062*	*0.055*	*21 IG*		*3.2±0.3*	*430±54*
(C)K-Cor^{H}/0.51/11°/0.06	*25.6±0.1*	*0.062*	*0.055*	*--*		*1.1±0.1*	*112±17*
(C)X-Cor$^{F}_{S}$/0.25/21°/0.24	*55.3±0.1*	*0.240*	*0.192*	*31IG*	*standard*	*2.4±0.1*	*264±30*
(C)X-Cor$^{H}_{S}$/0.25/21°/0.24	*23.7±0.1*	*0.240*	*0.192*	*--*	*standard*	*0.77±0.1*	*105±7*
(C)Foam 31 IG	*32.0±0.1*			*31 IG*		*0.4±0.1*	*21±1*
(C)Foam 21 IG	*22.6±0.1*			*21 IG*		*0.2±0.1*	*9±1*
(C)Nomex	*70.7±0.1*					*6.9±0.9*	*257±48*
(C)Al honeycomb	*72.0±0.1*					*2.5±0.1*	*198±10*

Table 6.2– *Experimental results and principal core characteristics*

6.2 Failure analysis and performance evaluation

6.2.1 Dominant failure mode

The behaviour exhibited by both the X-Cor and K-Cor in the configurations with and without foam is indicative of a buckling failure mechanism. This was observed in the testing phase (figure 6.8) and also confirmed by the stress-strain curves of the graphs of section 6.1.

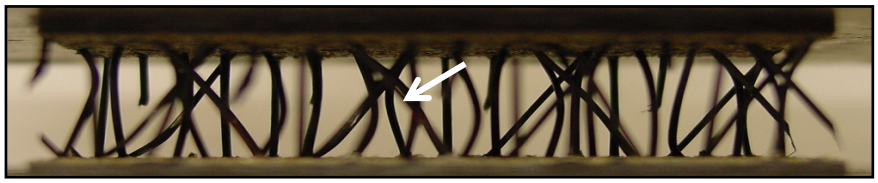

Figure 6.8– *Hollow K-Cor specimen under out-of-plane compressive loading. Sample characterised by very low pin areal density (0.040pin/mm^2), 22° pin insertion angle and 0.51mm pin diameter (preliminary tests)*

After an initial linear increase in the stress, there is a fairly sharp drop, followed by a collapse regime typical of a buckling failure [11]. In figure 6.9, the photographs showing the deformation of part of a unit cell, are related to the corresponding phases of the stress-strain curve; the specimen is a hollow X-Cor specimen (*(C)X-Cor^H_S /0.51/22°/0.13*).

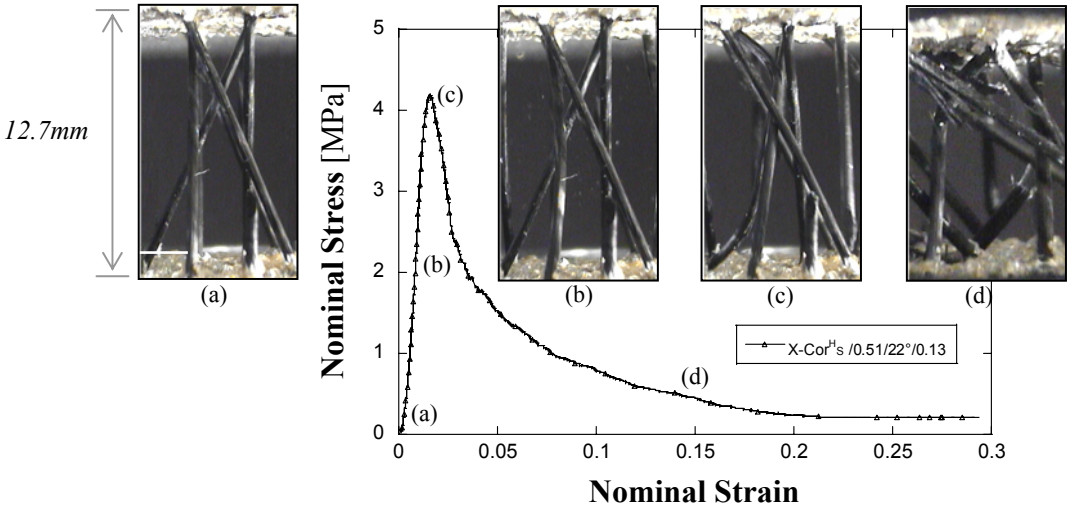

Figure 6.9– *(C)X-Cor^H_S /0.51/22°/0.13: optical microscope observations of pin buckling failure in out-of-plane compression*

Further confirmation of this failure mode can be obtained by comparing the stress value of core failure due only to pin axial compression. Such theoretical approach has been developed initially for a metal truss core sandwich [148]. It is argued that the assumption of a core made of frictionless pin-jointed trusses made from a rigid, ideally plastic material and sandwiched between two rigid skins, constitutes a simplified but adequate approximation for predicting plastic collapse of such core materials. Similarly, reference [11] extends the same assumption to X-Cor constructions made of titanium and carbon fibre pins of similar pin diameter (0.51mm). In the case of carbon pins the axial strength is set by the micro-buckling of the carbon fibres which make up the pultruded composite rods. The compressive strength σ_C for a pinned core according to [11] is:

$$\sigma_C = f\sigma_{1,T}\cos^2\theta_i \tag{6.1}$$

where f is the pin volume fraction (for the *(C)X-Cor^H_S/0.51/22°/0.13* samples is 0.0286), $\sigma_{1,T}$ is the pin elastic limit (1100 MPa, table 3.3) and θ_i the pin insertion angle. For the analysed X-Cor configuration equation 6.1 gives a core compressive strength of $27.0MPa$. The experimentally determined value is of $4.2\pm0.7MPa$. Those values correspond to an axial force acting on each pin of $-192.5N$ and of $-26.6\pm5.0N$ respectively. If a single pin is ideally considered as a simply supported column (shown in figure 6.10), it is possible to obtain the critical axial load by using the Euler formula [149], as follows:

$$N = -\frac{\pi^2 EI}{L^2} \tag{6.2}$$

Figure 6.10– *Pin represented as a simply supported column subjected to an axial load*

In equation 6.2, N is the axial load, E the material Young modulus, I the moment of inertia (for circular cross-section) and L the pin-column length. In the case of the X-Cor analysed (*(C)X-Cor$^{H}_{S}$/0.51/22°/0.13*), it gives the following result:

$$N_{critical} = -20.5N \tag{6.3}$$

The average value ($-26.6N$) experimentally found for the hollow X-Cor is close enough to the predicted value (eq. 6.3) to assume buckling failure.

6.2.2 Role of the foam: general considerations

As seen in section 6.1, specimens containing foam exhibit a significantly higher mechanical response to the applied out-of-plane compression load. There is a clear synergistic effect between the foam and the pins [11, 150]. The strength of the pin reinforced core is increased over and above the sum of the contributions of foam and pins alone. The synergistic strengthening observed increases the critical stress for the elastic buckling of the pins, thanks to the lateral support provided by the foam. The strength appears to be controlled by the onset of the buckling process [150]. Thus the action of the foam can be considered to be mainly in the delaying of the onset of the pin buckling process. In figure 6.11 a final densification region characterised by a rapidly increasing stress is also evident.

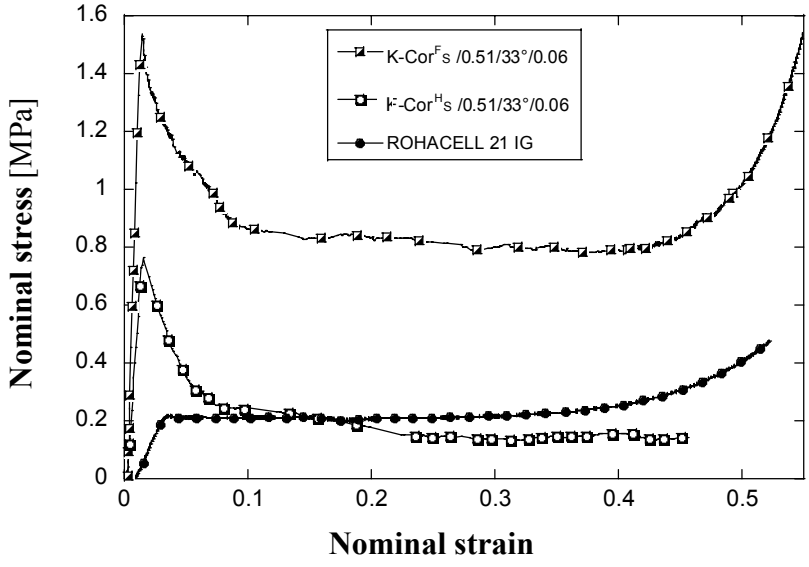

Figure 6.11– *Synergistic effect between foam and pins for K-Cor. Densification region is also evident*

This phenomenon is typical of cores containing foam [151]. Due to scaling reasons it was not visible in the graphs of section 6.1 (it is associated with a higher nominal strain). There is also an enhancement of the out-of-plane compression stiffness as shown in table 6.2 (a more detailed analysis is in section 6.2.4).

6.2.3 Influence of pin insertion angle on mechanical performance

The cores characterised by pins closer to vertical (and consequently by a lower insertion angle θ_i) are associated with the highest mechanical performance in terms of core strength and rigidity in out-of-plane compression loading (table 6.2 and graphs of section 6.1). The external load is introduced in the core perpendicularly with respect to the sandwich skin and it can be decomposed into an axial force acting along the pin and a force perpendicular (or shear**)** to the pin axis. The effect of the latter is to lower the buckling resistance of the pin. Figure 6.12 shows schematically the superimposition of the normal and bending stresses at a pin cross-section due to the two components of the applied force.

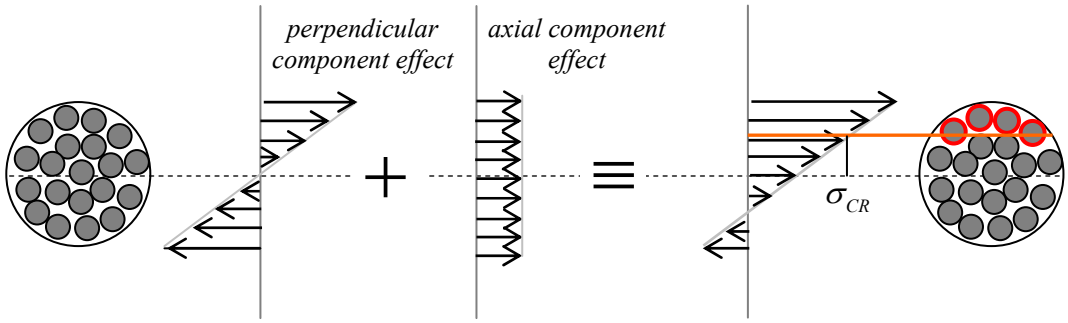

Figure 6.12– *Qualitative compression and tension stress distribution at a pin cross-section due to the axial and shear component of the applied external force*

The resisting section of the pultruded composite pin, and consequently the moment of inertia I (eq. 6.2), is reduced by the premature micro-buckling of the external bundles of fibres, due to the additional compression stresses introduced by the shear component. This effect is related to the pin insertion angle θ_i and its magnitude varies with the sine.

Thus the critical global buckling condition is reached for a lower applied load on the core.

6.2.4 X-Cor and K-Cor performance comparison

The basic idea of this analysis is to compare the benefits obtained by the presence of the foam as a function of pin insertion angle in both X-Cor and K-Cor structures for an out-of-plane compressive loading condition. All the configurations, considered for this analysis, are characterised by identical core parameters (0.062pin/mm^2 pin areal density, 0.51mm pin diameter and Rohacell 21 IG foam) and by two different pin insertion angles (θ_i=11°; 33°), which represent the extremes of the production range for these cores. The increase in performance achieved by the presence of the foam is evaluated in comparison to the hollow configuration. The two mechanical quantities considered are the compression stiffness (E) and the core strength (σ_C). The results are summarised in table 6.3.

	K-Cor		*increase in performance*	*X-Cor*		*increase in performance*
	*K-Cor^H /0.51/**33°**/0.06*	*K-Cor^F /0.51/**33°**/0.06*		*X-Cor$^H{}_I$ /0.51/**33°**/0.06*	*X-Cor$^F{}_I$ /0.51/**33°**/0.06*	
E [MPa]	*65±12*	*159±30*	*145%*	*133±19*	*297±16*	*123%*
σ_C [MPa]	*0.8±0.1*	*1.5±0.1*	*87%*	*1.3±0.3*	*4.2±0.3*	*223%*
	*K-Cor^H /0.51/**11°**/0.06*	*K-Cor^F /0.51/**11°**/0.06*		*X-Cor$^H{}_I$ /0.51/**11°**/0.06*	*X-Cor$^F{}_I$ /0.51/**11°**/0.06*	
E [MPa]	*112±17*	*430±54*	*284%*	*404±51*	*578±56*	*43%*
σ_C [MPa]	*1.1±0.1*	*3.2±0.3*	*191%*	*1.7±0.1*	*4.7±0.4*	*176%*

Table 6.3– *Performance comparison due to the presence of the foam between similar X-Cor and K-Cor samples*

The percentage increase in performance between X-Cor and K-Cor is similar except for the strength corresponding to a pin insertion angle of 33° and for the stiffness when pins are placed at 11°. It was pointed out earlier, that an axial and a shear force act on each

pin, due to its inclination with respect to the direction of the external applied load. For this reason the out-of-plane shear core properties play an important role in this loading case, especially for the case of cores with pins inserted at 33°. This represents a condition in which the shear component is about 50% of the applied force acting on each pin. Table 6.4 shows the shear properties of these cores characterised by a 33° pin insertion angle.

core identification	*out-of-plane shear strength [MPa]*	*out-of-plane shear stiffness [MPa]*
X-Cor$^F{}_1$/0.51/33°/0.06	*2.2±0.1*	*241±7*
K-Cor^F /0.51/33°/0.06	*0.8±0.1*	*129±2*

Table 6.4– *Shear properties of pinned cores: X-Cor$^F{}_1$/0.51/33°/0.06 and K-Cor^F /0.51/33°/0.06 (from Ch. 6)*

The X-Cor clearly outperforms the corresponding K-Cor structure (as seen in Ch. 5). The elastic support provided by the foam is, for the X-Cor structure, enough to limit the action of the shear component in lowering the pin buckling strength. Consequently the core strength value registered in presence of the foam is significantly higher. For the K-Cor configuration the effect of the foam support on strength is not as substantial.

The cores characterised by an 11° insertion angle have a low shear component acting on each pin which can be counteracted by the foam. This leads to a significant increase in core strength to be achieved in both pinned core types. The presence of the foam is also very beneficial for the K-Cor compression stiffness (+284%) if compared to the 43% increase for the X-Cor samples. This suggests that especially in K-Cor structures the foam carries also part of the core shear stresses contributing to the whole core rigidity.

For the case of K-Cor, it is possible to extend this analysis to another tested core, (*K-Cor^F /0.51/30°/0.10*), similar in terms of pin diameter (0.51mm) and effective insertion angle (32°) but characterised by a higher pin areal density (0.10pin/mm^2). This means that the number of load bearing pins in these samples is ~60% higher than that for the *(C)K-Cor^F /0.51/33°/0.06* samples previously analysed. Table 6.5 shows the percentage increase in performance.

	K-Cor		*increment in performance*
	*K-Cor^H /0.51/**30**°/0.10*	*K-Cor^F /0.51/**30**°/0.10*	
E [MPa]	*338±37*	*441±83*	*31%*
σ_C [MPa]	*3.8±0.4*	*6.1±0.6*	*60%*

Table 6.5– *Increase in performance due to the presence of the foam for K-Cor^F /0.51/30°/0.10*

The significantly higher values for strength and stiffness observed for this core in both configurations, show that the pin areal density plays a fundamental role in the out-of-plane compressive mechanical properties, as also indicated in [11]. Concerning the foam influence, it appears that the increase in performance depends also on the pin areal density being so different for these two K-Cor types. The highest increase corresponds to the core which has the lowest pin density. This result may be interpreted considering the foam as a medium that carries and redistributes the core stresses along with the function of supporting and stabilising the pins. It was noticed also that the positioning of the pins in a core plays a role in the external force distribution among them. If the pin lay-out in a unit cell is not symmetric with respect to the barycentre; it generates different reaction forces acting on each pin to satisfy the moment equilibrium. A detailed investigation (through FEA for example) on the force distribution in the unit cell of this core could support and further validate this analysis (similar results were obtained in the FE analysis for an out-of-plane shear loading condition, section 5.3.3.1). Figure 6.13 shows a typical premature pin buckling failure in a K-Cor specimen characterised by a very low pin areal density (0.040pin/mm^2) and an anisotropic pin lay-out (figure 3.21). It is possible to notice (from the photograph) that two homologous pins belonging to two different adjacent unit cells are experiencing buckling. As a consequence the load is re-distributed among the surviving pins which will be facing individually a higher force.

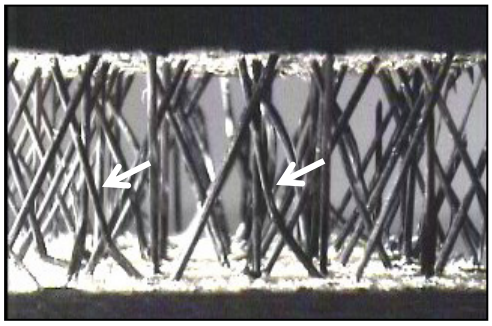

Figure 6.13– *Premature pin buckling in a hollow K-Cor specimen under out-of-plane compressive loading. Sample with very low pin areal density (0.040 pin/mm^2), 22° pin insertion angle and 0.51mm pin diameter (preliminary tests)*

Pin positioning seems to affect core strength; an ideal pin lay-out would have all the pins facing similar loads in order to reach a critical condition simultaneously, improving the pinned core strength. In this analysis the materials, pin interfaces, etc. were supposed to be ideal; in reality the difference in mechanical properties also favours an uneven load distribution.

6.3 Pin rotational constraint evaluation in out-of-plane compression: preliminary modelling

Similar X-Cor and K-Cor structures deliver different out-of-plane compression mechanical performance (section 6.1 and 6.2). As seen in Ch.3 they are characterised by a diverse way of obtaining structural integrity as part of a sandwich construction. The pin-skin (X-Cor) and the pin-adhesive film (K-Cor) interface impose a finite rotational constraint on the pins, which characterises the mechanical response of these sandwich structures. A preliminary model, developed for hollow cores, provides a way to measure this rotational constraint for out-of-plane compression and allows other considerations on pin insertion angle, manufacturing technique, interface materials and pin core lay-out to be made. Although at an early stage, the model can provide a better understanding of the mechanical behaviour and a base for approaching a complex problem. It could be

used to evaluate input parameters for pin interfacial elements implemented in a unit cell FE model in a similar way to that presented in section 5.3.

6.3.1 Theoretical model

The X/K-Cor pin is seen as a column of elastic, brittle material, with rotational springs (of unknown constant of rigidity K) at the ends, which simulate the interface mechanical properties. At one end the pin is subjected to an imposed displacement δ, which reflects the constant strain imposed on the sandwich core in the out-of-plane compression test as shown in figure 6.14.

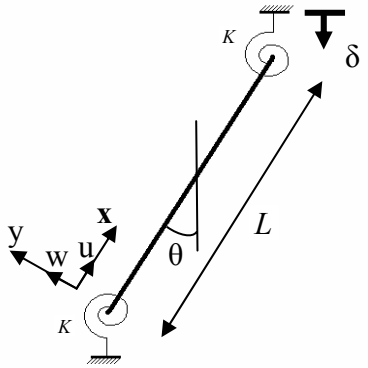

Figure 6.14– *X/K-Cor pin-column with* rotational *springs at the ends: theoretical approach to the problem*

The following assumptions are made:

The model considers only the axial component of the applied force on a single pin and follows the Euler-Bernoulli theory [152, 153]. It is based on the assumption that plane normal cross-sections remain plane and normal to the deflected centroidal axis of the column; the transverse normal stresses are considered negligible. This approximation is adequate only for pins where the effect of the shear component (and the consequent bending moment) can be considered negligible or limited. In spite of these restrictions, for a preliminary modelling approach, and as a basic investigative tool this model seems adequate.

A more refined analysis should consider a pin as a so called beam-column as it is in reality supporting both axial and transverse forces which affect the critical buckling load [154]. Moreover for beams made in a composite-type construction, the shear deformation (neglected in the Euler beam theory) can have a non-negligible effect and influence the critical axial load (Timoshenko beam theory [152, 153]).

The defined displacements according to the problem configuration are (figure 6.14):

$$\begin{cases} u(0) = 0 \\ w(0) = 0 \\ u(L) = -\delta\cos\theta \\ w(L) = -\delta\sin\theta \end{cases} \tag{6.4}$$

where L is the pin length and θ the pin angle with respect to the vertical direction. The axial force N (compressive force in this case) is the integral of the axial stress σ acting on the cross-sectional area A of the pin:

$$N = \int_A \sigma dA \tag{6.5}$$

Pins are pultruded composites which show elastic-brittle behaviour [11], thus the linear response can be described by Hooke's law. The axial force can be seen as:

$$N = \int_A E\frac{du}{dx}dA \tag{6.6}$$

$$N = EA\frac{du}{dx} \tag{6.7}$$

where E is the Young's modulus of the pin-column. The constant axial force ($N = \cos t$) along the pin, sets the following values for these derivatives:

$$\frac{dN}{dx} = 0 \tag{6.8}$$

$$\frac{d^2u}{dx^2} = 0 \tag{6.9}$$

Therefore the generic polynomial expression for $u(x)$ is:

$$u = C_1 x + C_2 \tag{6.10}$$

where C_1 and C_2 are two constants; for conditions 6.8 and 6.9 the term C_2 is equal to zero. Then, for $x = L$:

$$C_1 = \frac{-\delta \cos\theta}{L} \tag{6.11}$$

and so:

$$u = \frac{-\delta \cos\theta}{L} x \tag{6.12}$$

From equation 6.7 the compressive force acting on the beam is equal to:

$$N = -\frac{EA\delta}{L} \cos\theta \tag{6.13}$$

The equation for the buckling behaviour is a homogenous differential equation of the deflection of the axis of the column, [149, 152]. It is based on the assumptions that the material follows Hooke's law and the slope of the deflection curve is very small:

$$EIw^{IV} - Nw^{II} = 0 \tag{6.14}$$

where $I = \frac{1}{4}\pi R^4$ is the moment of inertia for a circular cross-section pin. Substituting the expression of the axial force (equation 6.13) into equation 6.14:

$$w^{IV} + \frac{A\delta}{IL} \cos\theta w^{II} = 0 \tag{6.15}$$

assuming:

$$\beta^2 = \frac{A\delta}{IL} \cos\theta \tag{6.16}$$

it becomes:

$$w^{IV} + \beta^2 w^{II} = 0 \tag{6.17}$$

Substituting the area $A = \pi R^2$ and $I = \frac{1}{4}\pi R^4$ the moment of inertia for circular cross-section into equation 6.16, it is possible to express β as:

$$\beta = \frac{2}{R}\sqrt{\frac{\delta\cos\theta}{L}} \tag{6.18}$$

To solve equation 6.17 it is necessary to determine the boundary conditions for this problem, which are:

$$\begin{cases} w(0) = 0 \\ w(L) = \delta\sin\theta \\ EIw^{II}(0) + Kw^{I}(0) = 0 \\ EIw^{II}(L) + Kw^{I}(L) = 0 \end{cases} \tag{6.19}$$

If a parameter α (adimensional) is defined as:

$$\alpha = \frac{EI}{KL} \tag{6.20}$$

the boundary conditions 6.19 then become:

$$\begin{cases} w(0) = 0 \\ w(L) = \delta\sin\theta \\ \alpha Lw^{II}(0) + w^{I}(0) = 0 \\ \alpha Lw^{II}(L) + w^{I}(L) = 0 \end{cases} \tag{6.21}$$

The general homogenous solution to equation 6.17 is:

$$w = A\cos\beta x + B\sin\beta x + Cx + D \tag{6.22}$$

After some computation, (indicated in Appendix B), the general solution of equation 6.17 is:

$$\begin{aligned} w = {} & \frac{\delta\sin\theta}{2\tan\frac{\beta L}{2} + \beta L\left[\alpha^2(\beta L)^2 + 1\right]} \times \\ & \times\left[\left(\tan\frac{\beta L}{2} + \alpha\beta L\right)(\cos\beta x - 1) + \left(\alpha\beta L\tan\frac{\beta L}{2} - 1\right)\sin\beta x + \beta\left(1 + \alpha^2\beta^2L^2\right)x\right] \end{aligned} \tag{6.23}$$

The buckling load is the load that makes the transversal displacement infinite, $w = \infty$, thus the denominator of equation 6.23 has to be equal to zero:

$$2\tan\frac{\beta L}{2}+\beta L\left[\alpha^2\left(\beta L\right)^2+1\right]=0 \tag{6.24}$$

Rearranging the terms for a more convenient interpretation:

$$-\tan\frac{\beta L}{2}=\frac{\beta L}{2}\left[\alpha^2\left(\beta L\right)^2+1\right] \tag{6.25}$$

6.3.2 Conditions of simply and rigidly supported pin

In the case of a simply supported pin, there are no rotational constraints at the pin ends. This is equivalent to the condition of having a rotational spring with a constant of rigidity $K=0$. This implies that the parameter $\alpha\to\infty$ (from eq. 6.20):

$$K=0\Rightarrow\alpha=\infty \qquad \tan\frac{\beta L}{2}=-\infty\Rightarrow\beta=\frac{\pi}{L} \tag{6.26}$$

from equation 6.14 and 6.17 substituting $\beta=\frac{\pi}{L}$ we obtain:

$$\beta=\sqrt{\frac{-N}{EI}} \tag{6.27}$$

which correctly yields the Euler formula of critical load for a column, previously mentioned:

$$N=-\frac{\pi^2 EI}{L^2} \tag{6.28}$$

In the case of rotational springs with infinite rigidity, $K\to\infty$ therefore $\alpha\to 0$ the pin is close to the condition of being fully clamped at the ends. This condition is the one of maximum stiffness, which gives the maximum buckling displacement and consequently the maximum buckling load. The graphical solution of the transcendental equation 6.25 is shown in figure 6.15.

$$K \to \infty \Rightarrow \alpha \to 0 \qquad -\tan\frac{\beta L}{2} = \frac{\beta L}{2} \tag{6.29}$$

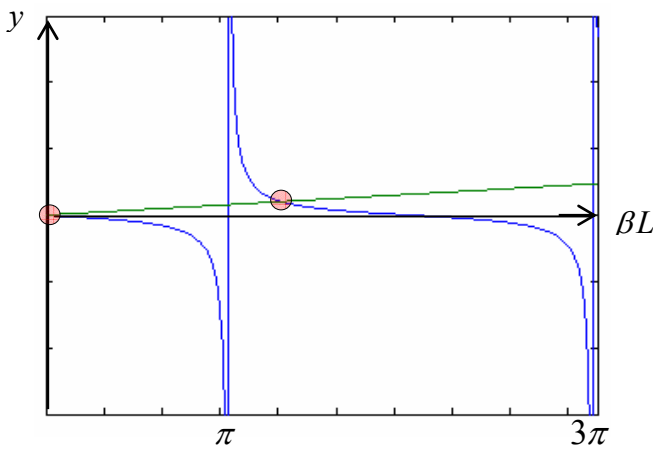

Figure 6.15– *Graphical solution of eq. 6.29 (case of rigidly supported pin*)

Except from the trivial solution, the other intersection gives $\beta L = 4.0575 = 1.2915\pi$. This is the solution that could be applied for both K-Cor and X-Cor if the pins were rigidly supported. It is therefore possible to determine the value of the pin axial load for this β, which is the highest possible value expected for the X/K-Cor pin. As mentioned before, for $K \to \infty$ and $\alpha \to 0$ the pin is "close" to a condition of being fully clamped. In the system of boundary conditions for this problem (eq. 6.19), the equation:

$$w(L) = \delta \sin\theta$$

allows a certain mobility to the end of the pin, which is then not rigidly supported, but still represents the condition of the highest degree of constraint on the pin for this problem (figure 6.16).

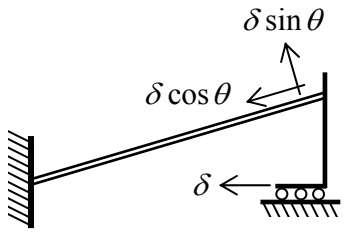

Figure 6.16– *Condition of pin maximum support for this problem. δ is the constant strain imposed in the out-of-plane compression test*

6.3.3 General condition on pin end constraints

The two critical load values found in the previous section represent the limits of validity for this approach. The pins for both X/K-Cor structures are in a condition between being simply and rigidly supported. In the ideal case of null shear component acting on the pin, it is possible to set a range in which the actual buckling load N_{CR} for the pins can be expected:

$$N_{SS} \leq N_{CR} \leq N_{RS}$$

where N_{SS} is the critical load for a simply supported pin and N_{RS} for a rigid support (section 6.3.2). For the general case it is necessary to solve the equation 6.25 for a particular value of the parameter α, (eq. 6.20), chosen in agreement with the experimental buckling load $N_{CR.EXP}$ previously determined. Through the parameter α it is possible to determine the constant of rigidity K of the rotational spring for the X/K-Cor examined. In figure 6.17 the solving algorithm is presented.

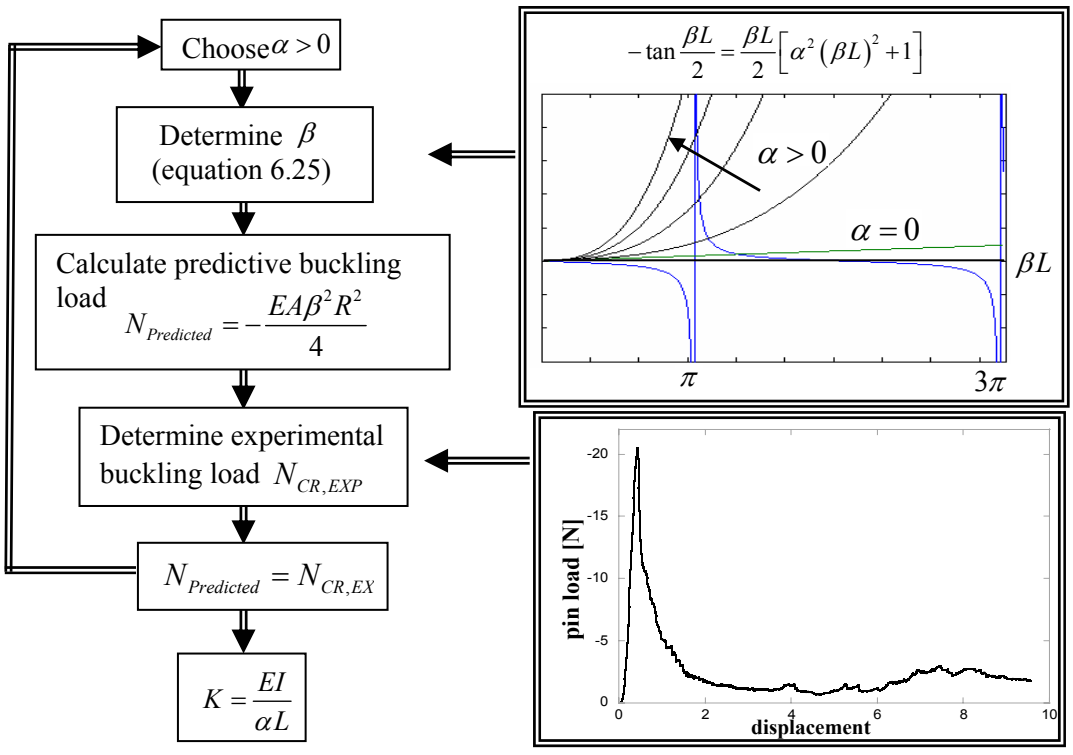

Figure 6.17– *Solving algorithm for the calculation of the predictive buckling load and of the constant of rigidity K for the* rotational *springs in the theoretical pin model*

It is critical to choose in different attempts a value of α which, when substituted in equation 6.25 provides a value for β and for the predicted axial force N, as close as possible to the buckling load experimentally determined.

6.3.4 Model considerations and results

The limits of validity of the model are set by the values of the axial critical load for a simply, N_{SS}, and a rigidly supported pin, N_{RS} determined for a specific core (section 6.3.2) in ideal conditions (only axial pin load). In reality the insertion angles are usually different from zero, which means that pins are also subjected to the perpendicular component of the applied force (section 6.2.3). The experimentally measured critical axial load $N_{CR,EXP}$ represents the average buckling load for a pin in a specific core configuration. If it is within the model validity range, it is then possible to determine a value for the constant of rigidity K which measures the average finite rotational constraint valid for a pin in that particular core configuration. Ideally it is like considering the same pin inserted perpendicularly with respect to the core plane (thus subjected only to an axial load), characterised by different end constraints representing the various core configurations. The value of the axial force N acting on each pin depends essentially on their insertion angle, density and lay-out in the core; the pin individual critical buckling load is related to the interface as well as to pin geometrical and elastic properties. As previously mentioned (section 6.2.4), pin positioning can influence the core strength. Premature pin failures cause load re-distributions and affect the whole core performance. The values determined for $N_{CR,EXP}$ and K are average core values and thus considered functions of the following parameters:

- Pin insertion angle (which determines the magnitude of the perpendicular or shear component acting on each pin)
- Interface properties (K-Cor / X-Cor constraint efficiency, manufacturing technique and combination of interface materials used)
- Core force distribution (pin lay-out / positioning in the core)

As long as the interface mechanical properties are concerned, it is possible to evaluate the K-Cor / X-Cor constraint efficiency by comparing two similar cores *X-Cor$^{H}_{I}$ /0.51/11°/0.06* and *K-Cor^{H} /0.51/11°/0.06* characterised by identical parameters: same insertion angle and similar pin positioning. This means that the shear component acting on each pin has the same magnitude. Table 6.6 shows the values of the pin critical axial load determined experimentally as well as for the ideal condition of simple and rigid support.

core identification	$N_{CR,EXP}$ *[N]*	N_{SS} *[N]*	N_{RS} *[N]*
X-Cor$^{H}_{I}$/0.51/11°/0.06	*-26.7±1.6*	*-24.8*	*-41.4*
K-Cor^{H} /0.51/11°/0.06	*-17.3±1.6*	*-24.8*	*-41.4*

Table 6.6– *Pin critical axial load determined experimentally and for the conditions of simple and rigid support*

The experimental value of the buckling load $N_{CR,EXP}$ for the X-Cor structure is within the range of validity of the model. This example is an indicator of the efficiency of the pin-skin and pin-adhesive film interface on the rotational constraint, as the effect of the other parameters is equal. The X-Cor structures manufactured with the 'improved' technique show higher interfacial properties than the corresponding K-Cor; this leads to higher mechanical properties in a similar out-of-plane loading condition. The value calculated for the constant of rigidity K of the rotational spring for the X-Cor$^{H}_{I}$ /0.51/11°/0.06 samples is $32.6 Nmm$. It is interesting to notice that the critical axial load value experimentally found for the *X-Cor$^{H}_{I}$/0.51/11°/0.06* pin is close to a condition of being simply supported. This value can be compared to the critical axial load found for the *X-Cor$^{H}_{S}$/0.51/22°/0.13* pin shown in table 6.7.

core identification	$N_{CR,EXP}$ *[N]*	N_{SS} *[N]*	N_{RS} *[N]*
X-Cor$^{H}_{S}$/0.51/22°/0.13	*-26.6±5.0*	*-20.5*	*-34.2*

Table 6.7– *Pin critical axial load determined experimentally and for the conditions of simple and rigid support*

The number of effective load-bearing pins in this core is almost double (+94%) with respect to the X-Cor$^{H}_{I}$ /0.51/11°/0.06 samples, which were also manufactured using the 'improved' technique. Despite the higher insertion angle (22°) and shear force component acting on each pin, as well as a pin-skin interface with lower mechanical properties ('standard' manufacturing technique, section 6.1), the *X-Cor$^{H}_{S}$ /0.51/22°/0.13* pins seem to be closer to an intermediate condition between simply and rigidly supported compared to the previous case. This result can be attributed to the pin lay-out; in the core characterised by a higher number of pins the external force is more evenly distributed (section 7.2.4). This maximises the global core strength (from $1.7 \pm 0.1 MPa$ to $4.2 \pm 0.7 MPa$) as the pins face a similar load condition.

6.3.5 Pin contact effect on mechanical performance

For a specific tested X-Cor, (*X-Cor$^{-F}_{T}$ /0.25/21°/0.24* and *X-Cor$^{-F}_{T}$ /0.25/21°/0.24*), due to the high value in pin areal density ($\rho_{th} = 0.24 pin/mm^2$), some of the pins are found to be in contact with each other. Figures 6.18(a) and 6.18(b) are respectively a close-up photograph of one hollow specimen and a 3-D representation of a unit cell of this core.

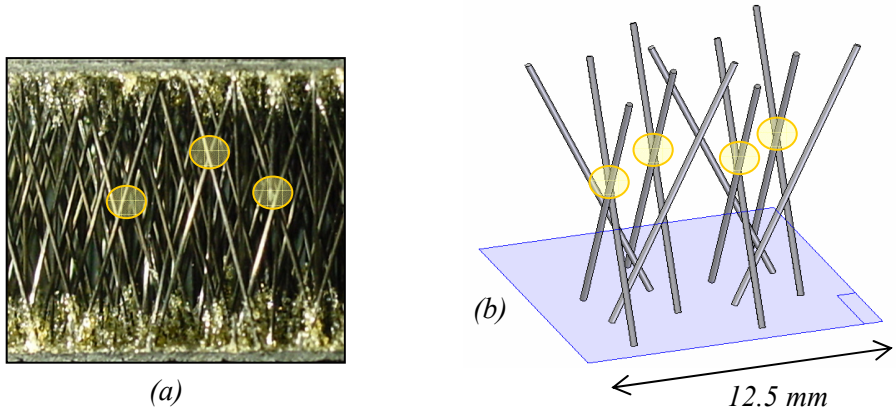

Figure 6.18– *(a) Close-up of a (C)X-Cor$^{F}_{T}$/0.25/21°/0.24 sample.*
(b) X-Cor$^{F}_{T}$/0.25/21°/0.24 unit cell 3D representation:
8 pins out of 12 are in contact

Throughout the out-of-plane compression test, new contacts are also encountered favoured by unit cells overlapping. The effect of this contact appears to enhance the strength of the material as if the pins were physically joined and are able to laterally support each other during the deformation. The compressive mechanical properties of the X-Cor sandwich are improved in comparison to a core characterised by a high enough distance between two or more neighbouring pins. As expected for this core, the theoretical schematisation of the pin with the two rotational springs is not adequate. In this case the experimental pin buckling load $N_{CR,EXP}$ found ($-3.2 \pm 0.4N$) exceeds the predicted value of the critical axial load also for a pin in a condition of being fully supported ($N_{RS} = -2.1N$). This result indicates that the support offered by the neighbouring pins has a non- negligible effect on the overall compressive behaviour of the material. The graph of figure 6.2 shows that the post elastic phase for these cores is not characterised by a sudden drop; the stress decrease seems more gradual, indicating that the interlocks created between the pins allow more load to be carried. A further investigation on the possible effects of manufacturing on pin lateral connections is required.

6.3.6 Model limitations and suggestions for improvement

The model of the pin as a column of elastic-brittle material with rotational springs at the ends is considered to be a good theoretical approximation of a pin belonging to a hollow configuration. There are three limiting factors for the approached used:

- The pin critical axial load is based on the experimentally measured core strength. An uneven force distribution among the pins leads to premature pin buckling failure, thus low core strength values. The pin buckling load $N_{CR,EXP}$ found and the value of the constant of rigidity K of the rotational springs appears to be influenced by pin positioning.

- The Euler-Bernoulli theory, besides the clear advantage of simplifying the analytical calculations, does not consider the influence of the shear component

of the external load applied on the pin which affects its buckling properties. Due to the pin positioning influence, it is not possible to correctly evaluate if this is an adequate approximation. Considering a pin as a beam-column (taking into account the transverse forces) and adopting the Timoshenko beam theory [152] should extend the validity of the model (and the determination of the pin end finite rotational constraint) to a wider range of core configurations.

- At high areal densities where pin contacts are observed, there is a non-negligible effect on the overall compressive behaviour of the pinned core (section 6.3.5). This is not taken into account in the theoretical model adopted. An assessment on the properties of these connections between neighbouring pins is necessary for an eventual development of an analytical model. Moreover, the fact that not all the pins interact with each other also needs to be considered in the core strength evaluation and certainly introduces a higher degree of complexity.

The value of the constant of rigidity K of the rotational springs should be a parameter depending only on:

- Manufacturing
- X/K-Cor constraint efficiency
- Interface material
- Pin properties (insertion angle and diameter)

Only in this case the K values could be used as interfacial elements in any unit cell FE model of a core made with those specific materials and a particular manufacturing procedure; the model could then evaluate different core configurations and optimise their pin lay-out. A way to determine such values for K, independent from pin positioning, is to combine a preliminary finite element analysis with a subsequent manufacturing and testing phase. A basic unit cell (and core) configuration with an optimised pin lay-out should be initially obtained. This approach can guarantee an even force distribution among the pins. The subsequent manufacturing and testing phase of such cores would provide the desired K values.

6.4 Chapter summary

1. The mechanical performance of different types of pinned core and competitor sandwich structures (Al and Nomex® honeycombs), chosen for their similar core densities and/or expected mechanical behaviour has been assessed for out-of-plane compressive loading. The tests were performed according to the ASTM C 365 standard.

2. The pinned core sandwich structures (K-Cor and 'standard' X-Cor), compared to the Nomex and Al honeycombs display a higher rigidity, between 50% and 150%. The strength of the X-Cor and K-Cor samples analysed is within a range of 4.2±0.7 - 6.1±0.6MPa. They outperform the Al honeycomb (2.5±0.1MPa), but have a lower peak value than the Nomex structures (6.9±0.9MPa). A K-Cor structure characterised by a 30º pin insertion angle shows a similar rigidity to that of a 'standard' X-Cor and a ~30% higher strength on the basis of similar core properties.

3. The 'improved' X-Cor manufacturing procedure significantly enhances the out-of-plane compressive mechanical properties of these constructions, when compared to similar K-Cor structures. The level of performance achieved is significantly higher especially for the samples characterised by a 33º pin insertion angle. The rigidity, for this case, is nearly twice as much as for all other configurations. There is also a 60% increase in strength for the hollow samples and a 180% for the specimens containing foam. With an 11º pin insertion angle the X-Cor exhibits a very high rigidity for both hollow and foam configurations (404±51 and 578±56MPa respectively). The corresponding K-Cor shows a comparable stiffness only in the samples containing foam (430±54MPa). In this configuration its strength is ~50% lower (3.2±0.3MPa) than the value recorded for X-Cor. In a comparison between 'standard' X-Cor (22º pin insertion angle) and 'improved' X-Cor (11º pin insertion angle) a similar performance is achieved for a core weight saving of ~34% in favour of the 'improved' manufactured core.

4. The behaviour exhibited by both the X-Cor and K-Cor in the configurations with and without foam is indicative of a buckling failure mechanism. This was observed during testing and confirmed by the stress-strain curves obtained. Moreover, if a single

pin is assumed as a column of elastic-brittle material then, the critical axial load determined experimentally is very close to the Euler buckling load.

5. All specimens containing foam exhibit a significantly higher mechanical response to the applied out-of-plane compression load. There is a clear synergistic effect between the foam and the pins as the strength of the pin reinforced core is increased over and above the sum of the single contributions of the foam and pins. The foam essentially provides a lateral support to the pins with the consequence of improving the buckling strength. For X-Cor structures with a 33º pin insertion angle, the core strength increases from 1.3±0.3MPa for the hollow configuration to 4.2±0.3MPa for the foam filled core. In regards to the enhancement of the compression stiffness, it appears that the foam also carries some of the core shear stresses, generated during the compressive load, contributing to the whole core rigidity. This is more evident in K-Cor samples, which are characterised by a much lower out-of-plane shear rigidity than the corresponding K-Cor specimens. The enhancement in rigidity for a core with an 11º pin insertion angle is ~284%.

6. The pin insertion angle influences the mechanical performance. Cores containing more vertical pins (and consequently with a lower insertion angle θ_i) are associated with a higher mechanical performance in terms of core strength and stiffness for out-of-plane compression loading. This is due to the fact that the external force generates two load components acting on each pin: an axial load and a load perpendicular to the pin axis. This latter component lowers the pin bucking resistance and introduces shear to the whole core. K-Cor with a foam filled core appears to maximise the benefits deriving from a variation of the pin insertion angle from 11º to 33º (*K-Cor^F /0.51/33°/0.06*: E=159±30MPa and σ_C=1.5±0.1MPa; *K-Cor^F /0.51/11°/0.06*: E=430±54MPa and σ_C=3.2±0.3MPa)

7. A preliminary analytical model to investigate the mechanical behaviour of hollow pinned cores was developed. It considers a pin as a column (according to the Euler-Bernoulli theory) of elastic-brittle material with rotational springs at the ends. The model is an initial attempt to measure the finite rotational constraint imposed by the pin-

skin (X-Cor) or the pin-adhesive film (K-Cor) interface, which characterises the mechanical response of these sandwich structures. Although the model could only be used in few cases, as there are some limitations to its applicability, it has allowed some realisations regarding the effect of pin insertion angle, manufacturing technique, interface materials and pin core lay-out to be made. The most restraining factor appears to be the dependency of the pin buckling load $N_{CR,EXP}$ and of the constant of rigidity of the rotational springs K, on the positioning of the pins. An uneven force distribution amongst the pins leads to premature pin buckling failure and therefore to low core strength values. The finite rotational constraint was measured for the *X-Cor$^{H}_{I}$ /0.51/11°/0.06* sample, its value is estimated to be 32.6Nmm.

Chapter 7

Energy absorption evaluation

In this chapter a first evaluation of the energy absorption capability and mechanical response of Z-pinned composite sandwich structures (X-Cor and K-Cor) is made under in-plane loading conditions. The findings are compared to those of competitor sandwich structures. A general literature survey on in-plane crushing for composite materials is followed by a more specific analysis on the crushing of composite flat plates and on different crushing tests employed in the past. A design guide for the development of a novel in-plane crush test on sandwich structures is gathered from a critical analysis of previous research work. A suitable data analysis methodology based on the specific energy absorption is presented, followed by test results. The specific energy absorption values of the out-of-plane compression tests are compared with the in-plane energy absorption values to allow an evaluation of the material energy absorption properties. The following section is dedicated to the crush zone morphology with the aim of proving that a correct progressive crushing is promoted by the new test configuration. The identification of the main damage mechanisms in pinned core sandwich structures completes the analysis.

7.1 Introduction

Previous studies have identified fibre reinforced composite materials to be efficient energy absorbing materials for application in aerospace and automotive structures [155-160]. They can be designed to provide energy absorption capabilities superior to those of metals, when compared on a weight basis. As a consequence, considerable research interest has been directed towards their use for crashworthiness applications [156]. Metal structures collapse under crush or impact, usually involving an extensive plastic deformation, typical of a ductile behaviour. On the contrary, most composites are

characterised by a brittle response to load. They fail through a sequence of fracture mechanisms involving fibre fracture, matrix crazing and cracking, fibre-matrix debonding, delamination and inter-ply separation [161].

The great number of variables interacting and controlling the mechanical behaviour, a result of the anisotropic nature of composite materials [156], and the fact that the energy absorption capability of a structure is dominated by the post-failure loading response [159], makes crash modelling of composite structures limited in application. It has not yet been demonstrated as an effective predictive tool [162]; as a result the most useful analytical results have come from semi-empirical methods that rely heavily on experimental data [163]. No standard test method currently exists for characterising the energy absorption capabilities of composite materials [155].

7.2 In-plane crushing

A major concern with composite materials in crashing applications is the so called 'crashworthiness'. The challenge is to design composite structures in such a way that impact energy can be absorbed in a controlled failure process, which should enable the maintenance of a gradual decay in the load profile during the absorption, providing greater safety [161]. The crashworthiness of a material is expressed in terms of its specific energy absorption (SEA), characteristic of that particular material and defined as the energy absorbed per unit mass of material.

Crashworthiness design has become in recent years a standard feature of vehicle design procedures. As far back as thirty years ago, a long series of publications on design and standard requirements providing design criteria and methodologies for maximising crashworthy performance have been published for the aerospace and automotive sectors. One of the first studies, MIL-STD-1290 [164], indicates the way for rotorcraft design to satisfy safety considerations. A rotorcraft under power loss is designed to descend with a maximum vertical velocity of 15 m/s. A crashworthy rotorcraft should include in its own design structures capable of withstanding such an impact, transmitting to the occupants accelerative forces which do not exceed the limits of human tolerance for survival. Structures made of composite materials are capable of

absorbing a large amount of energy in a controlled way only if the most effective and efficient failure modes are triggered. As indicated in references [157, 165, 166], this mode is a progressive collapse and it can be of two types. The first one is a progressive folding mode, typical of ductile metals and plastic tubes, achieved also in thin-wall composite tubes made with tough polymer fibre (such as Kevlar®) or at high temperature for particular combinations of glass fibres and polyester or epoxy resins. The second collapse mode is progressive crushing and implicates the formation of an extensive microfracture zone, at one end of the specimen, which propagates at the same speed as the crushing platen [167]. Significant amount of energy is absorbed in both types of progressive collapse, but the crushing failure is characterised by the highest values [157, 162]. The actual failure mechanisms and consequently the energy absorption capability in a composite structure are highly affected by the material, geometrical and experimental factors. Much of the experimental work to study the effects of fibre and matrix type [159, 160], fibre architecture [167], specimen and trigger geometry [155, 159, 168, 169], processing conditions [170, 171], fibre volume fraction [172] and testing speed and temperature [156, 163, 173], on the energy absorption capabilities of composite materials has been directed towards the axial crush analysis of composite thin-walled structural components, as the axial crush mode represents probably the most efficient design [156, 169].

Axisymmetric tube specimens have been used widely to study composite crushing phenomenology and one of their advantages is their inherent structural stability which allows using simple testing arrangements [162]. Substructural specimens like these are designed to suppress buckling and promote progressive crushing [163], and represent the most widespread shape of collapsible impact energy absorbers [174]. Other specimen designs include square tubes, angle and channel stiffeners, beams having various types of self-supporting webs [169], and other complex shapes used to suppress buckling and promote progressive crushing. All of these are complex and expensive test specimens, difficult to fabricate with consistency, particularly when compared with flat coupons [163].

Still today many issues are not properly addressed, in particular the relationship between full and subscale components; as a consequence, the primary means of determining energy absorption performance is to conduct a crush test. This makes the

process of incorporating crashworthiness very expensive, contributing further to high research and development costs [163, 169].

7.3 Flat laminate plate in-plane crushing test: a review

There has been a growing interest for inexpensive test methods for studying the energy absorption capability of composite structural elements. For a test method to be truly cost effective it should be designed for flat plate specimens [163, 175]. This is also supported by the fact that very similar failure mechanisms have been observed for both flat and tube specimen during progressive crushing [165]. One of the principal advantages is that the manufacturing process for producing flat coupons is relatively inexpensive and less time consuming if compared with more complex geometries. The other important benefit is the high degree of consistency in the specimen quality [176], and its consequences on experimental data reliability. The use of flat plate specimens can also be advantageous in a preliminary phase, as it offers a cost effective possibility of screening candidate material systems, optimum lay-ups and alternate different trigger geometries as well as evaluating scaling effects. Moreover, there are already enough material and/or laminate variables to consider when using flat coupons, without the introduction of complex structures.

The design of a flat plate crushing test is complicated in terms of testing fixture, specimen and trigger geometry. To crush flat plates, the laminates are stabilised in a support fixture which enables the localised crushing of the laminate to occur. The main problem with plate crushing is that the response can be significantly influenced by interaction with the support fixture, which complicates data analysis, modelling efforts [162], and influences the material damage mechanisms [161].

Different types of specimens and fixtures have been developed and used in the past; for clarity they have been divided into two categories and the reference works which either developed or employed them are indicated:

- 1st generation of flat specimen crush test [177-179]
- 2nd generation of flat specimen crush test [163]

The design improvement of a flat specimen crush test is based on the performance assessment of a new configuration compared to the previous ones and on a correlation in the trend of the crush data with composite cylinder specimens. In fact, axisymmetric tubes represent a widely used and studied configuration for axial crushing. This specimen configuration promotes a constant crushing load which is typical of a correct progressive crushing on a constant cross-section (figure 7.8).

In the first generation of crushing devices a movable platen slides on four guide posts fixed on a base plate. The flat specimen located between the guides, crushes at the bottom of the base plate. Despite the specimen constant cross-section, during the crushing a rising load is exhibited when the debris accumulated at the bottom and between the guides jams the relative movement between parts. A first unsuccessful attempt to solve this inconvenience was to enlarge the area for collecting the debris in the base plate, leaving enough unsupported specimen length to cause a different failure mechanism [175]. Another attempt to reduce the length of the guides giving more free crushing length to the specimen, without inducing global buckling, resulted in a magnitude of specimen out-of-plane deflection of being about 28% of the plate thickness [176].
Figure 7.1 shows a simplified sketch of a second generation crush fixture. It has proved to promote correct progressive crushing. The main change was to avoid a direct contact between the guide and the specimen by using knife edges that fit into the support posts and hold the specimen in place for almost the whole of the length.

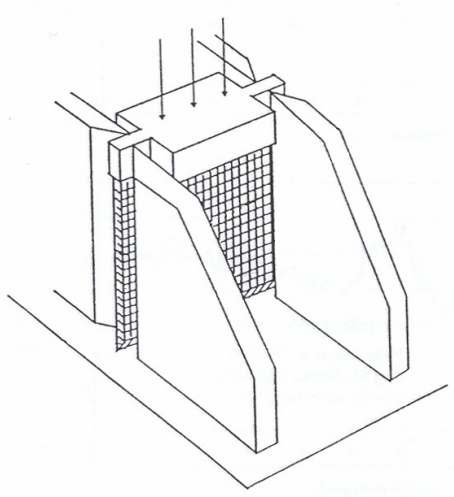

Figure 7.1– *Sketch of a second generation in-plane crush fixture, from [178]*

The load-displacement response of flat plates crushed in the new fixture is similar to the ideal response of self-stabilised composite cylinder [176].

It is important to mention at this stage a category of crush test configurations which represents a good compromise between the flat, low cost specimens and closed profile ones. These samples are also more similar in design to realistic energy absorbing structures; the most representative are cruciform columns and sine web shaped specimens [162, 169]. Such configurations are characterised by an inherent structural stability which allows the employment of fixtures with reduced coupon-testing jig interaction, as in the case of axisymmetric closed profile specimens. Moreover, it is possible to observe directly the damage evolution during crushing. Their disadvantages are related to the complex manufacturing procedures, if compared to flat plate specimens and to the difficulty in obtaining progressive crushing consistently, due to the numerous geometrical parameters deriving from their complicated shape.

7.4 Flat sandwich plate in-plane crushing test

Practical structures from X/K-Cor materials are most likely to be constructed using plate-like elements, at least at the time of writing. It is therefore of interest to see how they would behave as energy absorbing structures compared to other, more traditional, sandwich systems.

Most of the in-plane compression testing on flat sandwich plates is related to the analysis of their structural stability and the evaluation of skin-core interfacial bond strength [180-183]. The procedure described in ASTM C364 [184] provides a method for obtaining sandwich in-plane compressive properties and it is also employed to promote an induced buckling mode, which in the case of through-the-thickness reinforced sandwich structures could measure the effectiveness of the reinforcing method. This test does not evaluate the energy absorption capacity of a sandwich system. The challenge was to design a simple, cost effective test method which could promote a progressive crushing failure mode on foam, honeycomb and pinned cored sandwich structures and allow energy absorption evaluations to be made. It should allow to analyse the failure mechanisms and the role of the pins during the localised material collapse. A simple

specimen geometry is desirable for evaluating the influence of pin parameters in energy absorption. Flat coupon configurations have been used before only for laminate crushing. With sandwich constructions there are even more variables and interactive failure modes which compete in the collapsing process.

It is evident that a self-axially-stable specimen has advantages in terms of damage observations, fundamental in characterising novel materials, and in terms of data analysis, as there is no interaction with the support. The effect of a constraining fixture is to promote different damage mechanisms, affecting the material response [161]. Limitations on the manufacturing of other geometries rather than flat sandwich panel called for the adoption of a simple, flexible set-up (shown in figure 7.2). It is an open configuration; this means that the role played by a containing fixture for structural stability against global buckling and macroscopic delaminations is assumed by the specimen geometry.

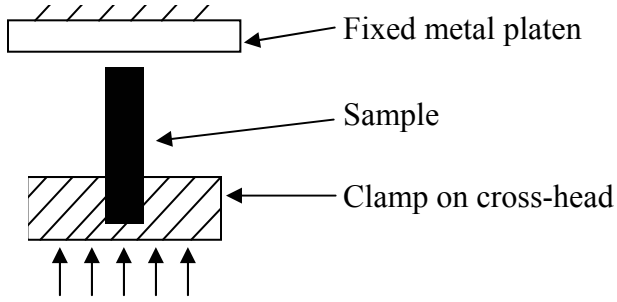

Figure 7.2– *Schematic of new in-plane crush fixture adopting for the in-plane crushing testing*

In most of the previously analysed test fixtures, the specimen is going downwards against the fixed crushing platen. A crush test where the specimen is clamped on a support which goes upwards against a fixed platen appears more appropriate. The debris will not accumulate in the crushed area giving three main advantages: no interference with the fixture and failure mechanisms, no obstacles to direct observation and no significant alteration in the relative friction coefficient between specimen and crusher. For sandwich specimens in particular, the debris problem is even more critical as they are made up of different materials characterised by a variety of properties and dimensions. In the previous fixtures, the specimen supporting guides interfere with the

failure mechanisms and usually do not allow close observation of the failure mechanisms. A direct observation during the test is considered essential for this work, as it is a first study on the in-plane crushing properties of X-Cor and K-Cor.

7.4.1 Materials and test parameter analysis

The tested X-Cor and K-Cor samples are characterised by the same pin areal density and lay-out and by a pin insertion angle of 11°. The role of the foam in the energy absorption capacity is evaluated by testing identical specimens in both hollow and foam filled configurations. A detailed description of these cores and the sample name convention can be found in Ch.3. All the results are compared to reference foam and honeycomb sandwich systems. Skins and adhesives employed were the same in terms of material and lay-up across the range of samples. Specimen dimensions and geometry are critical parameters for a correct test configuration and section 7.4.2 is dedicated to their evaluation.

The test was performed quasi-statically at a constant strain-rate on a displacement controlled universal testing machine, aware of the fact that this test condition is not a true simulation of an actual crash event. With impact testing, the striker speed decreases from the initial value to rest as the specimen absorbs the energy. A dynamic crash condition takes into account the strain rate sensitivity of the material, which is a critical parameter, often the subject of conflicting results. Energy absorption dependence on the crushing speed is related to the main failure mechanism which controls the crashing process; if this mechanism is a function of strain-rate then the energy absorption process of the composite specimen will be dependent on the crushing speed [156]. A quasi-static crushing test is appropriate especially when used as a first evaluation of the in-plane material behaviour. It could be a good indicator of the eventual energy absorption capabilities of the material. The principal advantages compared to a dynamic test are:

- Simple test, easy to control
- Failure mechanisms easily followed
- Dynamic (inertia) effects ignored

The test velocity was fixed at 5mm/min as found in numerous research studies [161, 162, 176, 178]. This crushing speed is a good compromise between a quasi-static loading condition and a convenient total test time. To reduce the friction effect between the metal platen and the crushing material, a procedure consisting of cleaning the striker surface with acetone and applying WD-40® was employed before each test.

7.4.2 Specimen geometry: initial design and design philosophy

Given the crushing fixture chosen previously (figure 7.2) and an in-plane quasi-static compression load, the main challenge was to determine a specimen geometry which would promote a failure by progressive crushing under a condition of global stability. Such geometry would have also represented a crashworthy design for flat sandwich plates as energy absorbers. Failure by end compression in sandwich structures as reported in references [73, 74, 180], occurs by a number of competing and interacting mechanisms which include global buckling collapse (Euler macrobuckling), macroscopic core shear buckling and facesheet wrinkling (microbuckling) and yielding.
The initial idea was to adopt a flat rectangular specimen with a trigger [168, 185], clamped on the base of the fixture and crushed by a flat metal platen. To produce uniform collapse in axially crushed composite specimens (tubes, webs, flat plates etc.) it is generally necessary to initiate the collapse process at one end of the specimen itself [169]. The failure initiator, or trigger, performs two functions: (i) reduces the magnitude of the initial load at which the collapse commences by a considerable factor and (ii) starts and propagates the collapse in a stable manner from one end rather than induce a catastrophic failure. The trigger geometry selected was the tulip configuration as it has the advantage to increase the crush stress and thus to enhance energy absorption capacity [168, 186]. This geometry was preferred also for practical reasons to a notch type (more difficult to manufacture) and a bevel shape (figure 9.3). The latter one is not suitable for a cored laminate as it does not allow a simultaneous crushing, in the initial phase, of all the parts of the sandwich construction. Moreover, in the case of pinned cores, in a portion of the trigger the pins would be unfastened from the skins.

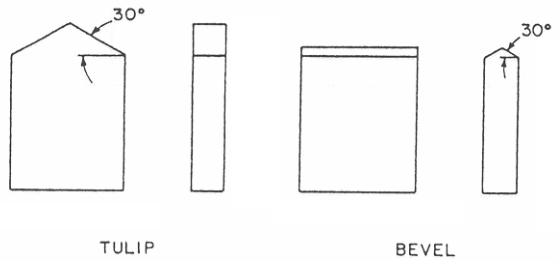

Figure 7.3– *Examples of trigger geometries from [168]*

The tulip trigger should have a half vertex angle of about 60° [168]. This imposes a constraint on the specimen width as the maximum clamping dimension on the fixture is fixed. It was also decided to have a crush length to specimen width ratio of at least close to one (the trigger length is discounted from the length calculation). The width was set at 40mm, this imposes a trigger height of 10mm to meet the geometrical requirements on the vertex angle. The clamped length, imposed by the fixture used, is 35mm (figure 7.4).

Rectangular plates loaded as columns (characterised by free lateral edges) may be considered as columns when the width-to-length ratio is less than 0.1 and as infinitely wide plates when the ratio is greater than 10 [187, 188]. The same study [187] also demonstrates that the critical stress may change as much as 10% from the Euler value depending on whether the plate-column is very narrow or very wide. For intermediate plate dimensions, as in this case and as for the samples tested in reference [180], the specimen is considered as a wide-column. This allows the use of a more straightforward and conservative approach in determining a stable specimen geometry for resisting axial compressive loads.

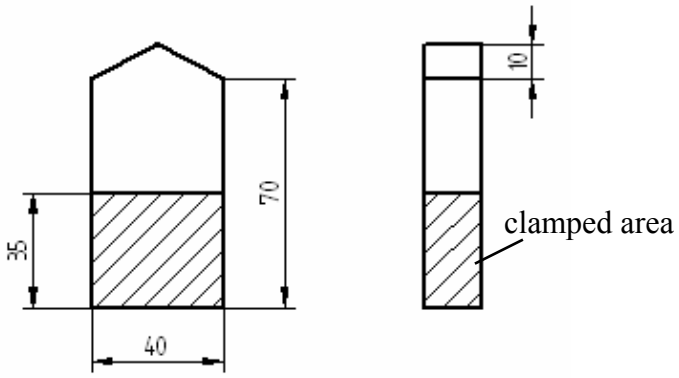

Figure 7.4– *First specimen configuration: nominal dimensions in mm*

The crushing test will be performed on different sandwich systems, but the sample geometry has to be determined on the basis of the most critical cases. Those are the tests on plain foam core sandwich specimen and a single skin crush test (reference configurations). The maximum load reached during a proper progressive crushing test is lower than the critical global buckling load of the specimen. Moreover, the presence of the trigger should lower the load value in the initial phase. This means that during the whole duration of the test the maximum load value experienced by the specimen $P_{\max}$ is lower than the critical value P_B. Two interacting failure modes influence the choice of the specimen length: global Euler buckling and macroscopic shear buckling. The flexural rigidity of the whole sandwich D is:

$$D = 2D_f + D_0 + D_c = \frac{E_f t_f^3 b}{6} + \frac{E_f t_f (t_f + t_c)^2 b}{2} + \frac{E_c t_c^3 b}{12} \tag{7.1}$$

where D_f is the flexural rigidity of the facesheet about its individual neutral axis, D_0 is the stiffness of the facesheets bending about the centroidal axis of the whole sandwich and D_c is the flexural rigidity of the core. As fully explained in references [73, 77], for the case of skin-core thicknesses and moduli ratios of the specimens considered (section 3.3) an equivalent flexural rigidity, D_{eq}, can be employed in the calculations incurring an error of under 1%. It follows:

$$D_{eq} \approx \frac{E_f t_f (t_f + t_c)^2 b}{2} \tag{7.2}$$

The above formula considers facesheets with no flexural rigidity on their own. The first critical buckling load (n=1) assumes the form of:

$$P_B = \frac{\dfrac{\pi^2 D_{eq}}{(\beta L)^2}}{1 + \dfrac{\pi^2 D_{eq}}{S(\beta L)^2}} \tag{7.3}$$

where the coefficient β depends on the boundary conditions, which in the case of a fixed-free column is:

$$\beta = 2 \tag{7.4}$$

S is the core shear buckling load that for thin skins is set by the equivalent shear rigidity of the core [151, 180]:

$$S \approx G_c t_c b \tag{7.5}$$

Equation 7.3 shows that for high values of S and L, the critical buckling load approaches the Euler load. At the same time, a finite buckling load is present even for weak cored sandwich specimens and/or for transition values of the slenderness ratio. Rearranging the terms of eq. 7.3, it can be written in a simpler form:

$$\frac{1}{P_B} = \frac{1}{P_E} + \frac{1}{S} \tag{7.6}$$

Here P_E is the Euler load for the specific constraint acting on the sample:

$$P_E = \frac{\pi^2 D_{eq}}{(\beta L)^2} \tag{7.7}$$

In the case of plain foam core samples, the shear buckling term of equation 7.6 is dominant and sets the value of the global critical load.

Although the smallest admissible crushing length for the specimen was chosen (to maintain a width-to-crush length ratio close to 1), the foam cored specimens failed by global buckling. The nominal dimensions are shown in table 7.1 and in figure 7.4.

	[mm]
Width	*40*
Total length	*80*
Crushing length	*45*
Trigger height	*10*
Clamped length	*35*

Table 7.1– *Specimen nominal dimensions*

According to eq. 7.3 the predicted value for the global buckling load of this set of samples was 5080N. After initial controlled crushing in the trigger portion, the specimen fails by global buckling (figure 7.5).

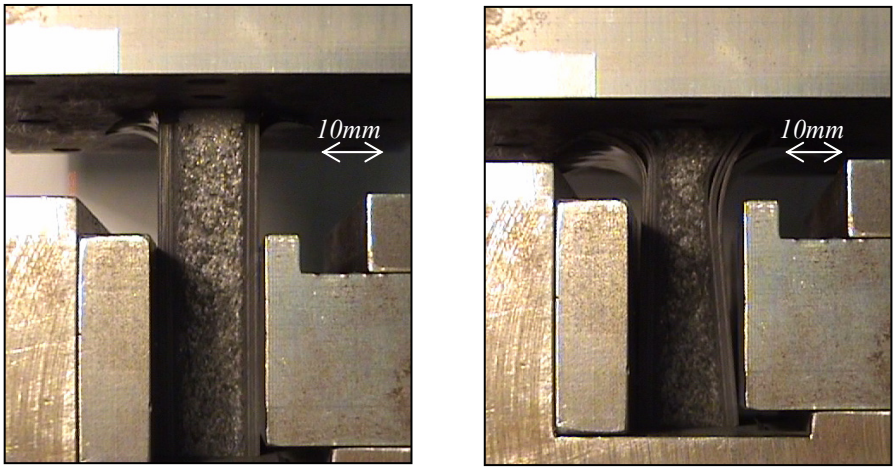

(a) *(b)*

Figure 7.5– *Rectangular foam core sandwich sample: (a) crushing of trigger; (b) global buckling*

In the case of the skin test, the same test set-up was used. The predicted buckling load and experimental peak load values are summarised in table 7.2.

	[N]
Wide-column theory predicted load	*4280*
Plate theory predicted load (FE analysis)	*4500*
Average experimental peak load	*4090*

Table 7.2– *Predicted and experimental load values for a skin sample (rectangular sample configuration)*

It was observed that the skin specimens did not experience global buckling. This was also confirmed by the predicted critical values which are higher than the maximum load reached during the test. In this case the presence of the trigger lowers the peak load and promotes a local collapse. For all the other core combinations, a local failure mechanism along most of the specimen length is achieved. A peak value in the region of 20kN for most of the pinned cores and of 10kN for the honeycomb cored samples were recorded. Those peak values are lower than the expected buckling loads according to eq. 7.3 when using the shear modulus values determined in Ch. 5.

Although global buckling has not been observed for the pinned, honeycomb cored and skin samples, the experimental evidence suggests that this specimen geometry is not suitable for promoting progressive crushing in flat plates (figures 7.22 and 7.24 sections

7.6 and 7.7 respectively). An unstable local failure mechanism, related to delamination of the laminae in the skins together with facesheet debonding from the core for the honeycomb samples, makes the collapse process neither controllable nor progressive. The load-displacement traces give a clear indication of unstable damage propagation in the sample (section 7.6). This means that the crush front in the specimen does not progress with the same velocity of the delamination front, as it should in a correct progressive crushing mechanism (a detailed critical analysis of the collapsing behaviour can be found in section 7.6.2).

7.4.2.1 Improved design

In the crushing of the trigger of the specimen, a progressive collapsed front was observed moving at the same speed as the platen. At least in the triangulated part of the sandwich flat specimen, a localised failure was achieved. This suggests that a self-triggering specimen of triangular geometry can undergo progressive crushing. A similar phenomenon is observed in the case of truncated cone shaped specimens. For the latter ones, a stable and progressive failure takes place with no need for a trigger [165]. Similar / comparable values of specific energy absorbed and failure modes between the two shapes are also achieved. There is a similarity between the close geometry and the open geometry specimens. Square flat plate specimens need like tubes a trigger at one end to initiate a progressive crushing and are both characterised by a constant cross-section opposing the crush load. Cones and triangular flat plate specimens are self-triggering shapes characterised by an increasing cross-section during the crushing event. Closed shaped specimens present the advantage of an inner stability towards global buckling, while for the open geometry shapes this is achievable either by choosing the supporting fixture or an appropriate specimen geometry.

The triangular specimen geometry employed is shown in figure 7.6. For manufacturing convenience the specimen width was maintained the same as in the previous configuration. The height was chosen so as to have the same vertex angle (~60°) at the top of the truncated pyramid.

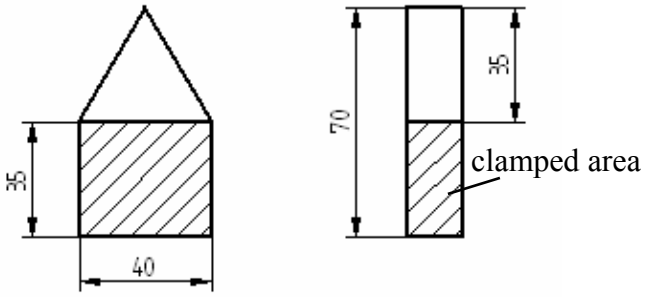

Figure 7.6– *Improved specimen configuration: nominal dimensions in mm*

7.4.2.2 Design for optimum work rate decay

Another advantage in terms of energy absorption capacity of a triangular shaped specimen comes from their geometry. During a crash event from a crashworthiness point of view, if we consider the specimens as absorbing devices, the sum between the kinetic energy and the work done by the structure to absorb it must be equal to zero. It is desirable that this energy will be absorbed over a large period of time, which means maintaining the rate of work, done by the absorbing device, as low as possible [189].

In a simplistic approach the amount of energy absorbed can be seen only as a function of the amount of crushed material. If we consider a triangular and a rectangular specimen characterised by the same volume, maximum width, thickness and material, the crush length required to absorb the same amount of energy and the time of the crushing process are doubled in the case of the triangular sample. Figure 7.7 shows this situation with the specimens overlapped.

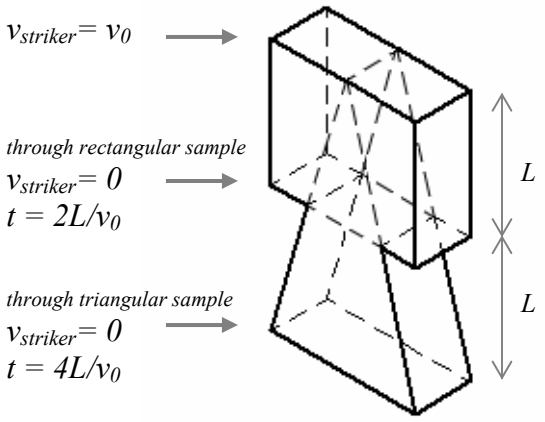

Figure 7.7– *Energy absorption rate for a triangular and rectangular samples of equivalent volume*

The rate of energy absorption for a triangular specimen is lower than for a rectangular one. The goal of crashworthiness is to absorb the kinetic energy possessed by the striker over a time frame as large as possible in order to achieve lower deformation and deceleration rates.

7.5 Data analysis: specific energy absorption calculation

The energy absorbed by crushing is usually expressed in terms of energy absorbed per unit mass of material that has been crushed. A progressive local collapse mechanism is achieved when the crush front moves at the same rate as the machine cross-head [165, 167]; this is a crucial characteristic of a correct in-plane crushing test. For specimens characterised by a constant cross-sectional area, (circular cross-section tubes, flat rectangular specimens, etc.), the size of the crush zone remains constant throughout the test [165]; the corresponding idealised crushing load-displacement curve is shown in figure 7.8.

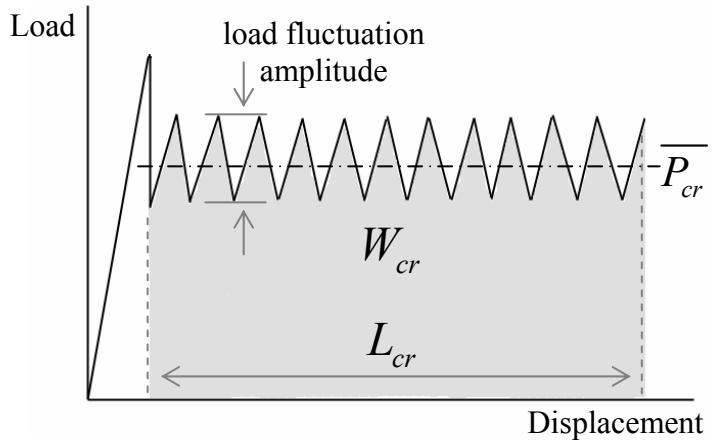

Figure 7.8– *Idealised crushing load-displacement curve for samples with constant cross-sectional area*

The initial slope of the load-displacement curve is almost linear and it is associated with elastic deformation of the specimen (tube or flat laminate in this case) up to a peak value. The load then drops to a constant crushing load that oscillates about an average value, $\overline{P_{cr}}$; the amplitude of the fluctuations, the peak load and the average sustained

load are found to follow a non linear relation, function of both the geometry of the trigger [165, 186], and of the specimen thickness, [165]. The specific energy absorption (SEA) is given by the following general formula:

$$SEA = \frac{W_{cr}}{M_{cr}} = \frac{\overline{P_{cr}}}{A\rho} = \frac{\overline{\sigma_{cr}}}{\rho} \tag{7.8}$$

where W_{cr} is the total crush work, M_{cr} is the specimen mass and ρ its density. A is the sample cross-section perpendicular to the in-plane load. The average crushing load, $\overline{P_{cr}}$, or stress, $\overline{\sigma_{cr}}$, can be determined from the energy absorbed in the crushing process, which is represented by the area under the curve shown in figure 7.8. For specimens characterised by a constant cross section the work done in crushing can be simply determined as:

$$W_{cr} = \overline{P_{cr}} L_{cr} \tag{7.9}$$

where L_{cr} represents the crushed length. In the case of flat triangular and conical specimens both the average load and the specimen cross-section change with the crush distance. A nearly linear increase in load with crush displacement for flat specimens is observed, just as for conical specimens [165]. An idealised crushing load-displacement curve for flat triangular and conical specimens is shown in figure 7.9.

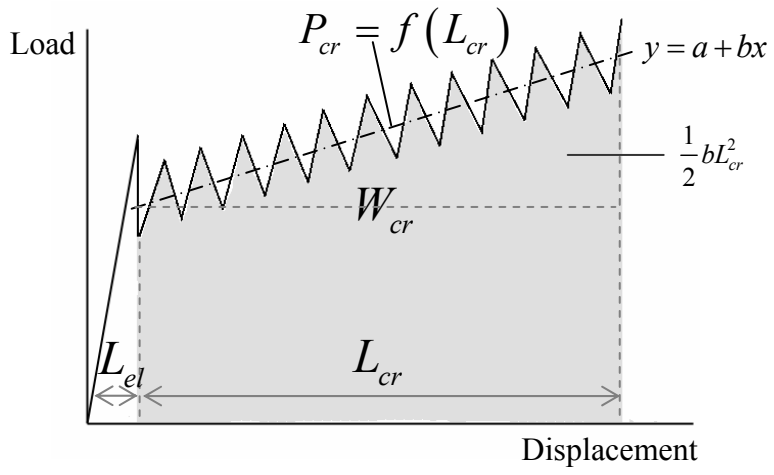

Figure 7.9– *Idealised crushing load-displacement curve for samples with linearly increasing cross-sectional area*

In this case in the specific energy absorption formula, eq. 7.8, both the crushing load P_{cr} and the perpendicular crushed area A_{cr}, are functions of the crush length L_{cr}.

Crushing load as function of L_{cr}

A linear equation 7.10 that best fits the sample data, as in figure 7.9, can be determined [190]; it expresses the change in crushing load P_{cr} as a function of the crushed length L_{cr}.

$$y = a + bx \tag{7.10}$$

This approach can be also associated to the previous case of constant cross-section; for the coefficients of eq. 7.10 will assume the following values:

$$\begin{cases} a = \dfrac{W_{cr}}{L_{cr}} = \overline{P_{cr}} \\ b = 0 \end{cases} \tag{7.11}$$

where the parameter a is associated with the crushing energy absorbed. Similarly for the case of increasing cross-section, the way proposed to evaluate the coefficient a of the regression line (eq. 7.10) is based on energy conservation. The parameter b is determined by the method of the least squares (figure 7.10). Thus the straight line (eq. 7.10) gives an average value of the load at each stage of crushing respecting the energy conservation. From figure 7.9, the expression of the crushing energy absorbed is given by:

$$W_{cr} = aL_{cr} + bL_{el}L_{cr} + \frac{b}{2}L_{cr}^2 \tag{7.12}$$

where L_{el} is the length associated with an elastic deformation of the sample prior to the crushing process. Hence the value of the coefficient a is:

$$a = \frac{W_{cr}}{L_{cr}} - bL_{el} - \frac{1}{2}bL_{cr} \tag{7.13}$$

The slope of the line b is evaluated by minimizing the error between the regression line and the experimental data population (as shown in figure 7.10).

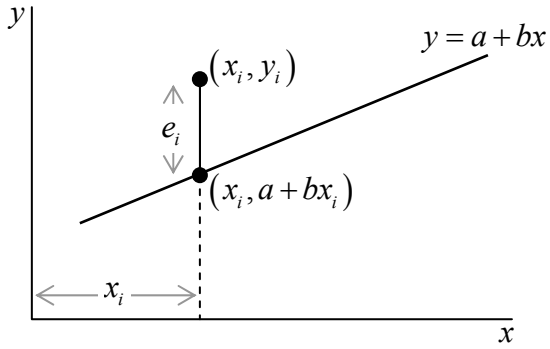

Figure 7.10– *Error between the regression line and the experimental data population*

It follows that the error e_i can be expressed as:

$$e_i = y_i - (a + bx_i) \tag{7.14}$$

and according to the least squares method:

$$\sum_{i=1}^{N} e_i^2 = \sum_{i=1}^{N} \left(y_i - (a + bx_i) \right)^2 \tag{7.15}$$

If we minimise this summation with respect to the unknown b we obtain:

$$\frac{\partial \sum_{i=1}^{N} e_i^2}{\partial b} = 0 \tag{7.16}$$

equivalent to:

$$\sum_{i=1}^{N} x_i y_i - a \sum_{i=1}^{N} x_i - b \sum_{i=1}^{N} x_i^2 = 0 \tag{7.17}$$

Eliminating a gives:

$$\begin{cases} a = \dfrac{W_{cr}}{L_{cr}} - bL_{el} - \dfrac{1}{2} bL_{cr} \\ b = \dfrac{\sum_{i=1}^{N} x_i y_i - \dfrac{W_{cr}}{L_{cr}} \sum_{i=1}^{N} x_i}{\sum_{i=1}^{N} x_i^2 - \left(L_{el} + \dfrac{1}{2} L_{cr} \right) \sum_{i=1}^{N} x_i} \end{cases} \tag{7.18}$$

which are the unknown coefficients of the straight line 7.10 which averages the crushing load as a function of the crush distance.

Crushed volume as function of L_{cr}

The other quantity that needs to be evaluated as a function of the crush length L_{cr} is the crushed volume. As shown in figure 7.11, a generic crushed volume of the triangular plate specimen is a truncated pyramid of volume given by the following expression:

$$V_{cr}\left(L_{cr}\right) = t(2L_{el} + L_{cr})L_{cr}\tan\alpha \tag{7.19}$$

where L_{el} is the displacement associated with the initial linear compressive response and α is half of the vertex angle of the pyramid.

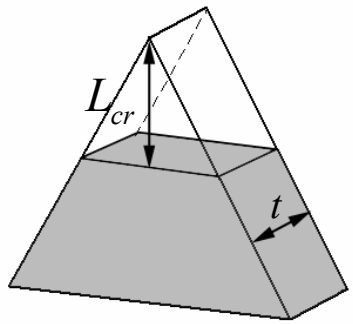

Figure 7.11– *Generic crushed volume of the triangular specimen*

For the triangular flat specimen the calculation of the specific energy absorbed in the crushing process is given by:

$$SEA = \frac{W_{cr}}{M_{cr}} = \frac{P_{cr}}{\rho t(2L_{el} + L_{cr})\tan\alpha} \tag{7.20}$$

Thus, both the crushing load (eq. 7.10) and the crushed volume (eq.7.19) can be expressed as functions of the crush length. This allows a 'punctual' estimation of the SEA to be made as the test progresses. It is an interesting tool that can provide insight on how the energy absorption capacity for material systems characterised by similar overall SEA values varies along the sample profile. It also allows to determine the critical minimum cross-section after which the SEA becomes constant.

7.6 Test results and performance analysis

The typical load-displacement traces for the two different test configurations (rectangular and triangular) analysed are shown in figures 7.12 and 7.13. In this case the in-plane crushing response for the skin specimens is shown. Similar trends in the load-displacement response for rectangular plate samples have been observed for the other material systems tested.

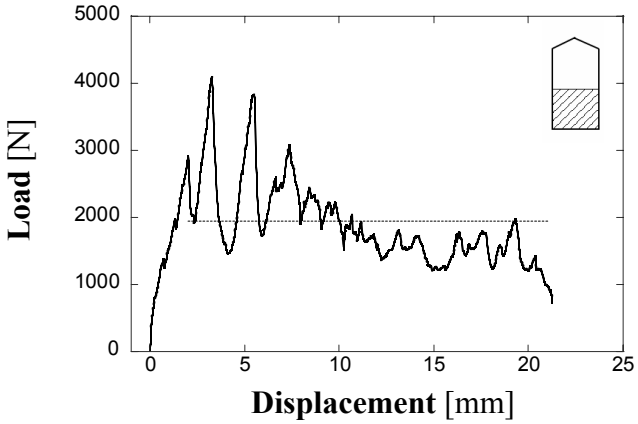

Figure 7.12– *Typical load-displacement curve for skin rectangular specimen*

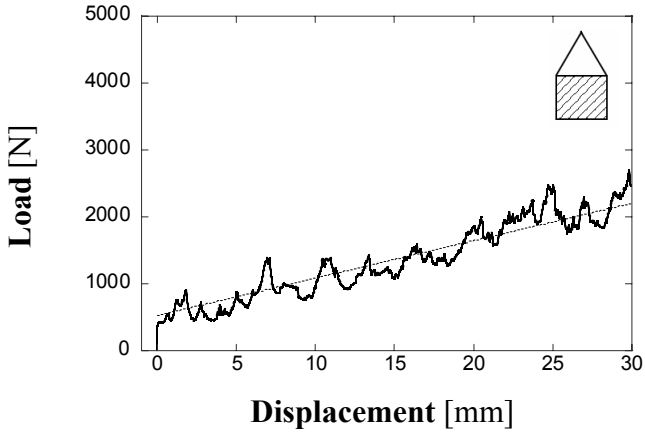

Figure 7.13– *Typical load-displacement curve for skin triangular specimen*

For both samples the load is serrated over the average crushing value which is indicated on the graphs with a dotted line and calculated according to the methodologies previously explained. The amplitude of these fluctuations was found always higher in the case of square plate specimens for all the different material systems tested. This may indicate that for the rectangular sample configuration, larger delaminations and unstable growth are taking place during in-plane loading. Moreover, Hull [157] shows that the heights of the serrations on the average crushing load P_{cr}, in a correct and ideal progressive crushing, should be independent of crush distance indicating that the failure mechanisms are constant throughout the crush. The curve of figure 7.12 resembles those observed for laminate samples with no lateral constraints [161, 168].

The graphs in figures 7.14-16 compare the typical in-plane crushing response and the average crush load values for the different material systems tested. The load-displacement behaviour of a foam cored specimen is compared to a honeycomb cored sample, figure 7.14. The other graphs show a pinned core and the corresponding hollow configuration crushing behaviour, figures 7.15 and 7.16.

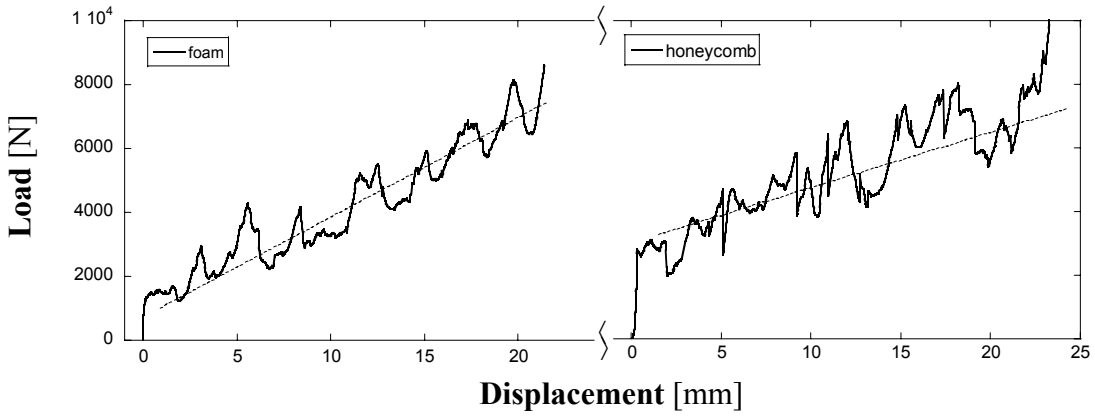

Figure 7.14– *Typical crushing curve (load-displacement) for foam and honeycomb core sandwich triangular specimens*

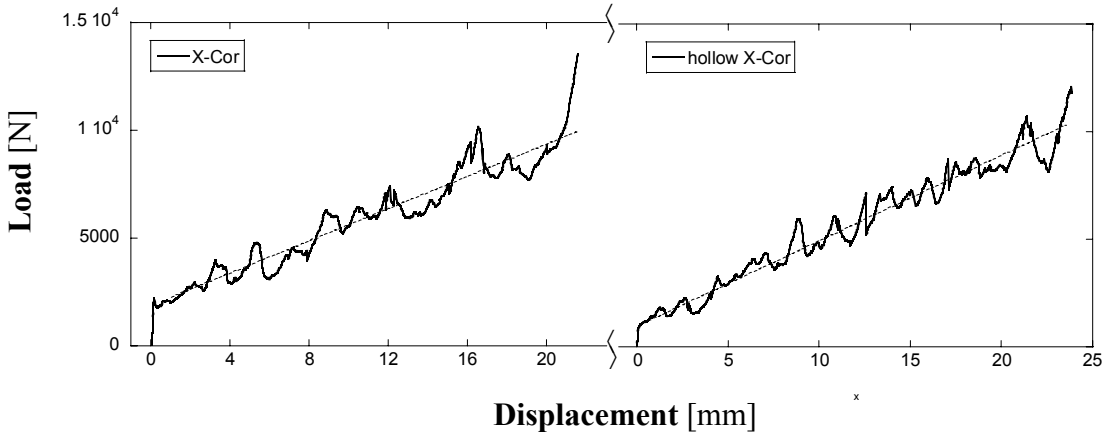

Figure 7.15– *Typical crushing curve (load-displacement) for foam-filled and hollow X-Cor triangular samples ((E)K-Cor^{F}/0.51/11°/0.06 and (E)X-Cor$^{H}_{I}$/0.51/11°/0.06)*

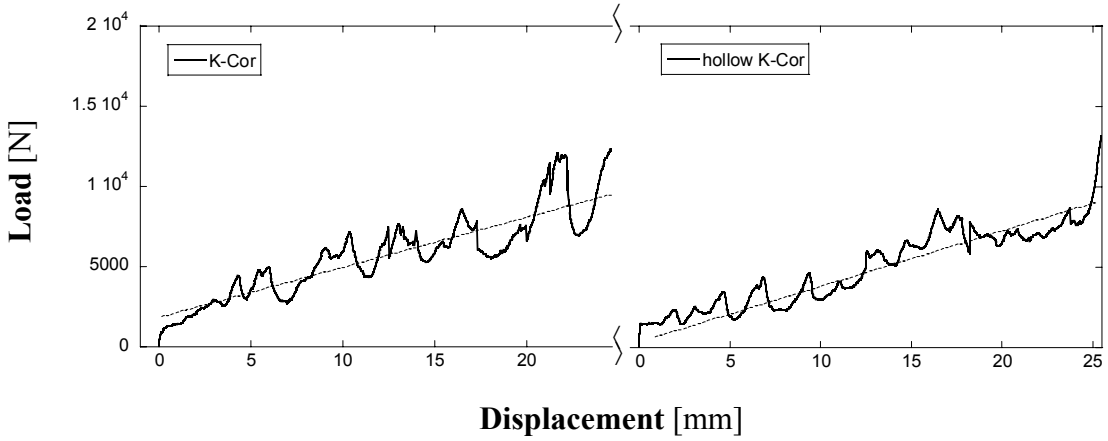

Figure 7.16– *Typical crushing curve (load-displacement) for foam-filled and hollow X-Cor triangular samples ((E)X-Cor$^{F}_{I}$ /0.51/11°/0.06 and (E)K-Cor^{H}/0.51/11°/0.06)*

Due to the load fluctuations, a superimposition of the curves would result in unclear graphs. A more effective and direct way to evaluate the degree of consistency and reliability of the experimental results for the new test configuration is to indicate the average and the standard deviation values of the parameters of the straight lines (eq. 7.10) for each case considered. As explained in section 7.5, those curves even out the crushing loads, maintaining the conservation of energy and represent a valid way of characterising the material crushing behaviour.

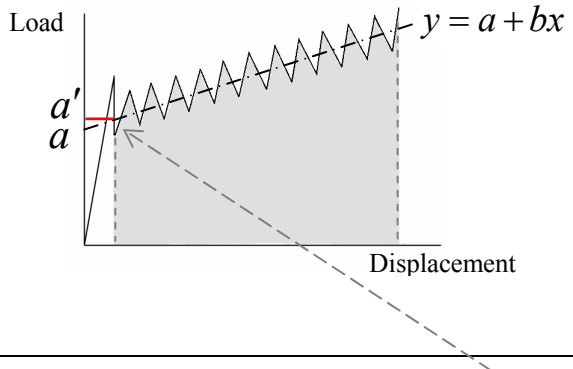

sample type identification	*b* *[Nmm^{-1}]*	*a* *[N]*	*a'* *[N]*
(E)Skin	*53±4*	*602±106*	*(609)*
(E)Foam 21 IG	*182±53*	*1619±309*	*(1647)*
(E)Al honeycomb	*174±21*	*3015±276*	*(3101)*
(E)X-Cor$^{F}_{I}$/0.51/11°/0.06	*453±83*	*1473±390*	*(1539)*
(E)X-Cor$^{H}_{I}$/0.51/11°/0.06	*403±37*	*1307±369*	*(1416)*
(E)K-Cor^{F}/0.51/11°/0.06	*438±5*	*1111±300*	*(1217)*
(E)K-Cor^{H}/0.51/11°/0.06	*300±35*	*777±366*	*(832)*

Table 7.3– *Experimental scatter for the parameters of eq.7.10*

The values of table 7.3 represent the slope b, the y-intercept a and the average load value at the beginning of the crushing process determined with eq. 7.10 and indicated in the table as a'. The calculated SEA values are summarised in table 7.4 and figure 7.17. The specimen total density is also indicated, as for in-plane loading all the parts of the sandwich construction take part in the crushing process. The value in parenthesis represents the expected global densities of the samples calculated simply by considering the volume and the density of each component that make up the sandwich sample.

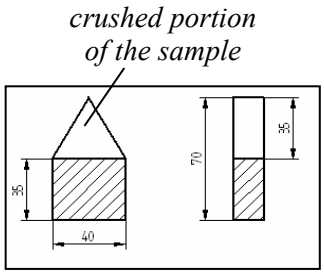

sample type identification	*no. sample*	*sample density[kgm^{-3}]*	*SEA [kJkg^{-1}]*
(E)Skin	*2*	*1578*	*23±1*
(E)Foam 21 IG	*3*	*464 (473)*	*41±3*
(E)Al honeycomb	*3*	*559 (552)*	*44±6*
(E)X-Cor$^{F}_{1}$/0.51/11°/0.06	*3*	*471 (464)*	*64±7*
(E)X-Cor$^{H}_{1}$/0.51/11°/0.06	*3*	*469 (442)*	*56±7*
(E)K-Cor^{F}/0.51/11°/0.06	*3*	*489 (489)*	*63±6*
(E)K-Cor^{H}/0.51/11°/0.06	*3*	*473 (460)*	*40±2*
(E)K-Cor^{F}/0.51/33°/0.06	*1*	*474 (469)*	*55*

Table 7.4– *Densities and SEA values of the materials tested*

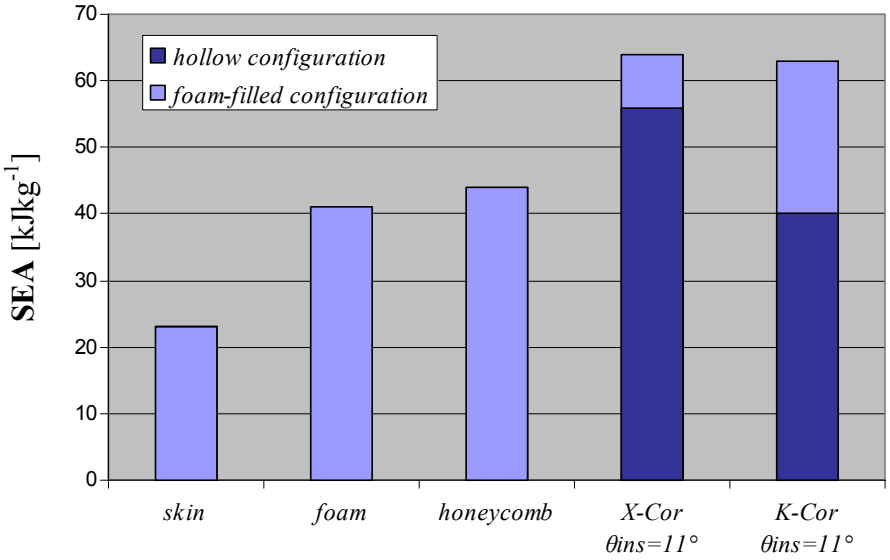

Figure 7.17– *SEA values of the materials tested*

The SEA values of table 7.4 show that when two skins are sandwiched with a foam or a honeycomb core, the total energy absorption capacity obtained is almost double the value obtained for a single skin. In the case of the foam filled X-Cor and K-Cor the SEA values are similar, but the respective hollow configurations are characterised by a substantial difference. The core contribution to the total specimen SEA is only a fraction of the contribution given by the composite skins; this is due to the cores much lower in-plane mechanical properties and densities (Ch. 3). The principal role of the core is to guarantee an out-of-plane support of the skins during the in-plane crushing process, keeping the relative distance between the skins constant and stabilising them during in-plane crushing. The core support maximises the SEA of the specimen. For this reason in

the case of X-Cor samples, due to the mechanical fastening between pins and skins a higher degree of structural stability is achieved and the foam removal accounts for about 10% of the total energy absorption capacity. In the case of K-Cor, for in-plane loading, the degree of structural stability provided by the pins adhesively bonded on the facesheets is 30% lower than in the case of the X-Cor samples. This is deducted from the difference in the SEA values for the hollow configurations. In K-Cor specimens the foam plays a fundamental role in in-plane crushing.

Another way to evaluate how the different sandwich systems behave in terms of energy absorption is to plot the variation of the specimen SEA during crushing as shown in the graphs of figure 7.19 and 7.20. In the abscissa of the graphs there is the width of the specimen cross-section (the thickness is constant), perpendicular to the load, varying linearly with the crush length (figure 7.18).

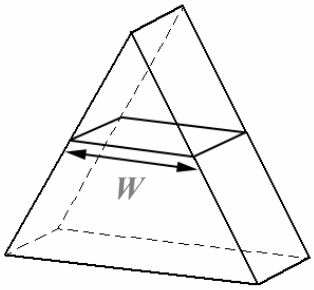

Figure 7.18– *Varying width of the specimen cross-section during the test*

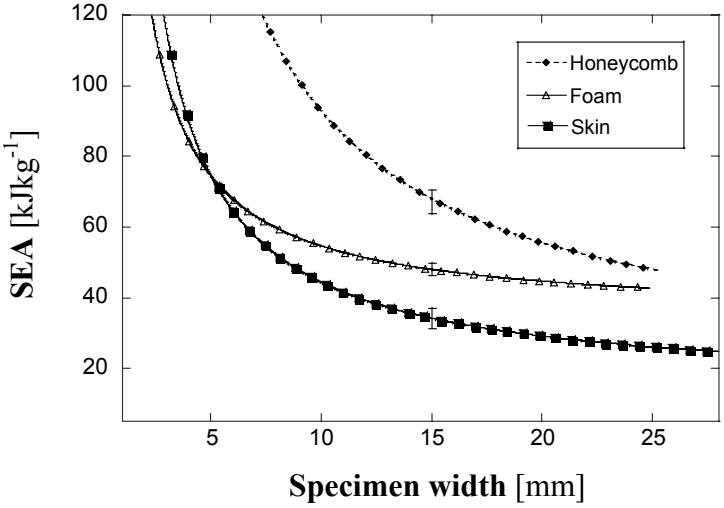

Figure 7.19– *Plot of SEA as a function of specimen width for skin, foam 21 IG and Al honeycomb samples*

Figure 7.19 shows the SEA capacity as a function of the width of the resisting section for foam and honeycomb cored sandwich specimens and for the skin samples. It is evident that for a small resisting portion of material along the specimen, honeycomb has a consistently higher energy absorption capacity. As the opposing cross-section increases, the SEA for the foam cored samples begins to approach honeycomb performance. Similar behaviour is exhibited by the K-Cor samples matching the X-Cor SEA values only for a width of the resisting section of at least 15mm (figure 7.20).

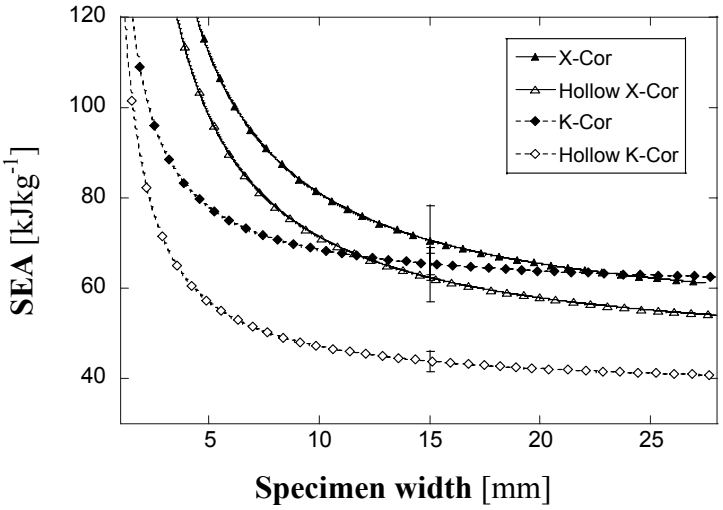

Figure 7.20– *Plot of SEA as a function of specimen width for (E)X-Cor$^{F}_{1}$ /0.51/11°/0.06, (E)X-Cor$^{H}_{1}$ /0.51/11°/0.06, (E)K-Cor^{F} /0.51/11°/0.06 and (E)K-Cor^{H} /0.51/11°/0.06 samples*

The bi-dimensional type of support offered by the honeycomb cell wall is effective, even for very small portion of material involved in the crushing process. The tested pinned cores have a low pin areal density (nominal value 0.062 pin/mm^2) and do not offer enough local skin support, if the resisting cross-section is too small. For very short specimen width there is a low probability first to encounter a pin and then that it is perfectly fastened to both sides (it is inserted in this case with an 11° angle). Figure 7.21 shows a specimen tip of a hollow K-Cor sample which indicates this situation. The out-of-plane support, for the pinned core samples, is provided in a continuous way only by a foam core characterised by a low-out-of-plane compression modulus (9±1 MPa, table 6.2) which for a small resisting section does not maximise the skin crushing process. As a consequence, for the pinned core samples, the SEA values associated with the very

initial stage of crushing are very low and comparable with the values found for simple skin specimens.

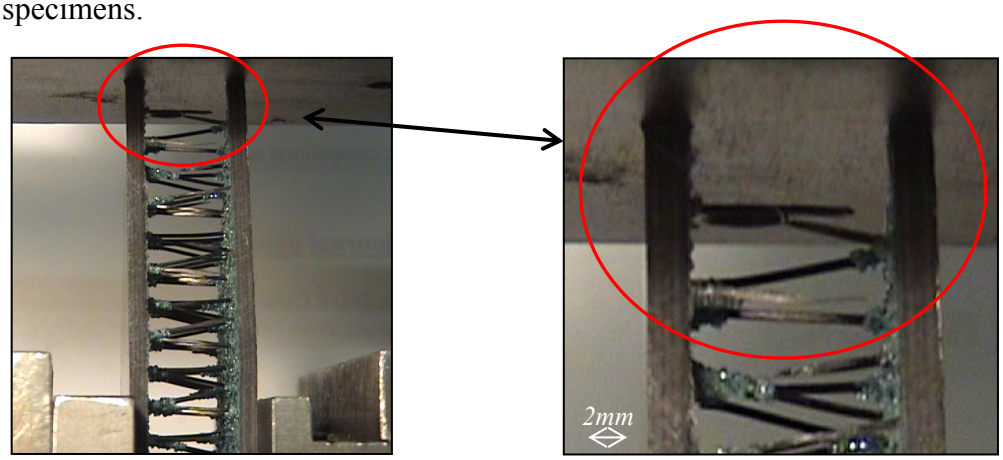

Figure 7.21– *Tip of a hollow K-Cor sample: there no pins bridging the two skins*

The performance in terms of SEA of the Al honeycomb cored sandwich samples can be considered equivalent to that of the hollow K-Cor. It is, in fact, outperformed by the pinned core sandwich sample although characterised by a higher out-of-plane modulus, (*198±10*MPa, Ch.3) which should provide more transverse support to the crushing skins. The K-Cor in the hollow configuration is the lowest performing among the pinned cores, characterised by an out-of-plane compression modulus of *112±17*MPa (Ch.6). The drawback exhibited by the honeycomb is typical of traditional sandwich systems characterised by a poor skin-to-core interfacial strength. As a consequence, debonding occurs (figure 7.22) during the in-plane crushing test, reducing the potential lateral support given by a stiff transverse modulus.

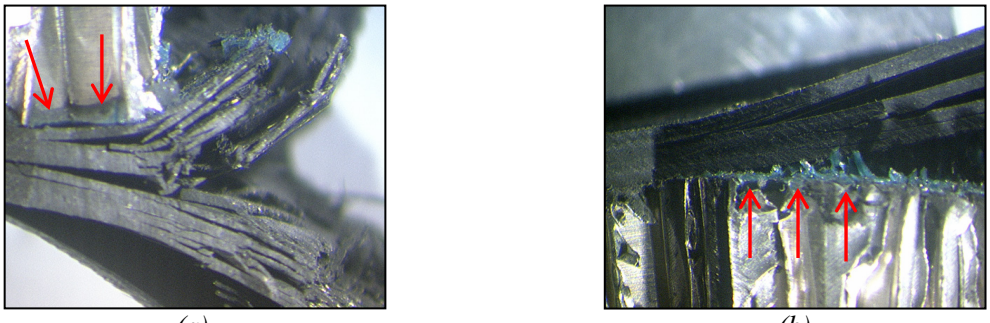

(a) *(b)*

Figure 7.22– *(a) Localised skin-honeycomb core debonding in triangular sample*
(b) Spread skin-honeycomb core debonding in rectangular sample

Passing from the first specimen configuration (flat rectangular plate with trigger) to the triangulated sample confined the skin-core debonding in a smaller portion of the specimen length (crush-damage front) as shown in figure 7.22(a). For the flat rectangular specimen configuration this debonding mechanism caused an irregular damaged front along the sample length (figure 7.22(b)).

7.6.1 Comparison with out-of-plane compression energy absorption results

To have a better overview of the energy absorption properties of the different cores studied, the SEA values obtained from the out-of-plane compression tests are reported here. For the method and the data analysis refer to sections 4.1.2, 4.3 and standard ASTM C365 [128]. For this test condition it is necessary to consider that the specimen in the post-elastic phase does not fail in a controlled manner as it is in the case of progressive crushing. The principal failure mechanism is set by pin buckling, leading to a catastrophic failure followed by a phase firstly characterised by a plateau and then by a densification region (Ch.6). The SEA values are calculated considering the whole test up to the beginning of the densification (initial brief elastic response included). For this loading condition the skins do not contribute to the energy absorption process but are indispensable to provide structural efficiency for X-Cor and K-Cor.

Table 7.5 summarises the experimental results for core densities and SEA values. The energy absorption values are calculated considering both the nominal and effective areas of the specimen according to the load-bearing pin approach, as explained in section 4.3.1. The results include also the findings for X/K-Cor characterised by the same pin areal density (nominal value 0.062 pin/mm^2) but different pin insertion angle (θ_{ins}=33°). A detailed description of the materials can be found in section 3.3.

sample type identification	*core density [kgm^{-3}]*	*nom SEA [kJkg^{-1}]*	*eff SEA [kJkg^{-1}]*
(C)Foam 21 IG	*22.60*	*8.60±0.10*	--
(C)Al honeycomb	*72.00*	*29.13±0.14*	--
(C) X-Cor$^{F}_{I}$/0.51/11°/0.06	*48.25*	*22.60±0.68*	*25.78±0.78*
(C) X-Cor$^{H}_{I}$/0.51/11°/0.06	*25.65*	*19.40±0.14*	*22.13±0.06*
(C)K-Cor^{F}/0.51/11°/0.06	*48.25*	*20.99±2.13*	*23.98±2.52*
(C)K-Cor^{H}/0.51/11°/0.06	*25.65*	*12.90±0.64*	*14.70±0.37*
(C)X-Cor$^{F}_{I}$/0.51/33°/0.06	*52.50*	*14.77±0.26*	*18.50±0.34*
(C)X-Cor$^{H}_{I}$/0.51/33°/0.06	*29.90*	*9.15±0.88*	*11.41±1.12*
(C)K-Cor^{F}/0.51/33°/0.06	*52.50*	*13.58±0.38*	*17.08±0.52*
(C)K-Cor^{H}/0.51/33°/0.06	*29.90*	*5.87±0.64*	*7.30±0.79*

Table 7.5– *Out-of-plane compression loading: energy absorption results (SEA values)*

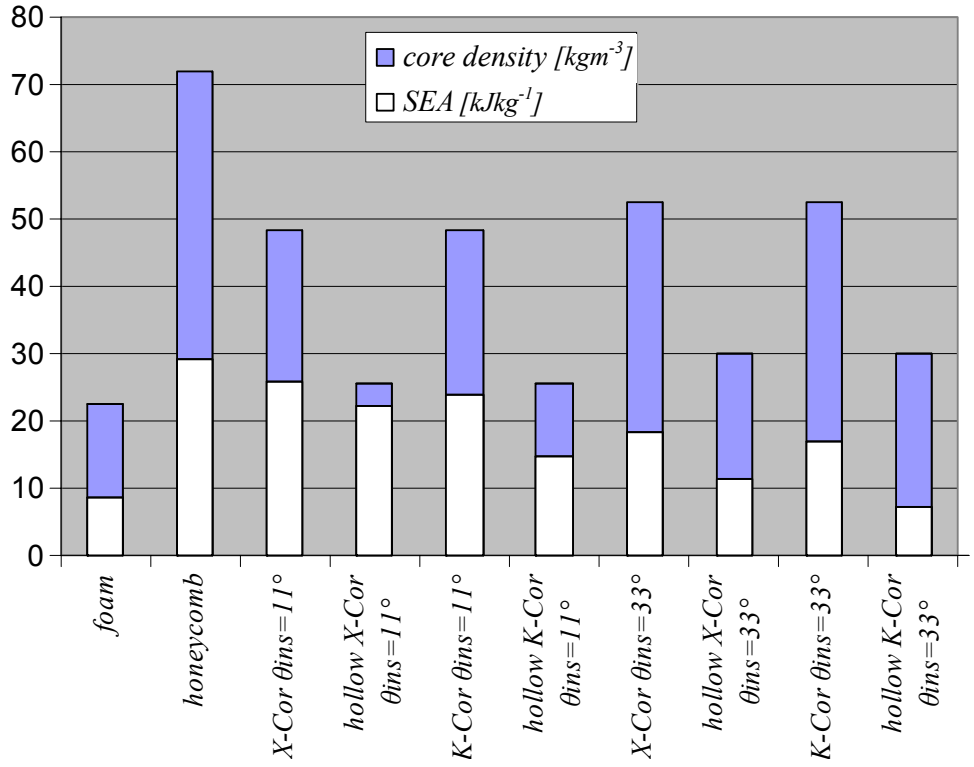

Figure 7.23– *Out-of-plane compression loading: energy absorption results (SEA values) and core density values*

From the table and the histogram graph it is evident that the honeycomb core has SEA values comparable to those of X/K-Cor characterised by a 10° pin insertion angle. As found in the out-of-plane compression behaviour (Ch.6), there is, accordingly, an insertion angle effect on the energy absorption which is maximised for a core with more vertical pins. Similarly as for the in-plane crushing results, the 11° X-Cor is not affected by the presence of the foam as are all the other pinned core configurations. The mechanical fastening typical of X-Cor plus an almost vertical pin insertion (10°) is an effective combination against a crushing load. In a flatwise condition the honeycomb core samples outperform the pinned cores in terms of energy absorption capacity. The out-of-plane loading direction promotes the most energy efficient crushing mechanisms for the honeycomb core (cell-wall buckling, followed by a post-elastic phase characterised by plastic deformation) without instigating skin-core debonding, one of the principal drawbacks in the in-plane loading of these sandwich structures.

7.7 Crush zone morphology and failure mechanisms identification

The first objective of this section is to assess by means of visual inspection whether the damage mechanism taking place in the triangular sample during in-plane loading can be defined as progressive crushing. The second part presents an analysis of the failure mechanisms competing in the crushing process.

Progressive crushing is recognised when the crush front and the delamination front are going through the specimen with the same velocity and in a regular manner. The serrated load-displacement curve is characteristic of progressive crushing and it is indicative of a stick-slip form of propagation in which the stresses required to initiate growth are higher than those of propagation. Load relaxation is associated with rapid crack growth in the crush zone [157].

In the case of unstable local collapse, delaminations and cracks propagate in the specimen irregularly, involving a variable damaged length during the application of the load. It is not possible to delineate a clear consistent delamination front, but it is evident

that the damage is not involving the full length of the specimen; it travels unevenly down the sample as the test carries on.

In the occurrence of global collapse, delaminations propagate in an irregular manner throughout the whole sample length. It is not possible to distinguish a delamination front.

These three failure modes (progressive crushing, unstable local collapse and global collapse) are competing mechanisms. It is also necessary to note that once the progressive crushing is established at the beginning of the crushing process, it needs to sustain itself throughout the whole sample length for the entire duration of the test.

It was observed for the first configuration of specimens considered (rectangular plate with a triggered end) in the case of honeycomb and pinned cores, that an unstable local failure was taking place. Figure 7.24 shows an advanced stage of the in-plane crushing process along rectangular specimens of different material configurations. The crush front, represented by the metal platen, does not proceed along the specimen at the same rate as the delamination/damage front.

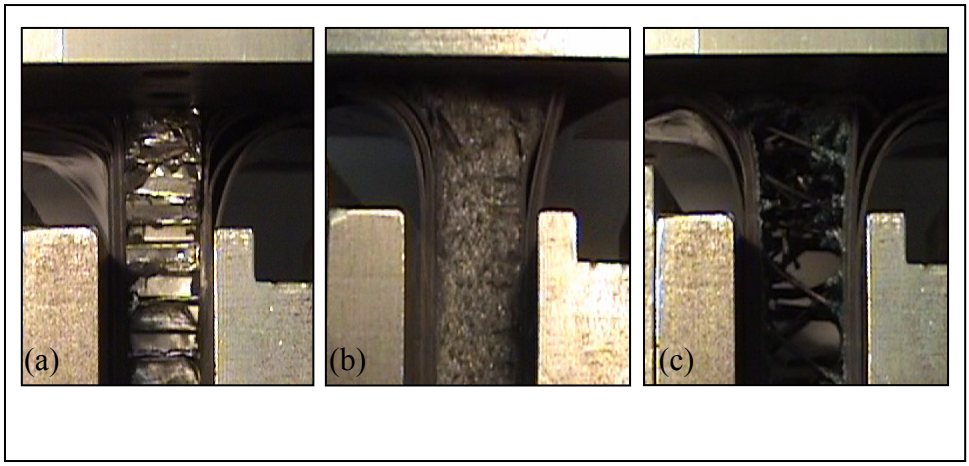

Figure 7.24– *In-plane crushing process in different rectangular shaped samples: (a) honeycomb; (b) X-Cor and (c) hollow K-Cor*

In the case of flat triangular specimens the crush and delamination fronts proceed simultaneously along the specimen. The progressive crushing mechanism is taking place throughout the duration of the test even for short lengths of the samples. The series of photographs (figures 7.25 – 7.27) show the phases of the crushing process for a foam cored, X-Cor and hollow K-Cor specimens. The damage process occurs in the

proximity of the crush platen. This can be assessed even once the test is stopped and the crusher removed, the portion of the specimen below the damaged end is intact.

Figure 7.25– *Different phases of progressive failure during in-plane crushing test on a foam cored triangular specimen, (E)Foam 21 IG*

Figure 7.25 shows a test on a foam cored sample which represents the most critical specimen configuration as the core is characterised by the lowest mechanical properties among the tested materials. In contrast the global buckling failure observed for rectangular samples (section 7.4.2, figure 7.5), in this case the in-plane loading promotes a smooth progressive crushing along the specimen length.

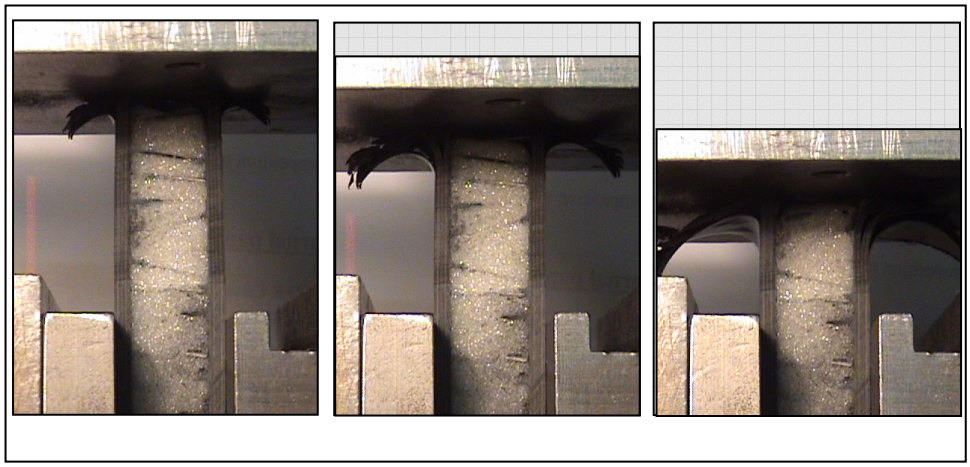

Figure 7.26– *Different phases of progressive failure during in-plane crushing test on an X-Cor triangular specimen*

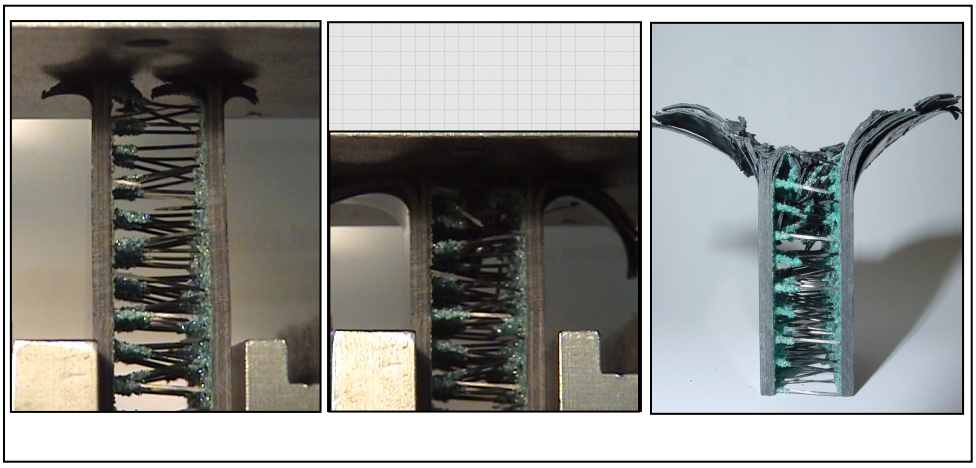

Figure 7.27– *Different phases of progressive failure during in-plane crushing test on a hollow K-Cor triangular specimen*

In the energy absorption there is a competition between collapse modes depending on geometrical, microstructural and testing parameters. As for composite tubes and cones, it was observed that also flat laminated samples experience two different competing crushing modes. These are essentially delamination (for closed profile is called "splaying") and fragmentation, as defined and described in reference [157]. The lay-up sequence of the skins plays a fundamental role. In this case the stacking sequence of each skin made up with unidirectional plies is $\left[\pm 45, 90, 0\right]_{2S}$ .The internal (towards the sample mid-plane) and the external layers support those 0° layers and minimise their premature buckling. Figure 7.28 shows a simple configuration of a laminate which undergoes progressive crushing under an in-plane loading. In this case, for a simple lay-up $\left[90, 0\right]_S$, the material exhibits a delamination failure mode during the progressive crushing.

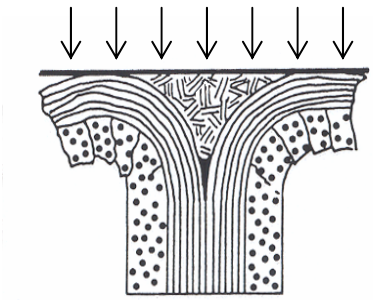

Figure 7.28- *Schematic of progressive crushing (delamination failure mode) in a* $\left[90, 0\right]_S$ *laminate, picture adapted from [157]*

Ideally there is a split of the 0° layer at the mid-plane; as the crushing progresses the 90° layers characterised by low mechanical properties in the direction perpendicular to the fibres fail. The test on the skin alone produced a pattern similar to that shown in figure 7.28 (figure 7.29).

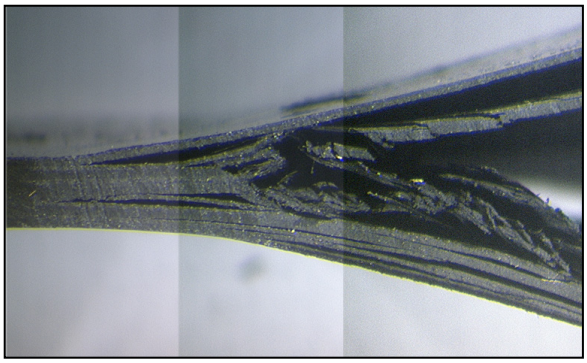

Figure 7.29- *Crushed skin sample,* $[\pm 45, 90, 0]_{2S}$ *lay-up*

In the case of sandwich samples, the presence of the core between the two skins plays a significant role in determining the dominant failure mode of the crushing process. In fact the specimen mid-plane is in this case is located at the middle of the core and all the delaminations of the internal layers and the damage of the core will be balanced by the other half of the specimen undergoing the same process. This creates favourable conditions for a fragmentation failure mode of the central section of the specimen, as shown in the schematic drawing of figure 7.30.

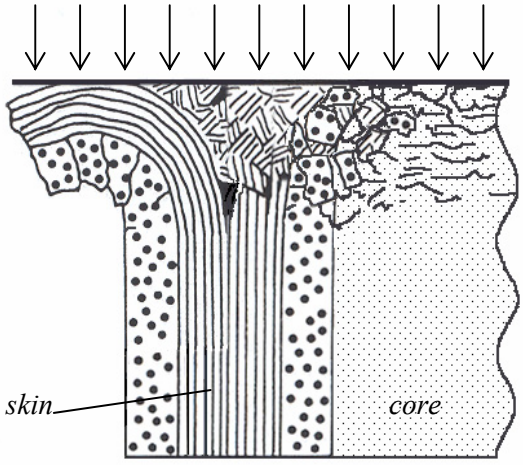

Figure 7.30- *Schematic of progressive crushing (delamination and fragmentation failure modes) in half sandwich structure with* $[90, 0]_S$ *laminate skins*

This mixed failure mode achieved in progressive crushing is noticeable in figure 9.31. The external skin layers of the hollow X-Cor specimen have delaminated and spread out from the inner part which underwent fragmentation.

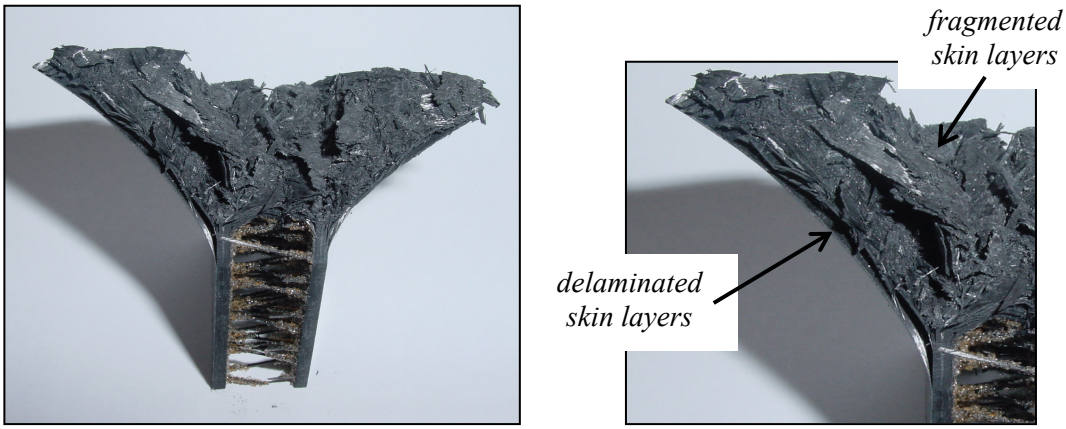

Figure 7.31- *Crushed hollow X-Cor (E)X-Cor$^{H}_{1}$/0.51/11°/0.06 specimen*

For both X-Cor and K-Cor a higher degree of fragmentation is achieved if compared to the foam and honeycomb cored samples. This explains the higher SEA values found. Figure 7.32 shows the side view of the crushed end for a hollow K-Cor sample.

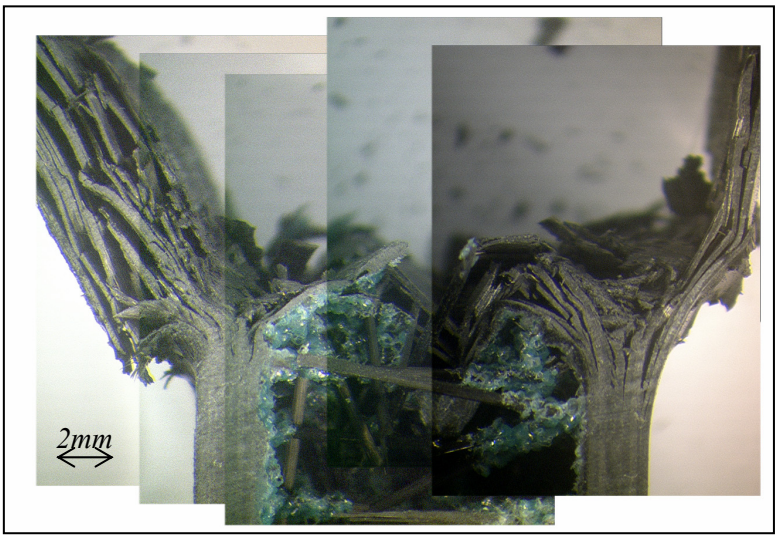

Figure 7.32- *Crushed hollow K-Cor (E)K-Cor^{H}/0.51/11°/0.06 specimen*

The higher stiffness of the pinned cores in the out-of-plane direction provides an effective support for the crushing skins, encouraging their fragmentation. This is clearly

indicated by the SEA values for X-Cor and K-Cor: very similar in their typical configuration and different in the hollow samples. The X-Cor is in fact only slightly penalised by the absence of the foam, due to the superior stability towards in-plane loads, attributable to the pin-skin mechanical fastening. The constraint provided in the out-of-plane direction reduces the delamination of the 0° layers. If skin-core bond does not delaminate, the stresses in the crushed zone will build up until critical values for interlaminar shear fracture are reached. The multiple bonds between the flattened pin-ends and the skins in the K-Cor samples prove to be very effective in suppressing the skin-core debonding typical for honeycomb and foam cored specimens.

The damage mechanism for X-Cor samples is governed by the pins inserted at a certain length inside the skin layers. The interlaminar skin properties are enhanced as well as the stability of the whole sample under the in-plane load. It seems also that the pins also promote a fragmentation mode of failure by avoiding delamination and by stopping the damage front from moving to the next pin (figure 7.33). The unpinned outer layers of the skins will eventually delaminate.

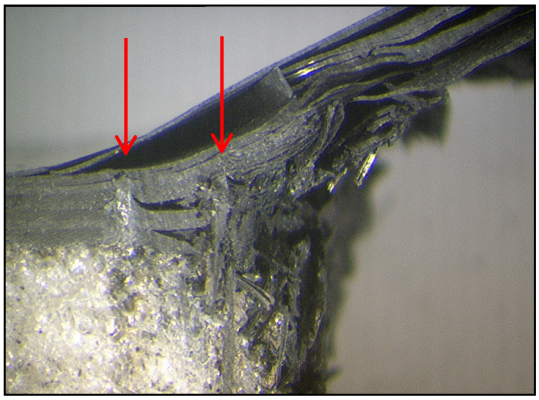

Figure 7.33- *Skin delamination between two pins in a crushed X-Cor (E)X-Cor$^{F}_{1}$/0.51/11°/0.06 specimen*

The pin reveal length (defined in section 3.1.1) plays an important part: a pin insertion through the full thickness of the skin may eventually provoke a higher degree of fragmentation beneficial for the SEA.

7.8 Chapter summary

1. A new test configuration has been developed successfully for quasi-static in-plane crushing of flat composite laminates and, for the first time, for flat sandwich samples. It consists of an open configuration where the specimen is clamped on the support which goes upwards against a fixed metal plate. It has proven to promote a progressive crushing failure mode and to be a cost effective test method.

2. The role played by a containing fixture, as in previous configurations, for structural stability against global buckling and macroscopic delaminations, is assumed in this case by a self-triggering specimen of triangular geometry. In this way the main drawback, consisting of interactions with the support fixture which influences the material damage mechanisms, is addressed. A direct observation of the failure mechanisms and a crushed area cleaner from debris are also achieved.

3. The flat rectangular specimen with a trigger used for a similar test set-up in previous studies [161, 168], has been found unsuitable for promoting progressive crushing in flat laminate and sandwich plates. Unstable local failure (delamination and debonding) makes the collapse process neither controllable nor progressive as exhibited by the load-displacement traces and by optical microscope analysis.

4. A suitable data analysis methodology for triangular specimens based on the conservation of energy and on a statistical approach has been developed successfully and adopted to analyse and interpret the experimental data. A definition of the specific energy absorption (SEA) as a function of the crush length allows the evaluation of the material behaviour during the crushing process.

5. The principal role of the core is to guarantee a transverse support of the skins during the in-plane crushing process, keeping the skins relative distance constant and stabilising them. Its contribution to the total specimen SEA is only a small fraction of the contribution given by the composite skins; this is due to the much lower in-plane

mechanical properties and density of the core. A stiffer core in the out-of-plane direction maximises the energy absorption capacity of the sample.

6. The in-plane crushing SEA values for the tested X-Cor and K-Cor samples, ((E)X-Cor$^{F}_{I}$ */0.51/11°/0.06* and (E)K-Cor^{F} */0.51/11°/0.06* samples characterised by: 10° pin insertion angle, 0.62 pin mm^{-2}pin areal density, Rohacell 21IG foam and same CF /epoxy laminated skins are similar and about ~60 kJkg^{-1}. The respective hollow configurations are characterised by a substantial difference. For X-Cor specimens the foam removal accounts for about 10% of the total SEA. This is a consequence of the mechanical fastening between pins and skins which allows a higher degree of structural stability during the crush event maximising the energy absorption. The tested K-Cor in the hollow configuration show similar SEA values, ~40 kJkg^{-1}, to the foam (Rohacell 21IG and same skins) and Al honeycomb (72kgm^{-3} and same skins).

7. For an out-of-plane loading condition the tested materials do not experience a progressive failure in the post-elastic phase as for in-plane crushing. The tested Al honeycomb (nominal density of 72 kgm^{-3}) outperforms the pinned cores (pin insertion angles of 10° and 30°, measured core densities of 48.25 kgm^{-3} and 52.50 kgm^{-3}), in terms of SEA: honeycomb has ~29 kJkg^{-1}, while X-Cor ~25 kJkg^{-1} and K-Cor have ~22 kJkg-^{1}. This loading condition maximises the energy absorbing mechanisms for the honeycomb core without promoting skin-core debonding.

8. All the pinned cored samples tested have shown a high degree of fragmentation of the composite skins, as well as the delamination of the outer layers in in-plane crushing. Fragmentation is a very efficient energy absorbing failure mode and a high out-of-plane modulus seems to create favourable conditions for its initiation and propagation throughout the sample length. In X-Cor the pins inserted in the skins, besides enhancing the interlaminar properties and limiting the delamination process, promote a suitable condition for this failure mode to take place.

Chapter 8

Overall discussion

X-Cor and K-Cor sandwich structures are novel materials belonging to the niche sector of high performance, aerospace grade materials. They are foam based lightweight structural cores reinforced with Z-Fiber® rods oriented in a truss pattern.

This work represents one of the first attempts to create a rigorous methodology for the analysis and evaluation of their mechanical performance. This investigation consisted of experimental testing in order to characterise the mechanical properties and provide an understanding of the materials behaviour. The experimental data gathered were also used to validate proposed theoretical and modelling approaches, analysing the material from a meso-scale level and allowing considerations of the pin truss structure and the core parameters to be made.
The process of implementation of X-Cor and K-Cor in engineering practice requires a parallel comparison with existing competitor cores and a critical evaluation of their performance in order to identify advantages/disadvantages and establish design guidelines.

Tests performed

To optimise the structural performance of a sandwich construction, a core material is required to provide a certain set of out-of-plane properties (shear and compression) essentially to prevent in-plane and out-of-plane relative movement of the skins [191]. These two fundamental tests were carried out according to ASTM C 273 and C 365. The data analysis methodology indicated by the standards had been developed essentially for honeycomb and foam cored sandwich panel. For this reason, a more

appropriate approach which discounts the pins not correctly fastened to both skins (usually along the edges) was adopted [11].

The material energy absorption properties were evaluated for the previously indicated loading cases as well as for in-plane crushing. A new quasi-static test for progressive crushing of flat sandwich laminates was designed. It solves the issues of invasive test support fixtures, which complicate the data analysis, modelling and influence material damage mechanisms. The structural stability of the specimen is achieved by adopting a self-triggering specimen of triangular geometry.

X/K-Cor structure differences in the modelling approach

The structural differences between X-Cor and K-Cor are at the base of a diverse mechanical response. In the case of X-Cor, the preform characterised by protruding pin tips, is laminated between prepreg composite skins and then co-cured. The pins pierce the facesheets and create a mechanical fastening between them and the core achieving in this way structural integrity. There is no need of an adhesive film for bonding the different parts together. In K-Cor structures the sandwich construction is achieved with the use of an adhesive film interleaving the preform and the skins. K-Cor preform has flattened pin tips, flush with the core surface. As for traditional honeycomb sandwich systems, both co-curing and co-bonding processes can be used.

The pin-skin and the pin-adhesive film interfaces impose different and finite rotational constraint at the pin tips, which characterises the mechanical response of the materials. Simplified pin physical models are used for obtaining analytical relations and models which relate the mechanical performance with core parameters. In particular, a pin is modelled as a column of elastic-brittle material with two rotational springs at the ends, which simulates the interface mechanical properties. In this way it is possible to assign a value to this rotational constraint. This value is used as an input parameter for a finite element model based on a core unit cell. A general FE modelling strategy for both X/K-Cor is provided for simulating their linear elastic response (stiffness and strength). The analysis followed a local-global approach and it was specifically developed for an X-

Cor material under out-of-plane shear loading. Both the analytical and the FE models are based on assumptions which simplify the complexity of the material structure, taking into account only principal features. The results allow a better understanding of the core mechanics and interactions among the different constituents and deductions to be made. Among all the parameters, pin positioning appears to be fundamental in determining the pinned core mechanical performance. Depending on their lay-out, pins experience a different loading condition essentially due to their non-symmetrical position in the unit cell. Once a pin faces a critical condition and fails, the load is re-distributed among the remaining pins. This suggests a way to optimise the core performance by placing the pins in a way that leads to as equal a distribution of the applied external load as possible (achievable with isotropic cores).

Manufacturing effect on X/K-Cor mechanical performance

X-Cor structures are manufactured with a co-cure process where the applied pressure and temperatures are chosen on the basis of core properties. High performance foams allow the ideal curing temperature for carbon/epoxy skins to be reached, although the lower pressure applied (3.1-3.4bar) could still cause compaction and porosity issues to the laminate facings. Moreover the presence of pin tips into the laminates creates a discontinuity which does not favour resin compaction.

An ‘improved’ manufacturing technique was designed with the aim of obtaining a higher quality pin-skin interface. The basic idea was to complete the initial stages of the pin insertion prior to the beginning of the curing process. The un-cured composite stack is debulked at 0.6bar and 50°-60ºC for 30 minutes, favouring a slow piercing of the prepreg skin. The following autoclave cycle mainly serves the functions of curing and consolidating. The obtained quality of each pin-skin interface is generally improved, as is the resulting mechanical performance. The graphs of figures 8.1-2 compare the out-of-plane specific shear and compressive stiffnesses and strengths of a ‘standard’ and an ‘improved’ X-Cor configuration; the corresponding mechanical quantities for relevant K-Cor structures are also indicated. All the samples have a nominal pin angle in the range of 30°-33°. The ‘standard’ X-Cor samples have a pin nominal areal density of

0.13 pin/mm^2 and Rohacell IG 31, while the 'improved' X-Cor only 0.06 pin/mm^2 and Rohacell IG 21. The K-Cor specimens have the same core properties as their respective X-Cor samples. The effective values of core density have been used to calculate specific stiffness and strength (table 3.11). From figure 8.1 it is evident that in terms of the stiffness the 'standard' X-Cor is a more rigid structure in both the loading conditions analysed (higher pin density). The increase in performance due to the improved manufacturing can be appreciated by comparing the results with the corresponding K-Cor structures. The 'improved' X-Cor has a higher stiffness in both cases.

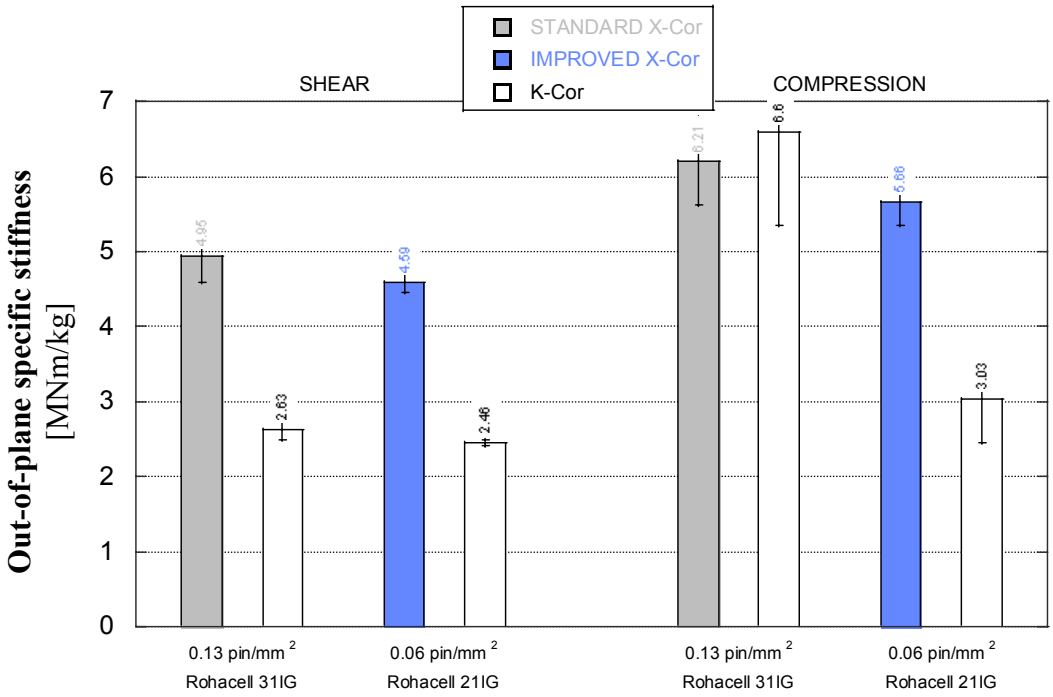

Figure 8.1– *Out-of-plane shear and compressive specific stiffness comparison between 'standard' and 'improved' X-Cor and K-Cor samples*

Figure 8.2 shows that the increase in performance due to the 'improved' manufacturing process affects mainly the core strength. The improved interface quality increases the rotational constraint acting on pin tips. This results in a higher strength, as the condition of critical stresses at the pin-skin interface are reached for higher applied loads.

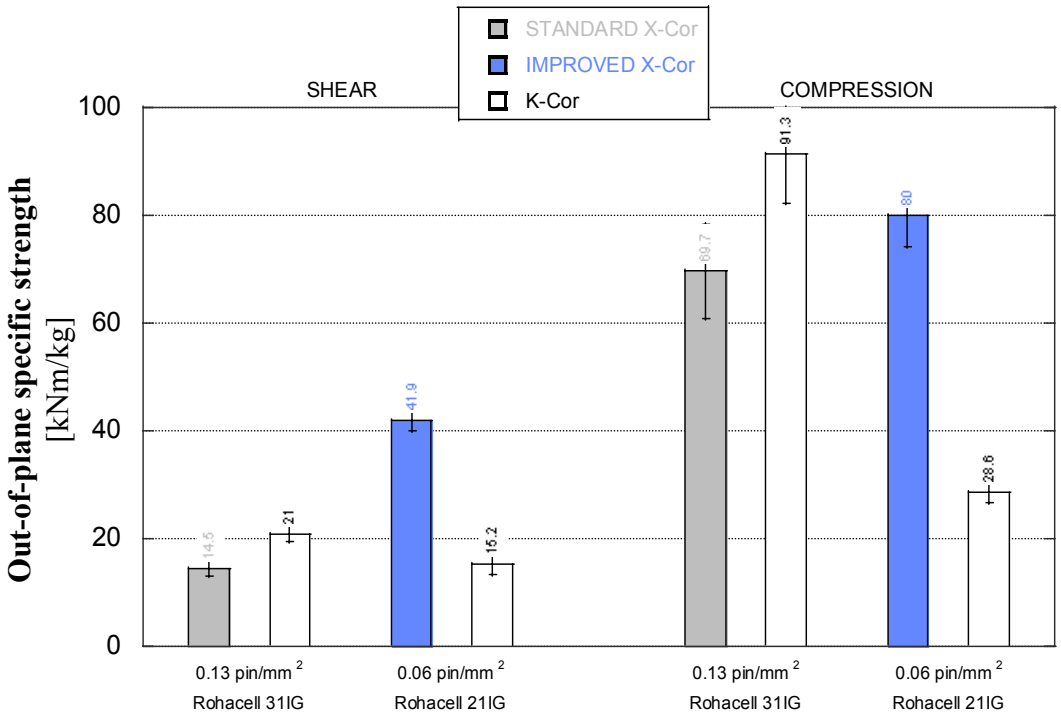

Figure 8.2– *Out-of-plane specific shear and compressive strength comparison between 'standard', 'improved' X-Cor and K-Cor samples*

Table 8.1 summarises the core types of this comparison and the main results.

CORE TYPE	*SHEAR*		*COMPRESSION*	
	specific stiffness [MNm/kg]	*specific strength [kNm/kg]*	*specific stiffness [MNm/kg]*	*specific strength [kNm/kg]*
X-Cor$^{F}_{S}$/0.51/30°/0.13	*4.95±0.36*	*14.51±1.45*	*6.21±0.58*	*69.67±8.71*
K-Cor^{F}/0.51/30°/0.10	*2.63±0.13*	*20.96±1.50*	*6.60±1.24*	*91.32±8.98*
X-Cor$^{F}_{1}$/0.51/33°/0.06	*4.59±0.13*	*41.90±1.91*	*5.66±0.30*	*80.00±5.72*
K-Cor^{F}/0.51/33°/0.06	*2.46±0.04*	*15.24±1.90*	*3.03±0.57*	*28.57±1.91*

Table 8.1– *Core types and comparison of results*

The co-bonding manufacturing process can be applied only for the production of K-Cor structures. The advantages offered by a co-bonded K-Cor can become a valid alternative as the skins, processed like monolithic laminates, achieve a higher degree of material compaction and consequently of mechanical properties. The eventual problems of core-crushing and heat distortion are not encountered in this process, and that makes it

suitable especially for low density foams. In the tests carried out, no differences in performance were noticed between co-bonded and co-cured K-Cor samples; the bond between the flattened pin part and the adhesive film, which constitutes the interface, seems unaffected.

The performance of X-Cor and K-Cor structures is highly sensitive to the manufacturing process as it determines the quality of the pin-skin, pin-adhesive interfaces. Such interfaces guarantee the sandwich construction integrity and determine the pin end constraint which makes this through-the-thickness reinforcement effective.

Influence of core parameters on the balance of mechanical properties

The core structure is determined before the curing process, when producing the pinned preform. It is at this stage that core parameters need to be tailored in order to achieve the desired mechanical performance. The curing process consolidates such core configuration into a sandwich construction.

The foam plays a fundamental part in the mechanical response; depending on the loading condition, it cannot be considered as a parasitic component. In out-of-plane compression a clear synergistic strengthening effect between the foam and the pins was noticed in both types of pinned core constructions [11, 150]. The strength of the pin reinforced core is higher than the sum of the contributions of foam and pins. The lateral support provided by the foam increases the critical stress for elastic buckling of the pins, as well as the out-of-plane rigidity of the core. A compression load in particular, due to the pin inclination with respect to the vertical direction, introduces an out-of-plane shear effect on the whole core. This influences the resulting mechanical behaviour and emphasises the differences in performance between X-Cor and K-Cor. X-Cor constructions exhibit a higher degree of out-of-plane shear rigidity as well as higher pin-skin interfacial properties when compared to K-Cor (section 6.3.4). The foam has a stronger effect in core strength enhancement rather than in increasing the overall rigidity. The shear component of the external force, which lowers the buckling strength,

is more effectively withstood due to the foam lateral support on the pins. In K-Cor structures the foam appears to carry part of the introduced shear stresses with a greater benefit in rigidity than in core strength. Only when the induced shear is relatively lower (for small pin insertion angles) the effect of the foam on strength is more evident. Figures 8.3-4 show the increase in performance (on compression stiffness and core strength) due to the presence of the foam for similar cores in the 'improved' X-Cor and K-Cor configurations. The pin insertion angles, for this comparison, are 11° and 33° respectively.

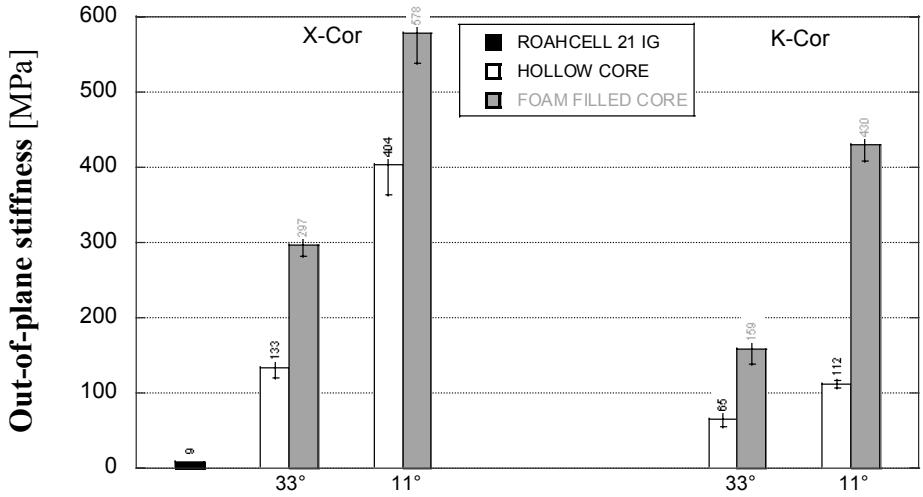

Figure 8.3– *Out-of-plane compression stiffness comparison between 'improved' X-Cor and K-Cor samples*

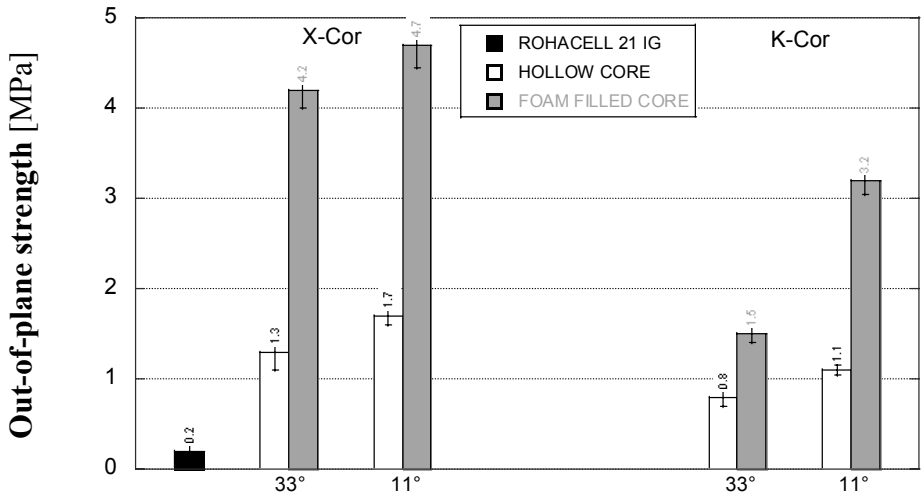

Figure 8.4– *Out-of-plane compression strength comparison between 'improved' X-Cor and K-Cor samples*

When X-Cor structures are under out-of-plane shear loading, the role of the foam appears to be negligible in the material linear response. This allows a potential ~40% core weight saving (calculated for Rohacell 31 IG foam) to be achieved with the hollow configurations whilst maintaining the same mechanical behaviour. Figure 8.5 shows the strength and the elastic modulus for two similar cores in both the hollow and the foam filled configurations ('standard' manufactured X-Cor samples: *(S)X-Cor$^{F}_{S}$/0.51/22°/0.13* and *(S)X-Cor$^{H}_{S}$/0.51/22°/0.13*).

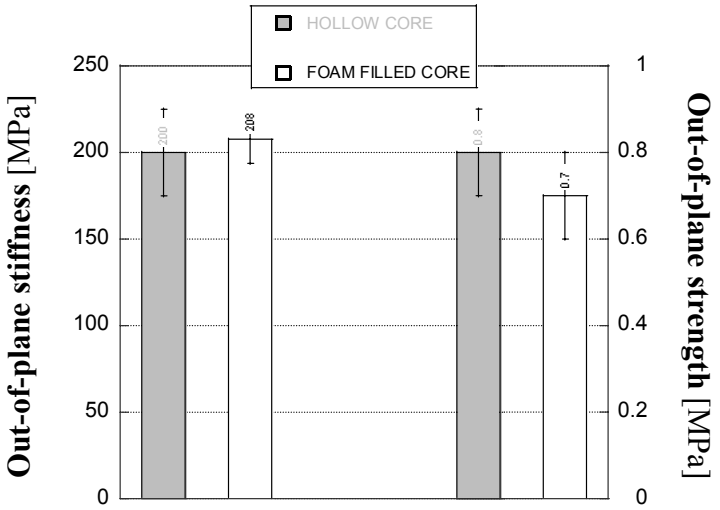

Figure 8.5– *Out-of-plane shear loading comparison: hollow and foam-filled X-Cor*

Pin insertion angle is a crucial parameter in determining the right blend of out-of-plane shear and compression properties for a pinned core. The best range of properties is achieved for a pin angle between 20°-30° as also suggested by the manufacturer [6] and by references [62, 99]. Especially in out-of-plane shear the rigidity of the core appears to be sensitive even to small differences in pin angle. The variation in stiffness (figure 8.6) was measured for a set of 'standard' manufactured X-Cor structures with the same core parameters and two different insertion angles: 22° and 32° (effective values).

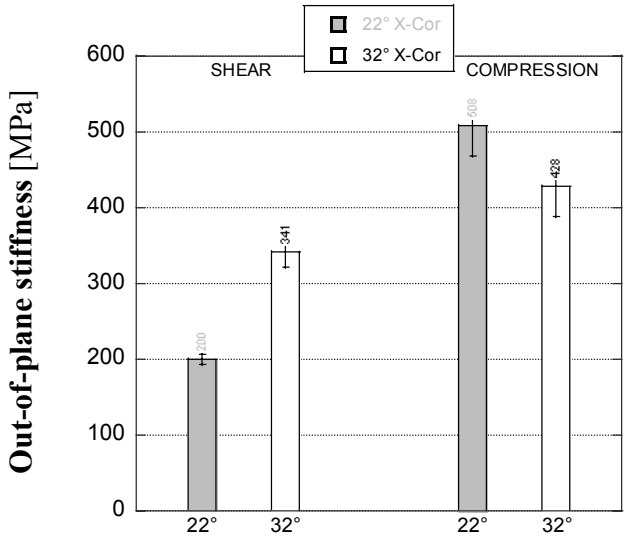

Figure 8.6– *Shear and compression out-of-plane stiffness comparison for a 'standard' X-Cor in 22° and 32° pin insertion angle configurations*

The results of the influence of the pin insertion angle in the out-of-plane compression behaviour for the 'improved' X–Cor and its corresponding K-Cor structures are summarised in figures (8.3-4). An increase in rigidity and strength is associated to a pin angle variation from 33° to 11° for both pinned core structures in the hollow and foam filled configurations. A smaller shear force component of the external load acting on each pin results into an equally smaller drop of the pin buckling load; consequently it is beneficial for core strength. In the hollow configurations this effect is more evident in comparison to the foam filled cores, where pins also experience foam lateral support.
Core rigidity is affected in the same way. X-Cor structures characterised by higher out-of-plane shear modulus benefit from a change in pin insertion angle in both hollow and foam filled configurations. In K-Cor structures the increase in rigidity is more evident for the foam filled configuration, as the foam contribution carrying the induced shear stresses is more significant.

A pin angle variation seems more beneficial for hollow X-Cor and for foam filled K-Cor structures under an out-of-plane compressive load with respect to all other possible configurations, although for such loading conditions the highest increase in performance is achieved by the presence of the foam. On the contrary, for an out-of-plane shear load

the pinned cores appear to be significantly more sensitive to a change in pin insertion angle.

The role of the foam and the variation of pin insertion angle were also considered in the energy absorption capacity; in this analysis the post-elastic behaviour of the pinned core materials is dominant. In out-of-plane compression the effect of the foam was evaluated in terms of the specific energy absorption (SEA) capability for each of the pinned core sandwich constructions. X-Cor structures appear to be less affected by the presence of the foam than K-Cor constructions with similar core parameters. The decrease in the energy absorption for the X-Cor hollow configuration is within 10-15% depending on the pin insertion angle; in the case of K-Cor it is more substantial and between 60-130%. For this loading condition, the highest values in SEA are achieved by modest pin insertion angles (with respect to the vertical direction). In foam filled core configurations X-Cor and K-Cor constructions have shown similar energy absorption capacity for this loading condition (table 7.5, figure 7.23).

In out-of-plane shear, the foam-filled specimens exhibit a higher energy absorption capability with respect to similar samples in the hollow configurations (table 5.3). Furthermore, the X-Cor samples manufactured with the 'improved' technique and characterised by a 25% lighter core (foam IG 21, 0.06 pin/mm^2 areal density, 33° pin insertion angle) have proved to have a higher energy absorbing capacity: ~18J compared to the ~6J absorbed for the same core deformation by a 'standard' X-Cor sample (foam IG 31, 0.13 pin/mm^2, 32° pin insertion angle) and ~14J by a similar K-Cor specimen (foam IG 21, 0.10 pin/mm^2, 32° pin insertion angle).

In the in-plane crushing test configuration the specific energy absorption is evaluated for the sandwich structure as a whole (Ch. 7). In this case, the principal role of the core is to guarantee an out-of-plane support of the facesheets during the in-plane crushing process, keeping their relative distance constant and stabilising them during in-plane crushing. The support provided by the core maximises the SEA capacity of the sample. For X-Cor specimens the foam accounts for about 10% of the total energy absorption capacity. This is a result of the higher degree of structural stability provided by the mechanical fastening between pins and skins. In the case of K-Cor, the adhesively

bonded pins offer a lower support to the in-plane load than an X-Cor specimen with a similar core configuration. A hollow K-Cor configuration absorbs about 30% less energy than a similar one with a foam filled core. As a result, in K-Cor structures the foam plays a fundamental role also in in-plane crushing (table 7.4).

Although a systematic testing to study the effect of pin density was not carried out, some considerations on its effect can be made thanks to the different core configurations analysed. The rigidity of X-Cor and K-Cor appears to be directly influenced by the pin areal density of the core for both out-of-plane shear and compression. In particular for X-Cor structures the out-of-plane stiffness seems to be affected more by the pin density than the manufacturing process used (‘standard’ or ‘improved'). The core strength, instead, appears to be dependent on the pin-skin, pin-adhesive film interface quality as well as on pin density and positioning. It was observed that, unless the pin lay-out is optimised, a core characterised by fewer pins is likely to have a more uneven load distribution when compared to a core with a higher pin density (section 6.2.4). A specifically high density core (0.24 pin/mm^2), where pin were found to be in contact with each other, showed that the neighbouring pin lateral support has a non-negligible effect on strengthening the material in the overall compressive behaviour.

Principal failure modes

A common failure mechanism is exhibited between X-Cor and K-Cor in out-of-plane shear loading. A skin-core interface failure is associated with an increasing skin separation due to the rotation of the load-counteracting pins. The non-counteracting pins consequently experience pull-out from their original positions. It has been demonstrated (sections 5.2.1-2) with simple pin-skin (X-Cor) and pin-adhesive film (K-Cor) interface models that the stress state reached is such that it damages those interfaces until complete failure occurs. As long as the foam is concerned, in the case of K-Cor the presence of an adhesive bonded interface localises the failure at this surface, while in X-Cor the damage is more spread throughout the volume due to the contact interactions with the pins and the skins.

In out-of-plane compression the dominant failure mode is pin buckling, exhibited by both X-Cor and K-Cor in configurations with and without foam; it is not pin-skin or pin-adhesive film interface failure.

In progressive crushing the crush front and the delamination front propagate through the specimen with the same velocity and in a regular manner. Progressive delamination and splaying out of external layers of the composite skin and a simultaneous fragmentation of the internal layers (close to the core) are observed for both X-Cor and K-Cor. The degree of fragmentation achieved by the pinned cores is higher than that in foam and honeycomb cored samples. Moreover, in X-Cor constructions the embedded pins appear to promote the fragmentation mode by delaying the damage front from moving to the next pin. Such promotion of the fragmentation mode is beneficial to the specific energy absorption capacity of the structures.

Core design suggestions

In a core design process for both X-Cor and K-Cor, the achievement of the requested shear properties in a panel should be a priority and determined essentially with the correct pin insertion angle. At this stage the right balance of mechanical properties can be achieved with the presence of the foam (even a very low density core) which increases substantially (due to the synergistic strengthening effect) the compressive response. In the case of a hollow core configuration, X-Cor appears to be a more sensible choice. The ‘improved’ hollow X-Cor, even in the optimal shear loading configuration (33° pin insertion angle), has shown superior mechanical properties in out-of-plane compression loading when compared to a corresponding hollow K-Cor with an 11° pin insertion angle. If strength is a fundamental design parameter, X-Cor structures manufactured with the ‘improved’ technique have shown the highest values in the loading conditions analysed. When choosing between ‘standard’ manufactured X-Cor and K-Cor, the latter becomes a logical alternative.

X/K-Cor performance comparison with competitor sandwich structures

Between the competitor materials tested, the best performing one was a Nomex® honeycomb core of effective density 70.7±0.1 kg/m^3. Its out-of-plane shear and compressive response was compared to those of pinned cores of similar densities (within the 66-73 kg/m^3 range). Same skins and adhesive systems were used to virtually obtain specimens characterised by similar weights (for details section 3.3). The X-Cor constructions specifically made for this comparison were all manufactured following the 'standard' procedure. The Nomex honeycomb sandwich, although characterised by a lower rigidity, exceeds both the pinned cores response in terms of shear and compression strengths, as well as energy absorbed associated to the deformation process for the loading conditions analysed (detailed results in tables 5.2 and 6.2) . Only the 'improved' manufactured X-Cor, although with a lower core density (52.5±0.1 kg/m^3), exhibits a performance comparable to that of the honeycomb structure. The 'improved' X-Cor chosen for this comparison is the configuration with the 33° pin insertion angle as it possesses a good balance of shear and compression properties (*X-Cor^F_I /0.51/33°/0.06* samples). Figures 8.7-8 show a comparison between the 'improved' X-Cor and the Nomex performance in terms of strength and stiffness for out-of-plane shear and compressive loading.

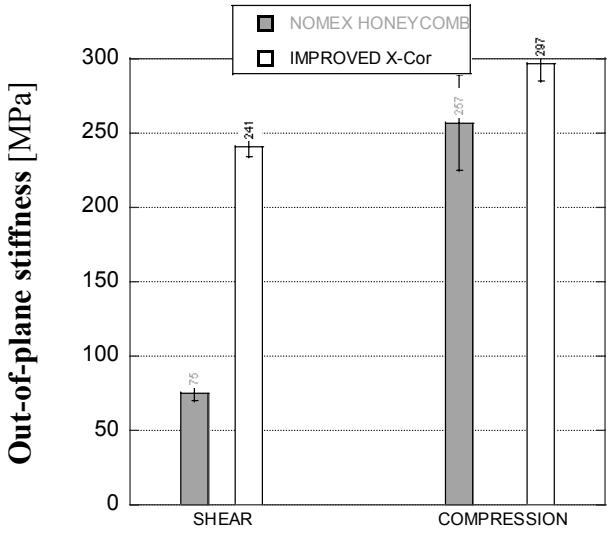

Figure 8.7– *Out-of-plane shear and compression stiffness comparison between a 70.7±0.1 kg/m^3 Nomex and a 52.5±0.1 kg/m^3 'improved' X-Cor*

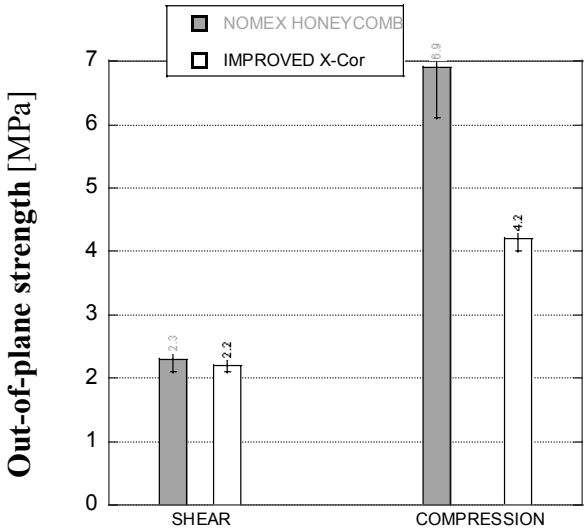

Figure 8.8– *Out-of-plane shear and compression strength comparison between a 70.7±0.1 kg/m^3 Nomex and a 52.5±0.1 kg/m^3 'improved' X-Cor*

Potential application guidelines

Besides all the weight sensitive applications, typical of the aerospace industry, where these cores could be potential alternatives to the currently utilised honeycombs, X-Cor and K-Cor structures seem to have also something different to offer. These materials can become an interesting alternative to traditional cores for a range of applications where, thanks to their particular structure, they are more versatile. One advantage with respect to honeycombs is the possibility to easily tailor the mechanical properties of a sandwich panel to specific design needs. This not only means a choice of a particular set of core parameters, but also the possibility to alter such parameters (pin density and insertion angles for example) within the same component especially in those areas subjected to particular loading conditions. It is possible to create a 3D engineered core which can offer the right blend of mechanical properties exactly where they are needed.

The hollow X-Cor configuration, for example, seems ideal to be used in a hostile environment to materials, such as space. As a potential multifunctional structure, miniature sensors to detect and evaluate loads or failure conditions could be embedded into the core, offering in this way a high degree of integration. Satellite components or parts of space antennas could eventually become a new area of application (figure 8.9).

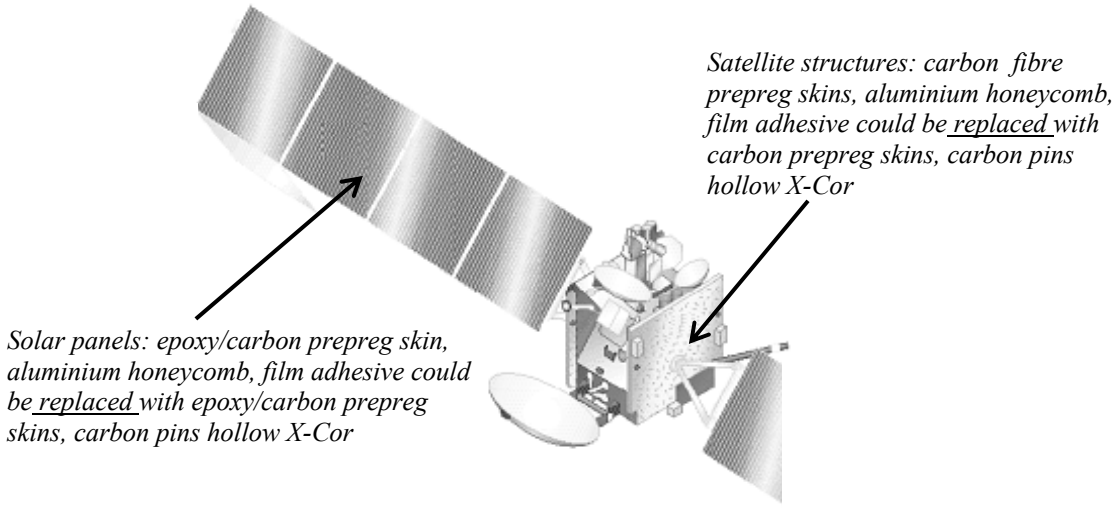

Figure 8.9– *Potential application of hollow X-Cor in satellite structures as replacement of Al honeycomb. Satellite schematic redrawn from [112]*

Chapter 9

Conclusions and suggestions for further work

9.1 Conclusions

The main conclusions drawn from this work are the following:

1. Structural differences between X-Cor and K-Cor are at the base of a diverse mechanical response.

2. The mechanical performance of X-Cor and K-Cor sandwich constructions is sensitive to the manufacturing process as it determines the quality of the pin-skin and pin-adhesive film interfaces.

3. The interface at the pin tips plays a fundamental role as:
   - It guarantees the sandwich construction integrity
   - It constitutes the pin end constraint which makes the through-the-thickness reinforcement effective
   - It imposes a finite rotational constraint at the pin tips

4. The ‘standard’ co-curing procedure for X-Cor structures can present some resin compaction issues, which affect the quality of the pin-skin interface (as found for pins of 0.51mm diameter). An alternative ‘improved’ manufacturing technique, consisting of a preliminary debulking phase before the autoclave cycle, has proved to be successful.

5. A K-Cor manufactured with a co-bonding process is usually a better alternative with respect to the same co-cured material. The skins achieve a higher degree of material compaction and mechanical properties. Eventual core-crushing and heat distortion are not encountered; it is suitable for low density foams.

6. A procedure to obtain hollow X-Cor and K-Cor structures through a convenient chemical foam removal procedure has been established. It is suitable for high pin density cores, large panels and structures. No material damage or contamination was noticed.

7. The mechanical behaviour of these novel core materials was evaluated under out-of-plane shear and compressive loading conditions (according to ASTM C 273 and C 365). The mechanical performance was compared to those of competitor honeycombs (Nomex and aluminium) chosen on the basis of similar core densities.

8. The material energy absorption properties were evaluated for the previous loading cases as well as for in-plane crushing. A new quasi-static test for progressive crushing on flat sandwich structures was designed successfully.

9. Analytical models have been developed in order to evaluate, together with the experimental results, the influence of core parameters on mechanical performance. A simplified pin physical model is developed to evaluate the out-of-plane compression behaviour. It considers a pin as a column of elastic-brittle material with rotational springs at the ends, which simulate the interface mechanical properties. Within the range of validity of the model, the finite rotational constraint at pin end can be successfully evaluated.

10. A general FE modelling approach based on a unit cell, representative of the entire core structure, has been developed for simulating the linear elastic response of K-Cor and X-Cor structures. It has been applied on the analysis of an X-Cor material (X-Cor$^{F}_{S}$ /0.51/30°/0.13) under out-of-plane shear loading. The assumptions made in the model development represent an effective compromise between the complexity of the core, its mechanical response and the necessity to produce a straightforward method of analysis. The predicted stiffness value underestimates the experimental shear rigidity (~20% lower). The material strength with the non linear analysis is obtained for a critical value of 1.39Nmm of the rotational moment applied at each pin-skin interface. The model can be used also as a tool for optimising pin positioning.

11. Depending on the loading condition, the presence of the foam in the core can play a fundamental role in the mechanical behaviour. If its contribution is negligible, a hollow configuration could be used achieving a consistent weight saving. The following was found:

- out-of-plane shear: the role of the foam appears to be negligible in the material linear response at least for ‘standard’ manufactured X-Cor structures (confirmed also with FE analysis)
- out-of-plane compression: synergistic strengthening between foam and pins was noticed in both types of constructions. In X-Cor the foam has a stronger effect in core strength enhancement; K-Cor benefits the most in overall rigidity

12. Pin insertion angle is a crucial parameter in determining the right blend of out-of-plane shear and compression properties. The main findings are:

- out-of-plane shear: core rigidity appears to be significantly affected even by small differences in pin angle
- out-of-plane compression: pin angle variation seems more beneficial to hollow X-Cor and foam filled K-Cor structures; for this loading condition the highest increase in performance is achieved by the presence of the foam

13. The rigidity of X-Cor and K-Cor appears to be directly influenced by the pin density of the core for both out-of-plane shear and compression. For X-Cor the out-of-plane stiffness does not seem to greatly depend on the manufacturing process used (‘standard’ or ‘improved'), leaving the pin density as one of the main controlling parameters.

14. Pin positioning appears to be critical in determining the pinned core mechanical performance. Depending on the lay-out, pins experience a different loading condition which leads to premature failures affecting the whole core mechanical response.

15. Core strength appears to be dependent on the pin-skin, pin-adhesive film interface quality as well as pin density and positioning.

16. The evaluation of the energy absorption capacity involves the post-elastic behaviour of the pinned core materials. The main findings are:

- out-of-plane shear: specimens containing foam exhibit a higher energy absorption capability (for similar strength and modulus); for X-Cor the manufacturing technique appears to play a critical role.
- out-of-plane compression: foam filled core configurations exhibit a similar energy absorption capacity. Highest values are achieved for 10°-20° pin insertion angles (with respect to the vertical direction). The decrease in energy absorption for the hollow X-Cor configuration is within 10-15%.
- in-plane crushing: the core provides out-of-plane support to the skins during the in-plane crushing process. X-Cor exhibits higher structural stability provided by the mechanical fastening between pins and skins. In K-Cor foam plays a critical role.

17. Tested Nomex honeycomb outperforms K-Cor and 'standard' manufactured X-Cor (of similar core density) in strength and energy absorption capacity, although it is characterised by lower out-of-plane rigidity. The 'improved' X-Cor shows a comparable compression and shear strength with a 25% weight saving.

18. The dominant failure mechanisms characterising each loading condition are as follows:

- out-of-plane shear: skin-core interface failure (pin-skin for X-Cor, pin-adhesive film for K-Cor) and increasing skin separation due to rotation of load-counteracting pins. Non-counteracting pins subjected to pull-out from original positions.
- out-of-plane compression: pin buckling exhibited by both X-Cor and K-Cor in configurations with and without foam (pin failure).
- in-plane crushing: progressive delamination and splaying out of external skin layers from the inner part of the facesheet, which undergoes fragmentation, was exhibited by both constructions.

9.2 Suggestions for further work

The following is a list of suggestions, regarding areas where more in-depth studies are needed as well as possible tests and potential material improvement solutions.

Modelling work

The analytical models used to determine the finite element analysis input parameters for the unit cell (Ch. 5 out-of-plane shear) or to calculate the rotational constraint acting on a pin (Ch. 6 out-of-plane compression) have shown some limitations. Creating models not based on some of the constraining assumptions made earlier would probably reproduce more effectively the material behaviour; at the same time more complex relations between experimental findings and core parameters are needed (sections 5.3.4 and 6.3.6).

In-plane crushing test

For what concerns the in-plane crushing test designed for flat sandwich panels, only one vertex angle configuration was investigated, chosen on the basis of the systematic testing on different trigger geometries by [168]. It would be of interest to vary this parameter and see how it affects the specific energy absorption capacity of sandwich samples. The out-of-plane deflection during in-plane crushing was monitored by the use of a video camera (some frames have been shown in Ch. 7) and was not addressed with the use of strain gauges (that could be attached at the bottom of the specimen before the clamp) or the use of any other means. Although a stable behaviour was observed, a cross-check with another device would have validated this point. The friction effect between the crushing material and the steel metal platen is inevitable in crushing tests, but it is rarely estimated. The use of a lubricant spray and constant cleaning of the surfaces guaranteed a similar friction coefficient for all the tests and it is the only precaution generally adopted for SEA calculations. A study to address this issue would be useful.

Pin-skin, pin adhesive interface analysis

Finding a way to improve the mechanical properties of this interface is beneficial to the whole structure performance. It seemed that the 'standard' manufacturing procedure for X-Cor with 0.25mm pin diameter is adequate. A comparison with the same material produced with the 'improved' technique is needed to confirm this assumption.

It could be worthwhile to manufacture K-Cor with skins made of self-adhesive prepreg materials (co-curing process) [192]. In this way it would be possible to obtain lighter K-Cor structure (no adhesive film, virtually same weight as an X-Cor panel made with the same materials). In order to assess the achieved pin interface quality simple flatwise tensile tests could be used [12]. This test is preferred for quality control as it induces an interface failure in both X-Cor and K-Cor sandwich structures [99, 193]. It is simpler to perform and requires smaller samples than the out-of-plane shear test.

A detailed FE analysis of the pin tip interface supported by systematic mechanical testing of cores with different pin 'reveal' and 'flattened' lengths could help in the optimisation of this parameter.

Facesheet / core delamination testing

The 'Modified Mode-I Cracked Sandwich Beam Fracture Test' [194], could be performed to evaluate and assess the interfacial fracture toughness of X-Cor and K-Cor and compared with that of traditional honeycomb structures. Figure 9.1 shows an example of the CSB test performed on a honeycomb core sandwich specimen (relevant studies in [195-196]). Higher values are expected due to the embedded pins (X-Cor) or the multiple bonds offered by flattened pin tips (K-Cor). This analysis could be extended to a K-Cor provided with a dry fabric pre-attached to the core for further enhancing damage tolerance [6] (figure 9.2).

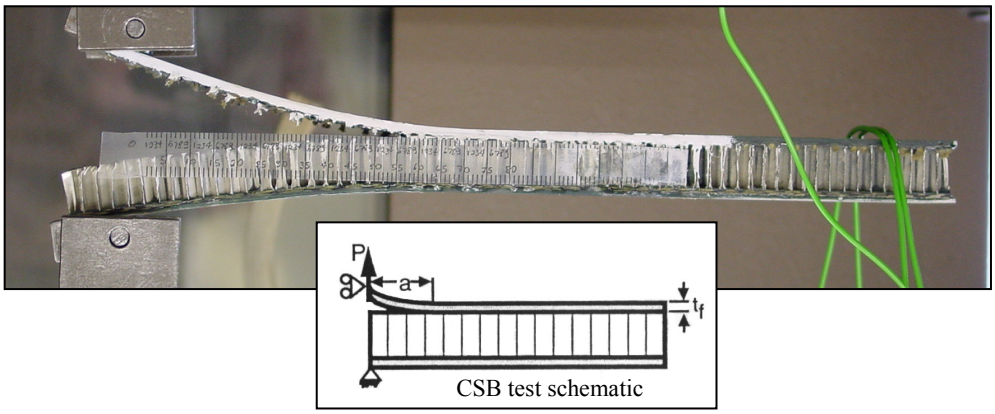

Figure 9.1– *Example of CSB test performed on honeycomb sandwich samples, from [197]*

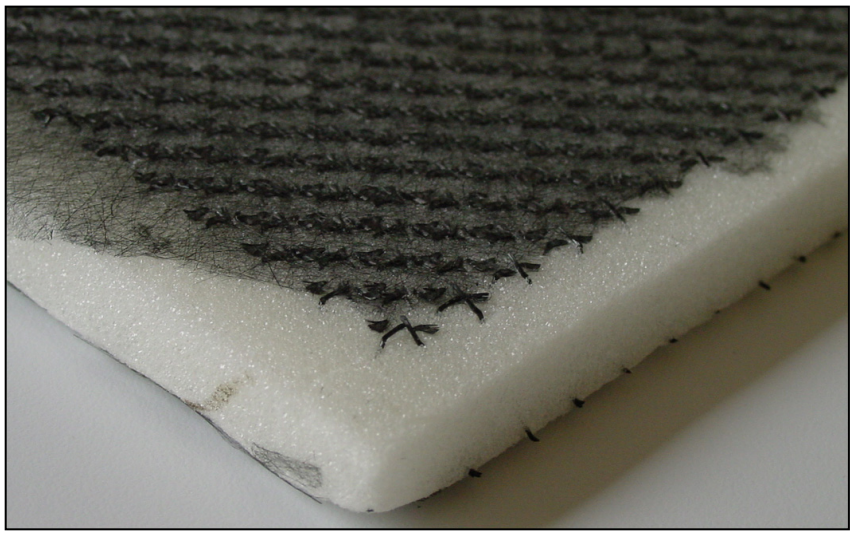

Figure 9.2– *Close-up of a K-Cor panel with a pre-attached dry fabric*

Core improvement suggestions

A hollow X-Cor with pins placed at more than one insertion angle could represent a solution for obtaining an optimum balance of mechanical properties even without the presence of the foam (Ch. 8).

An improvement in out-of-plane compression properties based on the exploitation of the synergistic strengthening offered by the simultaneous presence of pins and foam could be provided by an X-Cor (also valid for K-Cor structures) like the one shown in the schematic of figure 9.3.

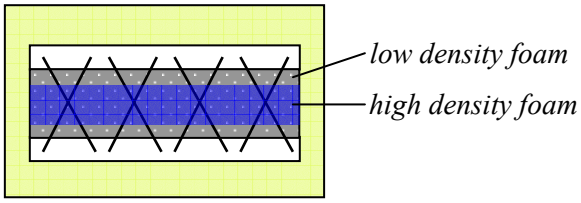

Figure 9.3– *Foam layer with a higher density in the central zone to enhance pin buckling support*

The presence of a foam layer of a higher density and mechanical properties in the middle should result in an enhanced core strength, as it provides a support against pin buckling where is most needed. This could be achieved by either utilising different layers of foam or by manufacturing ad-hoc foam layers with a higher density in the central zone (foam layers are exposed for a certain time to a heat source in order to obtain a uniform material density in the through-the-thickness direction of the panel as the central zone is, right after production, more dense).

As explained in section 6.3.5, contact between pins seems to be an effective way to push-up performance, especially for cores with small diameter pins (0.25mm). This could be obtained either with a high pin core density ($\geq$ 0.24 pin/mm^2 for 0.25mm pin diameter) or with 'intelligent' pin positioning. A complete set of tests (for compression results, section 6.1) needs to be carried out for out-of-plane shear and out-of-plane impact, where the highest benefits should be expected.

The FE analysis on a unit cell appears be an effective tool for improving pin lay-out in the core, in order to minimise as much as possible the performance dependency on positioning.

This study is one of the very early works on these new types of cores for sandwich structures. Both X-Cor and K-Cor show a potential for being used effectively as structural sandwich materials. Fundamental tests such as fatigue characterisation, thermal cycling, repairing capabilities as well as sub-structural component design and testing are just few of the issues that still need to be addressed.

References

1 Noor A K editor. Structures technology for Future Aerospace Systems (Progress in Astronautics and Aeronautics-Volume 188). AIAA, 2000

2 Marsh G. Composites in primary aerostructures. Reinforced plastic newsletter, 17 May 2004. (*URL: http://www.reinforcedplastic.com/ last access September 2005)*

3 Beumler T. Flying GLARE®. A contribution to aircraft certification issues on strength properties in non-damaged and fatigue damaged GLARE® structures. Ph.D. dissertation, 2004. Delft University Press

4 Department of Defense (DoD) Manufacturing Technology Program – ManTech *(URL: http://www.dodmantech.com/ last access August 2005)*

5 Dobyns A, Barr B and Adelmann J. RAH-66 Comanche building block structural qualification program. Composite Structures: Theory and Practice, ASTM STP 1383. Grant P and Rousseau C Q, Eds. American Society for Testing and Materials, West Conshohocken, PA, 2000; 140-157

6 Aztex Inc. website. (*URL*: *http://www.zfiber.com last access on August 2005)*

7 Bradley W L. Chapter 5: Relationship of matrix toughness to interlaminar fracture toughness. Application of Fracture mechanics to Composite Materials, editor Friedrich K, Elsevier, 1989

8 Singh S and Partridge I K. Mixed-mode fracture in an interleaved carbon-fibre/epoxy composite. Composites Science and Technology, 1995; 55(4): 319-327

9 Baker A, Dutton S and Kelly D. Composite materials for aircraft structures, (second edition). AIAA education series, Reston VA, 2004

10 Composite manufacturing technology center (CMTC) newsletter, fall 2002 *(URL: http://cmtc.scra.org/ last access September 2005)*

11 Cartié D D R and Fleck N A. The effect of pin reinforcement upon the through-thickness compressive strength of foam-cored sandwich panels. Comps Sci & Tech 2003; 63: 2401-2409

12 Stanley L E and Adams D O. Development and evaluation of stitched sandwich panels. NASA/CR-2001-211025, June 2001

13 Vaidya U K, Kamath M V, Hosur M V and Jeelani S. Low-Velocity Impact Response of Cross-Ply Laminated Sandwich Composites with Hollow and Foam-Filled Z-Pin Reinforced Core. Journal of Composites Technology and Research, 1999; 21(2): 84-97

14 Vaidya U K. Multifunctional sandwich composites. Proceedings of the SPIE (The International Society for Optical Engineering) conference: Smart Materials, Structures,

and Systems. Bangalore, India. 12-14 December 2002.

15 Sypeck D J. Cellular truss core sandwich structures. Applied Composite Materials, 2005; 12: 229-246

16 Vaidya U K, Hosur M V, Earl D and Jeelani S. Impact response of integrated hollow core sandwich composite panels. Composites: Part A, 31, 2000: 761-772

17 Mouritz A P, Bannister M K, Falzon P J and Leong K H. Review of applications for advanced three-dimensional fibre textile composites. Composites Part A, 1999; 30: 1445-1461

18 Lopresto V, Melito V, Leone C and Caprino G. Effect of stitches on the impact behaviour of graphite/epoxy composites. Composites Science and Technology, 2005; *(Article in press)*

19 Han N L, Suh S S, Yang J-M and Hahn H T. Resin film infusion of stitched stiffened composite panels. Composites Part A, 2003; 34: 227–236

20 Dransfield K A, Baillie C and Mai Y-W. Improving delamination resistance of CFRP by stitching- A review. Composites Science and Technology, 1994; 50: 305-317

21 Bucknall C B and Partridge I K. Effects of morphology, grafting and crosslinking on the toughness of rubber-modified plastics. Conference: Polymer Alloys: Structure and Properties, International Symposium. 16th Europhysics Conference on Macromolecular Physics, European Physical Soc; Groupe Francais d'Etudes et d'Applications des Polymeres, Fr, 1984; 25-31

22 Bucknall C B and Partridge I K. Phase separation in epoxy resins containing polyethersulphone. Polymer, 1983; 24: 639-644

23 Greenhalgh E and Hiley M. The assessment of novel materials and processes for the impact tolerant design of stiffened composite aerospace structures. Composites Part A, 2003; 34: 151–161

24 Troulis E. Effect of Z-Fiber pinning on the mechanical properties of carbon fibre/epoxy composites. Ph.D. Thesis. Cranfield University, School of Industrial and Manufacturing Science, Advanced Materials, 2003.

25 Lee S, Scott R F, Gaudert P C, Ubbink W H and Poon C. Mechanical testing of toughened resin composite materials. Composites, 1988; 19(4):300-310

26 Ishai O, Rosenthal H, Sela N and Drukker E. Effect of selective adhesive interleaving on interlaminar fracture toughness of graphite / epoxy composite laminates. Composites, 1988; 19(1): 49-54

27 Sela N, Ishai O and Banks-Sills L. The effect of adhesive thickness on interlaminar fracture toughness of interleaved CFRP specimens. Composites, 1989; 20(3): 257-265

28 Barrett D J. The mechanics of z-fiber reinforcement. Composite Structures, 1996; 36: 23-32

29 Baillie C, Emanuelsson J and Marton F. Building knowledge about the interface. Composites Part A, 2001; 32: 305-312

30 Buxton A and Baillie C. Study of the influence of the environment on the measurement of interfacial properties of carbon fibre/epoxy resin composites. Composites, 1994; 25(7):604-608

31 Liu D. Impact-induced delamination-a view of bending stiffness mismatching. Journal of Composite Materials, 1988; 22(7): 674-691

32 Hitchen S A and Kemp R M J. The effect of stacking sequence on impact damage in a carbon fibre/epoxy composite. Composites, 1995; 26: 207-214

33 Naik N K, Ramasimha R, Arya H, Prabhu S V and ShamaRao N. Impact response and damage tolerance of glass-carbon/epoxy hybrid composite plates. Composites Part B, 2001; 32:565-574

34 Brandt J, Drechslef K and Arendts F J. Mechanical performance of composites based on various three dimensional woven-fibre performs. Composites Science and Technology, 1996; 56: 381-386

35 Kamiya R, Cheeseman B A, Peter Popper and Tsu-Wei Chou. Some recent advances in the fabrication and design of three-dimensional textile preforms: a review. Composites Science and Technology, 2000; 60: 33-47

36 Dexter H B and Haskob G H. Mechanical properties and damage tolerance of multiaxial warp-knit composites. Composites Science and Technology, 1996; 56: 367-380

37 Bogdanovich A and Mungalov D. Recent advancements in manufacturing 3-D braided preforms and composites. Procs. of "Composite Systems – Macrocomposites, Microcomposites, Nanocomposites", SYDNEY, Australia, 21-25 July 2002. Eds: S. Bandyopadhyay et al: 61-72.

38 Hosur M V, Vaidya U K, Ulven C and Jeelani S. Performance of stitched/unstitched woven carbon/epoxy composites under high velocity impact loading. Composite Structures, 2004; 64: 455–466

39 Lee L, Rudov-Clark S, Mouritz A P, Bannister M K and Herszberg I. Effect of weaving damage on the tensile properties of three-dimensional woven composites. Composite Structures, 2002; 57(1-4): 405-413

40 Chou S, Chen H C and Wu C C. BMI resin composites reinforced with 3D carbon–fibre fabrics. Composite Science and Technology 1992; 43: 117–128

41 Callus P J, Mouritz A P, Bannister M K and Leong K H. Tensile properties and failure mechanisms of 3D woven GRP composites. Composites Part A, 1999; 30: 1277–1287

42 Bannister M K, Herszberg I, Nicolaidis A, Coman F and Leong K H. The manufacture of glass/epoxy composites with multi-layer woven architectures. Composites Part A, 1998; 29A: 293–300

43 Mungalov D and Bogdanovich A. Complex shape 3-D braided composite preforms:

structural shapes for marine and aerospace. SAMPE Journal, 2004; 40(3): 7-21

44 Ruan X and Chou T-W. Experimental and theoretical studies of the elastic behavior of knitted-fabric composites. Composites Science and Technology, 1996; 56: 1391-1403

45 Falconnet D, Bourban P-E, Pandita S, Mansona J-A E and Verpoest. I. Fracture toughness of weft-knitted fabric composites. Composites Part B, 2002; 33: 579–588

46 Pandita S D, Falconet D and Verpoest I. Impact properties of weft knitted fabric reinforced composites. Composites Science and Technology,2002; 62: 1113–1123

47 Ramakrishna S. Characterization and modeling of the tensile properties of plain weft-knit fabric-reinforced composites. Composites Science and Technology, 1997; 57: 1-22

48 Chou S, Chen H-C and Lai C-C. The fatigue properties of weft-knit fabric reinforced epoxy resin composites. Composites Science and Technology, 1992; 45: 283-291

49 Mouritz A P, Leong K H and Herszberg I. A review of the effect of stitching on the in-plane mechanical properties of fibre-reinforced polymer composites. Composites Part A, 1997; 28A: 979-99

50 Morales A. Structural stitching of textile performs. In Procs. 22nd Int. SAMPE Technical Conference, 6-8 November 1990; 22:1217-1230

51 Sickinger C and Herrmann A. Structural Stitching as a Method to design High-Performance Composites in Future. Publication from DLR (German Aerospace Center) web portal. *(URL: http://www.dlr.de/fa/publikationen/ last access September 2005)*

52 Dransfield K A, Jain L K and Mai Y-W. On the effects of stitching in CFRPs-I. Mode I delamination toughness. Composites Science and Technology, 1998; 58: 815-827

53 Jain, L K and Mai Y-W. On the effect of stitching on Mode I delamination toughness of laminated composites. Composites Science and Technology, 1994; 51: 331-345

54 Jain L K, Dransfield K A and Mai Y-W. On the effects of stitching in CFRPs-II. Mode II delamination toughness. Composites Science and Technology, 1998; 58: 829-837

55 Sankar B V and Sharma S K. Mode II delamination toughness of stitched graphite/epoxy textile composites. Composites Science and Technology, 1997; 57: 729-737

56 Gunnion A J, Scott M L, Thomson R S and Hachenberg D. Thickness effects on the compressive stiffness and strength of stitched composite laminates. Composite Structures, 2004; 66: 479-486

57 Farley G L, Smith B T and Maiden J. Compression response of thick layer composite laminates with through-the-thickness reinforcement. Journal of Reinforced Plastics and Composites, 1992; 11: 787-810

58 Hosur M V, Vaidya U K Ulven C and S. Jeelani. Performance of stitched/unstitched woven carbon/epoxy composites under high velocity impact loading. Composite Structures, 2004; 64: 455-466

59 Karal M. AST Composite Wing Program –Executive Summary. NASA/CR-2001-210650

60 Dell'Anno G. PhD annual review report, 2004 *(Unpublished)*

61 Poulin E A. Reinforcement of a T-joint by Z-Fiber® Pinning and Tufting. MSc Thesis. Cranfield University, School of Industrial and Manufacturing Science, 2004

62 Partridge I K, Cartié D D R and Bonnington T. Manufacture and performance of Z-pinned composites. Chapter 3 in: Advani S and Shonaike G, editors. Advanced Polymeric Materials: Structure-property relationships, CRC Press, 2003

63 Steeves C A and Fleck N A. In-plane properties of composite laminates with through-thickness pin reinforcement. International Journal of Solids and Structures, 2005; *(Article in press)*

64 Freitas G, Magee C, Dardzinski P and Fusco T. Fiber insertion process for improved damage tolerance in aircraft laminates. Journal of Advanced Materials, 1994; 25(4) 36-43

65 Cartié D D R. Effect of Z-fibres^{TM} on the delamination behaviour of carbon-fibre/epoxy laminates. Ph.D. Thesis. Cranfield University, School of Industrial and Manufacturing Science, Advanced Materials, 2000

66 Cartié D D R and Partridge I K. Delamination resistant laminates by z-fiber pinning. Part I: Manufacture and fracture performance. Composites Part A. 2005; 36 (1): 55–64

67 Graftieaux B, Rezai A and Partridge I K. Effects of Z-pin reinforcement on the delamination toughness and fatigue performance of unidirectional AS4/8552 composite. Proceedings of ECCM 9, Brighton, June 5-7, 2000

68 Bitsianis N. The influence of Z-pinning on toughness and impact performance of carbon fibre polymer composite materials. MSc Thesis. Cranfield University, School of Industrial and Manufacturing Science, 1999

69 Cartie´ D D R, Troulis M and Partridge I K. Delamination of Z-pinned carbon fibre reinforced laminates. Composites Science and Technology, 2005; *(Article in press)*

70 Grassi M. Numerical modelling of composite laminates with through-thickness-reinforcements. Ph.D. Thesis. Cranfield University, College of Aeronautics, 2004

71 Cartié D D R, Bitsianis N, Irving P E and Partridge I K. Z-fiber reinforcement: effects on the compression after impact performance of T300/914 laminates. Proceedings of JNC12, Cachan, Paris, France, 15-17 November 2000

72 Grassi M, Zhang X and Meo M. Prediction of stiffness and stresses in z-fibre reinforced composite laminates. Composites Part A, 2002; 33(12): 1653–1664

73 Allen H G. Analysis and design of structural sandwich panels. Pergamon Press Ltd. London, 1969

74 Zenkert D. The handbook of sandwich construction. UK Engineering Materials Advisory Services Ltd and Chameleon Press Ltd. London, 1997

75 Altstadt V, Diedrichs F, Lenz T, Bardenhagen H and Jarnot D. Polymer foams as core materials in sandwich laminates (comparison with honeycomb). Polymers and Polymer Composites, 1998; 6(5): 295-304

76 Herbeck L, Kleineberg M and Schöppinger C. Foam cores in RTM structures: manufacturing aid or high-performance sandwich? Publication from DLR web portal *(URL: http://www.dlr.de/fa/publikationen/ last access September 2005)*

77 Zenkert D. An introduction to sandwich construction. UK Engineering Materials Advisory Services Ltd and Chameleon Press Ltd. London, 1997

78 Pip W. Applications for PMI foam-cored sandwich material - why PMI? 28th International SAMPE Technical Conference, November 4-7, 1996

79 Wu C L, Weeks C A, Sun T C. Improving honeycomb-core sandwich structures for impact resistance. Journal of Advanced Materials, 1995; 26(4): 41-47

80 Vaidya U K, Nelson S, Sinn B and Mathew B. Processing and high strain rate impact response of multi-functional sandwich composites. Composite Structures, 2001; 52: 429-440

81 Vaidya U K, Ulven C, Pillay S and Ricks H. Impact damage of partially foam-filled co-injected honeycomb core sandwich composites. Journal of Composite Materials, 2003; 37(7): 611-626

82 Seibert H F. High-performance foam cores based on PMI definition of the position and recent developments. 42nd International SAMPE Symposium. May 4-8, 1997

83 Seibert H F, High-performance foam cores based on PMI definition of status and recent developments. In: Procs of the Fourth International Conference on Sandwich Construction, Stockholm, Sweden, June 9-11, 1998, Engineering Materials Advisory Services Ltd.

84 Akay M and Hanna R. A comparioson of honeycomb-core and foam-core carbon-fibre/epoxy sandwich panels. Composites, 1990; 21(4): 325-331

85 Laurin F and Vizzini A J. Energy absorption of sandwich panels with composite-reinforced foam core. Journal of Sandwich Structures and Materials, 2005; 5: 113-132

86 Sun C T, Hasebe R S and Hua Y. Properties of sandwich structures with reinforced core. American Society of Mechanical Engineers, Aerospace Division (Publication) AD. Analysis and Design Issues for Modern Aerospace Vehicles, 1997; 55: 323-333

87 Kim J H, Lee Y S, Park B J and Kim D H. Evaluation of durability and strength of stitched foam-cored sandwich structures. Composite Structures, 1999; 47: 543-550

88 Stanley L E, Gharpure S S and Adams D O. Mechanical property evaluation of stitched composite sandwich panels. 45th International SAMPE Symposium, May 21-25, 2000 Long Beach, California, USA

89 Lascoup B, Khellil K and Benzeggagh M. Stitched sandwich panel materials for resin infusion structures. SAMPE Journal, 2005; 41(1): 42-48

90 Potluri P, Kusak E and Cumellas A J. Structural performance of orthogonal and bias stitched sandwich structures with rigid close-cellular foams. 44th AIAA/ASME/ASCE/AHS/ASC Structures, Structural Dynamics, and Materials Conference. 7-10 April 2003, Norfolk, Virginia. AIAA 2003/1949; 7: 4991-4997

91 Raju K S and Tomblin. Energy absorption in stitched composite sandwich panels. Journal of Composite Materials, 1999; 33(8): 721-728

92 Potluri P, Kusak E and Reddy T Y. Novel stitch-bonded sandwich composite structures. Composite Structures, 2003; 59: 251-259

93 Singh P and La Saponara V. Experimental investigation on performance of angle-stitched sandwich structures. 45th AIAA/ASME/ASCE/AHS/ASC Structures, Structural Dynamics and Materials Conference. 19-22 April 2004, Palm Springs, California. AIAA-2004/1705

94 Glaessgen E H and Raju I S. Debonding of stitched composite sandwich structures. 41st AIAA/ASME/ASCE/AHS/ASC Structures, Structural Dynamics, and Materials Conference and Exhibit. 3-6 April 2000, Atlanta, Georgia. AIAA-2000/1614

95 Thurm T. Applications of one-sided stitching techniques for resin infusion preforms and structures. SAMPE Journal, 2005; 41(1): 64-67

96 Wittig J. In-mold-reinforcement of preform by 3-dimensional tufting. 47th International SAMPE Symposium, 12-16 May 2002, Long Beach, California, 47: 1043-1051

97 Wallace B T, Sankar B V and Ifju P G. Pin reinforcement of delaminated sandwich beams under axial compression. Journal of Sandwich Structures and Materials, 2001; 3: 117-129

98 Wallace B T, Sankar B V and Ifju P G. Effect of Z-pinning on buckling delaminated sandwich panels. 41st AIAA/ASME/AHS/ASC Structures, Structural Dynamics, and Materials Conference and Exhibit. 3-6 April 2000, Atlanta, Georgia. AIAA-2000/1403; 539-543

99 Carstensen T, Cournoyer D, Kunkel E and Magee C. X-Cor Advanced Sandwich Core Material. In: Proceedings of 33rd International SAMPE Technical Conference. Seattle, WA, November, 2001

100 Hosur M V, Adbullah M and Jeelani S. Studies on the low-velocity impact response of woven hybrid composites. Composite Structures, 2005; 67: 253–262

101 Wallach J C and Gibson L J. Mechanical behaviour of a three-dimensional truss material. International Journal of Solids and Structures, 2001; 38: 7181-7196

102 O'Brien K T and Paris I L. Exploratory investigation of failure mechanisms in transition regions between solid laminates and X-Cor™ truss sandwich. Composite Structures 2002; 57: 189-204

103 Vaidya U K, Palazotto A N and Gummadi L N B. Low velocity impact and compression-after-impact response of Z-pin reinforced core sandwich composites. Journal of Engineering Materials and Technology, 2000; 122: 434-442

104 Palazotto A N, Gummadi L N B, Vaidya U K and Herup E. Low velocity impact damage characteristics of Z-Fiber reinforced sandwich panels-an experimental study. Composite Structures, 1999; 43(4): 275–288.

105 Herup E J. Low velocity impact on composite sandwich plates. Ph.D. dissertation. Air Force Institute of Technology, Dayton, Ohio, 1996

106 Vaidya U K, Nelson S P, Ulven C and Mathew B. Vibration response of multi-functional Z-pin space core sandwich composites. American Society of Mechanical Engineers Proc, Noise Control and Acoustic Division (Publication) NCA, 2000; 27: 413-420

107 Kocher C, Watson W, Gomez M, Gonzalez I and Birman V. Integrity of sandwich panels and beams with truss-reinforced cores. Journal of Aerospace Engineering 2002; 15(3): 111-117

108 Mazumdar S K. Composites manufacturing – materials, product and process engineering – CRC Press, London, 2002

109 Karlsson K F and Astrom B T. Manufacturing and applications of structural sandwich components. Composites Part A, 1997; 28A: 97-111

110 Astrom B T. Manufacturing of polymer composites. Chapman & Hall, London 1997

111 *http:\\www.roehm.com last access August 2005*

112 Hexcel Composites Ltd, Duxford, Cambridge CB2 4QD, UK
(URL: http://www.hexcel.com/Products/ last access August 2005)

113 Cytec Engineered Materials Ltd**,** Abenbury Way, Wrexham, LL13 9UZ, UK
(URL: http://www.cytec.com/business/EngineeredMaterials/ last access August 2005)

114 Aztex Inc. Private communications.
Address: Aztex Inc, 303 Bear Hill Road, Waltham, MA, 02154-1196, USA

115 McKenzie M. Novel Core Materials for Use in Intrusion Resistant Composite Sandwich Panels, MSc Thesis, School of Industrial Manufacturing Science, Cranfield University, 2002

116 Yang Z L and Lee S. Heating cycle design for thick composite laminates using curing processes for thin laminates. Journal of Reinforced Plastics and Composites, 2002; 21(17): 1543-1559

117 Hsiao H M, Lee S M, Buyny R A and Martin C J. Development of core crush resistant prepreg for composite sandwich structures. Proceedings of 33rd International SAMPE Technical Conference - Advancing Affordable Materials Technology- Seattle, WA, Nov 5-8 2001

118 Rohacell® documentation CD, 2004 edition

119 Morrison R T and Boyd R N. Organic Chemistry -3rd edition-Prentice Hall International (UK) Limited, London, 1973

120 *www.Azom.com (On-line materials information directory, last access August 2005)*

121 Vantico Ltd. (now Huntsman Advanced Materials Ltd.), Duxford, Cambridge,CB2 4QA, UK, *(URL: http://www.huntsman.com/ last access August 2005)*

122 Staab G H. Laminar composites. Butterwoth-Heinemann, Boston, 1999

123 Chamis C C. 'Micromechanics strength theories'. Composite materials, vol. 5, 'Fracture and fatigue', Broutman L S, ed. Academic Press, New York, 1974

124 ASTM D 3039/D 3039M-95. Standard test method for tensile properties of polymer matrix composite materials, American Society for Testing Materials Annual Book of ASTM Standards, 1995

125 ASTM D 3410/D 3410M-95. Standard test method for compressive properties of polymer matrix composite materials with unsupported gage section by shear loading, American Society for Testing Materials Annual Book of ASTM Standards, 1995

126 DuPont de Nemours International S.A., P.O. Box 50, CH-1218 Le Grand-Saconnex, Geneva, Switzerland *(URL: http://www.dupont.com/ last access August 2005)*

127 ASTM C273 Standard Test Method for Shear Properties of Sandwich Constructions,American Society for Testing Materials Annual Book of ASTM Standards, 1995, Vol 03.01

128 ASTM C365 Standard Test Method for Flatwise Compressive Properties of Sandwich Cores, American Society for Testing Materials Annual Book of ASTM Standards, 1995, Vol 03.01

129 Zhang J and Ashby M F. The out-of-plane properties of honeycombs. International journal of mechanical sciences, 1992; 34(6): 475-489

130 Hodgkinson J M. Mechanical testing of advanced fibre composites. Woodhead Publishing and CRC Press. Cambridge, 2000

131 MIL-HDBK-17-3F. Volume 3, Polymer matrix composites: materials usage, design and analysis, 2002

132 O'Connor D J. A comparison of test methods for shear properties of the cores of sandwich construction. Journal of Testing and Evaluation, 1989; 17(4): 241-246

133 ASTM C 393-00 Standard Test Method for Flexural Properties of Sandwich Plates, American Society for Testing Materials Annual Book of ASTM Standards, 2000, Vol 15.03

134 Fukuda H, Itohiya G, Kataoka A and Tashiro S. Evaluation of Bending Rigidity of CFRP Skin–Foamed Core Sandwich Beams. Journal of sandwich structures and materials, 2004; 6: 75-92

135 Lingaiah K and Suryanarayana B G. Strength and stiffness of sandwich beams in bending. Experimental mechanics, 1991; 31(1): 1-7

136 Grédiac M and Dufort L. Experimental evidence of parasitic effects in shear test on sandwich beams. Experimental Mechanics, 2002; 42: 186-193

137 O'Connor D J. An evaluation of test methods for shear modulus of sandwich cores. The international journal of cement composites and lightweight concrete, 1984; 6(1): 3-12

138 Kanny K, Mahfuz H, Thomas T and Jeelani S. Static and dynamic characterization of polymer foams under shear loads. Journal of Composite Materials, 2004; 38(8): 629-639

139 Instron Corp., 825 University Ave., Norwood, MA 02062-2643
(URL: http://www.instron.com last access August 2005)

140 Instruction manual for model EIR LE-05, laser extensometer with 'multisegment' measurement. March 2000.
(EIR-Electronic Instrument Research Ltd., P.O. Box 678, Irwin, PA 15642,
URL: http://www.e-i-r.com/ last access August 2005)

141 National Instruments Corp., 11500 North MoPac Expressway, Austin, TX 78759
(URL: http://www.ni.com/uk last access August 2005)

142 Zupan M, Deshpande V S and Fleck N A. The out-of-plane compressive behaviour of woven-core sandwich plates. European Journal of Mechanics A/Solids, 2004; 23: 411–421

143 Kalidindi S R, Abusafieh A and El-Danaf E. Accurate characterisation of machine compliance for simple compression testing. Experimental Mechanics, 1997; 37: 210-215

144 Van Vuure A W, Pflug J, Ivens J A and Verpoest I. Modelling the core properties of composite panels based on woven sandwich-fabric preforms. Composites Science and Technology 2000; 60: 1263-1276

145 MSC. Nastran User Guide 2001

146 Cook R D, Malkus D S, Plesha M E and Witt R J. Concepts and application of finite element analysis (4th edition). John Wiley & Sons Inc., New York, 2002

147 Nguyen Q S. Stability and nonlinear solid mechanics. John Wiley & Sons Ltd, Chichester, 2000

148 Deshpande V S and Fleck N A. Collapse of truss core sandwich beam in 3-point bending. International Journal of Solids and Structures 38 (2001), 6275-6305

149 Gere J M and Timoshenko S P.Mechanics of materials. Fourth Edition, PWS Publishing Company, 1997

150 Marasco A I, Cartié D D R and Partridge I K. Mechanical behaviour of Z-pinned sandwich panels. Procs DFC7, University of Sheffield, 22-24 April 2003, UK

151 Gibson L J and Ashby M F. Cellular solids - structure & properties. Pergamon Press, Oxford, 1988

152 Timoshenko S P and Gere J M. Theory of elastic stability. Second Edition, McGraw-Hill, 1961

153 Wang C M, Wang C Y and Reddy JN. Exact solutions for buckling of structural members. CRC series in computational mechanics and applied analysis. CRC Press, 2005

154 Megson T H G. Aircraft structures for engineering students (third edition). Butterworth-Heinemann, Oxford,1999

155 Farley G L. Effect of specimen geometry on the energy absorption capability of composite materials. Journal of Composite Materials, 1986; 20: 390-400

156 Mamalis A G, Robinson M, Manolakos D E, Demosthenous G A, Ioannidis M B and Carruthers J. Crashworthy capability of composite material structures. Composite Structures, 1997; 37: 109-134

157 Hull D. A unified approach to progressive crushing of fibre-reinforced composite tubes. Composites Science and Technology, 1991; 40: 377-421

158 Kindervater C M and Georgi H. Composite strength and energy absorption as an aspect of structural crash resistance. In Proc. Symp. on Structural Crashworthiness and Failure, Liverpool, UK', Elsevier Applied Science, 1993: 189-235

159 Thornton P H. Energy absorption in composite structures. Journal of Composite Materials, 1979; 13: 247-262

160 Farley G L. Energy absorption of composite materials. Journal of Composite Materials, 1983; 17: 267-279

161 Jacob G C, Starbuck J M, Simunovic S and Fellers J F. New test method for determining energy absorption mechanisms in polymer composite plates. Polymer composites, 2003; 24: 706-715

162 Fleming D C and Nicot F. Crushing of flat graphite/epoxy laminates using a column specimen. Journal of Composite Materials, 2003; 37(24): 2225-2239

163 Lavoie J A and Kellas S. Dynamic crush tests of energy-absorbing laminated composites plates. Composites Part A, 1996; 27A: 467-475

164 Light fixed and rotary wings aircraft crashworthiness, MIL-STD-1290 (1974)

165 Price J N and Hull D. Axial crushing of glass fibre-polyester composite cones. Composites Science and Technology, 1987; 28: 211-230

166 Thornton P H and Edwards P J. Energy absorption in composites tubes. Journal of Composite Materials, 1982; 16(6): 521-545

167 Hull D. Axial crushing of fibre reinforced composite tubes. In 'Structural Crashworthiness', ed. Jones N and Wierzbicki T. Butterworths, London, 1983; 118-135

168 Thornton P H. The crush behaviour of glass reinforced plastic sections. Composites Science and technology, 1986; 27: 199-223

169 Hanagud S, Craig J I, Sriram P and Zhou W. Energy absorption behaviour of graphite epoxy composite sine webs. Journal of Composite Materials, 1989; 23: 448-459

170 Turner T A, Warrior N A, Robitaille F and Rudd C D. The influence of processing variables on the energy absorption of composite tubes. Composites Part A, 2005; 36: 1291-1299

171 Saito H, Chirwa E C, Inai R and Hamada H. Energy absorption of braiding pultrusion process composite rods. Composite Structures, 2002; 55: 407–417

172 Tao W H, Robertson R E and Thornton P H. Effects of material properties and crush conditions on the crush energy absorption of fiber composite rods. Composites Science and Technology, 1993; 47(4): 405-418

173 Farley G L. The effect of crushing speed on the energy-absorption capability of composite tubes. Journal of Composite Materials, 1991; 25: 1314-1329

174 Alghamdi A A A. Collapsible impact energy absorber: an overview. Thin-Walled Structures, 2001; 39:189-213

175 Lavoie J A and Morton J. Design and application of a quasi-static crush test fixture for investigating scale effects in energy absorbing composite plates. NASA/CR-1993-4526

176 Lavoie J A, Morton J, Jackson K. An evaluation of the energy absorption of laminated composite plates. Proceedings of the Institution of Mechanical Engineers, Part G: Journal of Aerospace Engineering, 1995; 209(3): 185-194

177 Jackson K, Morton J, Lavoie J A and Boitnott R. Scaling of energy absorbing composite plates. Journal of the American Helicopter Society, 1994; 39: 17-23

178 Soutis C, Ramany Bala Poubady V. Crush energy absorption of woven CFRP laminates. In: Foreign object impact & energy absorbing structure. Procs IMechE seminar, London, March 4, 1998

179 Bolukbasi A O and Laananen D H. Analytical and experimental studies of crushing behaviour in composite laminates. Journal of Composite Materials, 1995; 29: 1117-1139

180 Fleck N A and Sridhar I. End compression of sandwich columns. Composites Part A, 2002; 33: 353-359

181 Vadakke V and Carlsson L A. Experimental investigation of compression failure mechanics of composite faced foam core sandwich specimens. Journal of Sandwich Structures and Materials, 2004; 6: 327-342

182 Torre L and Kenny J M. Evaluation of energy absorption properties of crashworthy sandwich structures. Procs international SAMPE technical conference- Advancing affordable materials technology-, 5-8 November 2001, Seattle; Washington; 33:1478-1490

183 Ewiel I M, Gdoutos E E, Abot J L and Wang K-A. Deformation and failure of composite sandwich structures. Journal of Thermoplastic Composite Materials, 2003; 16(4): 345-364

184 ASTM C364 Standard Test Method for Edgewise Compressive Strength of Sandwich Constructions, American Society for Testing Materials Annual Book of ASTM Standards, 1995, Vol 03.01

185 Marechal A. Investigation into crush energy absorption of composite materials. MSc Thesis, School of Industrial Manufacturing Science, Cranfield University, 1997

186 Thornton P H. Effect of trigger geometry on energy absorption in composite tubes. Procs 'Fifth International Conference on Composite Materials', ICCM-V, San Diego, CA, USA, Metallurgical Soc Inc, 1985; 1183-1199

187 Houbolt J C and Stowell E Z. Critical stress of plate columns. NACA TN 2163, 1950

188 Singer J, Arbocz J and Weller T. Buckling experiments: experimental methods in buckling of thin-walled structures. John Wiley, New York, 2002.

189 Jacob G C, Fellers J F, Simunovic S and Starbuck J M. Energy absorption in polymer composite materials for automotive crashworthiness. Journal of Composite Materials, 2002; 36: 813-850

190 Rees D G. Foundation of statistics. Chapman and Hall, London , 1987

191 Pflug J, Vangrimde B and Verpoest I. Material efficiency and cost effectiveness of sandwich materials, SAMPE 2003 US, Long Beach, CA, May 11-15, 2003, pp 1925-1937

192 Lucas S and Pederson C. Self-adhesive prepreg materials for co-cured sandwich structure processes. International SAMPE Technical Conference, SAMPE 2004; 3685-3696

193 Marasco A I, Cartié D D R, Partridge I K and Rezai A. Mechanical properties balance in novel Z-pinned sandwich panels: Out-of-plane properties. Composites Part A, 2005 *(Accepted for publication)*

194 Smith S A and Shivakumar K N. Modified mode-I cracked sandwich beam (CSB) fracture test. Procs. 42nd AIAA/ASME/ASCE/ASC structures, structural dynamics and materials conference, Seattle; 2001 (AIAA 2011-1221)

195 Cantwell W J, Scudamore R, Ratcliffe J and Davies P. Interfacial fracture in sandwich laminates. Composite Science and Technology, 1999; 59: 2079-2085

196 Shivakumar K N and Smith S A. In situ fracture toughness testing of core materials in sandwich panels. Journal of Composite Materials, 2004; 38(8): 655-668

197 Temple M. Numerical simulation of F1 nose cone impact testing. MSc Thesis. Cranfield University, School of Industrial and Manufacturing Science, 2003

Appendix A

A1. Analytical model: quantities for the analysis

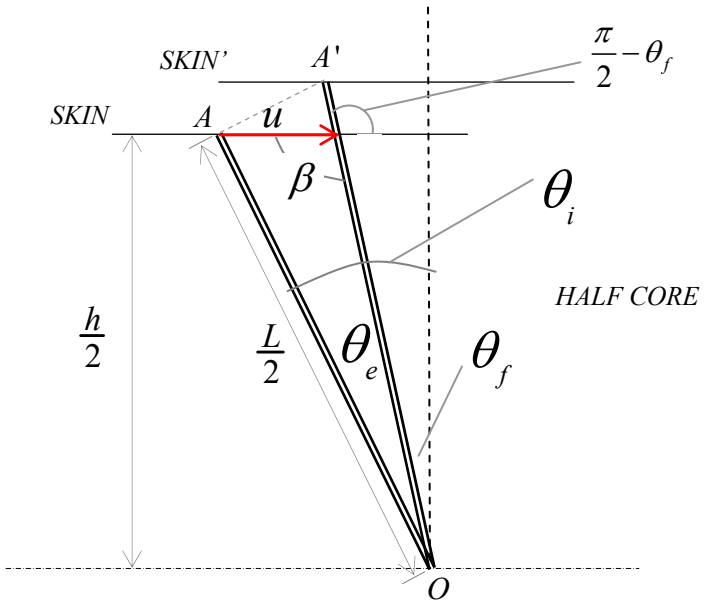

Figure A.1– *Local shear effect on rigid pin (quantities for the analysis shown)*

The triangle AOA' is isosceles; the two angles $\hat{A}$ and $\hat{A}'$ are equal. The correlation between the angle of the pin rotation in the elastic phase θ_e and the global shear strain γ measured in the material is determined. The quantity u is in reality half of the relative longitudinal displacement measured by the LVDT. The relation between γ and u follows:

$$\gamma = \frac{u}{(h/2)} \tag{A1}$$

A2. Pin element details for a hollow X-Cor model

All the pins present in the unit cell model (counteracting and non-counteracting) and the rigid connecting elements between boundary pins are shown in figure A.2. Foam solid elements have been omitted for clarification.

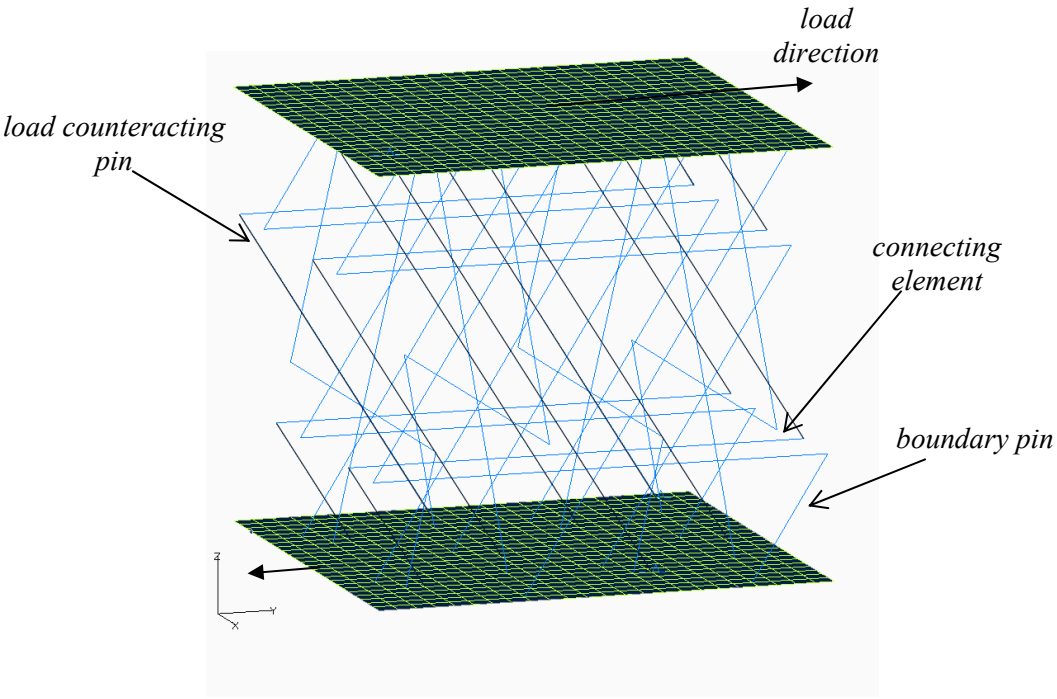

Figure A.2– *Pin and connecting elements in a* X-Cor$^{F}_{S}$ */0.51/30°/0.13 unit cell model*

A3. Errors in predicted stiffness values: evaluation of a non-rigid pin analytical model

The assumption of rigid pin in the analytical model presented in section 5.3.1 means that all the deformability goes into the rotational springs located at the tips of the counteracting pins. This probably leads to an underestimation of the constant of rigidity of the rotational spring elements employed in the FE model. To prove this, a non-rigid pin is adopted in the same analytical approach. In this case a core measured property (G modulus) is related to both the deformation of the load counteracting pins and the deformation occurring in the rotational springs. It is again assumed that all the pins face the same shear force F and that they undergo the same deformation. For simplicity the model here presented accounts only for vertically inserted counteracting pins. More complex calculations are produced by insertion angles different from zero, although leading to similar conclusions. The model schematisation of figure A.3 shows half core; the pin length $2L$ coincide with the core thickness h. The boundary and load conditions indicated are the same as those used in the FE model. Points (or nodes) B and C are

coincident, but here for convenience are sketched separate. They are connected with a rotational spring and with a rigid connection -not indicated- which in the model represent the fact that the pin head remains embedded in the skin.

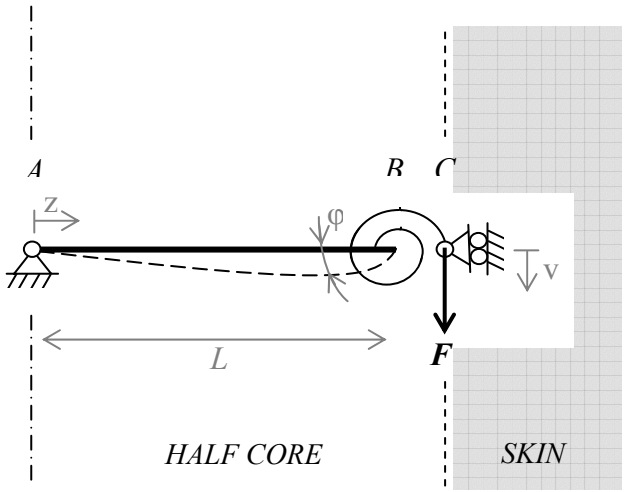

Figure A.3– *Non-rigid pin model*

The force F acting on each counteracting pin of the core is considered equally distributed between them and it is calculated as follows:

$$F = \frac{T}{N_C} \tag{A2}$$

where T is the total applied force on the sample and N_C is the number of the counteracting pins. The displacement $v(B) \equiv v(C)$ at pin tip is related to the core shear strain γ:

$$\gamma = \frac{v(B)}{L} \tag{A3}$$

The relation between the shear modulus G and the pin tip (and skin) displacement is the following:

$$G = \frac{\tau}{\gamma} = \frac{TL}{vA} \tag{A4}$$

To calculate the pin displacement the following differential equation needs to be solved:

$$\frac{d^2v}{dz^2} = -\frac{Fz}{EI_z} \tag{B5}$$

In equation A5, E is the pin Young's modulus and I_z the moment of inertia. After some computation and considering the following boundary conditions:

$$\begin{cases} v(0) = 0 \\ \gamma(L) = \dfrac{FL}{k_M} \end{cases} \tag{A6}$$

where k_M is the constant of rigidity of the rotational spring, we obtain this equation for the displacement at pin tip:

$$v(B) = \frac{L^3F}{3EI_z} + \frac{L^2F}{k_M} \tag{A7}$$

The following relation allows the constant k_M to be determined once the G value has been experimentally determined

$$G = \frac{N_C}{A\left(\dfrac{L^2}{3EI_z} + \dfrac{L}{k_M}\right)} \tag{A8}$$

Table A1 shows a comparison between the constant of rigidity k_M of the rotational springs obtained with this model and with the previous based on rigid pins (section 5.3.1.2). They are valid only for cores made up of vertically inserted pins ($\theta_{ins} = 0$).

Rigid pin model	*Non-rigid pin model*
$k_{M_R} = \dfrac{GAL}{N_C}$	$k_{M_{NR}} = \dfrac{GAL}{\left(N_C - \dfrac{GAL^2}{3EI_z}\right)}$

Table A1-*Comparison between rigid and non-rigid pin models*

The ratio between the two constants of rigidity shows that considering a non-rigid pin in the analytical model leads to higher stiffness values for the rotational spring element to be used in the FE analysis.

$$\frac{k_{M_{NR}}}{k_{M_R}} = \frac{N_C}{N_C - \left(\frac{GAL^2}{3EI_z}\right)} \tag{A9}$$

In fact the quantity in parenthesis in equation A9 assumes positive values, this implies that $k_{M_{NR}} > k_{M_R}$ which means that a higher constant of rigidity, to be implement in the FE code, is obtained with a non-rigid pin analytical model.

Appendix B

B.1 Detailed calculations for solving the differential equation for the buckling behaviour of the pin-column model

General homogenous solution of equation 6.17 (section 6.3.1):

$$w = A\cos\beta x + B\sin\beta x + Cx + D \tag{B1}$$

From the first boundary condition (eq. 6.21):

$$A + D = 0 \Rightarrow D = -A \tag{B2}$$

Therefore the general solution becomes:

$$w = A\left(\cos\beta x - 1\right) + B\sin\beta x + Cx \tag{B3}$$

From the second condition:

$$A\left(\cos\beta L - 1\right) + B\sin\beta L + CL = \delta\sin\theta \tag{B4}$$

The derivatives of the general solution (B3) are:

$$\begin{aligned} w' &= -AB\sin\beta x + \beta B\cos\beta x + C \\ w'' &= -AB^2\sin\beta x - \beta^2 B\sin\beta x \end{aligned} \tag{B5}$$

The third condition yields to:

$$-A\alpha\beta^2 L + \beta B + C = 0 \tag{B6}$$

The fourth condition yields to:

$$-A\alpha\beta^2 L\cos\beta L - \alpha\beta^2 BL\sin\beta L - A\beta\sin\beta L + \beta B\cos\beta L + C = 0 \tag{B7}$$

thus:

$$-\left(\alpha\beta^2 L\cos\beta L + \beta\sin\beta L\right)A + \left(-\alpha\beta^2 L\sin\beta L + \beta\cos\beta L\right)B + C = 0 \tag{B8}$$

The unknown constants A, B, C in the general solution are given by solving the following linear system:

$$\begin{cases} (\cos\beta L - 1)A + (sin\beta L)B + LC = \delta sin\theta \\ -\alpha\beta^2 LA + \beta B + C = 0 \\ -(\alpha\beta^2 L\cos\beta L + \beta sin\beta L)A + (-\alpha\beta^2 Lsin\beta L + \beta\cos\beta L)B + C = 0 \end{cases} \tag{B9}$$

The unknowns are determined by applying the Cramer's rule. The determinant of the matrix coefficient of the previous system (B9):

$$\overline{M} = \begin{pmatrix} \cos\beta L - 1 & \sin\beta L & L \\ -\alpha\beta^2 L & \beta & 1 \\ -\alpha\beta^2 L\cos\beta L - \beta\sin\beta L & -\alpha\beta^2 L\sin\beta L + \beta\cos\beta L & 1 \end{pmatrix} \tag{B10}$$

After some computation:

$$\det\overline{M} = \beta\sin\beta L\left\{2\tan\frac{\beta L}{2} + \beta L\left[\alpha^2(\beta L)^2 + 1\right]\right\} \tag{B11}$$

The unknown coefficients A, B and C are evaluated as follows:

$$\begin{cases} A = \dfrac{\begin{pmatrix} \delta\sin\theta & \sin\beta L & L \\ 0 & \beta & 1 \\ 0 & -\alpha\beta^2 L\sin\beta L + \beta\cos\beta L & 1 \end{pmatrix}}{\det\overline{M}} \\ B = \dfrac{\begin{pmatrix} \cos\beta L - 1 & \delta\sin\theta & L \\ -\alpha\beta^2 L & 0 & 1 \\ -\alpha\beta^2 L\cos\beta L - \beta\sin\beta L & 0 & 1 \end{pmatrix}}{\det\overline{M}} \\ C = \dfrac{\begin{pmatrix} \cos\beta L - 1 & \sin\beta L & \delta\sin\theta \\ -\alpha\beta^2 L & \beta & 0 \\ -\alpha\beta^2 L\cos\beta L - \beta\sin\beta L & -\alpha\beta^2 L\sin\beta L + \beta\cos\beta L & 0 \end{pmatrix}}{\det\overline{M}} \end{cases} \tag{B12}$$

After some calculations, the constants A, B and C solution of the linear system (eq. B9) are:

$$\begin{cases} A = \delta \sin\theta \dfrac{\tan\dfrac{\beta L}{2} + \alpha\beta L}{2\tan\dfrac{\beta L}{2} + \beta L\left[\alpha^2(\beta L)^2 + 1\right]} \\ B = \delta \sin\theta \dfrac{\alpha\beta L \tan\dfrac{\beta L}{2} - 1}{2\tan\dfrac{\beta L}{2} + \beta L\left[\alpha^2(\beta L)^2 + 1\right]} \\ C = \delta \sin\theta \dfrac{\beta(1+\alpha^2\beta^2 L^2)}{2\tan\dfrac{\beta L}{2} + \beta L\left[\alpha^2(\beta L)^2 + 1\right]} \end{cases} \tag{B13}$$

which give (eq. 6.23 in section 6.3.1):

$$w = \frac{\delta \sin\theta}{2\tan\dfrac{\beta L}{2} + \beta L\left[\alpha^2(\beta L)^2 + 1\right]} \times \\ \times\left[\left(\tan\frac{\beta L}{2} + \alpha\beta L\right)(\cos\beta x - 1) + \left(\alpha\beta L\tan\frac{\beta L}{2} - 1\right)\sin\beta x + \beta\left(1+\alpha^2\beta^2 L^2\right)x\right] \tag{B14}$$